


8-2018

The Role of Perivascular Fibrosis in Post-Stroke Glymphatic Impairment and Cerebral Amyloid Angiopathy

Matthew D. Howe

Follow this and additional works at: https://digitalcommons.library.tmc.edu/utgsbs_dissertations

 Part of the [Biology Commons](#), [Cellular and Molecular Physiology Commons](#), [Molecular and Cellular Neuroscience Commons](#), [Pharmacology Commons](#), and the [Translational Medical Research Commons](#)

Recommended Citation

Howe, Matthew D., "The Role of Perivascular Fibrosis in Post-Stroke Glymphatic Impairment and Cerebral Amyloid Angiopathy" (2018). *UT GSBS Dissertations and Theses (Open Access)*. 875.
https://digitalcommons.library.tmc.edu/utgsbs_dissertations/875

This Dissertation (PhD) is brought to you for free and open access by the Graduate School of Biomedical Sciences at DigitalCommons@TMC. It has been accepted for inclusion in UT GSBS Dissertations and Theses (Open Access) by an authorized administrator of DigitalCommons@TMC. For more information, please contact laurel.sanders@library.tmc.edu.

THE ROLE OF PERIVASCULAR FIBROSIS IN POST-STROKE GLYMPHATIC
IMPAIRMENT AND CEREBRAL AMYLOID ANGIOPATHY

By

Matthew David Howe, B.S.

APPROVED:

Louise McCullough, MD, PhD

Jaroslawn Aronowski, MD, PhD

Andrew Bean, PhD

Shane Cunha, PhD

Ruth Heidelbergger, MD, PhD

Claudio Soto, PhD

APPROVED:

Dean, The University of Texas
MD Anderson Cancer Center UT Health Graduate School of Biomedical Sciences

THE ROLE OF PERIVASCULAR FIBROSIS IN POST-STROKE GLYMPHATIC
IMPAIRMENT AND CEREBRAL AMYLOID ANGIOPATHY

A

DISSERTATION

Presented to the Faculty of

The University of Texas

MD Anderson Cancer Center UTHealth

Graduate School of Biomedical Sciences

in Partial Fulfillment

of the Requirements

for the Degree of

DOCTOR OF PHILOSOPHY

by

Matthew David Howe, B.S.
Houston, Texas

August, 2018

This work is dedicated to

- DAVID CARLETON HOWE -

*A remarkable man
who survived a stroke at 57,
passed away at 87,
and continues to inspire us all
with his kind manner,
his sense of humor,
and his fighting spirit.*

ACKNOWLEDGEMENTS

I would like to thank my entire thesis committee—including Professors Jarek Aronowski, Andy Bean, Shane Cunha, Ruth Heidelberger, and Claudio Soto—for their mentorship over the past three years. I always looked forward to our meetings, and felt that they really helped me stay on track. I would especially like to thank my thesis advisor, Dr. Louise McCullough, not just for helping me write grants, apply for scholarships and publish papers, but also for taking the time to mentor me as a future scientist and to challenge me to do the best work that I can do. Growing up, I never saw myself living in Texas, but I am so glad that I took a chance and moved here with you just a few short months after we started working together in Connecticut—thank you so much for the opportunity to grow, both personally and professionally, in a new state. I would also like to thank my co-advisor, Dr. Akihiko Urayama, who has steadily guided my research, and provided both moral and technical support through some ambitious projects. You are a gifted teacher and a brilliant scientist. I have learned so much from you, and I am excited to see where you take this research program in the coming years.

I would also like to give a big thank you to the many research technicians that assisted with this research over the years, especially Yan Xu, Monica Spsychala, Rachael Rosow, Ye Sun, Gabe Spiegel, Eric Mohan, Louise Atadja, John d’Aigle, Weldon Furr and Yashee Munshi. Thank you all for the amount of hard work that you put into these projects, and for all of the good times that we had along the way. Yan is a senior research technician in our laboratory, and has the big responsibility of managing our enormous colony of wild-type and transgenic mice, including breeding pups for my cell culture work and procuring

aged animals for many of our *in vivo* studies. Thank you, none of our projects would be possible without your hard work behind the scenes. Monica has helped me with behavior and data analysis since the beginning, when she moved here from Connecticut with our lab, and has been one of the few constants in my research since the beginning of my education. Rachael and Ye were summer students at UConn, who helped with the initial behavioral studies and also did the early characterization of angiogenesis and aquaporin expression in our mouse model of stroke. Gabe spent a year in our lab in Texas, and helped me perform some of our very early physiology experiments, and assisted with the associated histology (detailed in Chapter 3). I don't know where I would be without Louise Atadja's help with all of the behavioral studies (Chapter 4). Her patience, perseverance and careful work with our animals continue to be essential to our research program, and I wish her the best of luck as she starts medical school next year. John was a big help in teaching me how to harvest primary cells, and keep them alive for long enough to get data! He also helped harvest cells for some of the last cell culture experiments, when I really needed the assistance (shown in Chapter 5). He's going to be a phenomenal graduate student. Weldon has been an amazing technician, who has done the most work for me over the past year. He is very talented and hardworking, and has helped with everything from physiology experiments, to histology, to biochemical assays, including help with western blots and ELISA (shown in Chapter 5). He has a bright future ahead of him in the medical profession. Finally, Yashee was indispensable for the PCR experiments (also in Chapter 5). She performed most of the RNA isolation, and all of the cDNA synthesis and qPCR assays. Whether it is science, medicine or something else, I'm excited to see where her career takes her next.

Other individuals also played important roles in my education and research projects. Fellow graduate students Ted Koelhoff, Tony Patrizz, Meaghan Roy-O'Reilly and Jake Hudobenko provided a ton of technical help, and great conversations over the years as we worked across the bench from each other. We all made it through this crazy journey together, and I know each of them will be very successful in their future careers. Postdoctoral fellows Hilda Ahstedt and Anjali Chauhan are incredibly generous people, who mentored me early on in my research. Even today, they are great resources for advice at the bench, and I thank them for their help. Michael Maniskas, one of our newer postdoctoral fellows, has been a major help this past year, both in finishing some remaining projects and taking the reins for our future projects involving two-photon microscopy. He is a very gifted scientist, and I know he will do well here. Professors Sean Marelli, Fudong Liu, Venu Venna and Jun Li have also provided helpful advice, and are leaders in our shared research program. It has been fun working with all of you over the years, and I wish you the best of luck. I would also like to thank Dr. Nancy Edwards, who generously provided all of the human samples and clinical data that we used for our analysis in Chapter 6. Our administrative team, including Diego Morales, Lori Capozzi and Kayla Hurt, also deserves recognition. You all made my research possible by maintaining the animal protocols, ordering reagents, making sure I had the animals that I needed, and overall just making the lab run smoothly and working to maintain a positive, collaborative environment for all of us.

In addition to the individuals that helped me at school and in the lab, my family also deserves thanks for their love and support over the years. Both of my parents were great role models and helped me to become the person that I am today. They encouraged my interest in science as a kid, and made sure that I always tried my best in school growing up. My mom

saw the importance of exposing me to the medical field as a teenager, and made sure that I had summer jobs and volunteer opportunities working in the different hospitals and practices that she was working in at the time. Both of my parents supported my unusual choice to pursue training in an MD/PhD program, even though we all knew it would be a long road. Finishing this dissertation brings me a big step closer to completing this journey, and I am so lucky to have them taking it with me, every step of the way.

Finally, I also want to thank my wife for everything that she does. Megan, you've been my best friend since we met sophomore year in college. We've been through a lot since then, and there is no way that I could have done any of this without you. Thank you for being there for me, whether it was helping me study, taking care of things at home if I had to work late, or coming into lab on the weekends to hang out while I finished those extra-long experiments. Thank you for the sacrifices that you have made to make my education possible, which are too many to count, and all of the things you have done along the way to help, as recently as editing this dissertation. Above all, thank you for being my partner in life. I look forward to starting our next chapter together with our little girl Ainsley.

THE ROLE OF PERIVASCULAR FIBROSIS IN POST-STROKE GLYMPHATIC IMPAIRMENT AND CEREBRAL AMYLOID ANGIOPATHY

Matthew David Howe, B.S.

Advisory Professor: Louise McCullough, M.D., Ph.D.

In healthy brain tissue, toxic amyloid- β ($A\beta$) proteins are transported by the pulsatile flow of cerebrospinal fluid (CSF) along perivascular drainage pathways. Ischemic stroke may disrupt this process, leading to a perivascular build-up of $A\beta$, termed cerebral amyloid angiopathy (CAA). I hypothesize that an abnormal pattern of extracellular matrix deposition within the vascular basement membrane, termed fibrosis, impairs $A\beta$ drainage from the aged brain after stroke. I further hypothesize that inhibition of astrocytic transforming growth factor- β (TGF- β) signaling can reverse these phenotypes. Finally, I also hypothesize that serum biomarkers of perivascular fibrosis can be used to diagnose CAA following intracerebral hemorrhage (ICH). To test these hypotheses, I first performed experimental stroke in young and aged wild-type mice, then measured basement membrane fibrosis and CSF flow using a variety of biochemical and physiological techniques. I also evaluated the contribution of astrocytes to these phenotypes using a primary cell culture model. Then, I treated aged mice with a TGF- β antagonist, and measured the impact on fibrosis and CSF flow. Finally, I explored the relevance of these findings to humans by measuring serum biomarkers of fibrosis after ICH, and correlating them to CAA etiology, injury severity and functional outcomes. Overall, my findings support a role for fibrosis in impairing perivascular $A\beta$ drainage after stroke, which could lead to CAA and progressive cognitive decline in stroke survivors.

TABLE OF CONTENTS

| | |
|---|-------------|
| • <i>Approval Sheet</i> | <i>i</i> |
| • <i>Title Page</i> | <i>ii</i> |
| • <i>Dedication</i> | <i>iii</i> |
| • <i>Acknowledgements</i> | <i>iv</i> |
| • <i>Abstract</i> | <i>viii</i> |
| • <i>Table of Contents</i> | <i>ix</i> |
| • <i>List of Illustrations</i> | <i>x</i> |
| • <i>List of Tables</i> | <i>xiii</i> |
| • <i>Abbreviations</i> | <i>xiv</i> |
| • Chapter 1: Background and Significance..... | <i>1</i> |
| • Chapter 2: Specific Aims of Dissertation Research..... | <i>30</i> |
| • Chapter 3: Early Validation of Perivascular CSF Flow in the Murine Brain..... | <i>34</i> |
| • Chapter 4: Fibronectin Induces the Perivascular Deposition of CSF-derived Amyloid- β in Aging and After Stroke..... | <i>52</i> |
| • Chapter 5: TGF- β Stimulates A2 Astrocytes to Remodel the Basement Membrane and Impair the Perivascular Flow of CSF After Stroke..... | <i>96</i> |
| • Chapter 6: Serum Biomarkers of Basement Membrane Fibrosis Are Diagnostic of CAA After Intracerebral Hemorrhage..... | <i>155</i> |
| • Chapter 7: Discussion and Future Directions..... | <i>171</i> |
| • Chapter 8: References..... | <i>201</i> |
| • Chapter 9: Vita..... | <i>247</i> |

LIST OF ILLUSTRATIONS

Chapter 2

- **Figure 2-1:** Reactive astrocytes may secrete fibronectin and impair the perivascular transport of CSF-derived A β_{1-40} after stroke..... 30

Chapter 3

- **Figure 3-1:** Visualization of CSF influx by intracisternal dye injection..... 43
- **Figure 3-2:** CSF influx occurs along perivascular routes..... 46
- **Figure 3-3:** Kinetics of influx and efflux of injected tracers..... 48

Chapter 4

- **Figure 4-1:** Aging and DMCAO disrupted the transport of CSF and enhanced A β_{1-40} distribution in the superficial cortex..... 63
- **Figure 4-2:** Infusion technique, representative images and raw tracer uptake values..... 65
- **Figure 4-3:** Comparison of cortical atrophy, motor and cognitive impairments in young and aged mice with DMCAO..... 69
- **Figure 4-4:** DMCAO selectively increased the uptake of A β_{1-40} in the injured cortex of aged animals..... 71
- **Figure 4-5:** Distribution of dextran does not predict A β_{1-40} distribution in aged animals..... 74
- **Figure 4-6:** Lectin staining predicted A β_{1-40} distribution in all experimental groups..... 75
- **Figure 4-7:** DMCAO increased the expression of fibronectin and integrin- $\alpha 5$ at

| | |
|--|----|
| 7 DPI..... | 77 |
| • Figure 4-8: DMCAO upregulated the expression of fibronectin and integrin $\alpha 5$ in young and aged mice..... | 78 |
| • Figure 4-9: DMCAO reduced LRP1 expression in aged mice..... | 79 |
| • Figure 4-10: Fibronectin expression colocalized with sites of CSF $A\beta_{1-40}$ deposition..... | 81 |
| • Figure 4-11: Integrin- $\alpha 5$ expression colocalized with sites of CSF $A\beta_{1-40}$ deposition..... | 83 |
| • Figure 4-12: Fibronectin conjugation altered the perivascular transport of $A\beta_{1-40}$ | 85 |

Chapter 5

| | |
|---|-----|
| • Figure 5-1: Reactive astrogliosis occurs after DMCAO and is worse in aged animals..... | 121 |
| • Figure 5-2: TGF- β signaling is differentially activated by aging and DMCAO... | 123 |
| • Figure 5-3: OGD alters activation status and expression of ECM genes in primary astrocytes..... | 126 |
| • Figure 5-4: Expression of TGF- β -related genes in primary astrocytes following acute stimulation..... | 131 |
| • Figure 5-5: Expression of inflammatory genes in primary astrocytes following acute stimulation..... | 133 |
| • Figure 5-6: TGF- β stimulation increases $A\beta_{1-40}$ binding and fibronectin expression..... | 136 |

- **Figure 5-7:** OGD increases A β ₁₋₄₀ binding in primary astrocytes..... 138
- **Figure 5-8:** TGF- β stimulation alters AQP4 polarization and impairs water uptake..... 141
- **Figure 5-9:** Age-specific effects of subacute TGF- β R1 antagonism following DMCAO..... 143
- **Figure 5-10:** Delayed TGF- β R1 antagonism reduces fibrosis and improves perivascular flow following DMCAO in aged mice..... 146

Chapter 6

- **Figure 6-1:** Biomarkers of small vessel fibrosis discriminate between CAA and hypertensive hemorrhage..... 166

Chapter 7

- **Figure 7-1:** Working model of CAA pathogenesis..... 184

LIST OF TABLES

Chapter 5

- **Table 5-1:** PCR assay design..... 111
- **Table 5-2:** Effects of perfusion, co-stimulation and interaction on gene expression in primary astrocytes..... 128

Chapter 6

- **Table 6-1:** Demographics and admission variables by study group..... 162
- **Table 6-2:** Early cytokine levels and their relation to initial injury scores..... 163
- **Table 6-3:** Early cytokine levels as predictors of functional outcome scores..... 164
- **Table 6-4:** Comparison of serum cytokine values in CAA and hypertensive hemorrhage patient populations..... 165

ABBREVIATIONS

| <i>Abbreviation</i> | <i>Definition</i> |
|---|---|
| 647-Aβ₁₋₄₀ | <i>AlexaFluor-647-conjugated human amyloid-β, amino acids 1-40</i> |
| A.U. | <i>Arbitrary units</i> |
| AAALAC | <i>Association for Assessment and Accreditation of Laboratory Animal Care</i> |
| ACA | <i>Anterior cerebral artery</i> |
| aCSF | <i>Artificial cerebrospinal fluid</i> |
| AD | <i>Alzheimer's disease</i> |
| AGRN | <i>Agrin (gene)</i> |
| ANOVA | <i>Analysis of variance</i> |
| APOE ϵ4 | <i>Apolipoprotein E ϵ4</i> |
| APP | <i>Amyloid precursor protein</i> |
| AQP1 | <i>Aquaporin-1</i> |
| AQP4 | <i>Aquaporin-4</i> |
| AUC | <i>Area under the curve</i> |
| Aβ | <i>Amyloid-β peptide</i> |
| Aβ₁₋₄₀ | <i>Amyloid-β peptide, amino acids 1-40</i> |
| Aβ₁₋₄₂ | <i>Amyloid-β peptide, amino acids 1-42</i> |
| BBB | <i>Blood-brain barrier</i> |
| BSA | <i>Bovine serum albumin</i> |
| BSS | <i>Balanced salt solution</i> |
| CAA | <i>Cerebral amyloid angiopathy</i> |
| CB-d3 | <i>Cascade blue dextran (MW = 3 kilodalton)</i> |
| cDNA | <i>Complementary DNA</i> |
| CNS | <i>Central nervous system</i> |
| COL164A1 | <i>Collagen XVI (gene)</i> |
| CP | <i>Choroid plexus</i> |
| CPM | <i>Counts per minute</i> |
| CSF | <i>Cerebrospinal fluid</i> |
| CSPG | <i>Chondroitin sulfate proteoglycan</i> |
| CT | <i>Cycle threshold (value)</i> |
| CXCL10 | <i>C-X-C motif chemokine 10</i> |
| CXCL16 | <i>C-X-C motif chemokine 16</i> |
| DAPI | <i>4',6-diamidino-2-phenylindole</i> |
| DIV | <i>Days in vitro</i> |
| DMCAO | <i>Distal middle cerebral artery occlusion</i> |
| DMEM | <i>Dulbecco's modified eagle medium</i> |
| DPI | <i>Days post-injury</i> |
| DPM | <i>Disintegrations per minute</i> |

| | |
|--|---|
| DVR | <i>8-vinyl reductase</i> |
| EBA | <i>Evans blue albumin</i> |
| EBD | <i>Evans blue dye</i> |
| EC₅₀ | <i>50% Effective Concentration</i> |
| ECM | <i>Extracellular matrix</i> |
| FBLN5 | <i>Fibulin-5 (gene)</i> |
| FDR | <i>False discovery rate</i> |
| FITC-Aβ₁₋₄₀ | <i>Fluorescein isothiocyanate conjugated recombinant human amyloid-β, amino acids 1-40</i> |
| FITC-Aβ₁₋₄₂ | <i>Fluorescein isothiocyanate conjugated recombinant human amyloid-β, amino acids 1-42</i> |
| FITC-d2000 | <i>Fluorescein isothiocyanate dextran (2000 kilodaltons)</i> |
| FITC-d70 | <i>Fluorescein isothiocyanate dextran (70 kilodaltons)</i> |
| FN1 | <i>Fibronectin (gene)</i> |
| GAG | <i>Glycosaminoglycans</i> |
| GCS | <i>Glasgow Coma Scale</i> |
| GFAP | <i>Glial fibrillary acid protein</i> |
| HBSS | <i>Hank's Balanced Salt Solution</i> |
| HCl | <i>Hydrochloric acid</i> |
| HEPES | <i>4-(2-hydroxyethyl)-1-piperazineethanesulfonic acid</i> |
| HSPG | <i>Heparan sulfate proteoglycan</i> |
| HSPG2 | <i>Perlecan (gene)</i> |
| IACUC | <i>Institutional Animal Care and Use Committee</i> |
| ICC | <i>Immunocytochemistry</i> |
| ICH | <i>Intracerebral hemorrhage</i> |
| ICP | <i>Intracranial pressure</i> |
| IHC | <i>Immunohistochemistry</i> |
| IL-1β | <i>Interleukin-1β</i> |
| IL-6 | <i>Interleukin-6</i> |
| IL-10 | <i>Interleukin-10</i> |
| IQR | <i>Interquartile range</i> |
| ISF | <i>Interstitial fluid</i> |
| ITGA5 | <i>Integrin-α5 (gene)</i> |
| ITGB1 | <i>Integrin-β1 (gene)</i> |
| IVH | <i>Intraventricular hemorrhage</i> |
| kD | <i>Kilodalton</i> |
| KeV | <i>Kiloelectron-volt</i> |
| LPS | <i>Lipopolysaccharide</i> |
| LRP1 | <i>Lipoprotein receptor protein 1</i> |
| LSC | <i>Liquid scintillation counter</i> |
| MCA | <i>Middle cerebral artery</i> |
| MCAO | <i>Middle cerebral artery occlusion</i> |

| | |
|---------------------------------|--|
| MCI | <i>Mild-cognitive impairment</i> |
| MIPAV | <i>Medical Image Processing, Analysis, and Visualization</i> |
| MMP | <i>Matrix metalloproteinases</i> |
| MRI | <i>Magnetic resonance imaging</i> |
| mRNA | <i>Messenger RNA</i> |
| mRS | <i>Modified rankin scale</i> |
| NIHSS | <i>National Institute of Health stroke scale</i> |
| NO | <i>Normoxia</i> |
| NORT | <i>Novel object recognition test</i> |
| NVU | <i>Neurovascular unit</i> |
| OGD | <i>Oxygen-glucose deprivation</i> |
| PBS | <i>Phosphate-buffered saline</i> |
| PCA | <i>Posterior cerebral artery</i> |
| PET | <i>Positron emission tomography</i> |
| PFA | <i>Paraformaldehyde</i> |
| PGP | <i>P-glycoprotein</i> |
| PBS | <i>Phosphate buffered saline</i> |
| PiB | <i>Pittsburgh compound B</i> |
| PMSF | <i>Phenylmethylsulfonyl fluoride</i> |
| PS1 | <i>Presenilin-1 (gene)</i> |
| PVDF | <i>Polyvinylidene fluoride</i> |
| PVS | <i>Perivascular space</i> |
| qPCR | <i>Quantitative polymerase chain reaction</i> |
| RAGE | <i>Receptor for advanced glycation endproducts</i> |
| RIPA | <i>Radioimmunoprecipitation assay buffer</i> |
| ROC | <i>Receiver operating characteristic</i> |
| ROI | <i>Region of interest</i> |
| RPM | <i>Revolutions per minute</i> |
| SD | <i>Standard deviation</i> |
| SDC2 | <i>Syndecan-2 (gene)</i> |
| SEM | <i>Standard error of the mean</i> |
| SPP1 | <i>Osteopontin (gene)</i> |
| TCT | <i>Triton carrageenan tris buffered saline solution</i> |
| TGF-β | <i>Transforming growth factor-β (isoforms 1, 2 and 3)</i> |
| TGF-βR1 | <i>TGF-β receptor-1</i> |
| TGF-βR2 | <i>TGF-β receptor-2</i> |
| Tgfr2 | <i>Transforming growth factor-β receptor-2 (gene)</i> |
| TMA | <i>Tetramethylammonium</i> |
| TNF-α | <i>Tumor necrosis factor-α</i> |
| tPA | <i>Tissue plasminogen activator</i> |
| TR-d3 | <i>Tetramethylrhodamine dextran (3 kilodaltons)</i> |

CHAPTER 1

Background and Significance

1.1: Stroke is a major risk factor for cognitive decline in the elderly.

Ischemic stroke occurs when a blood clot acutely reduces blood flow to a region of brain tissue, leading to acute infarction of the affected area.¹ This type of stroke affects approximately 800,000 people every year within the U.S.,^{1,2} and is a leading cause of acquired disability.³ With approximately 7 million stroke survivors currently alive in the U.S.,² there is a desperate need to better understand the long-term cognitive consequences of stroke and to develop tailored strategies to address the unique clinical challenges in this vulnerable population.

The most common type of stroke is a large vessel occlusion of the middle cerebral artery (MCA). During the acute phase of injury, this type of stroke typically damages the cortex and basal ganglia.⁴ Following blockage by a thrombus or embolus, acute ischemia in these brain regions produces confusion and hemiparesis, as well as different cortical signs depending on which side of the brain is affected.⁴ Tissue plasminogen activator (tPA) represents the only available pharmacologic treatment for acute stroke, and must be used within hours of stroke onset to be efficacious in reducing injury severity.⁵ However, even when properly treated, stroke frequently leads to long-term disability, including chronic motor, sensory and cognitive impairment.³ Recent studies in the clinical literature suggest that in addition to acute deficits in cognitive function, stroke commonly leads to a slowly progressive form of cognitive decline, termed ‘vascular’ dementia.⁶ However, this disease

has proven challenging to model in mice, and the underlying mechanisms leading to this phenotype are a subject of intense debate.

There is significant evidence in the clinical literature that stroke is an independent risk factor for progressive cognitive decline. The Framingham heart study found that stroke doubles the risk of cognitive decline, with 35% of stroke survivors progressing to dementia within ten years of the initial insult.⁷ Furthermore, the Rotterdam study confirmed that stroke doubles the risk of dementia, and that this occurs independently of pre-stroke cognitive function and, importantly, in the absence of recurrent stroke.⁸ More recent work has shown that in addition to an acute loss of cognitive function, stroke also accelerates the trajectory of underlying progressive cognitive decline, suggesting a synergistic relationship between chronic neurodegenerative disease and acute injury.⁹ Overall, these data from multiple, large clinical studies indicate that stroke is a major, yet largely unrecognized independent risk factor for progressive cognitive decline. However, the lack of a coherent disease mechanism presents a major roadblock to developing potential treatments for post-stroke dementia.⁶

Stroke may induce acute cognitive impairment due to the initial loss of brain tissue associated with the primary injury.⁴ However, this progressive impairment, described above, requires the exploration of additional, more chronic mechanisms. This has mainly been studied with experimental MCA occlusion (MCAO) models in mice.⁶ One plausible hypothesis is that stroke initiates a neuroinflammatory cascade, which contributes to widespread neuronal loss and dementia by autoimmune mechanisms.¹⁰ For example, one previous study showed that young mice subjected to a small, cortical stroke developed progressive cognitive decline over seven weeks after injury, due to a neuroinflammatory response involving B cell activation.¹¹ Similarly, previous work by our lab has shown that

aging exacerbates chronic T cell responses to stroke,¹² which could also impair cognitive function. Others have shown that sterile inflammation, modeled by lipopolysaccharide (LPS) stimulation, impairs cognitive function in mice.¹³ Furthermore, this can be abolished by treatment with anti-inflammatory drugs at the time of LPS exposure, indicating a detrimental effect of immune activation on cognition.¹³ However, based on the fact that cognitive impairment continues to progress years after the peak of inflammation has subsided, there could be other, non-immune mechanisms at play that have not been adequately explored in animal models.

Alzheimer's disease (AD) provides a relatively well-understood alternative prototype for progressive cognitive decline, which serves as a useful starting point to explore additional potential mechanisms of post-stroke dementia. In classic AD-type dementia patients, a toxic protein called amyloid- β ($A\beta$) accumulates and forms plaques in the hippocampus, which is associated with progressive impairment of cognitive function.¹⁴ Similarly, when humanized amyloid protein is overexpressed in the brains of mice, they also begin to develop progressive cognitive decline with aging,¹⁵ further supporting the so-called 'amyloid cascade hypothesis' of neurodegeneration in AD.^{16,17} As hippocampal amyloid pathology forms early in the disease course, AD patients develop deficits in hippocampal dependent tasks, such as short-term and working memory. Additionally, in most AD patients, $A\beta$ deposits in the walls of cortical vessels, which can lead to a loss of vessel integrity and recurrent microhemorrhage.¹⁸⁻²⁰ This special type of vascular pathology is termed cerebral amyloid angiopathy (CAA).¹⁹ The appearance of microhemorrhage is often associated with impairment in multiple other 'extra-hippocampal' cognitive domains, including executive function, language and facial recognition; although some patients are cognitively normal

until late stage disease.²¹ While the literature supports that A β accumulation plays a major role in AD pathogenesis,¹⁷ it is not known if CAA contributes to post-stroke dementia.⁶

Stroke patients tend to exhibit early problems with ‘cortical’ domains of cognitive function.^{9,21} In particular, compared to AD, a marked loss of executive function occurs early in post-stroke dementia, suggesting damage to the frontal cortex or white matter.²²

Additionally, patients with post-stroke dementia often follow a stepwise loss of cognitive function, suffering repeated vascular insults, including microhemorrhage and microinfarction throughout the cortex, in a similar distribution to that seen in AD-associated CAA.⁹

Therefore, it stands to reason that CAA could play a major, early role in driving the progression of post-stroke dementia. It is not known how stroke induces conditions that could favor the formation of CAA deposits,¹⁷ but understanding this process could shed light on the pathogenesis of both post-stroke dementia and lead to new disease-modifying treatments.

In summary, ischemic stroke is a leading cause of dementia in the elderly, however, the mechanism driving cognitive decline in these patients is not known. Both AD and post-stroke dementia may involve the accumulation of A β , however, differences in the disease course and impact on specific domains in cognitive function suggest that this accumulation occurs in different locations; therefore, they likely occur by distinct pathophysiological mechanisms. In particular, the cognitive symptoms and clinical course of post-stroke dementia suggest a pattern of cortical vascular amyloid deposition that is consistent with CAA.²³

In the remainder of this chapter, the evidence that stroke induces CAA pathology in human patients will be extensively explored. Additionally, the multiple mechanisms by

which A β deposition induces vessel damage and cognitive decline will also be reviewed in detail. Finally, a new potential mechanism by which stroke induces vascular A β deposition in the cerebrovascular basement membrane will be introduced. A better understanding of these mechanisms may lead to new diagnostic tools and therapeutic avenues for stroke survivors at risk of cognitive decline.

1.2: CAA drives cognitive decline in aging and after stroke.

CAA is pathologically defined as the appearance of amyloid (“sugar-like”) deposits in vessels accompanied by vessel wall hypertrophy, fibrinoid necrosis and/or hemorrhage.¹⁹ These amyloid deposits form in the brain extracellular perivascular space (PVS) and are primarily composed of amyloid- β (A β), a 4 kD peptide with a unique biochemical profile.²⁰ Importantly, the majority of dementia patients suffer from mixed brain pathologies, and have histological evidence of both macroscopic infarction, caused by prior stroke, and Alzheimer’s disease (amyloid deposition) at autopsy.^{18,24,25} This association between stroke and CAA is clearly evidenced in the clinical literature by both histopathological and imaging studies.

First, several postmortem histopathological studies of human patients support an association between ischemic stroke and CAA. One study found that cerebral infarction and amyloid pathology synergize to worsen cognitive impairment in elderly individuals.²⁴ Importantly, this association also occurs in patients with mild-cognitive impairment (MCI), indicating that vascular and amyloid pathologies co-exist even in the earliest stages of dementia.¹⁸ CAA pathology is associated with executive dysfunction in MCI patients, further supporting the notion that vascular amyloid pathology impairs specific domains of cognitive

function.²⁶ Overall, these studies show that stroke and amyloid pathology frequently co-occur, and are associated with both early and late stages of disease.

Further supporting the relationship between stroke and CAA, data from positron emission tomography (PET) studies support a relationship between ischemia and amyloid deposition using the Pittsburgh compound B (PiB) retention ratio.²⁷ Ischemic stroke patients exhibit significantly higher amyloid burden in the area of infarction during the subacute phase of injury,²⁸ which correlates with both magnetic resonance imaging (MRI) biomarkers of CAA, and dementia, in elderly stroke patients.²⁹ Furthermore, stroke patients with high amyloid burden are also more likely to develop hemorrhagic transformation, suggesting that these post-stroke amyloid deposits are associated with underlying small vessel disease.³⁰

Finally, MRI studies also support a relationship between stroke and small vessel disease phenotypes that are characteristic of CAA. MRI can be used to meet a probable diagnosis of CAA by measuring several types of secondary brain injuries, termed the ‘Boston criteria,’ including the presence of cerebral microbleeds, lacunar infarction (small ischemic strokes), leukoairiosis (white matter hyperintensity), superficial siderosis, cortical atrophy and enlarged PVS.^{31,32} Stroke survivors with imaging biomarkers of CAA have worse functional outcomes 3 months after stroke.³³ They exhibit higher levels of leukoairiosis, which positively correlates with cognitive decline after stroke.^{34,35} Additionally, stroke survivors commonly develop enlarged visible PVS.^{32,33,36} Overall, these studies demonstrate (1) that stroke patients are at a high risk of developing the secondary injuries associated with CAA, and (2) that stroke patients with more severe CAA exhibit increased rates of cognitive impairment after stroke.

While these findings clearly support a relationship between stroke and CAA, this may be complicated by the fact that stroke and AD share several major risk factors.³⁷ Sporadic AD and stroke share genetic risk factors, including apolipoprotein E ϵ 4 genotype,³⁸ methylenetetrahydrofolate reductase polymorphisms³⁹ as well as regulators of C-reactive protein and plasma lipids.⁴⁰ In addition, the two diseases also share several modifiable risk factors, including hypertension,⁴¹ hypercholesterolemia,⁴² diabetes mellitus,⁴³ obesity,⁴⁴ sedentary lifestyle⁴⁵ and smoking.⁴⁶ All of these shared factors could confound even the best-designed retrospective study, and highlight the need for more prospective studies with baseline imaging and cognitive testing. While these shared risk factors between AD and stroke may confound the clinical literature, they also raise the question as to how the underlying pathophysiology of stroke and CAA are related.

In theory, the causative relationship between stroke and CAA would be best illustrated by studies in the animal literature, because they avoid many of the confounding variables of shared risk factors, described above, by the use of littermate controls. A few interesting studies using wild-type rats have shown that stroke increases the levels of soluble A β within the thalamus after MCAO, which may be a result of secondary injury.⁴⁷⁻⁵¹ These studies support the notion that stroke independently increases amyloid burden, but do not perfectly mimic the findings seen in stroke patients involving CAA pathology and amyloid plaque deposition in the area of infarction. However, these papers provide consistent support for a causative relationship between stroke and amyloid deposition.

Overall, data from diverse studies using histopathology as well as MRI and PET imaging strongly support an association between ischemic stroke, CAA and cognitive decline. However, the causative nature of stroke on CAA progression is difficult to infer in

these clinical studies, due to both unavoidable shortcomings in study design, as well as the significant overlap of risk factors for AD and stroke. Additional studies of long-term histological and cognitive outcomes in transgenic AD mice with experimental stroke are needed to confirm the directionality of the relationship between stroke and CAA, as well as to better understand the potential mechanism of CAA induction after stroke.

1.3: Increased vascular A β deposition mediates vascular pathology in CAA.

CAA is associated with maladaptive vascular phenotypes that could contribute to cognitive decline in stroke survivors by negatively affecting neurons and other brain cells that rely on affected vessels for perfusion. Based on a review of the existing literature, it is clear that the vascular phenotypes and cognitive loss observed in CAA are, in large part, a direct consequence of A β deposition into cerebral blood vessels. Therefore, therapies that reduce the production, aggregation or deposition, or conversely, enhance the clearance of A β from the PVS, could slow the progression of CAA.

The A β peptide is a metabolic product that is derived from the much larger amyloid precursor protein (APP), which is an 87 kD integral membrane-spanning protein.⁵² In the healthy brain, APP plays an important role in synapse formation,⁵³ synaptic plasticity⁵⁴ and iron metabolism.⁵⁵ Importantly, APP is degraded during the course of normal neurotransmission, and A β is produced and released into the extracellular space, where it undergoes two sequential cleavage steps by two enzymes: β -secretase and γ -secretase.⁵⁶ The major A β isoforms that are associated with CAA and Alzheimer's disease are A β peptides containing the amino acid residues numbered 1-40 and 1-42 (denoted as A β ₁₋₄₀ and A β ₁₋₄₂, respectively). Both isoforms exhibit extensive beta sheet structure, which causes monomeric

A β particles to assemble into dimers, oligomers and eventually large insoluble aggregates, which are found as abnormal deposits within the vascular basement membrane.¹⁷ A β ₁₋₄₀ is most commonly associated with CAA plaques,⁵⁷ potentially due to its improved solubility compared to the longer A β ₁₋₄₂ isoform,⁵⁸ which could allow for it to travel further from the synapse and associate with the vasculature.

While there is a strong association between CAA and dementia, there is historical debate as to whether A β ₁₋₄₀ represents a cause or a consequence of the underlying small vessel pathology. The most direct evidence that A β is causally related to small vessel disease comes from studies of early-onset, genetic forms of CAA. For example, patients with Down syndrome (Trisomy 21) exhibit overexpression of APP and develop AD pathology and CAA at increased rates.⁵⁹ Additionally, in familial AD, activating mutations in γ -secretase (presenilin-1 [PS1]) increase the generation of A β from APP,^{56,60,61} leading to extensive A β plaques and early-onset cognitive decline,⁶² and certain PS1 mutations induce vascular amyloid deposition and multiple hemorrhage.⁶³⁻⁶⁵ Finally, rare cases of familial CAA, caused by specific mutations in the A β coding region of the APP gene, comprise a small group of diseases termed hereditary cerebral hemorrhage with amyloidosis.⁶⁶⁻⁶⁹ While total APP expression is unaffected, altered cleavage by γ -secretase leads to relative increases in A β ₁₋₄₀ compared to A β ₁₋₄₂.^{70,71} While the causative nature of A β overproduction is clearly linked to early-onset familial CAA, the mechanism driving late-onset sporadic CAA is not as clear in the literature.

These genetic mutations are such powerful drivers of disease, that simply inducing their expression in mice is sufficient to recapitulate many of the nuances of CAA. For example, one of the most widely used models of AD is the Tg2576 mutant mouse, which

possess the APP(KM670, 671NL [Swedish]) mutation.⁷² This strain exhibits slowly progressive, age-associated cognitive impairments, and begins to develop more widespread parenchymal and vascular pathology by 9 – 10 months of age.⁷² In contrast, another strain, termed APP/PS1, harbors two mutant alleles: mutant-APP(KM670N, 671NL [Swedish]), as well as PS1(L166P).⁷³ Due to the additional genetic manipulation, these mice develop parenchymal amyloid pathology much earlier in life, leading to neuronal loss, astrogliosis and cognitive impairment by 6 – 8 months of age.⁷³ This particular mutation induces very high production of A β ₁₋₄₂ compared to A β ₁₋₄₀, which likely explains the apparent lack of CAA until very advanced age in this model.⁷³

On the other end of the disease spectrum, another strain, termed TgSwDI, exhibits CAA-like pathology very early in life.⁷⁴ These animals possess three disease-associated transgenes: APP(KM670N, 671NL [Swedish]), APP(E693Q [Dutch]) and APP(D694N [Iowa]).⁷⁴ The Dutch and Iowa ‘vasculotropic’ APP mutations were isolated from families with hereditary cerebral hemorrhage with amyloidosis.^{66,75} As such, these animals develop early elevations in A β ₁₋₄₀ and widespread vascular amyloid pathology from 3 – 6 months of age.⁷⁴ They also develop some of the earliest cognitive impairment of any AD model, performing worse than their wild-type counterparts on cognitive tasks by 3 months of age.⁷⁶ Overall, these transgenic models of familial disease support increases in A β ₁₋₄₀ as a major driver of small vessel disease and cognitive decline in CAA.

In contrast with familial cases, the epidemiology of late-onset CAA points to disruption of A β ₁₋₄₀ clearance as a potential driver of so-called ‘sporadic’ disease. In contrast to genetic forms of CAA, the vast majority of CAA patients develop the sporadic form of the disease in old age, with mild CAA pathology present in approximately half of elderly brains,

and in 80 - 90% of Alzheimer's disease brains.^{77,78} While less common, even moderate to severe CAA is present in 8% of patients aged 75 to 84, and grows to 12.1% of patients over the age of 85 years.²⁰ This is likely to become even higher in the future as our population continues to age, as preclinical studies have shown that aging impairs the clearance of soluble $A\beta_{1-40}$ from the brain.⁷⁹⁻⁸² Further work in mouse models indicate that other CAA risk factors can further impair $A\beta_{1-40}$ clearance and accelerate amyloid deposition, including hypertension,⁸³ hyperlipidemia,⁸⁴ diabetes/obesity,⁸⁵ apolipoprotein E $\epsilon 4$ (APOE $\epsilon 4$) genotype^{78,86} and sedentary lifestyle.⁸⁷ Overall, impaired $A\beta_{1-40}$ clearance is a plausible mechanism of sporadic CAA, which could also occur after stroke.

Taken together, this review of the literature indicates that $A\beta_{1-40}$ directly contributes to cognitive decline in both familial and sporadic forms of CAA. While overproduction of $A\beta_{1-40}$ is the major cause of early-onset CAA, impaired clearance of $A\beta_{1-40}$ represents an alternative, additional driver of sporadic CAA, and is implicated in nearly all of the known risk factors that are common in elderly CAA patients. Therefore, stroke likely also disrupts the process of $A\beta_{1-40}$ transport and clearance from the vasculature. However, further work is needed to confirm that this occurs in animal models of stroke, which will aid in determining which specific $A\beta_{1-40}$ clearance mechanisms fail in stroke patients.

1.4: The basement membrane is the initial site of $A\beta_{1-40}$ deposition in CAA.

It is clear from the existing literature that increases in $A\beta_{1-40}$, whether from increased production or reduced clearance, lead to small vessel disease and cognitive decline in CAA. However, the impact of $A\beta_{1-40}$ on vessel function remains understudied. Cerebral arteries penetrate from the surface of the cortex and branch into descending arterioles, which further

split to form capillary beds, where nutrients and waste products are exchanged with the brain parenchyma.^{88,89} Cerebral capillaries are comprised of a monolayer of endothelial cells surrounded by a unique extracellular structure called the vascular basement membrane,⁹⁰ which also contains pericytes and astrocytic endfeet.⁹⁰ Together, these structures coordinate cerebral blood flow and neuronal activity to optimize cognitive function, in a synergy termed the ‘neurovascular unit’ (NVU), which becomes impaired in CAA.⁹¹ The current literature suggests that CAA begins within the basement membrane, and leads to cognitive decline due to repetitive brain injury as well as impaired NVU regulation.

In early CAA, A β ₁₋₄₀ preferentially deposits within distinct regions of the cerebrovascular tree.⁹² CAA is predominantly observed within the cerebral cortex and cerebellum, and generally spares the deeper nuclei of the cerebrum and brainstem, as well as the white matter.⁷⁷ Within these affected brain areas, CAA first spreads through the leptomeningeal and superficial cortical vessels, and later involves the majority of small arteries, arterioles and capillaries within the cortex.⁹³ The initial deposits associated with CAA form along the outer layer of basement membrane, providing a ‘seed’ for the eventual growth of CAA plaques.⁹⁴ However, it is not known why certain individuals develop these initial basement membrane deposits.

In advanced CAA, A β ₁₋₄₀ deposits invade the deeper layers of the vessel wall. In particular, the walls of small arteries, arterioles and capillaries are often replaced entirely by amyloid deposits, while sparing the inner endothelial lining.^{77,95} During this process, astrocytes aggregate and become dystrophic around large capillary plaques, indicating potential involvement of these perivascular glial cells in modulating CAA pathology.⁹⁴ Finally, advanced CAA induces several pathognomonic vasculopathies, including duplication

of the vessel lumen, destruction of the vessel wall, hyalinosis, formation of microaneurysms as well as fibrinoid necrosis.^{19,95,96} Taken together, these findings indicate that CAA begins within the basement membrane of cortical vessels, and involves perivascular astrocytes as well as invasion of deeper portions of the vessel wall, leading to severe and widespread vasculopathy throughout the affected brain structures.

CAA vasculopathies can be broadly separated into changes favoring both hemorrhagic and ischemic injury, which both contribute to impaired cognitive function via progressive loss of brain tissue. In hemorrhagic injury, CAA reduces vessel wall integrity and leads to the formation of microaneurysms, which can spontaneously rupture and lead to both microbleeds⁹⁵ and intracerebral hemorrhage (ICH).⁹⁷ Additionally, small ischemic injuries, termed ‘microinfarctions’ can also occur during CAA,^{98,99} and results from invasion of the small vessel lumen by vascular amyloid deposits, leading to occlusive disease and leukoairiosis on imaging.^{100,101} Together, both microbleeds and microinfarction contribute to loss of cognitive function via impairing white matter connectivity,^{102–104} inducing cortical atrophy,¹⁰⁵ as well as promoting local inflammatory responses.^{106,107} Overall, induction of ischemic and hemorrhagic brain injury occur via different mechanisms, but similarly contribute to cognitive decline in CAA patients.

In addition to focal brain injury, there is also significant evidence that CAA induces chronic disruption of the NVU. Preclinical studies have shown that $A\beta_{1-40}$ inhibits cerebral autoregulation, leading to vasoconstriction of cerebral arteries in isolated preparations and intact cortex.¹⁰⁸ In advanced CAA, vascular amyloid deposits impair vasomotor function in a dose-dependent manner.¹⁰⁹ In addition, $A\beta_{1-40}$ can also induce direct damage to the cells of the NVU due to increased free radical formation.¹¹⁰ Specifically, $A\beta_{1-40}$ damages

neurons,^{111,112} vascular smooth muscle cells,¹¹³ pericytes¹¹⁴ and endothelial cells.¹¹⁵ These changes impair NVU function which may disrupt neurotransmission along axons.¹¹⁶ The net results of NVU disruption in human CAA patients include impaired perfusion of small vessel beds,^{117,118} reduced vessel integrity^{119–121} as well as reduced neurovascular coupling^{122–124}. In conclusion, while CAA is a major cause of focal brain injury, A β_{1-40} also contributes to progressive cognitive decline via altered autoregulatory responses as well as direct cytotoxicity to cellular components of the NVU.

In summary, A β_{1-40} deposition is initiated at the cerebrovascular basement membrane and then spreads to invade the vessel wall. This deposition leads to microhemorrhages as well as microinfarction, which both contribute to stepwise cognitive decline in CAA patients. Additionally, A β_{1-40} impairs cerebrovascular reactivity and induces cytotoxicity, causing dysfunction of the NVU and contributing to progressive cognitive decline. Therefore, a better understanding of the molecular, cellular and physiological processes that contribute to the initial deposition of A β_{1-40} within the basement membrane is critical to formulating therapies to slow CAA progression. Furthermore, successful prevention of basement membrane A β_{1-40} deposition could prevent amyloid-induced vasculopathy and improve cognitive function in stroke survivors. In theory, this could be accomplished by targeting the various transport mechanisms that are involved in depositing and removing A β_{1-40} from the PVS.

1.5: Cerebrospinal fluid is a potential source of perivascular A β_{1-40} deposits in CAA.

Previous work has shown that the vascular basement membrane is the initial site of amyloid pathology in CAA. However, the physiological route of A β_{1-40} deposition is not

known. This deposition may occur due to alterations in the perivascular transport of cerebrospinal fluid (CSF), which acts as a 'lymphatic' fluid that is pumped through the cerebrovascular basement membrane. This process is key for removing waste products from the PVS in healthy individuals.¹²⁵ However, this function may become impaired, or even maladaptive, in aging and stroke, potentially favoring the deposition of CSF-derived A β within the basement membrane. Therefore, I hypothesize that the CSF is a major potential source of A β ₁₋₄₀ that becomes deposited within the basement membranes of CAA patients. I further hypothesize that aging and stroke reduce the flow rate of CSF, further contributing to impaired transport of A β ₁₋₄₀ through the basement membrane.

CSF is produced within the choroid plexus (CP), a cuboidal epithelial monolayer that lines the brain ventricles.¹²⁶ This unique epithelial layer displays a high degree of polarity, with a basement membrane on its basolateral surface, and apical microvilli with ciliary projections extending into the ventricle lumen.¹²⁷ The CP secretes approximately 600 mL of CSF per day in healthy individuals,^{128,129} which is supported by several factors including dense vascularization,¹²⁷ high rates of blood flow,¹³⁰ enriched mitochondrial content¹²⁷ and the presence of high surface area secretory microvilli.¹²⁷ In healthy individuals, the CP provides a barrier between the plasma and CSF.¹²⁶ Together, these qualities allow for rapid turnover of CSF, while still maintaining the blood-CSF barrier.

Importantly, the transport of water within the CP takes place by distinct transcellular and paracellular pathways. In both cases, these processes are driven by favorable ion gradients that are primarily driven by the continuous activity of Na-K-ATPase, which enable the osmotic transport of water.^{131,132} Transcellular diffusion occurs through the epithelial cells, and is enabled by the membrane expression of aquaporin-1 (AQP1).¹³³⁻¹³⁷ In contrast,

in paracellular transport, claudin-2 allows for the movement of water moves through selectively permeable extracellular pores.^{138,139} This continuous production of CSF provides a driving force for the bulk flow of CSF through the brain ventricular system, displacing the existing fluid from the ventricular system to the subarachnoid space surrounding the brain.¹⁴⁰

Upon exiting the ventricular system, CSF then flows along the surface of the brain through the cisterns, which are a series of hollow chambers that generally contain the major arteries within the subarachnoid space. The majority of the CSF drains into the bloodstream via the subarachnoid granulations,^{141,142} dural lymphatic vessels,^{143,144} the nasal cribriform plate¹⁴⁵ and along cranial/spinal nerve sheaths.¹⁴⁶ This process of CSF drainage allows for homeostatic waste clearance to occur.¹⁴⁷ The relative contribution of these various pathways, and how they may be modulated by aging, stroke and neurodegenerative disease remain an area of highly active investigation.¹⁴⁸ The CSF contains a variety of waste products, including $A\beta_{1-40}$, which are derived from its function in clearing waste products from the brain parenchyma. Previous work has shown that, in patients with AD and CAA, this homeostatic balance abnormally shifts over the course of disease, leading to predictable fluctuations in CSF $A\beta_{1-40}$ concentration.¹⁴⁹ Most importantly, increases in CSF $A\beta_{1-40}$ are a pathological hallmark of early CAA,¹⁵⁰ and may actively contribute to disease by crossing a critical threshold to favor the aggregation and deposition within the cerebrovascular basement membrane.

While it is clear that CSF $A\beta_{1-40}$ levels rise during the early stages of CAA, it is not clear whether this is simply a biomarker of disease, or if this increase contributes to the formation of the initial basement membrane amyloid deposits. The precise perivascular routes, and the potential regulators of this process are not known. In addition to changes in

the total amount of CSF A β ₁₋₄₀, increased affinity of the basement membrane for circulating CSF A β ₁₋₄₀ could further accelerate the formation of CAA plaques in aging and after stroke.

1.6: Basement membrane fibronectin may promote the formation of CAA pathology.

In healthy adults, the vascular basement membrane is predominantly comprised of heparan sulfate proteoglycans (HSPGs), collagen, laminin and integrins.¹⁵¹ Together, these proteins create a porous, flexible structure that permits the flow of CSF in the healthy brain. However, aging and stroke-induced basement membrane fibrosis could sequester A β ₁₋₄₀ and lead to CAA. Therefore, I hypothesize that stroke abnormally increases basement membrane fibronectin expression, which worsens with aging and contributes to the development of CAA pathology.

Fibronectin is a modular glycoprotein that is composed of two 230 kD – 270 kD subunits.¹⁵² It plays a central role in organizing the molecular structure of the basement membrane during development, anchoring cellular components to the HSPG matrix, and is also upregulated during the response to injury.^{90,153–155} Fibronectin is a highly modular protein that is predominantly composed of three different repeats, termed Type I – III.¹⁵⁶ The Type I region is involved in the polymerization of fibronectin into large insoluble aggregates, a process called fibrillogenesis, which occurs during wound repair.¹⁵⁶ The Type II region binds collagen, and the Type III region binds integrins and HSPGs.¹⁵⁶ Together, each of these domains plays an important role in linking the protein components of the basement membrane to each other, as well as anchoring the cellular components via integrin receptors.

Fibronectin plays an important role in organizing the HSPG matrix within the basement membrane. HSPGs are very large (> 1000 kD) proteoglycans that are formed by

numerous, negatively charged heparan-sulfated glycosaminoglycans (GAG) side-chains that surround a relatively small, positively charged protein core.¹⁵⁷ HSPGs are the major component of the cerebrovascular basement membrane, which expresses several subtypes, including perlecan,¹⁵⁸ agrin,^{159–161} collagen XVIII¹⁶² and syndecan-4.¹⁶³ In particular, syndecan-4 binds fibronectin with high affinity via the Type III domain.¹⁶⁴ In addition to providing structural integrity, HSPGs are involved in a number of processes, including support of vascular development, maintenance of blood-brain barrier (BBB) integrity, and angiogenic responses to focal injuries, such as stroke.^{157,165} They also may be important in maintaining CSF flow in the healthy brain.

Integrins are a family of cell membrane receptors which contain both α and β subunits, and play a major role in anchoring cells to the basement membrane and enabling cell motility. Different classes of $\beta 1$ integrin are expressed by endothelial cells ($\alpha 1\beta 1$, $\alpha 3\beta$, $\alpha 6\beta 1$, $\alpha v\beta 1$),^{166–169} pericytes ($\alpha 4\beta 1$)¹⁷⁰ and astrocytes ($\alpha 1\beta 1$, $\alpha 5\beta 1$, $\alpha 6\beta 1$).¹⁶⁹ Importantly, the major receptor for fibronectin in the brain is $\alpha 5\beta 1$ integrin, which is expressed on the outer surface of astrocytic endfeet.^{171–173} The $\beta 1$ subunit contains a binding site for fibronectin, while the $\alpha 5$ subunit plays a role in modulating the binding affinity.^{174–177} Integrins also provide the major anchor points for attaching the astrocytic endfeet to the endothelium via binding to β -dystroglycan, another protein expressed within the basement membrane.^{178,179} This anchoring to the basement membrane creates the ‘double-barreled’ structure of the PVS, which supports normal CSF transport.

CAA is associated with major changes in the basement membrane, including a ‘thickened’ morphology as well as well as altered protein composition. Studies of AD patients have found that the outer basement membrane layer, which is normally produced by

astrocytes, is selectively thickened.¹⁸⁰ Further studies found that these alterations occur in areas with increased amyloid pathology,^{181,182} and that these changes can occur prior to development of amyloid pathology.¹⁸³ Specific basement membrane proteins, including collagen IV, laminins and nidogen are *downregulated* in amyloid plaques and have been shown to prevent amyloid deposition in the healthy brain.^{184,185} However, both fibronectin and perlecan *increase* in mouse models of AD.^{181,182,186} While both perlecan and fibronectin have been shown to bind A β aggregates *in vitro*,¹⁸⁷ the physiological relevance of this phenomenon has never been examined *in vivo*. Overall, a better understanding of how alterations in basement membrane composition contribute to the development of CAA is needed, and may help to better understand how aging and stroke induce the formation of CAA plaque pathology.

There is limited data available on the impact of aging on basement membrane morphology and composition. Aging induces thinning of the basement membrane in the cortex, hippocampus and thalamus, but not the striatum.¹⁸¹ Additionally, aging reduces collagen IV, laminin and nidogen 2 expression, but upregulates fibronectin and perlecan expression in the cortex.¹⁸¹ While similar increases in total fibronectin expression is observed in other brain regions, this is not associated with reductions in other basement membrane proteins, suggesting that the relative amount of fibronectin may be most important in determining the cortical location of sporadic CAA pathology.¹⁸¹

In contrast with normal aging, stroke induces a ‘biphasic’ effect on basement membrane thickness and composition. During the acute phase of injury, stroke increases BBB permeability, allowing for the influx of serum and cellular factors into the brain parenchyma that degrade the basement membrane via increased exposure to proteases and

inflammatory cytokines.¹⁸⁸⁻¹⁹¹ In particular, upregulation of matrix metalloproteinases (MMP's) leads to a general loss of basement membrane proteins during the acute phases of ischemia, including reductions in collagen IV, laminin, agrin, perlecan and fibronectin.^{188,191-193} However, few studies have examined the chronic effects of stroke on the basement membrane. It is known that newly forming vessels upregulate both fibronectin and perlecan during the chronic angiogenic response after stroke.^{165,194} These changes are similar to what is seen in the aging brain at baseline, and may further exacerbate age-related changes in basement membrane proteins. However, it is not known whether these changes accelerate the formation of CAA pathology.

In conclusion, it is clear from the literature that CAA is associated with changes in basement membrane composition, which are similar to what has been observed in both normal aging and the chronic phase of stroke. Pathological upregulation of basement membrane proteins, including various integrin receptors or fibronectin could favor the development of CAA. This may occur by altering the transport of CSF-derived $A\beta_{1-40}$ through the basement membrane, which could favor the initial formation of CAA pathology in elderly stroke patients.

1.7: CSF bulk flow transports $A\beta_{1-40}$ through the vascular basement membrane.

The cortical distribution of CAA pathology gives clues to its pathophysiological mechanism. As described in earlier sections, CAA is initiated in the leptomeningeal arteries, and 'descends' along cerebral arteries, arterioles and eventually capillary beds, sparing the venous system almost entirely. Previous studies have shown that CSF $A\beta_{1-40}$ levels rise in the early stages of CAA,^{149,150} providing a potential source for the 'outside to inside'

distribution of CAA pathology within the surface cortex.¹⁹ Both classical studies of perivascular anatomy, and the physiology of perivascular flow of CSF explain how and why amyloid pathology spreads through the cortex in this distinctive pattern. Therefore, I hypothesize that the transport of CSF A β ₁₋₄₀ along perivascular routes is a major driver of CAA pathology in aging and after stroke.

Importantly, both the macroscopic and microscopic anatomy of the Virchow-Robin space allow for a route of CSF flow along perivascular routes.¹⁹⁵ A merging of the innermost meningeal membrane (pia mater) with the outermost layer of cortex (glia limitans) produces this small, but important anatomical space, allowing for the subarachnoid space to involute and extend into the brain alongside each individual penetrating artery.¹⁹⁶ Distal to this region of pial involution, the glia limitans then fully envelopes each penetrating artery in a monolayer of astrocytic endfeet.¹⁹⁷ Components of the vessel wall, primarily smooth muscle cells in the arteries, and eventually endothelial cells and pericytes in the capillary beds secrete a glycosylated matrix of proteins, termed the ‘inner’ basement membrane.^{81,151} Similarly, the astrocytic endfeet also secrete their own distinct ‘outer’ basement membrane along their edges.¹⁹⁶ Therefore, as the Virchow-Robin space narrows, the astrocytic endfeet and vessel wall are brought closer together, and eventually merge to form a single basement membrane with 2 - 4 layers.¹⁹⁶ This multilayered, largely acellular basement membrane structure provides a unique avenue for CSF, and the solutes contained therein, to flow into the brain with minimal resistance. This may allow for efficient CSF-ISF exchange.^{125,196}

In addition to this anatomical evidence, numerous studies of brain solute exchange, diffusion and bulk flow provide physiological evidence for the existence of a perivascular circulation of CSF. Beginning in the 1970s, pioneering work showed that when various sized

tracers, including polyethylene glycol and albumin, were infused into the brains of rats, they all cleared from the interstitial fluid (ISF) at the same rate, regardless of molecular weight.^{198–201} These findings suggest that solute movement within the PVS is primarily driven by convective bulk flow, rather than purely by osmotic diffusion, which would predict that solutes of different sizes would clear from the brain at different rates.²⁰² Additional work showed that the ISF moves at a rate of 10.5 $\mu\text{m}/\text{min}$, and that this ISF is a major source of ‘extra-choroidal’ CSF.²⁰³ Interestingly, Rennels *et al.* (1985) subsequently found that proteins infused into the cisterna magna, a major CSF compartment on the surface of the brain, rapidly penetrated into the brain within minutes.²⁰⁴ Taken together, these studies indicate that bulk flow is the major transport mechanism of CSF flow, completing the physiologic ‘circuit’ for perivascular solute transport.

Nearly 30 years later, this perivascular exchange was later ‘re-discovered’ using two-photon microscopy, and shown to be important for the clearance of $\text{A}\beta_{1-40}$ in a process termed glial-lymphatic (‘glymphatic’) flow. Since then, the importance of glymphatic flow has been further supported by a series of recent papers, confirming that CSF drives the bulk flow of ISF within the PVS.^{82,125,205–209} In this initial model, the arterial beds act as a positive ‘source’ of bulk influx of CSF, and the venous system acting as a negative ‘sink’ for the bulk clearance of ISF. Further work newly showed that aquaporin-4 (AQP4), expressed on astrocytic endfeet, provides a semipermeable barrier for the exchange of CSF and ISF, which is required for the clearance of intraparenchymally injected $\text{A}\beta_{1-40}$.¹²⁵ More recent studies have updated this model, and have subsequently found that the perivascular influx of CSF occurs within the outer basement membrane (associated with the glia limitans astrocytes), and that the clearance of ISF can simultaneously occur in the opposite direction along the inner

basement membrane of cerebral arteries.¹⁹⁶ However, more work is needed to clarify how CSF and ISF are exchanged within the perivascular microenvironment, and the role of the basement membrane in regulating this process in health and disease.

Overall, given that (1) high levels of CSF $A\beta_{1-40}$ predispose individuals to the development of CAA, (2) CSF is in continuous contact with the basement membrane, (3) that CSF drives the clearance of $A\beta_{1-40}$ from the brain, and (4) the basement membrane is the initial site of amyloid pathology in CAA, it is highly likely that this physiological route is involved in the early stages of CAA development. However, the specific molecular and cellular factors within the basement membrane that regulate CSF flow, and $A\beta_{1-40}$ deposition, have yet to be identified. A better understanding of how aging and stroke impact the molecular composition of the basement membrane could shed important light on the pathogenesis of CAA. Furthermore, this work could help to identify novel molecular targets that could help to shield the basement membrane from $A\beta_{1-40}$ deposition, allowing for new disease-modifying therapies to be developed.

1.8: Theoretical considerations for CSF $A\beta_{1-40}$ distribution in the basement membrane.

The vascular basement membrane is essential to maintaining the structural organization of the PVS. In addition to providing structural integrity, disease-associated basement membrane proteins, like fibronectin, may induce the deposition of CSF $A\beta_{1-40}$ by impairing the free diffusion of molecules. As CSF solutes are delivered to the PVS by bulk flow, solutes must diffuse through the basement membrane, which could modulate regional transport of solutes. Diffusion within the PVS is thermodynamically governed by Brownian movement, which is described by the Stokes-Einstein equation, given as:

$$D = \frac{k_B T}{3\pi\eta(d_H)} \times 10^{13}$$

Where D = free diffusion coefficient (cm^2/s), k_B = Boltzmann's constant (1.38065×10^{-23}), η = viscosity ($Pa \times S$) and d_H = hydrodynamic diameter of the molecule (nm).²⁰² This equation indicates that the rate that a molecule diffuses through the PVS is directly related to temperature, and inversely related to the diameter of the molecule and viscosity of the diffusing medium (in this case, CSF within the basement membrane). For a given molecule under physiological conditions ($37^\circ C$), this equation predicts that the major determinant of solute diffusion will be the viscosity (or "stickiness") of the basement membrane, as well as the hydrodynamic radius of the diffusing molecule.

Several basement membrane properties may impair the diffusion of CSF solutes following injury. These include increased geometric path length around cells, increased dead spaces between cells, alterations in the electrical charge of the basement membrane, general increases in viscosity due to weak interactions, as well as upregulation of specific receptors for the diffusing molecule of interest.²⁰² The simplest way to describe impairment of diffusion in biological systems, such as the basement membrane, is an experimentally defined measurement called tortuosity (λ). Using tortuosity, it is possible to describe the *relative* diffusion rate of molecules between two different experimental conditions (such as aging or ischemia), making it a simple, yet powerful tool to get an overall picture of diffusion rates within living brain tissue. Tortuosity is given by the following equation:

$$\lambda = \lambda_g \times \frac{\lambda_1}{\lambda_g} \times \frac{\lambda_2}{\lambda_1} \dots \frac{\lambda}{\lambda_n} = \sqrt{\frac{D}{D_g} \times \frac{D_g}{D_1} \times \frac{D_1}{D_2} \dots \frac{D_n}{D^*}} = \sqrt{\frac{D}{D^*}}$$

Where λ = tortuosity, D = diffusion in the control condition, and D^* = diffusion in the experimental condition.²⁰² In this equation, the subscripts denote the contribution of

individual factors. For example, λ_g and \mathbf{D}_g would correspond to the tortuosity and rate of diffusion attributable to geometric path length, respectively, with other numbers representing the contribution of other hypothetical factors. However, the individual factors can be “cancelled out” by measuring the diffusion rate as a whole, dramatically simplifying quantification under experimental settings. Diffusion can be experimentally measured in several ways, including tetramethylammonium (TMA) iontophoresis, radioligand injection as well as the tracking of fluorophores.²⁰² Regardless of the technique that is used, tortuosity can be determined simply by comparing the rate of diffusion between two states.

As a final point, tortuosity is also related to the volume fraction (α) of the extracellular space (ECS), given by the following equation:

$$\alpha = \frac{V_{ECS}}{V_{tissue}}$$

Where α = volume fraction, V_{ECS} = volume of the ECS, and V_{tissue} = total volume of tissue.²⁰²

While tortuosity and volume fraction intuitively should co-vary (all things being equal, increased free space for diffusion *should* result in faster diffusion, measured as reduced tortuosity), they do not always correlate well under biological conditions. This is most likely due to the contribution of some of the other factors outlined in the preceding paragraphs, which are all taken into account by the tortuosity equation.

Both human and murine cortex exhibit relatively high tortuosity, with diffusion occurring approximately ~2.5 times more slowly than what is observed in a free medium.^{210–212} In pathological states, changes in basement membrane composition may further increase tortuosity, restricting diffusion and favoring the deposition of CSF A β_{1-40} . There is limited data available that suggests both aging and ischemia further increase the tortuosity of whole

brain tissue,^{213,214} however, more specific studies are needed to determine the impact of aging on tortuosity of the vascular basement membrane, specifically.

While the *in vivo* impact of focal stroke on brain parenchymal tortuosity and volume fraction is not known, the acute impacts of global hypoxia or ischemia on these parameters of brain diffusion are well described, largely using *in vitro* slice physiology. One study found that hypoxia dramatically reduced volume fraction and increased tortuosity in adult rat cortex,²¹⁵ with an additional study finding that hypoxia alone induced more modest increases in tortuosity in adult rat cortex.²¹⁶ While this work supports the notion that aging and hypoxia may broadly reduce the diffusion of solutes through the extracellular space, one major caveat is that these techniques do not specifically assess basement membrane tortuosity, rather, they rely on measurements of whole brain slices in an *ex vivo* setting.

In my experimental setting, increased fibronectin expression may be a major driver of increased tortuosity of the basement membrane after stroke, which could have major consequences *in vivo*. This could occur due to its activity as a nonspecific ‘obstacle’ to diffusion, as it may increase the viscosity and complexity of the structure for molecules to diffuse through. Additionally, fibronectin may have selective effects on the diffusion of A β ₁₋₄₀, as one study found that fibronectin binds amyloid aggregates via the type I domain.²¹⁷ However, it is not known if fibronectin can bind soluble A β ₁₋₄₀ within the perivascular microenvironment. Increased expression of basement membrane fibronectin could lead to the specific trapping of CSF A β ₁₋₄₀ within the PVS, in addition to the nonspecific reductions in diffusibility due to changes in basement membrane composition or structure.

1.9: Astrocytic TGF- β signaling may mediate basement membrane fibrosis and CAA.

Previous work indicates that transforming growth factor- β (TGF- β) levels are elevated in mouse models of CAA,²¹⁸ and that overexpression of TGF- β in wild-type mice leads to astrogliosis, fibronectin expression and microvascular damage.^{219,220} However, it is not known whether TGF- β mediates post-stroke basement membrane fibrosis. This section will first review the potential TGF- β signaling mechanisms involved in post-stroke fibronectin expression. Then, the impact of aging and stroke on TGF- β expression and astrocyte phenotypes will be examined.

TGF- β is a member of the TGF- β cytokine superfamily, which also contains glial derived neurotrophic factor, activin, 8-vinyl reductase (DVR), and growth differentiation factor subfamilies.²²¹ The TGF- β subfamily contains 3 different isoforms: TGF- β 1, TGF- β 2 and TGF- β 3, which are differentially expressed during development of the central nervous system (CNS), and nearly absent from the adult brain under homeostatic conditions.²²² However, following stroke, activated microglia secrete high levels of TGF- β 1 during the acute phase of injury.²²³ Previous work has shown that TGF- β activates TGF- β receptor-1 and receptor-2 (TGF- β R1/R2), which dimerize upon TGF- β binding within the cell membrane.²²⁴ Following dimerization, TGF- β R1 phosphorylates Smad proteins, including Smad2 and Smad3, which then complex with other Smad proteins and translocate to the nucleus.²²⁵ These complexes subsequently influence gene expression by binding to enhancer/repressor sites within the genome, influencing cell differentiation and the expression of ECM proteins in astrocytes during development and after brain injury.²²⁶

TGF- β signaling after stroke has several beneficial pro-survival effects, including expression of anti-apoptotic proteins Bcl-2 and Bcl-x1, leading to reduced neuronal death

during the acute phase of injury.²²⁷ These early beneficial effects, which have only been studied in young animals, have led to TGF- β being labeled as an anti-inflammatory molecule in the context of acute brain injury.^{228,229} However, TGF- β is a highly pleiotropic cytokine, and also induces astrogliosis and ECM deposition, which have well-documented detrimental impacts, including inhibition of axonal regrowth^{230,231} and angiogenesis²³² due to the abnormal production of ECM proteins. Furthermore, other work has shown that TGF- β expression is disproportionately increased in aged animals after stroke, which may increase the likelihood of detrimental affects in the chronic phase of injury.²²³ Along these lines, previous studies by our laboratory have shown that aged animals exhibit increased glial scarring in the ischemic penumbra after MCAO, which is associated with delayed behavioral recovery.²³³ Even in young animals, inhibition of TGF- β signaling may reduce astrogliosis within the glial scar, however, the impact of this treatment on long-term cognitive function is not known.²²⁹ Overall, the role of TGF- β during brain injury remains controversial, and the few studies performed in aged animals suggest a detrimental effect of TGF- β signaling on functional recovery, which could be due to abnormally high levels of astrogliosis.

Astrocytes are a major type of glial cell in the brain that, under normal conditions, perform numerous homeostatic functions including support of BBB integrity,²³⁴ metabolism²³⁴ and waste clearance.¹²⁵ Astrocytes interface with the perivascular niche via numerous small endfeet, and regulate the composition of the outermost basement membrane layer, which is involved early in the pathogenesis of CAA.^{181,196} Furthermore, reactive astrocytes are associated with impaired CSF flow during normal aging,²³⁵ multiple microinfarction,^{236,237} traumatic brain injury²³⁵ and Alzheimer's disease.^{209,238} However, the role of reactive astrocytes in basement membrane remodeling is understudied, and it is not

known whether inhibiting TGF- β signaling in astrocytes can restore CSF flow under pathological conditions.

Recent work has shown that reactive astrocytes generally exhibit two major phenotypes, defined by their gene expression pattern – A1 (modeled by peripheral stimulation with LPS) and A2 (modeled by MCAO).²³⁹ While A1 astrocytes have been recently shown to induce inflammation, downregulate AQP4 and secrete toxic products that are detrimental to neuronal survival,²⁴⁰ the functions and phenotypes of A2 astrocytes are not known. Furthermore, excess TGF- β signaling, as occurs after stroke in the aged brain,²²³ could further impact A2 astrocyte responses to ischemic injury and induce the abnormal production of ECM proteins. If true, astrocytes may hold the key to preventing CAA after stroke.

Overall, previous work has shown that TGF- β increases in aging and stroke, and may also contribute to the formation of CAA pathology. However, it is not known whether TGF- β mediates basement membrane fibrosis after stroke, or if inhibiting astrocytic TGF- β signaling is sufficient to improve CSF flow and prevent the perivascular deposition of CSF A β ₁₋₄₀ within the basement membrane. Elucidating the role of TGF- β would significantly improve our understanding of the molecular and cellular regulation of basement membrane composition in pathological states. Furthermore, modulating the function of A2 astrocytes with TGF- β inhibitors could also lead to new therapeutic targets for post-stroke CAA in aged populations.

CHAPTER 2

Specific Aims of Dissertation Research

2.1: Overview.

CAA may be caused, in part, by a failure of $A\beta_{1-40}$ transport through the vascular basement membrane of cerebral blood vessels after stroke. The basement membrane transports $A\beta_{1-40}$ via facilitating CSF flow within the PVS. Therefore, impairment of CSF flow may contribute to CAA after stroke. I propose that TGF- β signaling pathologically increases the expression of fibronectin within the basement membrane, reducing CSF flow through the cortex. I further propose that increases in fibronectin selectively favors the binding of CSF $A\beta_{1-40}$ to the basement membrane, accelerating the formation of amyloid pathology in the proximal regions of cortical vessels after stroke (Fig. 2-1). Therefore, my overall hypothesis is that TGF- β -driven increases in basement membrane fibronectin leads to increased perivascular deposition of $A\beta_{1-40}$ after stroke, contributing to increased CAA burden and accelerated cognitive decline. To test this hypothesis, I propose the following specific aims:

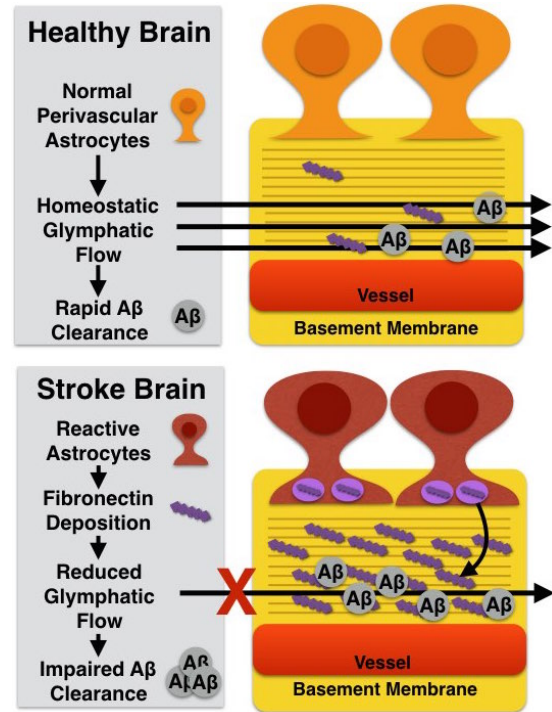


Figure 2-1: Reactive astrocytes may secrete fibronectin and impair the perivascular transport of CSF-derived $A\beta_{1-40}$ after stroke.

2.2: Specific Aims.

Aim 1. To determine whether aging and stroke induce the deposition of CSF A β ₁₋₄₀ within the vascular basement membrane. While the clinical literature suggests that focal stroke may be a risk factor for CAA, there is a lack of studies examining whether stroke induces CAA in mouse models of focal stroke. Additionally, the potential pathophysiological sources of basement membrane A β ₁₋₄₀ deposits are not known. I hypothesize that aging and stroke impair perivascular CSF flow and induce the trapping of CSF A β ₁₋₄₀, which contributes to increased CAA pathology and cognitive decline. To test this hypothesis, I propose the following sub-aims:

- Sub-Aim 1A: To assess how aging and stroke impact perivascular CSF flow.
- Sub-Aim 1B: To characterize how aging and stroke modulate the perivascular transport of CSF A β ₁₋₄₀ through the basement membrane.

Aim 2. To determine if astrocytic TGF- β signaling mediates basement membrane fibrosis and A β ₁₋₄₀ deposition in aging and after stroke. While previous work has shown that stroke induces basement membrane fibrosis in young animals, characterized by increased expression of fibronectin, it is not known whether aging worsens post-stroke basement membrane fibrosis. Furthermore, it is not known whether these changes in protein composition mediate the initial trapping of CSF A β ₁₋₄₀ or the eventual formation of CAA plaques. Finally, the impact of aging and TGF- β on perivascular astrocyte phenotype and function are understudied, or if blocking TGF- β can reduce basement membrane fibrosis after stroke. Therefore, I hypothesize that stroke induces basement membrane fibrosis in a

TGF- β -dependent manner, which worsens with aging. To test this hypothesis, I propose the following sub-aims:

- Sub-Aim 2A: To characterize how aging and stroke impact the structure and composition of the cerebrovascular basement membrane.
- Sub-Aim 2B: To examine whether fibronectin mediates post-stroke A β ₁₋₄₀ deposition, and if this worsens with aging in mice.
- Sub-Aim 2C: To evaluate whether TGF- β activates A2 astrocytes to produce fibronectin using both *in vitro* and *in vivo* systems.
- Sub-Aim 2D: To explore whether blocking TGF- β signaling reduces perivascular gliosis and basement membrane fibrosis in young and aged mice with stroke.

Aim 3. To explore whether peripheral markers of small vessel fibrosis predict CAA diagnosis and disease progression. Previous work has shown that CAA can be diagnosed using cortical biopsy or a set of imaging guidelines, termed the “Boston criteria.” However, CAA diagnosis and management has been hampered by a lack of blood biomarkers that can easily and reliably predict the presence of pathology or correlate with long-term functional outcomes. Therefore, I hypothesize that serum markers of basement membrane fibrosis (soluble fibronectin, TGF- β and MMPs) may predict CAA diagnosis and functional recovery in human ICH patients. To test this hypothesis, I propose the following sub-aims:

- Sub-Aim 3A: To test the clinical utility of biomarkers of fibrosis in diagnosing CAA pathology after ICH.
- Sub-Aim 3B: To evaluate whether biomarkers of fibrosis are predictive of long-term functional outcomes after ICH.

2.3: Translational statement.

This research is significant because it impacts our understanding of a new potential mechanism by which stroke induces cognitive decline. Additionally, these findings shed light on a new physiological route by which $A\beta_{1-40}$ becomes deposited in the basement membrane of aged mice with stroke, which may have relevance for human stroke patients, as well as elderly patients with sporadic CAA. Fibronectin may be a major mediator of perivascular CSF $A\beta_{1-40}$ deposition in aging and after stroke, which could be secreted by astrocytes in response to TGF- β signaling. Furthermore, blocking TGF- β signaling to astrocytes by peripheral pharmacological treatment may reverse basement membrane fibrosis, which could lead to new therapies for CAA in stroke survivors. Finally, this preclinical research could be used to develop new biomarkers for CAA in human ICH patients, which could be translated to the clinic as a diagnostic panel, potentially improving CAA diagnosis and management.

CHAPTER 3

Early Validation of Perivascular CSF Flow in the Murine Brain

3.1: Introduction

3.1.1: Overview.

Previous studies showed that brain ISF solutes are cleared by bulk flow,²⁰⁰ despite the fact that the BBB tight junction proteins preclude significant bulk influx of plasma.²⁴¹ One potential explanation for these disparate findings is that CSF, contained within the cisterns, exchanges with brain ISF via the PVS.²⁰⁴ More recent work has shown that this process of perivascular CSF flow drives the bulk flow of ISF,¹²⁵ and is required for the clearance of A β ₁₋₄₀ via the meningeal lymphatic system.¹⁴³ This process is thought to be critical to maintaining brain homeostasis, and may help to prevent CAA in healthy individuals.

3.1.2: Significance.

We hypothesized that CSF flow occurs along perivascular routes, and that diffusion through the basement membrane is dependent on the size of the injected tracer. While these findings have been previously shown in the literature, given that these techniques are largely new to our laboratory, it was important for us to internally validate our techniques. Therefore, prior to undertaking our studies in mouse models of stroke, we wished to replicate previous physiological studies in our own laboratory using naive young animals. This also afforded us a chance to develop and troubleshoot our own techniques to study CSF flow, helping to ensure the success of our future experiments. While many of our findings were in

agreement with the existing literature, we found an interesting phenomenon of size exclusion within basement membrane sublayers that deserves further study.

3.1.3: *Experimental design.*

We sought to replicate previous work using intracisternal injection of tracers in anesthetized mice, which have been used previously as an experimental model of perivascular CSF flow. To accomplish this, we developed a custom injection apparatus and used it to infuse a variety of tracers, starting with Evans blue dye, which is visible to the naked eye and allows for quick confirmation of successful injection. We then progressed to using simultaneous injection of dyes into the vasculature and cisterna magna, which allowed us to assess the perivascular localization of CSF dye by conventional fluorescence microscopy in fixed brain tissue. Next, we tested multiple dextran particles of different molecular weights, and assessed their transport through the basement membrane by *in vivo* two-photon microscopy. We also confirmed our findings by intracisternal injection of radiolabeled ^{14}C -Inulin and $^3\text{H}_2\text{O}$, which allowed us to easily quantify the amount of tracer taken up into the brain ISF and facilitated the creation of optimal time-courses for our later experiments. Finally, we also compared the clearance rate of ^{125}I -A β_{1-40} to ^{125}I -Albumin to evaluate whether it is removed solely via bulk flow, or if other clearance mechanisms are involved.

3.2: Methods

3.2.1: Animals.

Wild-type young (2 – 3 month-old) male C57BL/6 mice were obtained from Charles River. Mice were kept on a 12-hour light-dark cycle, and fed standard dry chow with *ad libitum* access to food and water. Mice were examined regularly by trained members of the lab and the veterinary staff for any signs of illness, as well as gross pathology at the time of sacrifice. Importantly, all studies were carried out in accordance with the recommendations in the guide for the Care and Use of Laboratory Animals of the National Institutes of Health. The protocols were approved by the UTHealth Institutional Animal Care and Use Committee (IACUC) and carried out in a facility approved by the Association for Assessment and Accreditation of Laboratory Animal Care (AAALAC). Animals were randomized to experimental conditions, and investigators were blinded to treatment.

3.2.2: Preparation of fluorescent tracers.

Artificial CSF (aCSF) containing Na⁺ (150 mM), K⁺ (3 mM), Ca²⁺ (1.4 mM), Mg (0.8 mM), P (1.0 mM) and HCO₃ (24.1 mM) was freshly prepared in sterile distilled water prior to the experiment. First, on the day of the experiment, a 2% solution of Evans blue dye (*Sigma*) was created in aCSF and mixed 1:1 with aCSF alone or aCSF containing 10% bovine serum albumin (BSA, *Sigma*) in aCSF, then filtered using a molecular-weight cutoff filter (MW cutoff = 50 kD) to create 1% working stocks of Evans blue dye (EBD) or Evans blue albumin (EBA) conjugate. Additionally, for subsequent multi-color experiments, various lyophilized dextran conjugates were first obtained from Thermo Fisher and then reconstituted separately in aCSF. Then, 4% stock solutions of 2000 kD fluorescein

isothiocyanate dextran (FITC-d2000), lysine-fixable 70 kD FITC dextran (FITC-d70) and lysine-fixable 3 kD tetramethylrhodamine dextran (TR-d3) were prepared and stored at -20°C prior to the experiments. Then, on the day of the experiment, fluorescent tracers were then further diluted/combined in aCSF to a working concentration of 1%. To measure fluorescent background signal, aCSF with no tracers was also retained for injection into control animals. Tracer mixtures were kept on ice for up to 4 hours prior to use, and vortexed for 5 seconds immediately before infusion.

3.2.3: Preparation of ¹²⁵I-radiolabeled tracers.

Recombinant human A β ₁₋₄₀ (Anaspec, Fremont, CA) or BSA (Sigma) was first dissolved to a concentration of 1 μ g/ μ L in sterile, chloride-free 250 mM sodium phosphate buffer (pH = 7.4). Then, peptides were conjugated to Iodine-125 (¹²⁵I) with chloramine T as previously described.²⁴² ¹²⁵I-peptide was separated from free ¹²⁵I by washing the mixture through a Sephadex G-10 column. Successful conjugation was measured by TCA precipitation, and fractions retaining > 95% counts per minute (CPM) values in the solid phase were then combined and lyophilized overnight for later use.

3.2.4: Preparation of ¹⁴C-Inulin/³H₂O tracer cocktails.

¹⁴C-Inulin and ³H₂O were purchased directly from Perkin-Elmer, and stock solutions of ¹⁴C-Inulin (Perkin-Elmer, $\sim 2 \times 10^5$ disintegrations/minute/microliter [DPM/ μ L]) and ³H₂O (Perkin-Elmer, $\sim 2 \times 10^6$ DPM/ μ L) were dissolved in aCSF and radioactivity normalized via liquid scintillation counting. Then, stock solutions were combined to a final concentration of 1×10^5 DPM/ μ L ¹⁴C-Inulin and 1×10^6 DPM/ μ L ³H₂O in aCSF.

3.2.5: Intracisternal injection.

Mice were deeply anesthetized with an intraperitoneal injection of Ketamine-Xylazine dissolved in 0.9% saline (120 mg/kg Ketamine, 10 mg/kg Xylazine), then placed in a stereotaxic frame. The hair over the cervical spine was then shaved, and then the skin was aseptically prepared and incised. Following this, a 30 gauge needle attached to catheter tubing was inserted through the superficial neck musculature and into the cisterna magna as previously described.¹²⁵ Tracer was slowly infused into the cisterna magna (1 μ L/min) over 10 minutes, after which mice were transferred to a warmed cage. Then, 15, 30 or 60 minutes after the initiation of the injection, mice were sacrificed by Avertin overdose (250 mg/kg), followed by transcardial perfusion with phosphate buffered saline (PBS) supplemented with 0.2% heparin, then 4% paraformaldehyde (PFA) in PBS for histological experiments. Tissues (brain and skull) were dissected and stored at 4% PFA for histology, or snap frozen and stored at -80°C for radiouptake measurements.

3.2.6: Intravenous injection.

Mice were deeply anesthetized with an intraperitoneal injection of Ketamine-Xylazine dissolved in 0.9% saline (120 mg/kg Ketamine, 10 mg/kg Xylazine). Two minutes prior to sacrifice, a 2 cm midline incision was made on the skin covering the ventral neck musculature, and the jugular vein visualized. Then, a 100 μ L bolus of 5% EBA was injected into the jugular vein, and allowed to circulate for 30 seconds. Successful injection was confirmed via inspection of the mucous membranes for gross darkening. Mice were sacrificed by Avertin overdose (250 mg/kg), followed by cervical dislocation. Then, tissues were dissected and post-fixed in 4% PFA until later use.

3.2.7: Intraparenchymal injection.

Mice were deeply anesthetized with an intraperitoneal injection of Ketamine-Xylazine dissolved in 0.9% saline (120 mg/kg Ketamine, 10 mg/kg Xylazine), then placed in a stereotaxic frame. A craniotomy was performed and a Hamilton syringe was then advanced into the striatum (0.4 mm anterior to Bregma, lateral 2.2 mm, ventral 3.5 mm). Then, 2 μ L dH₂O containing 1×10^6 CPM of reconstituted tracer solution was then infused at a rate of 1 μ L/min. To reduce inflammation, the needle was left in place for the duration of the experiment. Mice were sacrificed by Avertin overdose (250 mg/kg) after 60 minutes, and successful injections confirmed by inspection of the needle tract. Finally, brains were snap frozen and stored at -80°C prior to gamma counting.

3.2.8: Brain sectioning.

Following perfusion, brains were extracted and post-fixed for 24 hours in 4% PFA. Then, brains were dehydrated in 30% sucrose, frozen to -20°C and sectioned to 24 μ m (immunohistochemistry [IHC]/cresyl violet staining) or 100 μ m (tracer quantification) sections. Sections were then mounted onto slides and coverslipped with Fluoromount G or Vectashield + DAPI (4',6-diamidino-2-phenylindole, Vector Laboratories).

3.2.9: Fluorescence microscopy.

Sections were imaged under fluorescence with a Leica DMI8 microscope at 10X magnification. A blinded investigator imaged the lateral cortex (0.38 mm anterior to Bregma, 2.5 mm lateral, 1.5 mm deep). Then, 100 μ m Z stack images were obtained, and

maximum intensity projections performed with LAS X software. Single-plane mosaic images were also obtained at 10X magnification with autofocus.

3.2.10: Two-photon microscopy.

Mice were deeply anesthetized with an intraperitoneal injection of Ketamine-Xylazine dissolved in 0.9% saline (120 mg/kg Ketamine, 10 mg/kg Xylazine), then placed in a stereotaxic frame. Immediately following acute installation of a glass coverslipped cranial window over the right dorsal forebrain, tracer was infused into the cisterna magna, and cortex was imaged through the window. Briefly, animals were imaged using a custom-built two-photon microscope (Bruker Nano, WI) with femto-second pulse lasers (Spectra physics). Fluorophore was excited at 810 nm and emission of photon was collected by two-channel top-mount GaAsp detectors equipped with dual emission filters (525/70m-2P and 595/50m-2P). Two-photon image acquisition was performed with a imaging software Prairie View. A water immersion objective lens (Nikon CFI 16x/0.80) was used throughout the imaging session. Upon completion of imaging experiments, mice were sacrificed by Avertin overdose (250 mg/kg) and then cervically dislocated.

3.2.11: Gamma counting.

Frozen brain samples were thawed on ice, then manually homogenized in 30% TCA in glass test tubes. Then, whole homogenates were centrifuged at 5000 x g for 15 minutes, and the supernatant removed to a separate tube. Then, the amount of peptide-bound (pellet) and free iodine (supernatant) were quantified using a gamma counter (Packard Cobra II), courtesy of Dr. Claudio Soto.

3.2.12: Liquid scintillation counting.

Samples were thawed on ice, then placed in 5 mL glass vials and dissolved in 1 mL Solvable (Perkin Elmer) overnight at 37°C. Then, homogenates were vortexed and mixed with 4 mL Hionic-Fluor scintillation cocktail (Perkin Elmer). Following this, β -emissions were measured using a Tri-Carb T2900 Liquid Scintillation Counter (LSC) (Perkin Elmer), with $^3\text{H}_2\text{O}$ emissions counted at less than 20 keV, and ^{14}C -Inulin measured counted between 20 and 150 KeV. Control vials containing aCSF alone, aCSF + ^{14}C -Inulin and aCSF + $^3\text{H}_2\text{O}$ were used to account for background radiation, as well as to normalize emission signals from samples for subsequent analyses.

3.2.13: Statistics. All data are presented as mean (+/-) SEM, with the number of animals per experimental group (n). Statistically significant changes over time were determined by one-way analysis of variance (ANOVA). Statistical significance in total clearance was calculated by Student's t-test. Significance is denoted as * $p < 0.05$, ** $p < 0.01$, *** $p < 0.001$.

3.3: Results

3.3.1: CSF traveled through the brain along perivascular routes.

First, to test the hypothesis that CSF solute exchange occurs within the PVS in a size-dependent manner, I compared the distribution of intracisternally injected Evans blue (EBD, ~500 Da) to Evans blue albumin (EBA, 70 kD) at 60 minutes post-injection. Upon gross examination, I found that EBD spread from the circle of Willis and diffused bilaterally across the dorsal surface of the brain along vascular tracts, including the MCA, as well as the posterior cerebral artery (PCA) and the anterior cerebral artery (ACA) (**Fig. 3-1A**). The dye formed a visible diffusion gradient, appearing to spread from the arterial structure to the surrounding parenchymal tissue (**Fig. 3-1A**). Unexpectedly, EBA, the larger molecule, was more tightly associated with surface vessels than EBD (**Fig. 3-1B**). Examination under fluorescence revealed that this vascular association continued within the PVS of deep brain vessels, and appeared more strongly with EBA injection (**Fig. 3-1C**). These studies confirm that CSF flow occurs along the surface of the brain, and follows perivascular routes, rather than simply diffusing randomly throughout the brain. They also suggest a size-exclusion property of the pial membrane, which allows for the rapid diffusion of EBD, but not EBA, away from the major vessels and into surface capillaries and interstitial spaces.

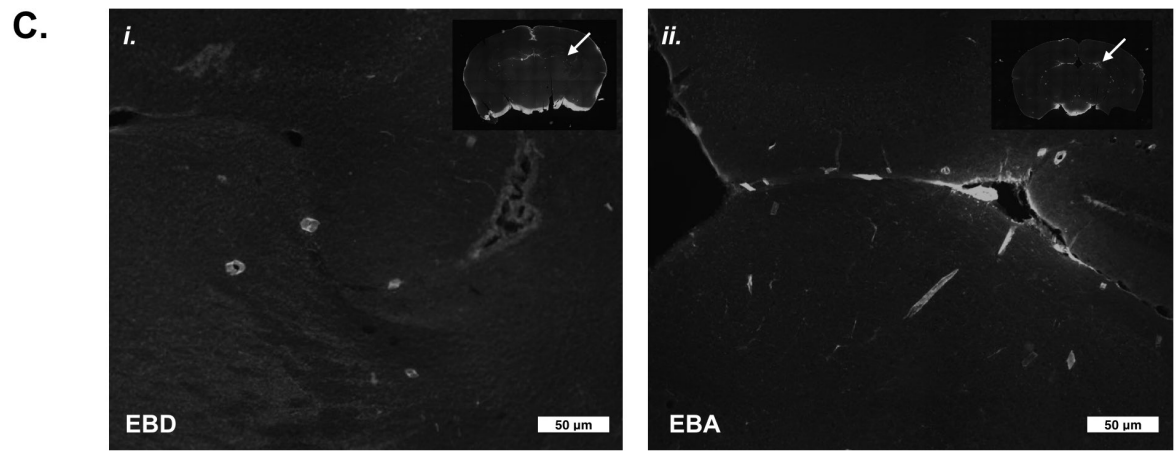
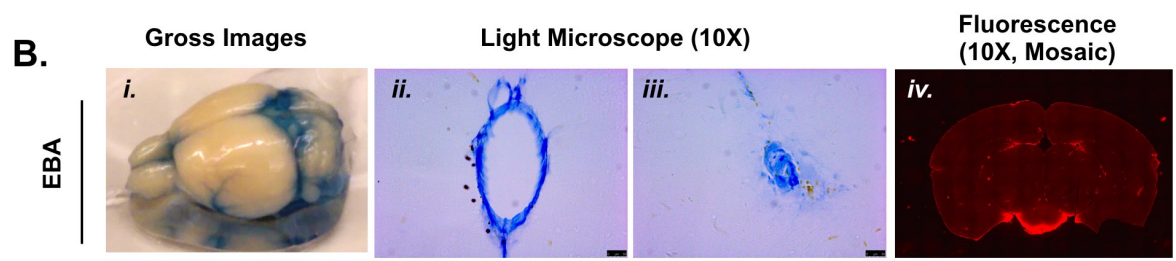
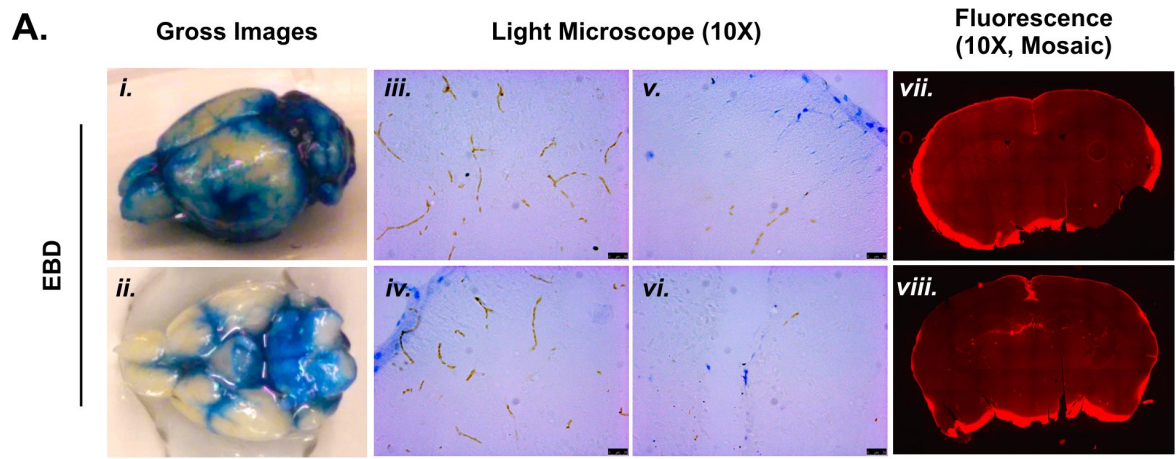
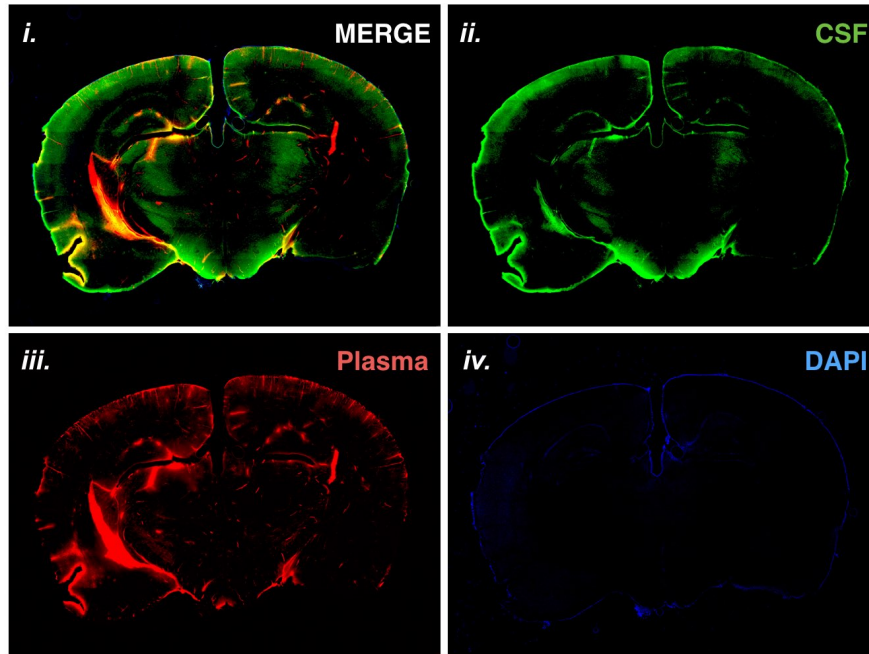


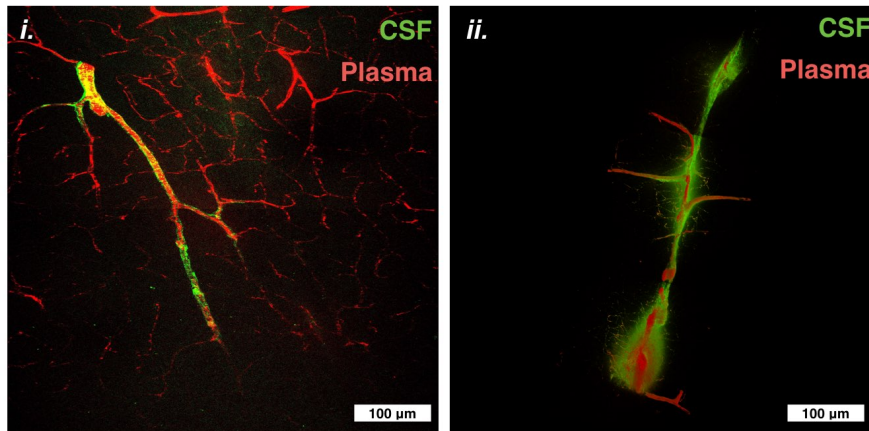
Figure 3-1: Visualization of CSF influx by intracisternal dye injection. (A.) Photograph of (i.) dorsolateral and (ii.) ventral mouse brain 30 minutes after intracisternal injection with Evans blue dye (EBD, 500 Da). (iii. – vi.) Light micrograph showing intraparenchymal EBD distribution within coronal sections. (vii. – viii.) Fluorescent mosaic micrographs from two mice showing EBD influx along the superficial surfaces of the brain. **(B.)** Photograph of (i.) dorsolateral mouse brain 30 minutes after intracisternal injection with Evans blue albumin (EBA, 70 kD). (ii. – iii.) Light micrograph showing perivascular EBA distribution within coronal sections. (iv.) Representative fluorescent mosaic image showing EBA influx along the superficial surfaces of the brain. **(C.)** Fluorescent micrographs showing how (ii.) EBA exhibits stronger perivascular localization than (i.) EBD. Scale bar (black, white) = 50 μm .

Then, to confirm that CSF influxes into the deeper structures of the brain along penetrating arterial beds, I double-labeled CSF and plasma by injecting FITC-dextran (70 kD, FITC-d70) into the cisterna magna, and then injecting EBD into the jugular vein immediately prior to sacrifice (**Fig. 3-2A**). I found that the injected CSF FITC-d70 tracer strongly localized to the injected plasma EBD tracer, and distributed along arteries, arterioles and capillary beds, extending into the deepest structures of the brain (**Fig. 3-2B**). These findings were later confirmed with two-photon microscopy, where CSF flow was observed to occur within the PVS of young mice in real-time. When different size tracers were simultaneously injected (2000 kD, FITC-d2000; 4 kD, 594-d3), we found that the smaller tracer traveled more closely to the vessel wall, while the larger tracer was excluded from this region and diffused along the outer surface (**Fig. 3-2C**). This intriguing finding suggests that the basement membrane layers exhibit size-exclusion properties, potentially filtering larger particles out of the inner basement membrane layers. In addition to being interesting from a biophysical perspective, this could have significance for the ability of to efficiently transport smaller monomeric vs larger oligomeric amyloid species.

A.



B.



C.

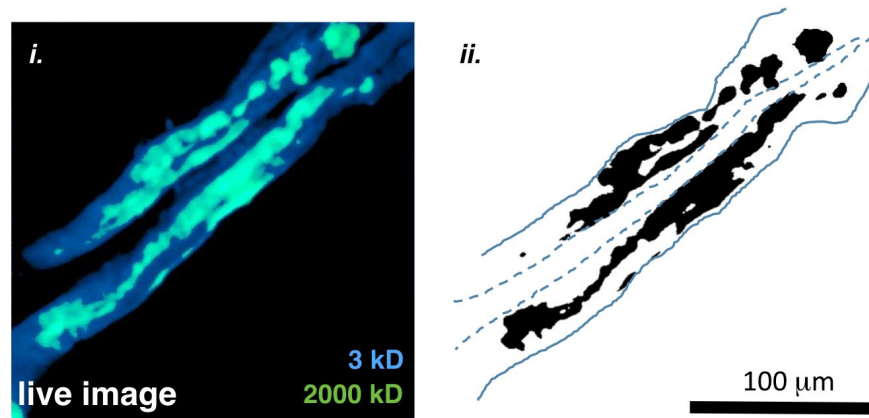


Figure 3-2. CSF influx occurs along perivascular routes. (A.) (i.) Representative fluorescent mosaic micrograph showing (ii.) plasma (red) colocalizing with (iii.) CSF. (iv.) Nuclei were counterstained with DAPI. (B.) (i.) High-resolution confocal micrograph showing CSF influx along perivascular routes. (ii.) 3-dimensional reconstruction of CSF influx showing diffusion away from the perivascular regions. (C.) Representative *in vivo* two-photon image showing differential distribution of FITC-d2000 and TR-d3. Scale bar (black, white) = 100 μm . *Note: Panel C was used with permission from Dr. Akihiko Urayama (unpublished data).*

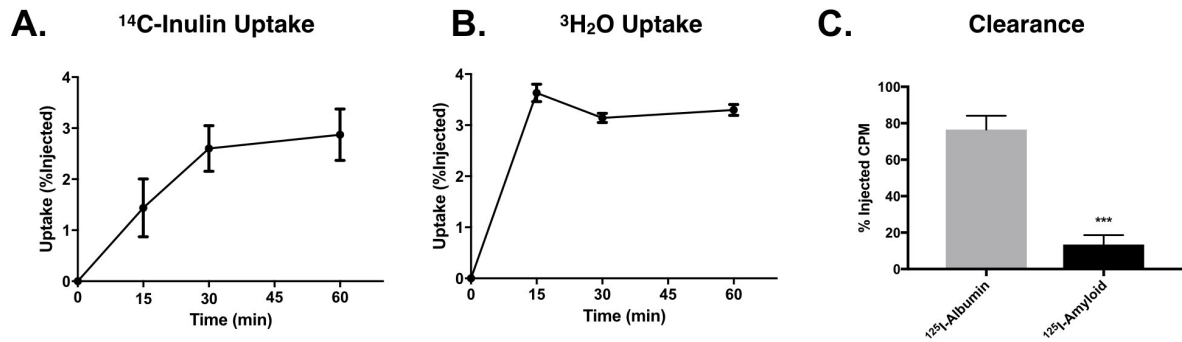


Figure 3-3. Kinetics of influx and efflux of injected tracers. (A.) Intracisternally injected ¹⁴C-Inulin levels increase within the brain interstitial fluid over time and equilibrates by 30 minutes. *n* = 5 – 8 per time-point. **(B.)** Intracisternally injected ³H₂O reduces and equilibrates with the brain by 30 minutes. *n* = 5 – 8 per time-point. **(C.)** Intraparenchymally injected ¹²⁵I-Albumin (70 kD) clears more slowly from the brain than ¹²⁵I-Aβ₁₋₄₀ (4.5 kD) over 60 minutes. *n* = 5 per group. Data are analyzed by Student's *t*-test, *** *p* < 0.001.

3.3.2: CSF solutes rapidly achieve equilibrium with the brain interstitial fluid. Next, to assess the time-course of diffusion of CSF solutes, we performed intracisternal injections of ¹⁴C-Inulin and ³H₂O. ¹⁴C-Inulin was selected as a marker for extracellular diffusion of CSF, due to the fact that it is soluble in water but cannot cross lipid bilayers. ³H₂O was used to measure the intracellular uptake of CSF, which largely occurs in astrocytes via AQP4. I found that ¹⁴C-Inulin levels gradually increased over time ($F[3, 34] = 9.87, p < 0.001$). In contrast, I found that ³H₂O levels rapidly increased, and then plateaued ($F[3, 36] = 230.6, p < 0.001$). These findings indicate that both intracellular and extracellular uptake occur over different time courses, and provide support for choosing a 30-minute duration for subsequent studies, as injected extracellular tracers will have reached equilibrium.

In a separate experiment, we measured the clearance rate of solutes within the interstitial fluid by performing intraparenchymal injection of ^{125}I -Albumin or ^{125}I - $\text{A}\beta_{1-40}$. Unlike previous studies that have found that intraparenchymally injected solutes all move at the same rate, regardless of molecular weight, I found that ^{125}I - $\text{A}\beta_{1-40}$ (4 kD) cleared much more rapidly than ^{125}I -Albumin (70 kD) ($t[7] = 14.9$, $p < 0.001$), being removed almost entirely from the brain by 60 minutes post-injection. This may be due to additional clearance mechanisms for interstitial $\text{A}\beta_{1-40}$.

3.4: Discussion

Even after 30 years of extensive research,²⁰² the existence of physiologically meaningful perivascular CSF flow remains controversial.^{243,244} However, newer studies with two-photon microscopy¹²⁵ have helped this concept gain wider acceptance within the scientific community. Importantly, our work provides further evidence for the perivascular flow of CSF within the healthy brain using multiple types of measurements, including *ex vivo* fluorescence imaging, brain radiouptake measurements as well as *in vivo* two-photon imaging.

Unlike previous studies of interstitial clearance,²⁰⁰ we newly found that the influx of CSF solutes through the basement membrane is size-dependent, with the transport of large solutes (2000 kD) occurring in a separate layer of basement membrane than smaller solutes (70 kD). This may have disease relevance to CAA, as monomeric A β ₁₋₄₀ is small (~4.5 kD), but can form larger oligomers and eventually enormous, insoluble plaques,²⁴⁵ potentially affecting different layers of the basement membrane at different disease stages. Alterations in the composition or communication between these layers could further reduce the transport rate of CSF solutes, which could further worsen deposition of A β ₁₋₄₀ within the basement membrane. Similar to CSF influx, we additionally found that that intraparenchymally injected albumin cleared more slowly from the brain than A β ₁₋₄₀ in naïve animals, measured at 60 minutes post-striatal injection. While this could be due to size differences (molecular weight of albumin is 70 kD), more likely, our observed differences are due to the existence of specific BBB transporters that are involved with the active clearance of A β ₁₋₄₀, which could increase the rate of A β ₁₋₄₀ clearance from the brain compared to other compounds, such as albumin.^{246,247} Further work is needed to determine how aging and stroke alter the ability of

these active transport mechanisms in clearing $A\beta_{1-40}$ across the BBB, which could protect the brain from CAA even under conditions that would otherwise favor the deposition of $A\beta_{1-40}$ within the basement membrane.

In summary, these initial studies confirm that CSF flows from the cisterns into the brain parenchyma, and that this transport occurs within the PVS. They further indicate that the transport of solutes is segregated by molecular weight, with larger molecules excluded from the inner regions of the PVS. They also suggest that microstructural differences within the basement membrane sub-layers, which may produce the size-exclusion properties to different CSF solutes, becomes altered with disease and could sensitize the brain to CAA in pathological states.

CHAPTER 4

Fibronectin Induces the Perivascular Deposition of CSF-derived A β in Aging and After Stroke

4.1: Introduction

4.1.1: Significance.

While CAA is a pervasive finding in stroke survivors, the pathophysiological mechanisms underlying progressive vascular A β_{1-40} accumulation remain understudied. Recent studies suggest that the clearance of A β_{1-40} from blood vessels is mediated via a perivascular route of CSF flow, termed the glymphatic system.¹²⁵ During glymphatic flow, the pulsation of arteries pushes CSF from the meningeal cisterns along penetrating arterioles and eventually capillary beds through the PVS,²⁴⁸ which is bordered on either side by the vascular basement membrane and astrocytic endfeet.^{181,249} Interestingly, Peng *et al.* (2016) showed that in addition to clearing A β_{1-40} from the brain, the glymphatic system can also redistribute CSF A β_{1-40} back into the brain along perivascular routes. This process can be exacerbated by brain pathology, as they further showed that CSF-derived A β_{1-40} selectively accumulates in the brains of aged APP/PS1 mice, and colocalizes with pre-existing cortical A β plaques. Taken together with clinical data showing that CSF A β_{1-40} levels fluctuate over the course of disease in dementia patients,²⁵⁰ these findings suggest that CSF A β_{1-40} may deposit within perivascular regions involved in glymphatic flow. While increased perivascular redistribution of CSF A β_{1-40} could lead to CAA, the molecular and cellular factors that induce A β_{1-40} deposition in CAA, especially in the context of ischemic stroke, remain understudied.

The perivascular flow of CSF may be dependent on the vascular basement membrane which consists of a glycosylated protein matrix that can be stained with tomato lectin. This protein matrix may act as a filtration path that could restrict, in part, the redistribution of solutes dissolved in the CSF. We postulate that this novel basement membrane function may become dysregulated after ischemic stroke, which stimulates the overexpression of fibronectin and its receptor, $\alpha 5\beta 1$ integrin. Cellular fibronectin is a dimeric 440 kD basement membrane glycoprotein that links cell membrane integrins to HSPGs.¹⁷¹⁻¹⁷³ Importantly, fibronectin is also expressed in CAA plaques²⁵¹ and may exhibit affinity for aggregated $A\beta$.^{217,252} Therefore, we hypothesize that stroke-induced increases in basement membrane fibronectin leads to perivascular deposition of soluble, CSF-derived $A\beta_{1-40}$ by direct binding.

4.1.2: Experimental Design.

We show that both aging and focal stroke inhibit the bulk flow of CSF along perivascular routes within the brain, which is associated with impairment of cognitive function. Furthermore, we also demonstrate that CSF $A\beta_{1-40}$ is abnormally deposited within the basement membrane after stroke in aged animals, and that this deposition strongly correlates with the peri-infarct basement membrane labeled by lectin. We identified that fibronectin and the integrin- $\alpha 5$ receptor subunit are upregulated basement membrane proteins in aged animals with stroke, which enhanced the deposition of CSF $A\beta_{1-40}$. Based on our findings, we propose targeting fibronectin as a strategy to treat age and stroke-related CAA.

4.2: Methods

4.2.1: Animals.

Wild-type young (2 – 3 month-old) and aged (18 – 20 month-old) male C57BL/6 mice were obtained from Charles River and the National Institute of Aging, respectively. Mice were kept on a 12-hour light-dark cycle, and fed standard dry chow with *ad libitum* access to food and water. Mice were examined regularly by trained members of the lab and the veterinary staff for any signs of illness, as well as gross pathology at the time of sacrifice. The protocols were approved by the UTHealth IACUC and carried out in an AAALAC-approved facility, as described in the preceding chapter. Animals were randomized to experimental conditions, and investigators were blinded to treatment.

4.2.2: Permanent distal middle cerebral artery occlusion.

Mice were subjected to permanent distal middle cerebral artery occlusion (DMCAO) as previously described.²⁵³ Briefly, mice under isoflurane anesthesia were placed in a prone position inside a sterile surgical field, and body temperature maintained at 37°C. Following this, the right dorsolateral cranium was shaved and aseptically prepared. Then, local anesthetic was injected (Marcaine, 0.05 mL), the skin and underlying temporalis muscle were incised, and a 2 mm burr hole was drilled to expose the MCA, which was then cauterized to induce ischemia. After successful cauterization, the burr hole was closed with dental cement, the temporalis muscle repaired with Vetbond and the skin incision closed with Vicryl 5-0 nylon sutures. Sham surgeries were performed following an identical procedure, except that no cauterization was performed. Ischemia was confirmed by Laser Doppler flow measurement immediately following MCA cauterization.

4.2.3: Behavioral tests

- **DigiGait.** The impact of aging and stroke on motor function was assessed using DigiGait (Mouse Specifics) at 3 and 7 days post-injury (DPI) in a double-blinded manner. Mice were first acclimated to the system, and then the speed was gradually increased to 15 centimeters/second. Gait was recorded for 60 seconds, and the degree of left forepaw rotation was measured using automated DigiGait analysis software over 10 steps by a separate blinded investigator.
- **Barnes Maze.** Hippocampal-dependent spatial reference memory was assessed at 28 DPI using a one day training-testing paradigm, modified from previously described work²⁵⁴. Following habituation, mice were trained to find the escape hole in an illuminated, elevated Barnes maze (Mouse Specifics). This training was repeated 4 times, and then tested 4 hours later in a 3 minute probe trial. The latency to find the escape hole, number of errors and total distance moved were quantified using EthoVision XT software in a blinded manner.
- **Open Field.** Spontaneous exploratory behavior was assessed at 28 DPI by open field testing. Mice were allowed to explore a 40 cm² opaque chamber for 5 minutes. Absolute distance traveled (centimeters) was recorded and quantified using EthoVision XT software in a blinded manner.

4.2.4: Preparation of fluorescent tracers.

aCSF containing Na⁺ (150 mM), K⁺ (3 mM), Ca²⁺ (1.4 mM), Mg (0.8 mM), P (1.0 mM) and HCO₃ (24.1 mM) was prepared in sterile distilled water on the day of the experiment. Stock solutions of lysine-fixable 3 kD cascade blue dextran (CB-d3, 3,000 MW, anionic, 4% stock, Thermo Fisher) and 2000 kD FITC dextran (FITC-d2000, 2,000,000 MW, anionic, 4% stock, Thermo Fisher) were prepared in aCSF. Additionally, AlexaFluor-647-conjugated human amyloid- β_{1-40} (647-A β_{1-40} , 100 μ M stock, Anaspec), FITC-conjugated recombinant human amyloid- β_{1-40} (FITC-A β_{1-40} , 100 μ M stock, Anaspec), and FITC-conjugated recombinant human amyloid- β_{1-42} (FITC-A β_{1-42} , 100 μ M stock, Anaspec) were also prepared in aCSF. Tracers were then combined to a solution 1 (2% CB-d3, 1% FITC-d2000 and 10 μ M 647-A β_{1-40}), solution 2 (10 μ M FITC-A β_{1-42} and 10 μ M 647-A β_{1-40}) or solution 3 (10 μ M FITC-A β_{1-40} alone). In other experiments, recombinant human fibronectin (R&D Systems, cat. 4305-FN) or aCSF was added to the tracer mixture to a concentration of 500 nM and incubated for 1 hour at room temperature prior to infusion. Tracer mixtures were kept on ice for up to 4 hours prior to use, and vortexed for 5 seconds immediately before infusion. To measure fluorescent background signal, zero control animals received aCSF with no tracers.

4.2.5: Tracer injection.

Mice were deeply anesthetized with an intraperitoneal injection of Ketamine-Xylazine dissolved in 0.9% NaCl (120 mg/kg Ketamine, 10 mg/kg Xylazine), then placed in a stereotaxic frame. The skin over the cervical spine was then shaved, aseptically prepared and incised. Following this, the needle was inserted through the superficial neck musculature

and into the cisterna magna as previously described.¹²⁵ Tracer was slowly infused into the cisterna magna (1 μ L/min) over 10 minutes, after which mice were transferred to a warmed cage. Then, 30 minutes after the initiation of the injection, mice were sacrificed by Avertin overdose (250 mg/kg), followed by transcardial perfusion with 0.2% heparin-PBS, then 4% PFA. Tissues were dissected and stored in 4% PFA until later use.

4.2.6: Fluorescent microscopy and tracer imaging.

Following perfusion, brains were extracted and post-fixed for 24 hours in 4% PFA. Then, brains were dehydrated in 30% sucrose, frozen to -20°C and sectioned to 24 μ m (IHC/cresyl violet staining) or 100 μ m (tracer quantification) sections. Sections were then mounted onto slides and coverslipped. For experiments involving colocalization with lectin, sections were first stained with *Lycopersicon esculentum* (Tomato) lectin (see *Immunohistochemistry*). Sections were imaged under fluorescence with a Leica DMI8 microscope at 10X magnification. A blinded investigator imaged the lateral cortex (0.38 mm anterior to Bregma, 2.5 mm lateral, 1.5 mm deep). Then, 100 μ m Z stack images were obtained, and maximum intensity projections performed with LAS X software. Images were then quantified in ImageJ (see *Data Analysis*).

4.2.7: Immunohistochemistry.

IHC was performed on fixed brain sections (24 μ m) that were mounted onto slides and incubated with *Lycopersicon esculentum* lectin (1:100, $\lambda = 594$, Vector Laboratories, cat. DL-1177), anti-fibronectin (Rabbit, 1:100, abcam, cat. ab2413), anti-integrin- α 5 (Rabbit, 1:100, abcam, cat. EPR7854) or anti-glial fibrillary acid protein [GFAP]-Cy3 (Mouse,

1:1000, Millipore Sigma, cat. C9205,) antibodies. Then, sections were incubated with secondary antibodies (Goat anti-Rabbit (Abcam, Alexa-Fluor, 1:500, $\lambda = 488, 594$ or 647 nm). Finally, sections were cover-slipped with Vectashield containing DAPI (Vector Laboratories, H-1200).

4.2.8: Protein isolation, SDS-PAGE and western blotting.

The right cortex was perfused with heparinized PBS, homogenized and lysed in buffer containing 1% NP-40, 1 mM phenylmethylsulfonyl fluoride (PMSF), cOmplete (Roche) and PhosSTOP (Roche). Following centrifugation, the supernatant was removed and diluted to 4 mg/mL in 4x Laemmli Sample Buffer (Bio-Rad, 161-0737) supplemented with 4% β -mercaptoethanol, then heated to 95°C for 5 minutes. Following sample preparation, 10 μ L of each lysate was run on a 4-15% Criterion TGX 26-well gels (Bio-Rad, cat. 5671085), and SDS-Page performed at 120V for 60 minutes in Tris-Glycine-SDS buffer (Bio-Rad). Protein bands were subsequently transferred to a polyvinylidene fluoride (PVDF) membrane and probed with anti-fibronectin (Rabbit, 1:1000, abcam, cat. ab2413), anti- α 5 Integrin (Rabbit, 1:1000, abcam, cat. EPR7854) or anti-vinculin antibody (Rabbit, 1:10,000, abcam, cat. EPR8185). Blots were then probed with HRP-conjugated goat anti-rabbit secondary antibody (1:10,000, Vector Laboratories, cat. PI-1000) and imaged using a Bio-Rad ChemiDoc Imager.

4.2.9: Generation of radiolabeled amyloid- β .

Recombinant human A β ₁₋₄₀ (Anaspec, Fremont, CA) was first dissolved to a concentration of 1 μ g/ μ L in sterile, chloride-free 250 mM sodium phosphate buffer (pH =

7.4). Then, A β ₁₋₄₀ was conjugated to 2 mCi Iodine-125 (¹²⁵I) with chloramine T (1 μ g/ μ L) as previously described.²⁴² The labeling reaction was terminated by adding sodium metabisulfate (10 μ g/ μ L) to the reaction. ¹²⁵I-A β ₁₋₄₀ was separated from free ¹²⁵I by washing the mixture through a Sephadex G-10 column. Successful conjugation was measured by TCA precipitation ratio, calculated as $\% \text{ precipitation} = \text{CPM} (\text{pellet}) / (\text{CPM} [\text{pellet}] + \text{CPM}[\text{supernatant}])$. Fractions retaining > 95% CPM values in the solid phase were then combined and lyophilized overnight for later use.

4.2.10: Fibronectin-¹²⁵I-A β ₁₋₄₀ binding assay.

To measure the binding affinity of radiolabeled ¹²⁵I-A β ₁₋₄₀ for fibronectin, an *in vitro* assay was developed that relies on separation of free ¹²⁵I-A β ₁₋₄₀ (4.2 kD) from fibronectin-¹²⁵I-A β ₁₋₄₀ conjugates (> 220 kD) based on molecular weight. First, serially diluted recombinant human fibronectin (1 x 10³ to 1 x 10⁸ ng/ml) (R&D Systems, cat. 4305-FN) was incubated with ¹²⁵I-A β ₁₋₄₀ (1 x 10⁵ CPM) at room temperature for 1 hour. Reaction mixtures were then centrifuged in a molecular weight cutoff spin column (> 50 kD, Amicon Ultra, Millipore-Sigma). The columns were washed with 400 μ L of sterile PBS and centrifuged 3 times for 5 minutes at 5,000 x g. Finally, the remaining ¹²⁵I-A β -fibronectin conjugates were resuspended in sterile PBS and the amount of fibronectin-bound ¹²⁵I-A β quantified by a gamma counter (Packard Cobra II). See *Data Analysis* for the calculation of the standard curve.

4.2.11: Data Analysis.

- **Atrophy quantification.** High resolution images of cresyl violet-stained coronal brain sections (24 μm) were obtained (**Fig. 4-1**). Then, ventricular volume and hemisphere size were quantified as previously described (Harris *et al.*, 2016; Verma *et al.*, 2014). Tissue atrophy percentage was calculated by the formula: $\% \text{ tissue loss} = 100 - ([\text{total ipsilateral tissue}/\text{total contralateral tissue}] \times 100)$.
- **Tracer intensity.** Tracer influx was quantified by measuring intensity as a function of tissue depth using ImageJ (**Fig. 4-1**). Then, average intensity values were imported into Excel, and integrated into 50 μm bins. Absolute binned intensity values were then plotted as raw intensity (arbitrary units, [A.U.]). To normalize potential age-induced differences in background intensity, the relative tracer intensity was calculated by subtracting each binned value from intensity values obtained from age-matched control mice that did not receive tracer injections (Δ Intensity [A.U.]).
- **Immunohistochemical quantification.** IHC images were acquired and quantified in a double-blinded manner. Based on lectin staining, regions of interest (ROI's) were drawn around 3 peri-infarct vessels/image across 3 brain sections for a total of 27 vessels/brain. Threshold was held constant between brains, and the area and average pixel intensity of fibronectin was measured relative to the ROI.
- **Calculation of 50% Effective Concentration (EC_{50}).** The EC_{50} was quantified using a sigmoidal E_{Max} model by plotting the \log [Fibronectin] against the $\%A\beta$ binding (calculated as $\text{CPM [X]}/\text{CPM [Max]}$). A sigmoidal regression line was fit with Prism, and the EC_{50} was interpolated from the curve. Each measurement at each concentration was replicated 3 times.

4.2.12: Statistics.

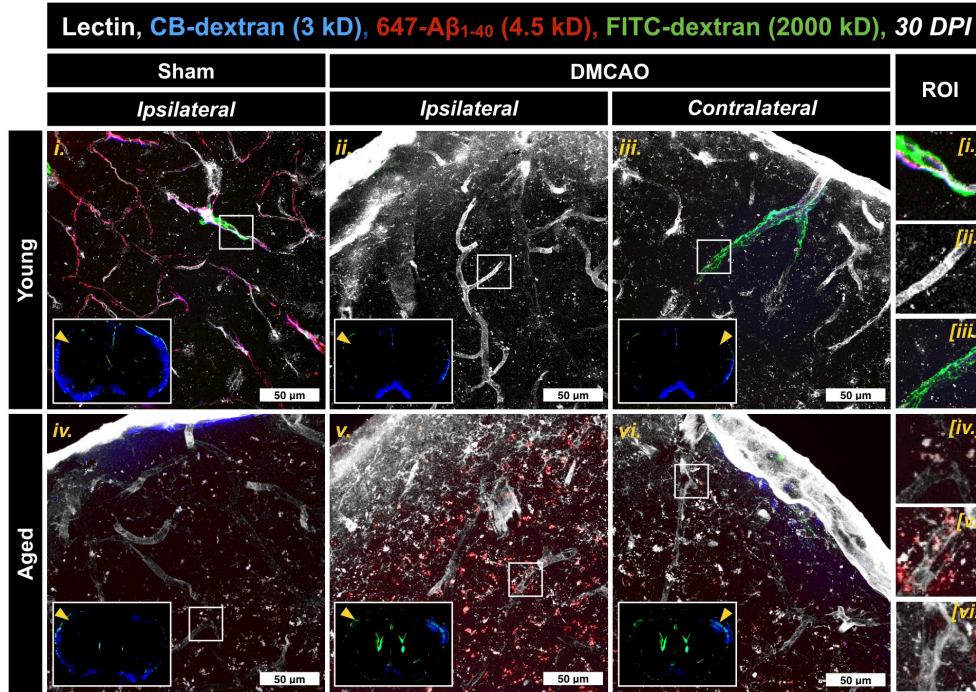
Data are expressed as mean (+/-) SEM with the number of animals per group (n). The physiology data measured at different depths was analyzed by repeated measures two-way ANOVA, with factors of aging and DMCAO. Repeated measures one-way ANOVA was used for repeated measures with only one factor. For immunohistochemical quantification of area or intensity, as well as for analysis of band intensity of western blots, two-way ANOVA was used, examining the effects of aging and DMCAO on the dependent variable. All of the above analyses were followed by Sidak's post-hoc test. Scatter plots were provided and linear mixed-effects models were used to study the association between the dextran intensity and $A\beta_{1-40}$ intensity, and between the lectin intensity and the tracer intensity. Statistical significance is denoted as * $p < 0.05$, ** $p < 0.01$, *** $p < 0.001$, ns, no significance.

4.3: Results

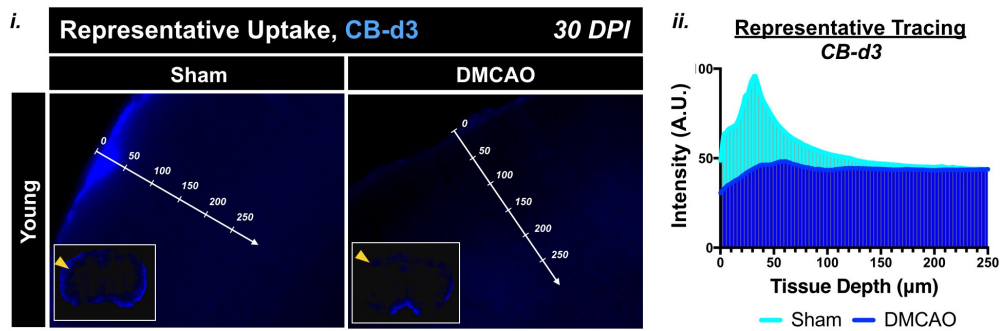
4.3.1: Aging and DMCAO impaired the perivascular flow of CSF.

Previous work has shown that aging impairs glymphatic flow,²³⁵ and that multiple microinfarction disrupts CSF flow in middle-aged mice (12 months-old).²⁰⁸ However, it was not known whether a single focal stroke, modeled by DMCAO, induces glymphatic impairment, or if this would further worsen underlying impairments in aged mice (generally considered to be > 18 months of age). Therefore, to assess the impact of aging and DMCAO on overall perivascular CSF flow, we injected fluorescent tracer into the cisterna magna at 30 days post-DMCAO, and quantified the uptake 30 minutes later (**Fig. 4-1, Fig. 4-2**). We found that CSF influx, measured as the distribution of dextran-derived fluid space markers, occurred along the superficial surfaces of the brain (**Fig. 4-2**). Furthermore, we found that the distribution of both low (CB-d3, 3 kD) and high (FITC-d2000, 2000 kD) molecular weight dextran colocalized with lectin-stained vessels, supporting a perivascular route for CSF influx (**Fig. 4-1A**). When raw CB-d3 uptake values were examined, we found reduced CSF flow occurred in aged animals at baseline (**Fig. 4-2D**, iii, Main Effect: Age, [F(1, 19) = 6.2, p = 0.022]). We then measured how CSF influx changed in the injured cortex, relative to the contralateral hemisphere, and found the distribution of CB-d3 was inhibited by DMCAO in both young and aged animals (**Fig. 4-1C**, i., [F(1, 18) = 52.3, p < 0.001]). Taken together, these data indicate that DMCAO produced a unilateral impairment of bulk CSF influx through the lectin-stained basement membrane, even in aged mice, which exhibit baseline reductions in CSF flow.

A.



B.



C.

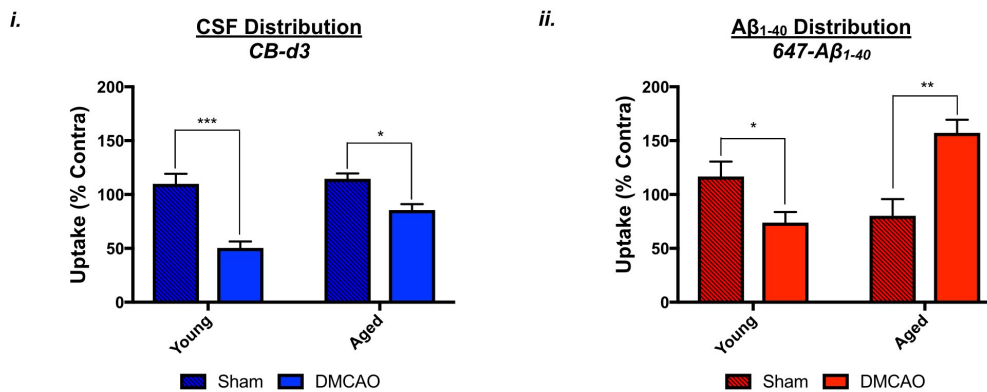


Figure 4-1. Aging and DMCAO disrupted the transport of CSF and enhanced A β ₁₋₄₀ distribution in the superficial cortex. (A.) Representative images of tracer uptake (CB-d3, 647-A β ₁₋₄₀, FITC-d2000) and colocalization with lectin⁺ basement membrane. **(B.)** (i.) Representative 10X magnification images from young sham and DMCAO animals showing axis of tracer quantification, (ii.) Comparison of intensity tracings from young sham and DMCAO animals. **(C.)** Quantification of (i.) CB-d3 tracer uptake and (ii.) 647-A β ₁₋₄₀ from ipsilateral (injured/sham) cortex, 1 – 250 μ m depth. Data are normalized to contralateral hemisphere. *All experiments, n = 5 – 8 per group. Data are analyzed by two-way ANOVA with Sidak's post-hoc test. *p < 0.05, **p < 0.01, ***p < 0.001. Scale bar = 50 μ m.*

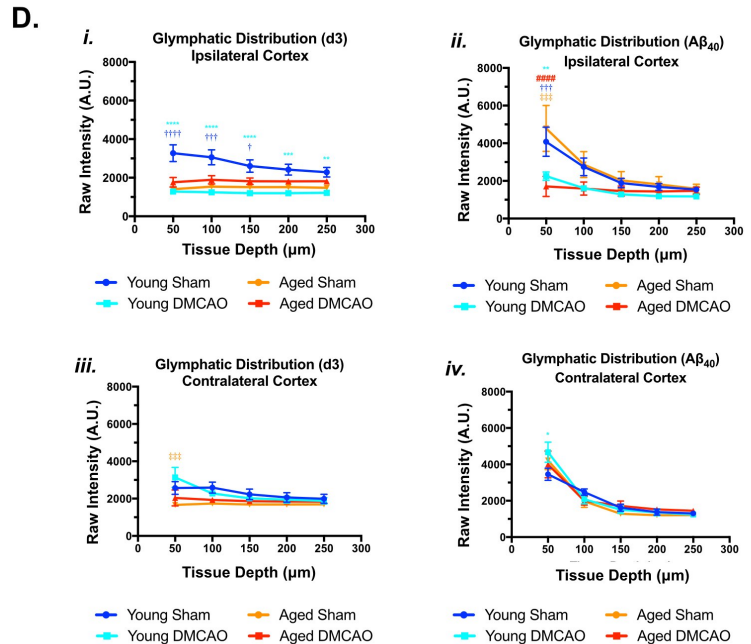
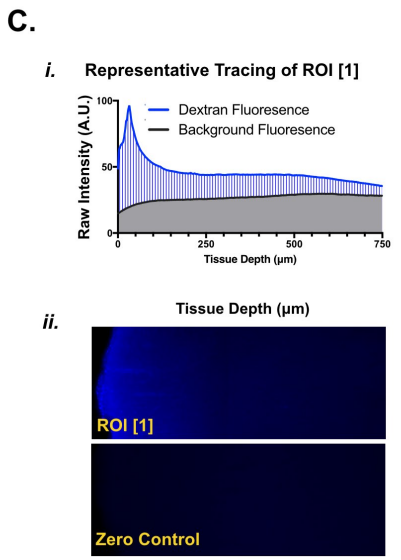
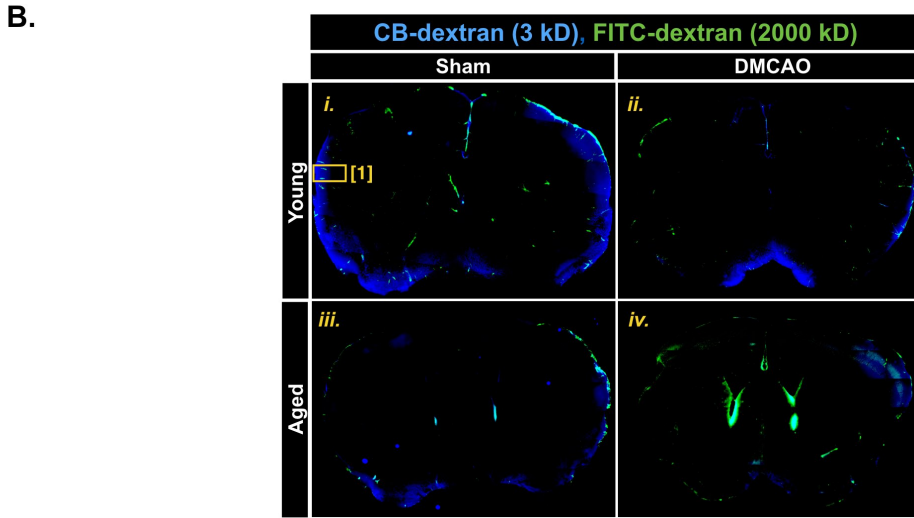
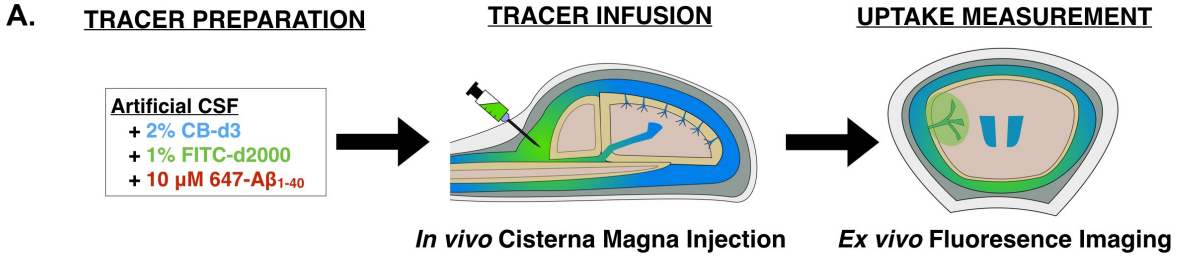


Figure 4-2. Infusion technique, representative images and raw tracer uptake

values. (A.) Measurement of glymphatic flow by tracer uptake. **(B.)** Representative images

of tracer uptake (CB-d3, FITC-d2000) changes with aging any stroke. **(C.)** Representative

raw tracing of dextran uptake in a tracer infused and non-tracer infused mouse

brain. **(D.)** Aging and stroke both reduced glymphatic flow compared to young sham

animals in the injured cortex. *Data are analyzed by repeated measures two-way ANOVA*

*with Tukey's post-hoc test. *young sham vs. young stroke, #aged sham vs aged stroke, †young*

*sham vs. aged sham, ‡young stroke vs. aged stroke. * $p < 0.05$, ** $p < 0.01$, *** $p <$*

0.001. Scale bar = 50 μm .

4.3.2: DMCAO increased the perivascular distribution of CSF A β ₁₋₄₀, which worsens with aging.

Previous work has shown that the glymphatic system provides a perivascular route for the deposition of CSF A β ₁₋₄₀ in mouse models of Alzheimer's disease with pre-existing A β pathology,²⁰⁹ but it was not known whether stroke would induce *de novo* A β ₁₋₄₀ deposition, given the absence of pre-existing A β plaques in wild-type mice. Therefore, to determine whether stroke selectively induced the 'trapping' of CSF A β ₁₋₄₀, we first examined whether DMCAO increased the total amount of A β ₁₋₄₀ deposition within the brains of young and aged wild-type mice by quantification of 647-A β ₁₋₄₀ distribution. While we did not observe an impact on aged animals at baseline, we found an interesting interaction effect, which showed a paradoxical increase in 647-A β ₁₋₄₀ distribution in aged animals with DMCAO (**Fig. 4-1C, ii.**, $F[1, 18] = 21.7$, $p < 0.001$). Importantly, these differences between young and aged mice with DMCAO were not associated with significant differences in tissue atrophy ipsilateral to the injury (**Fig. 4-3B**, $p = 0.96$), suggesting that other mechanisms, aside from infarct volume, could play an important role in determining the fate of CSF A β ₁₋₄₀. Taken together, these data indicate that both aging and DMCAO induced the abnormal deposition of CSF A β ₁₋₄₀, with a major effect of DMCAO on the injured hemisphere, and a major effect of aging on the contralateral hemisphere.

Then, to determine whether this effect was truly specific to A β ₁₋₄₀, we compared the distribution of 647-A β ₁₋₄₀ to FITC-A β ₁₋₄₂ in aged animals with sham and DMCAO in a separate cohort (**Fig. 4-4A**). This analysis confirmed that 647-A β ₁₋₄₀ was increased in aged animals with DMCAO (**Fig. 4-4B, i.**, $p = 0.015$), with no significant impact on FITC-A β ₁₋₄₂ distribution (**Fig. 4-4B, ii.**, $p = 0.596$). Normalization of these values confirmed that 647-

$A\beta_{1-40}$ / FITC- $A\beta_{1-42}$ ratio was significantly increased with DMCAO (**Fig. 4-4B**, iii., $p = 0.045$). Given that the same amount of $A\beta_{1-40}$ and $A\beta_{1-42}$ were infused into the brain, and that the proteins are similar in molecular weight, these data indicate a specific effect of DMCAO on the transport of CSF $A\beta_{1-40}$ through the aged basement membrane after DMCAO, which we next explored by correlation analysis.

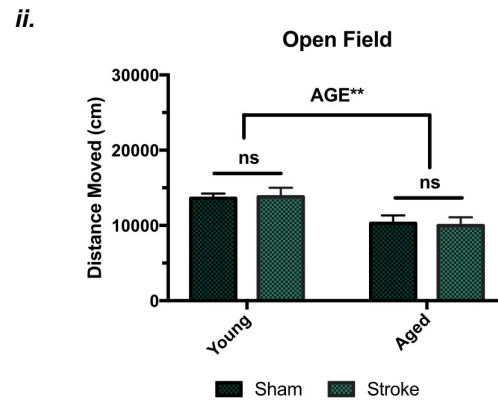
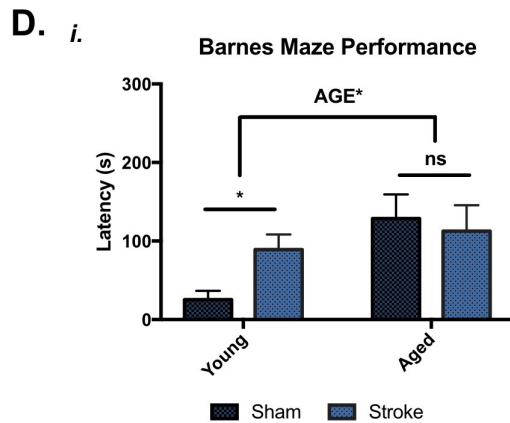
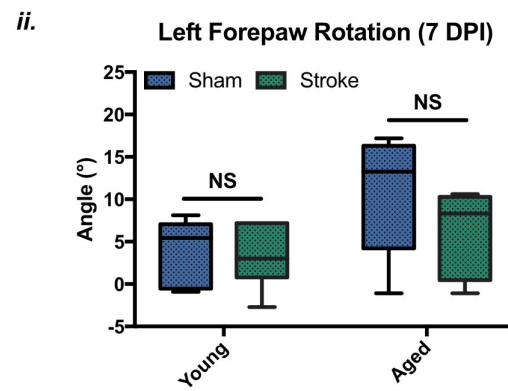
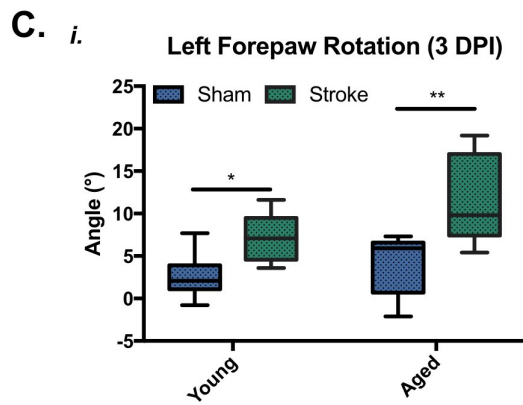
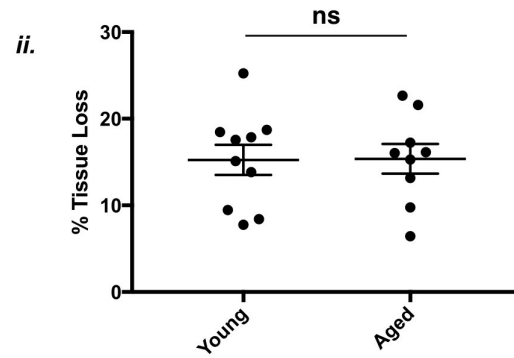
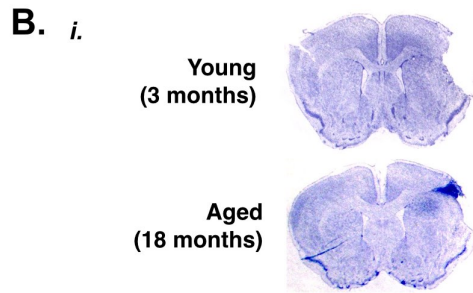
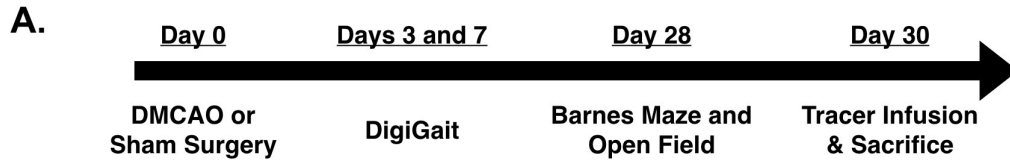


Figure 4-3. Comparison of cortical atrophy, motor and cognitive impairments in young and aged mice with DMCAO. (A.) Timeline of stroke surgery and behavioral tests. (B.) (i.) Cresyl violet staining of DMCAO brains revealed focal damage to the lateral cortex in both young and aged mice at 30 DPI. (ii.) DMCAO induced similar degrees of atrophy in young and aged mice at 30 DPI (*Data are analyzed by Student's t-test, n = 10 per group*). (C.) DMCAO induced alterations in forepaw rotation at day 3, which recovered by day 7 as measured by Digigait. *n = 5 - 12 per group* (D.) (i.) Aging and stroke impaired performance on the Barnes maze. (ii.) Aging reduced exploratory behavior on the open field test. *n = 7 - 8 per group*. *Data from panels C and D are analyzed by two-way ANOVA with Sidak's post-hoc test. *p < 0.05, **p < 0.01. ns, no significance.*

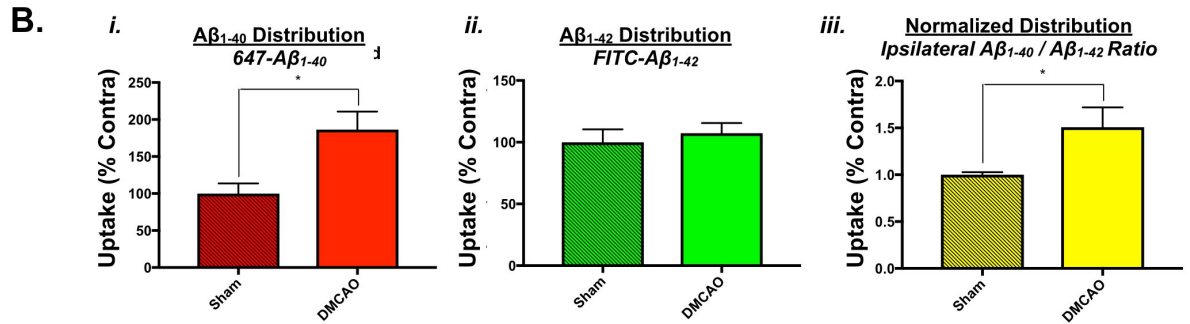
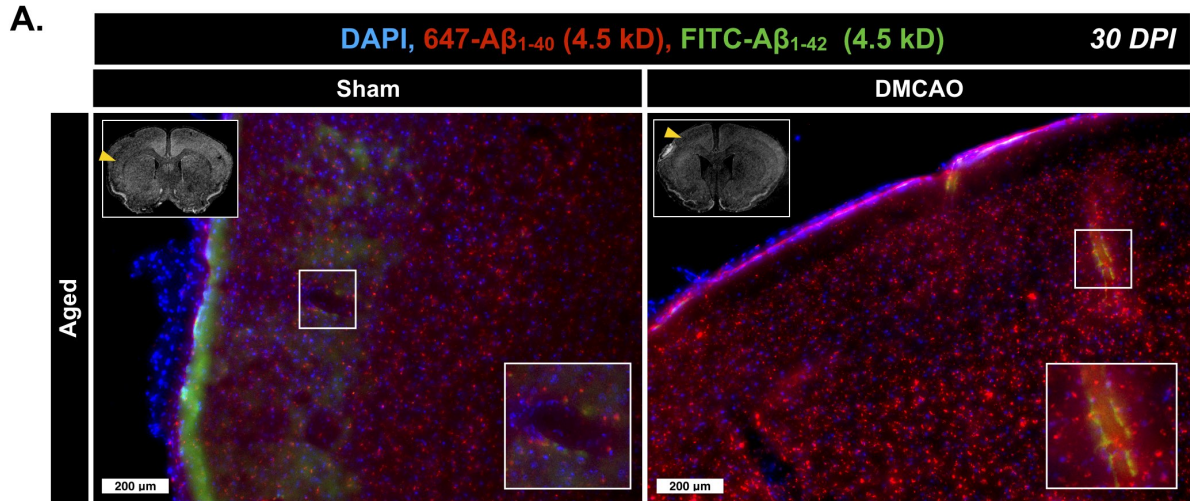


Figure 4-4. DMCAO selectively increased the uptake of A β_{1-40} in the injured cortex of aged animals. (A.) Representative images comparing the distribution of 647-A β_{1-40} to FITC-A β_{1-42} in aged animals treated with sham or DMCAO at 30 DPI. **(B.)** Quantification of (i.) 647-A β_{1-40} uptake, (ii.) FITC-A β_{1-42} uptake and (iii.) 647-A β_{1-40} /FITC-A β_{1-42} ratio. All data are acquired from 1 – 250 μ m depth of superficial cortex, and normalized to the contralateral hemisphere. $n = 5$ per group. Data are analyzed by Student's t -test, $*p < 0.05$.

4.3.3: Aging decoupled $A\beta_{1-40}$ transport from CSF flow.

To examine whether abnormal $A\beta_{1-40}$ deposition is related to the bulk flow of CSF, the average intensity of 647- $A\beta_{1-40}$ and CB-d3 (CSF fluid space marker) were compared within each 50 μm bin for the ipsilateral hemisphere (5 bins/animal) (**Fig. 4-5, A-B**). Comparison of CB-d3 and 647- $A\beta_{1-40}$ influx curves revealed similar distribution kinetics as a function of tissue depth in young sham animals (**Fig. 4-5A**). Furthermore, linear regression revealed a positive correlation (non-zero slope) of CB-d3 and 647- $A\beta_{1-40}$ uptake in young sham (**Fig. 4-5C, i.**, [t(21) = 5.89, $p < 0.001$]) and young stroke animals (**Fig. 4-5C, ii.**, [t(25) = 3.25, $p = 0.003$]). However, CB-d3 uptake did not predict $A\beta_{1-40}$ uptake in aged sham [t(17) = 0.9, $p = 0.379$] or aged stroke animals [t(17) = 1.89, $p = 0.076$]. These findings indicate that age-induced disruption of bulk CSF influx did not predict the behavior of $A\beta_{1-40}$, implying that other mechanisms, such as altered diffusion of $A\beta_{1-40}$ through the basement membrane, may have played a more important role in determining CSF $A\beta_{1-40}$ deposition with aging, which may be further changed by DMCAO.

Since bulk flow did not significantly predict CSF $A\beta_{1-40}$ deposition in disease states, we then broadly assessed whether components of the basement membrane are associated with CSF $A\beta_{1-40}$ accumulation *in vivo*. To accomplish this, the average intensity of 647- $A\beta_{1-40}$ and CB-d3 were each compared to the expression of glycosylated basement membrane matrix proteins, measured by the intensity of 594-lectin staining (**Fig. 4-6**). Interestingly, linear regression of 594-lectin vs. 647- $A\beta_{1-40}$ intensity revealed a highly significant positive correlation in all experimental groups (**Fig. 4-6C, i. – iv.**; young sham, [F(1, 23) = 10.1, $p < 0.001$]; young stroke, [F(1, 27) = 67.91, $p < .0001$]; aged sham, [F(1, 19) = 26.4, $p < 0.001$]; aged stroke, [F(1, 19) = 17.61, $p < 0.001$]). In contrast, linear regression of 594-lectin vs.

CB-d3 intensity (used as a fluid space marker and to control for potential non-specific trapping within the extracellular space) revealed a positive relationship in young sham animals (sham, **Fig. 4-6B**, i., $t(23) = 3.7$, $p = 0.001$], but not in young DMCAO animals (**Fig. 4-6B**, ii., [$t(27) = 0.4$, $p = 0.685$]). Additionally, in aged animals, 594-lectin intensity did not correlate with CB-d3 intensity in sham (**Fig. 4-6B**, iii., [$t(19) = 0.9$, $p = 0.384$]) or DMCAO mice (**Fig. 4-6B**, iv., [$t(19) = 0.5$, $p = 0.619$]). Overall, these data showed that basement membrane proteins were more strongly associated with 647-A β_{1-40} than CB-d3 controls, indicating an association of lectin-stained basement membrane proteins on A β_{1-40} levels. This difference was further exacerbated by aging and DMCAO.

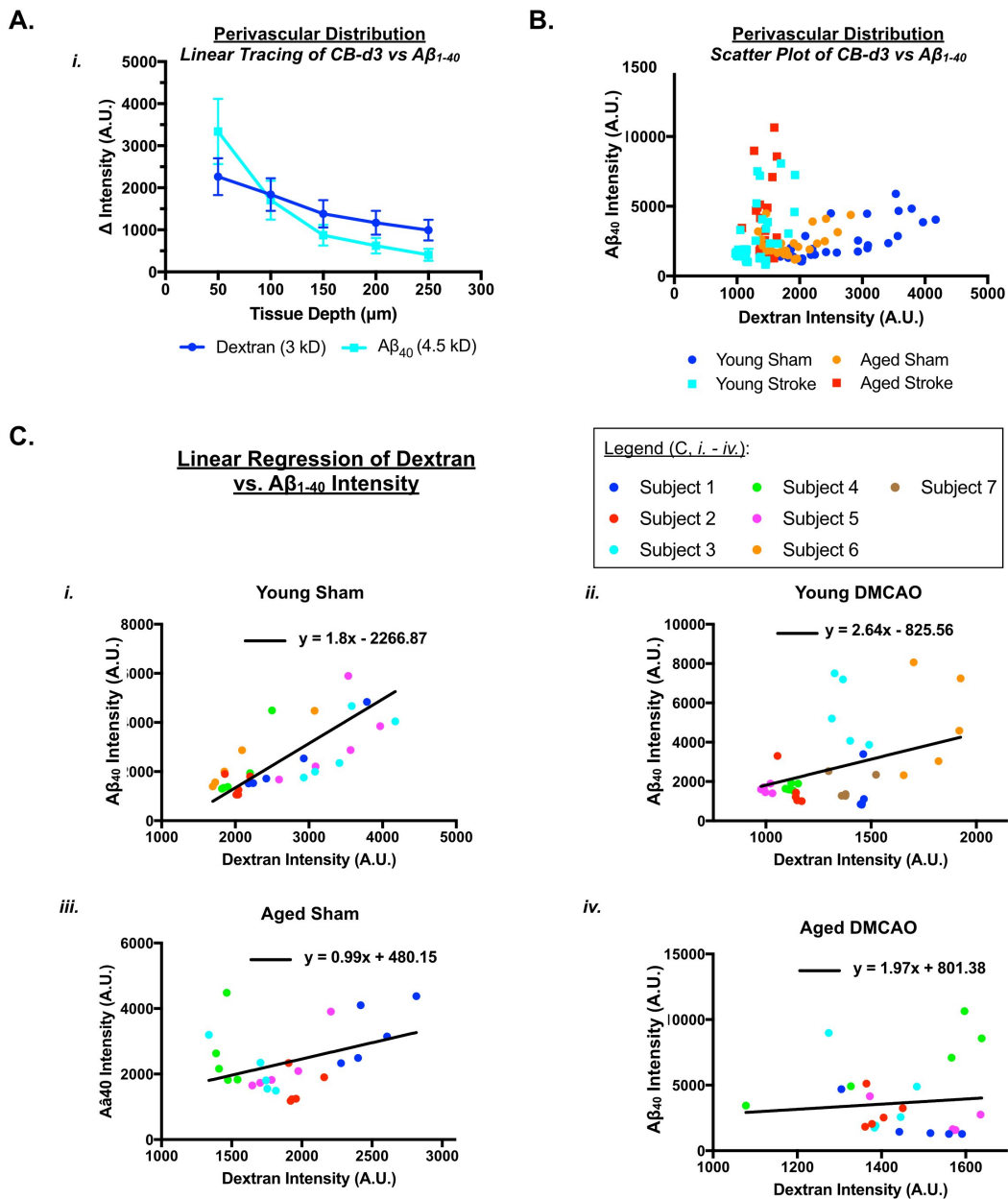


Figure 4-5. Distribution of dextran did not predict $A\beta_{1-40}$ distribution in disease conditions. (A.) Distribution of $A\beta_{1-40}$ and dextran by tissue depth in young sham animals, (B.) Correlation plot of dextran and $A\beta_{40}$ uptake in all experimental groups. (C.) (i. - iv.) Linear regression of dextran vs. $A\beta_{1-40}$ uptake. A - C, $n = 5 - 7$, 5 bins/animal. Data are analyzed by a linear mixed effect model to control for within-subject correlations.

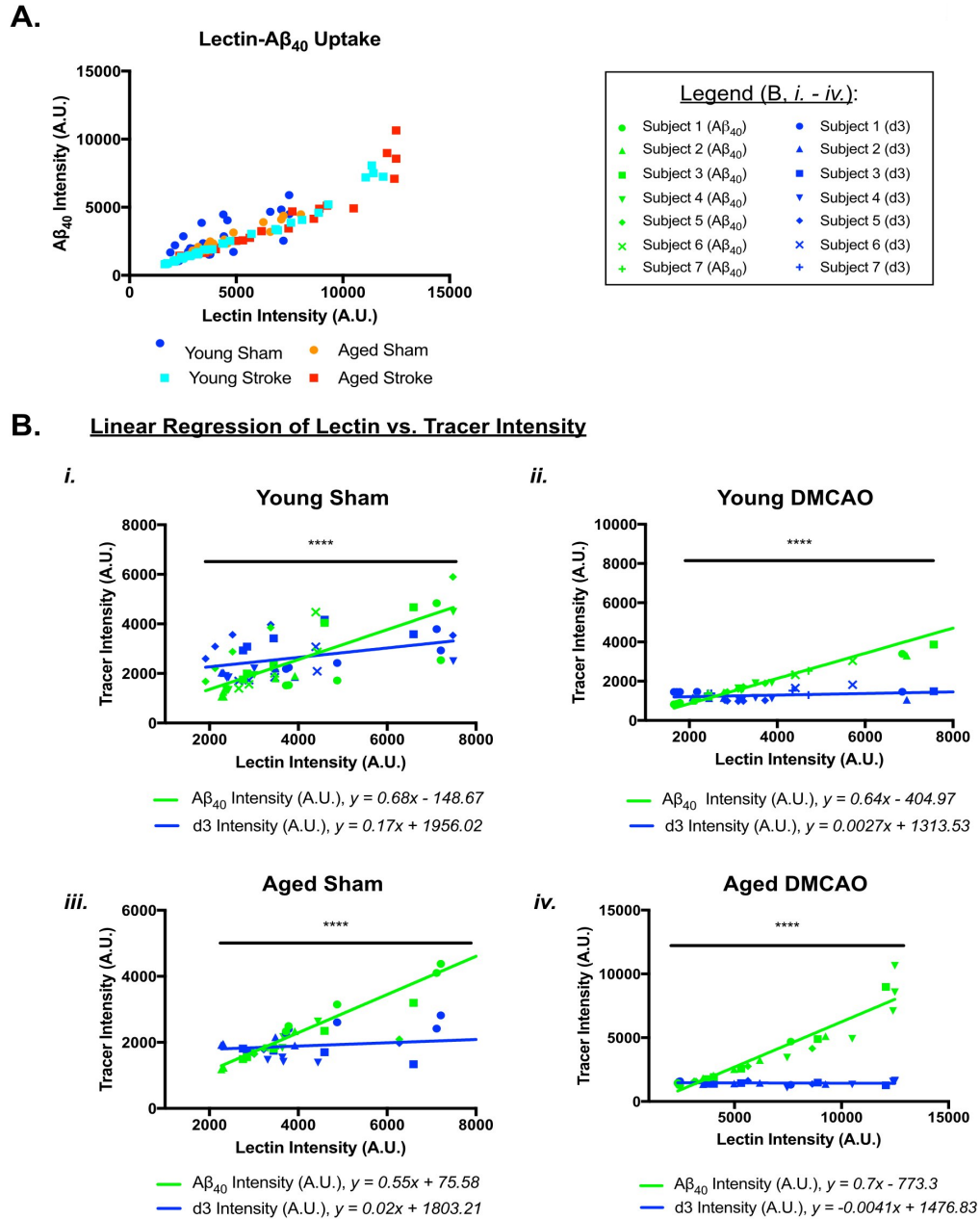


Figure 4-6. Lectin staining predicted A β_{1-40} distribution in all experimental groups.

(A.) Correlation plot of lectin staining and A β_{1-40} uptake in all experimental groups. (B.)

Comparison of lectin-A β slopes across experimental groups. (C.) (i. - iv.) Linear regression

of lectin vs. A β_{40} uptake and lectin vs. dextran (3 kD) uptake. A - C, $n = 5 - 7$. Data are

analyzed by a linear mixed effect model to control for within-subject correlations.

4.3.4: DMCAO increased fibronectin and integrin- α 5 expression in young and aged animals.

We next examined how the expression of fibronectin changes in the context of the PVS, bordered by astrocytic endfeet and the lectin-stained basement membrane matrix. IHC revealed increases in fibronectin expression at 7 DPI (**Fig. 4-7A**). To confirm these findings, total protein levels of fibronectin and integrin- α 5 were then assessed by western blot of the peri-infarct cortex (**Fig. 4-7B, Fig. 4-8**). Stroke increased fibronectin expression (**Fig. 4-7C**, i., [F(1, 19) = 63.8, p < 0.001]), with no additional effects of aging [F(1, 19) = 0.06, p = 0.81] or interaction [F(1, 19) = 0.1, p = 0.733]. In contrast, integrin- α 5 levels were increased by both DMCAO (**Fig. 4-7C**, ii., [F(1, 19) = 34.6, p < 0.001]) and aging [F(1, 19) = 5, p = 0.038], with no significant interaction effect [F(1, 19) = 1.5, p = 0.232]. These data indicate that perivascular fibronectin deposition occurred by 7 DPI, which was also accompanied by further increases in integrin- α 5 expression in aged animals with DMCAO. We also observed acute reductions in LRP1 following DMCAO in aged animals (**Fig. 4-9**), which may further impair the clearance of A β ₁₋₄₀ from the basement membrane across the BBB in the aged brain.⁸⁰

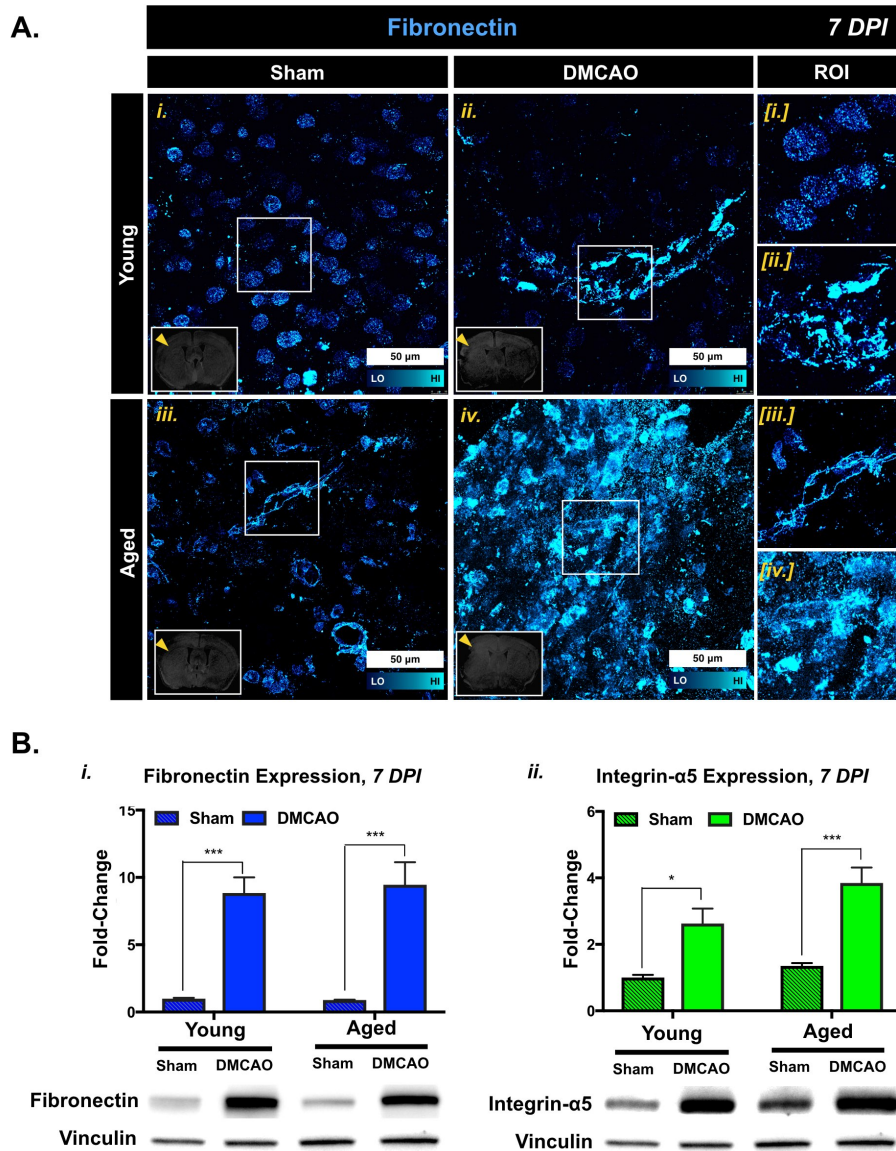


Figure 4-7. DMCAO increased the expression of fibronectin and integrin- α 5 at 7 DPI.

(A.) Representative images of fibronectin expression in young and aged animals, taken at 7 DPI (40X magnification). (B.) Representative blots and quantification of fibronectin, integrin- α 5 and vinculin (loading control) expression of these proteins at 7 DPI. Data are analyzed by two-way ANOVA with Sidak's post-hoc test, $n = 5 - 7$ per group, $*p < 0.05$, $***p < 0.001$. Scale bar = 50 μ m.

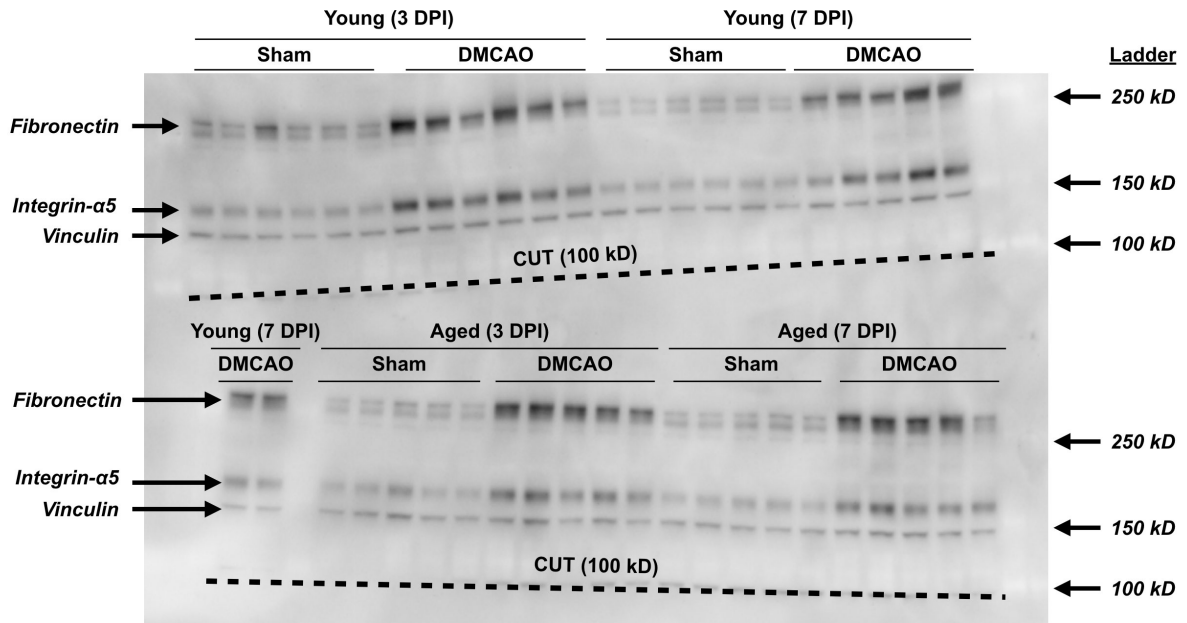
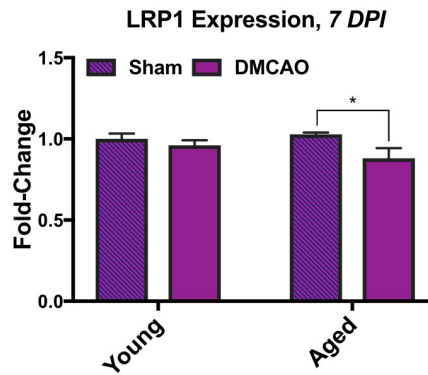


Figure 4-8. DMCAO upregulated the expression of fibronectin and integrin $\alpha 5$ in young and aged mice. Western blot image showing upregulation of basement membrane proteins at 3 and 7 DPI in both young and aged mice. Gels were run in parallel, cut at 100 kD, then transferred to the same PVDF membrane. Proteins were identified by molecular weight using Bio-Rad Precision Plus Dual Color standards.

A.



B.

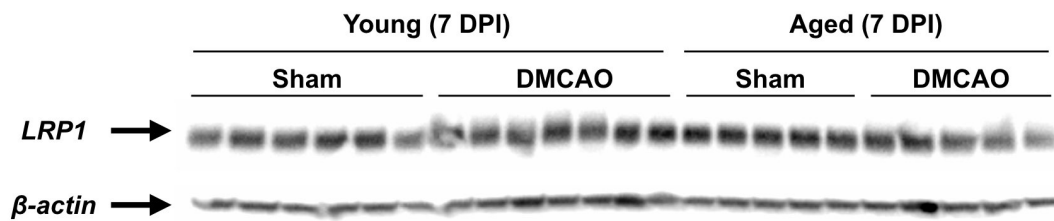


Figure 4-9. DMCAO reduced LRP1 expression in aged mice. (A.) Quantification of LRP1 expression in young and aged mice at 7 DPI. (B.) Western blot showing reduced expression of LRP1 in aged mice with DMCAO. $n = 5 - 7$. Data are analyzed by two-way ANOVA with Sidak's post-hoc test, $*p < 0.05$.

4.3.5: CSF-derived $A\beta_{1-40}$ colocalized with fibronectin, the integrin- $\alpha 5$ subunit and lectin-stained basement membrane components, which increased with DMCAO.

Based on our data showing that aging and DMCAO cause increased association of CSF $A\beta_{1-40}$ with the lectin-stained basement membrane, we next assessed the contribution of fibronectin and the integrin family of receptors to this phenotype. In addition to fibronectin, we selected integrin- $\alpha 5$ because previous work has shown that it is strongly expressed in the basement membrane,^{257,258} regulates the binding of multiple beta subunits to fibronectin,²⁵⁹ and is associated with increased $A\beta$ accumulation in disease states.²⁶⁰

Image quantification at 30 DPI revealed that DMCAO increased the expression of FITC-lectin-stained basement membrane components (**Fig. 4-10B**, ii., [F(1, 19) = 5.756, p = 0.0269]). Aging also exhibited a trend for increased FITC-lectin staining, but it failed to reach statistical significance [F(1, 19) = 3.252, p = 0.0872]. Additionally, we found that perivascular fibronectin staining increased with DMCAO in both young and aged animals (**Fig. 4-10B**, i., F[1, 12] = 19.5, p < 0.001) and colocalized with the lectin-stained basement membrane (**Fig. 4-10A**). Furthermore, intracisternally injected FITC- $A\beta_{1-40}$ colocalized with fibronectin within the basement membrane across all conditions, and was most apparent in aged animals with DMCAO (**Fig. 4-10A**). This indicates that fibronectin was a marker of sites within the basement membrane that were predisposed to $A\beta_{1-40}$ deposition, which further increased with aging and DMCAO. This suggests a potential mechanism of $A\beta_{1-40}$ deposition via its association with fibronectin.

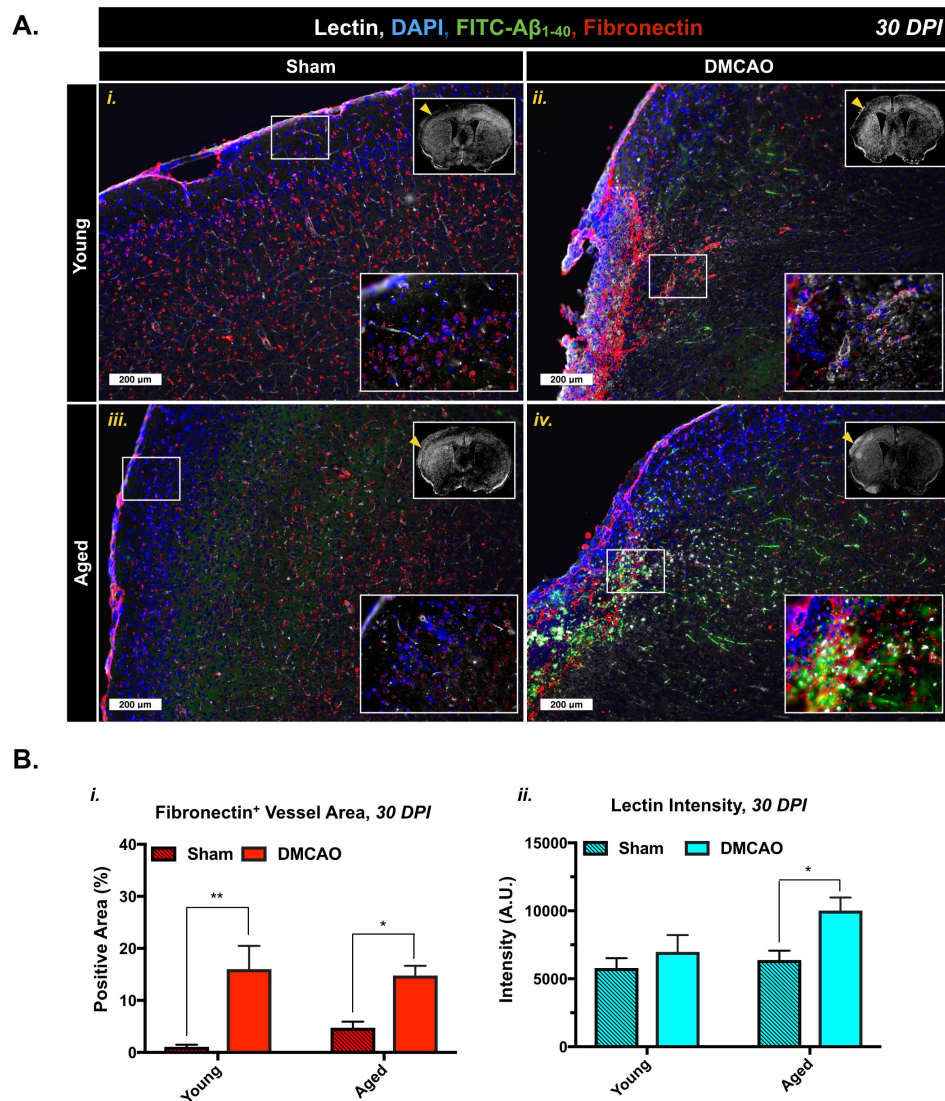


Figure 4-10. Fibronectin expression colocalized with sites of CSF A β_{1-40} deposition. (A.)

Colocalization of intracisternally injected FITC-A β_{1-40} with fibronectin occurs within the lectin stained basement membrane at low levels in young sham mice, which worsens with aging and DMCAO. Low-power images were acquired at 10X magnification, and high power images were acquired at 40X magnification. **(B.)** Quantification of *(i.)* fibronectin and *(ii.)* lectin staining at 30 DPI. $n = 3 - 5$ per group for all experiments. Data are analyzed by two-way ANOVA with Sidak's post-hoc test. $*p < 0.05$, $**p < 0.01$. Scale bar = 200 μ m.

Despite observing colocalization with $A\beta_{1-40}$, we did not observe consistent increases in fibronectin expression in aged animals. Therefore, we next explored the impact of aging and DMCAO on its major receptor, integrin- $\alpha 5$, to determine whether it could further modulate $A\beta_{1-40}$ distribution in the aged brain. We found that perivascular integrin- $\alpha 5$ staining in the aged brain further increased with DMCAO, and colocalized with the lectin-stained basement membrane (**Fig. 4-11A**). Furthermore, intracisternally injected FITC- $A\beta_{1-40}$ colocalized with integrin- $\alpha 5$ within the basement membrane across all conditions, and was, again, most apparent in aged animals with DMCAO (**Fig. 4-11A**). Total expression of vascular integrin- $\alpha 5$ was highest in aged animals with DMCAO (**Fig. 4-11B**), with main effects of DMCAO ($F[1, 12] = 344.6, p < 0.001$) and aging ($F[1, 12] = 15.1, p = 0.002$) on increased expression, with a significant interaction effect ($F[1, 12] = 27.9, p < 0.001$). Increased expression of integrin- $\alpha 5$ could alter the affinity of the basement membrane by complexing with its major ligand, fibronectin. Alternatively, it could possess additional binding sites for $A\beta_{1-40}$.

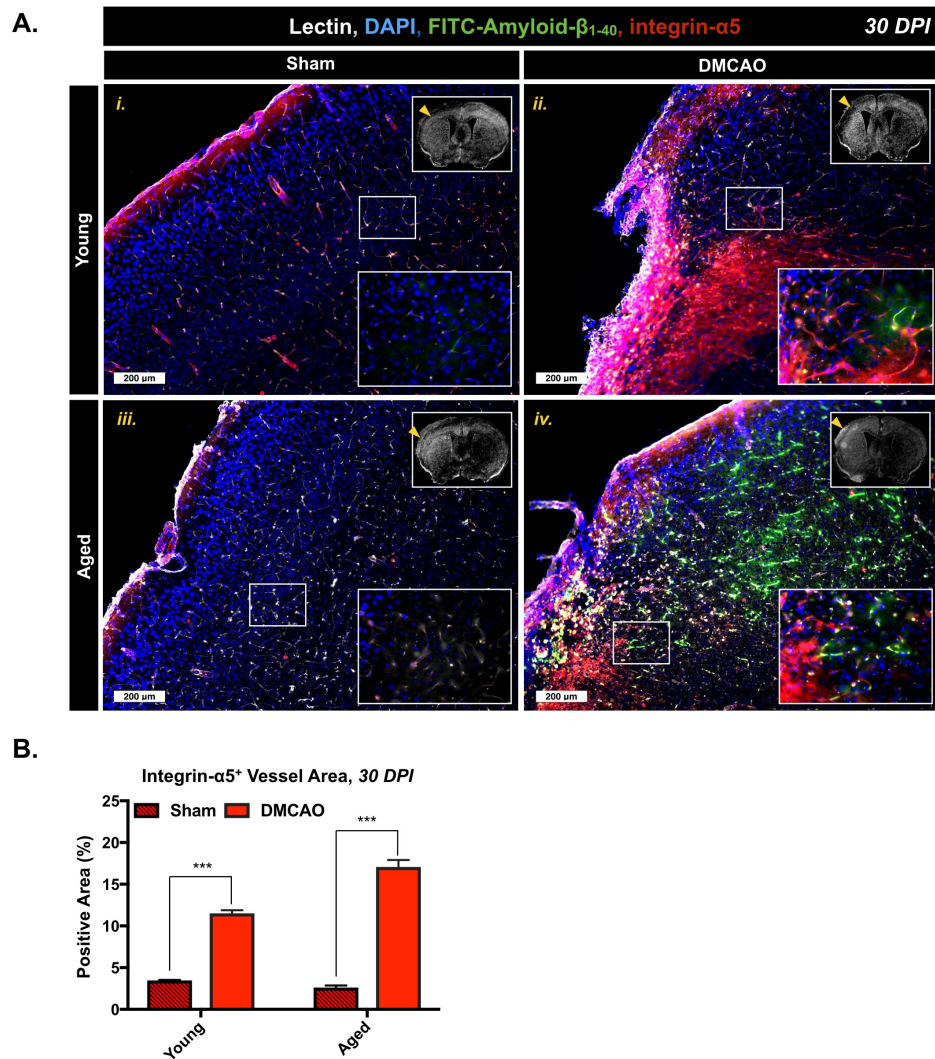


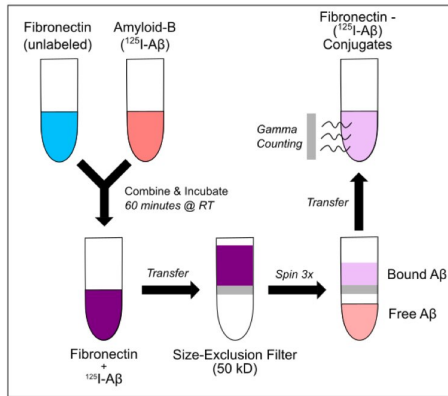
Figure 4-11. Integrin- $\alpha 5$ expression colocalized with sites of CSF $A\beta_{1-40}$ deposition. (A.)

Colocalization of intracisternally injected FITC- $A\beta_{1-40}$ with integrin- $\alpha 5$ occurs within the lectin stained basement membrane at low levels in young sham mice, which worsens with aging and DMCAO. Low-power images were acquired at 10X magnification, and high power images were acquired at 40X magnification. **(B.)** Quantification of integrin- $\alpha 5$ staining at 30 DPI. $n = 3 - 5$ per group for all experiments. Scale bar = 200 μm . Data are analyzed by two-way ANOVA with Sidak's post-hoc test. $*p < 0.05$, $**p < 0.01$. Scale bar = 200 μm .

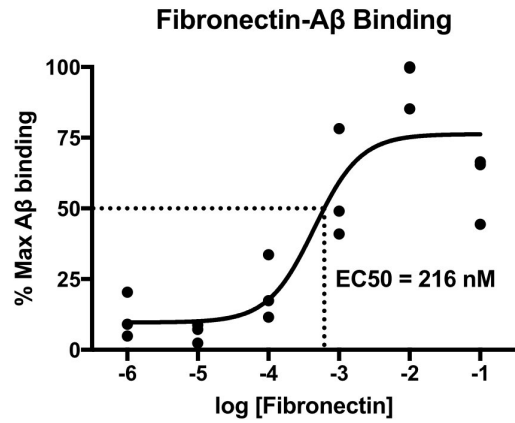
4.3.6: Fibronectin treatment increased the perivascular deposition of CSF A β ₁₋₄₀.

Previous work has suggested that plasma fibronectin may bind serum amyloid species via the fibronectin type I domain,²¹⁷ but there are a lack of studies examining its potential affinity to the A β ₁₋₄₀ fragment, especially in the context of the brain microenvironment. Therefore, to first assess the binding characteristics of fibronectin to A β ₁₋₄₀, recombinant fibronectin was incubated with ¹²⁵I-A β ₁₋₄₀ (**Fig. 4-12A**, i.). We found that fibronectin bound A β ₁₋₄₀ *in vitro* with an EC₅₀ of 216 nM (**Fig. 4-12A**, ii.). Then, to determine whether fibronectin impacted CSF flow or A β ₁₋₄₀ deposition, fibronectin or vehicle control was incubated with CB-d3 and 647-A β ₁₋₄₀, and then injected intracisternally (**Fig. 4-12B**). Fibronectin treatment increased the 647-A β ₁₋₄₀/CB-d3 ratio (**Fig. 4-12C**, [F(1, 8) = 11.2, p = 0.01]), which decreased with tissue depth [F(4, 32) = 18.1, p < 0.001]. Furthermore, an interaction between fibronectin treatment and tissue depth was also observed [F(4, 32) = 3.1, p = 0.028]. Treatment did not affect total CB-d3 ([F(1, 8) = 0.05, p = 0.835]) or 647-A β ₁₋₄₀ influx ([F(1, 8) = 0.6, p = 0.468]). These data demonstrate that fibronectin-A β ₁₋₄₀ binding occurred, and that this interaction was sufficient to induce the selective accumulation of A β ₁₋₄₀ within the superficial cortex, without impacting bulk CSF influx.

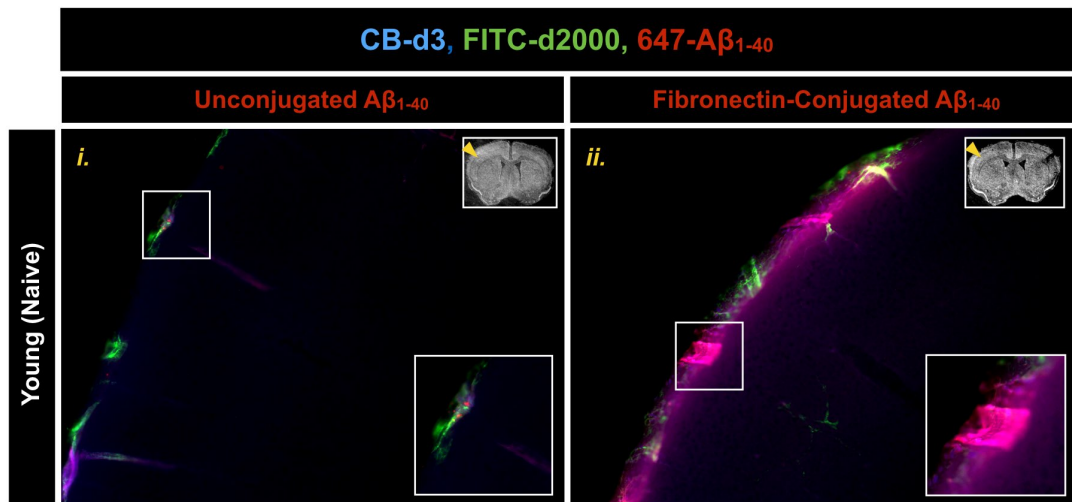
A. *i.*



ii.



B.



C.

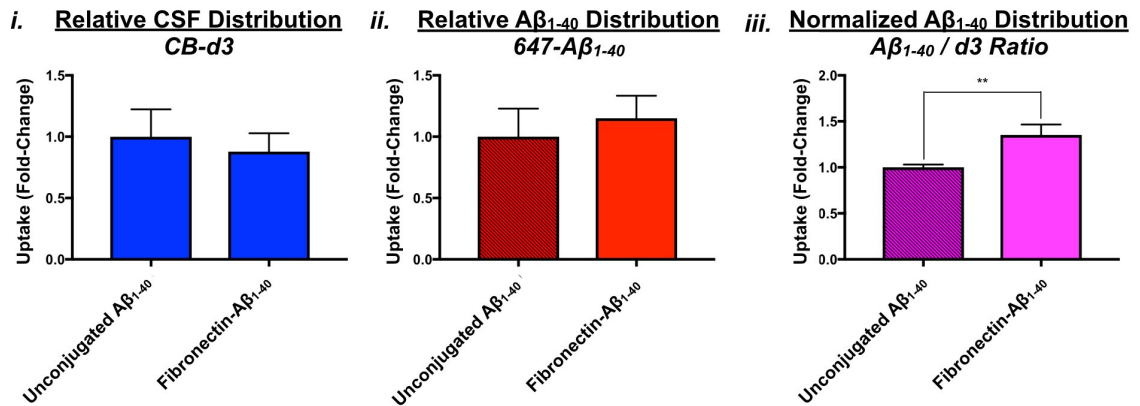


Figure 4-12. Fibronectin conjugation altered the perivascular transport of A β ₁₋₄₀. (A.)

(i.) Experimental design of *in vitro* fibronectin binding assay. **(ii.)** Binding kinetics of fibronectin and ¹²⁵I-A β ₁₋₄₀. **(B.)** Representative images showing increased distribution of fibronectin-A β ₁₋₄₀ *conjugates* compared to unconjugated A β ₁₋₄₀ following intracisternal injection into naïve young mice. **(C.)** Comparison of (i.) CB-d3 uptake, (ii.) 647-A β ₁₋₄₀ uptake and (iii.) 647-A β ₁₋₄₀/CB-d3 ratio. *n* = 5 - 6 per group for all experiments. Data are analyzed by Student's *t*-test, **p* < 0.05.

4.3.6: Aging and DMCAO induced impairments in motor function, cognition, and exploratory behavior.

Previous work has shown that young mice develop cognitive impairment after DMCAO.¹¹ To evaluate whether aging and DMCAO induced similar behavioral changes in our animals, we tested mice on DigiGait, Barnes maze and open field (**Fig. 4-3, C-D**). We found that stroke induced left forepaw rotation at 3 DPI (**Fig. 4-3C**, [F(1, 31) = 21.4, $p < 0.0001$]), which resolved by 7 DPI ([F(1, 21) = 1.6, $p = 0.214$]). Aging also induced mild forepaw rotation at 3 DPI [F(1, 31) = 4.7, $p = 0.037$] and 7 DPI [F(1, 21) = 5.6, $p = 0.028$]. No significant interaction of aging and DMCAO were observed at 3 DPI [F(1, 31) = 0.9, $p = 0.35$] or 7 DPI [F(1, 21) = 1, $p = 0.333$]. These data indicate that both aging and DMCAO induce motor impairment, with DMCAO-induced motor deficits recovering by 7 DPI.

Aging increased the latency to find the escape hole on the Barnes maze (**Fig. 4-3D**, [F(1, 26) = 8.3, $p = 0.008$]). No major effect of DMCAO on latency was observed [F(1, 26) = 1.2, $p = 0.287$], likely due to a trending interaction between aging and DMCAO [F(1, 26) = 3.3, $p = 0.082$], as DMCAO worsened Barnes maze performance in young (Sidak test, $p = 0.049$), but not aged animals ($p = 0.8784$). Finally, aging reduced total movement on open field testing (F(1, 26) = 12.6, $p = 0.002$), with no effect of DMCAO [F(1, 26) = 0.003, $p = 0.96$] or interaction observed [F(1, 26) = 0.06, $p = 0.817$]. Taken together, these data indicate that cognitive deficits existed in conditions of reduced CSF flow, even when motor deficits were no longer detectable by gait measurement.

4.4: Discussion

4.4.1: Aging and stroke impair the perivascular flow of CSF through the basement membrane.

Previous work has shown that aging⁸² and multiple types of brain injury, including traumatic brain injury,²⁶¹ multiple microinfarction²⁰⁸ and AD,²⁰⁹ all reduce the perivascular bulk flow of CSF. However, it was not previously known whether focal ischemic stroke impairs the perivascular flow of CSF. Furthermore, no study had examined whether normal aging or stroke impact the deposition of CSF A β ₁₋₄₀ within the basement membrane.

In agreement with previous studies of CSF influx, we found that both aging and stroke impaired the transport of CSF through the basement membrane. However, we newly showed that these effects occurred independently of each other: while stroke reduced CSF influx in young animals, it showed minimal further reduction in aged animals, who were already severely impaired at baseline. This is surprising, because recent work showed that age-related glymphatic impairment significantly worsened with experimental induction of multiple microinfarction.²⁰⁸ However, our study differed in several important respects:

1. *Injury model differences.* We performed a single, focal stroke (modeled by distal MCA occlusion), while their model relied on the induction of multiple small infarctions via intravenous latex microbead injection. Differences in the pathophysiology of these two diseases could explain disparate findings, and suggest that focal and repeated infarction may have distinct effects on CSF flow in the aged brain.
2. *Age differences.* Their study used 12-month-old mice as their aged population, while we used much older 20 month-old mice that are more

analogous to elderly stroke patients. Given that Kress *et al.* (2014) found that CSF influx continues to decline between 12 and 18 months,⁸² indicating major differences in baseline CSF flow, these further reductions could have made it more difficult to detect stroke-induced impairment in our aged animals.

3. *Tracer differences.* Third, their study used fluorescent ovalbumin (45 kD), while ours used fluorescent dextrans (3 and 2000 kD). Given that our early validation studies, detailed in Chapter 3, showed molecular size-dependent distribution of CSF solutes in the basement membrane, it is possible that their study measured CSF flow in a different layer of basement membrane than where A β_{1-40} (~4.5 kD) is transported.

Overall, further work using multiple experimental stroke models and differently sized tracers is required to definitively determine if stroke worsens age-related impairments in perivascular CSF flow.

In addition to changes in total CSF flow, our study also examined whether aging and stroke had specific impacts on the deposition of CSF A β_{1-40} . One recent publication found that A β_{1-40} can re-enter the brain from the CSF and associate with pre-existing amyloid plaques within the brain parenchymal extracellular space.²⁰⁹ In this case, the distribution of A β_{1-40} was altered by binding to these pre-existing plaques, which trapped them within the brain tissue rather than allowing them to circulate back out to the cisterns. Based on these data, CSF A β_{1-40} is ideally positioned to contribute to the perivascular A β deposits that are characteristic of CAA.

This novel source of A β ₁₋₄₀ could explain several interesting characteristics of CAA pathophysiology, including the early involvement of leptomeningeal and penetrating arteries, the initial deposition within the basement membrane, as well as the primarily ‘outside-in’ cortical distribution of plaques, with worse pathology being observed in the superficial cortical layers. We newly discovered that aging and stroke selectively increase the deposition of CSF A β ₁₋₄₀, which occurs independently of changes in bulk CSF flow. This finding suggests that other factors, such as the diffusion of A β ₁₋₄₀ between glycosylated extracellular basement membrane proteins (stained with lectin), play a major role in determining the amount and location of A β ₁₋₄₀ deposition within the basement membrane, particularly in aging and stroke. One potential implication of this finding is that the movement of A β ₁₋₄₀ within the PVS cannot be approximated by dextran flux, which is problematic for all but one²⁰⁹ of the previously discussed studies of glymphatic flow. Other factors, including the degree of basement membrane glycosylation, play a more important role in modulating the distribution of CSF A β ₁₋₄₀.

Overall, my work supports the notion that aging and brain injury both reduce the perivascular flow of CSF. It also newly shows that stroke specifically disrupts the transport of CSF-derived A β ₁₋₄₀, which correlates with upregulation of lectin-stained basement membrane proteins, as well as fibronectin. This deposition of CSF A β ₁₋₄₀ occurs even in wild-type mice that do not have pre-existing amyloid plaque pathology. These studies provide a potential new mechanism by which aging and stroke sensitize cortical vessels to the development of CAA pathology.

4.4.2: Aging and stroke interact to remodel the vascular basement membrane.

My findings suggest multiple facets of a potential new mechanism of CAA development, including both the physiological route of the initial perivascular A β deposition after stroke, as well as the specific extracellular matrix components that pathologically enhance this A β deposition after stroke. While previous studies have examined the independent effects of aging and stroke on basement membrane composition,^{165,181,194} there is a significant gap in the literature with respect to the impact of stroke on the aged basement membrane. A better understanding of how aging and stroke impact the regulation of basement membrane composition is critical to developing new and effective therapies to combat CAA.

I first examined how aging and stroke impact the overall morphology of the vascular network by staining the basement membrane with lectin. Similar to previous studies, I found that stroke increased the density of microvessels. Following stroke, aged animals also produced new vessels. However, many of these peri-infarct vessels appeared “string-like,” which is a sign of nonperfused vasculature. Given the dependence of bulk flow on the pulsation of arteriolar blood vessels, these likely do not contribute to effective CSF flow. As such, these vessels may be the most prone to the development of CAA after stroke, given that they exhibited reduced ability to transport CSF through the PVS.

I then hypothesized that post-stroke basement membrane fibrosis includes chronic changes in both fibronectin and a subunit of its receptor, integrin- α 5, which together ‘prime’ the basement membrane matrix for the binding of CSF-derived A β . Indeed, my findings indicate that stroke induces the chronic deposition of extracellular fibronectin as well as lectin⁺ matrix proteins (which are most likely enriched for HSPG) and integrin- α 5.

Surprisingly, while the total amount of fibronectin dramatically increased after stroke, this response was not different between young and aged animals. However, I did detect increased lectin⁺ matrix and integrin- α 5 expression in aged animals with stroke. Both of these proteins directly interact with fibronectin within the basement membrane. Given that fibronectin is a highly modular protein that is subject to alternative splicing, post-translational modification and fibrillogenesis, the “quality” of fibronectin, rather than the “quantity,” may change with aging. Further work with targeted mass spectrometry is needed to sequence fibronectin and determine if any of its domains are being altered with aging, and whether this can enhance its affinity for A β ₁₋₄₀ in aged animals with stroke.

Overall, I found that stroke chronically alters basement membrane morphology and composition in a way that strongly resembles CAA plaques. These changes are characterized by increases in lectin⁺ matrix and fibronectin content, within foci of basement membrane thickening. Targeting these early changes may help to reduce CAA in stroke survivors.

4.4.3: Fibronectin may trap A β ₁₋₄₀ within the basement membrane by multiple mechanisms.

I found that CSF A β ₁₋₄₀ selectively deposited in regions of thickened basement membrane, which displayed high levels of lectin⁺ matrix, fibronectin and integrin- α 5. Furthermore, I also found that treatment with fibronectin increases CSF A β ₁₋₄₀ deposition within superficial cortical layers (**Fig. 5**). Finally, I confirmed these findings in a cell-free *in vitro* assay, where I found that fibronectin binds A β ₁₋₄₀ with high affinity. Fibronectin may impact multiple physiological factors that could play a role in determining the degree to which CSF A β ₁₋₄₀ becomes deposited in the aged brain, which might be further altered with

brain injury such as stroke. In particular, fibronectin may alter several distinct factors that modulate the diffusion of $A\beta_{1-40}$ through the extracellular space (Reviewed in Syková & Nicholson, 2008).²⁰²

First, there is significant evidence that astrogliosis increases the geometric tortuosity of brain tissue, which may also apply to the basement membrane.^{212,262,263} I found that areas of increased fibronectin expression also exhibited increased numbers of GFAP⁺ perivascular reactive astrocytes (see Chapter 5), which may act as a cellular barrier to the diffusion of $A\beta$, effectively ‘trapping’ it within the PVS. Second, post-stroke angiogenesis, which also involves fibronectin, may induce the focal trapping of CSF solutes by increasing the volume of physiologic dead space within the PVS (i.e. regions that do not participate in CSF flow). I found that stroke increased the thickness of the lectin-stained basement membrane, which also exhibited increased branching and lacunarity. Third, fibronectin overexpression may increase the viscosity of the basement membrane, which could trap CSF $A\beta_{1-40}$. Previous work has shown that cortical stab wound in rats leads to local astrogliosis and increased deposition of numerous ECM proteins throughout the injured hemisphere, although fibronectin levels were not examined.²⁶⁴ However, the above factors appear to play a minor role in $A\beta_{1-40}$ deposition due to the fact that we did not observe the same increases in size-matched dextran levels, as examined the preceding chapter. This points to a specific property of $A\beta_{1-40}$ that is independent of molecular weight, which we investigated in the present experiments.

Rather than exploring these more nonspecific mechanisms, we evaluated whether fibronectin was a novel ECM receptor for CSF $A\beta_{1-40}$, which could explain the unique pattern of deposition that we observed in the basement membrane. Increased fibronectin may

positively charge the basement membrane,²⁶⁵ which could contribute to selective binding of negatively charged CSF proteins, such as A β ₄₀ peptide (pI = 5.17). Under normal conditions, the basement membrane retains a negative charge due to the high glycosaminoglycan content.²⁴¹ This protective effect may be lost following injury due to increases in positively charged proteins, including fibronectin, although this may be balanced in some regions with increases in HSPG content, although this would need to be verified by more specific staining.

Due to its charge, numerous potential binding sites and its central role in the assembly of the basement membrane, increases in fibronectin may selectively mediate the deposition of CSF A β ₁₋₄₀ by direct binding. Previous work has shown that plasma fibronectin binds aggregated amyloid proteins via the Type 1 domain, and colocalizes with amyloid plaques in human AD brain sections.²¹⁷ I newly found that fibronectin bound soluble A β ₁₋₄₀ *in vitro* with high affinity, and that these conjugates deposited more readily within the murine basement membrane than free A β ₁₋₄₀. This suggested an additional binding partner, which I identified as integrin- α 5, which strongly colocalized with the distribution of A β ₁₋₄₀ in all conditions. Overall, these data indicate that fibronectin binds soluble A β ₁₋₄₀, which then becomes sequestered in the basement membrane by binding to integrin- α 5. These interactions most likely occur via Type I and Type III fibronectin domains, respectively. However, more work with specific blocking antibodies or fibronectin mutants are required to confirm the specific amino acid residues that are involved in this process.

This work clearly establishes the role of fibronectin and integrin- α 5 in contributing to the *initial phases* of post-stroke CSF A β ₁₋₄₀ deposition via direct binding to the A β ₁₋₄₀ peptide, especially in aged animals. While other factors such as increased cellularity, dead space and viscosity generally impair the bulk flow of solutes deep into the brain, within the

superficial layers of cortex, I found that even low levels of bulk flow supported abnormal $A\beta_{1-40}$ deposition within peri-infarct vessels.

CHAPTER 5

TGF- β Stimulates A2 Astrocytes to Remodel the Basement Membrane and Impair the Perivascular Flow of CSF After Stroke

5.1: Introduction

5.1.1: Overview.

The results outlined in the preceding chapters demonstrate that aging and stroke simultaneously impair the bulk flow of CSF and induce the perivascular deposition of CSF-derived A β ₁₋₄₀. They further indicate that fibronectin/integrin- α 5 complexes contribute to this phenomenon by sequestering soluble CSF A β ₁₋₄₀ within the basement membrane, and that they may also act as a physical barrier to perivascular CSF flow. Importantly, these complexes could be expressed by perivascular astrocytes, providing a link between reactive astrogliosis, abnormal AQP4 expression and A β ₁₋₄₀ deposition. However, it is not known how stroke and TGF- β alters the phenotype of perivascular astrocytes, or whether these ubiquitous cells are the major source of fibronectin and integrin- α 5 expression after stroke.

5.1.2: Significance.

Astrocytes are the most common glial cell in the brain,²⁶⁶ and are in direct communication with neurons,²⁶⁷ oligodendrocytes,²⁶⁸ microglia²⁴⁰ and blood vessels.⁹¹ In addition to maintaining homeostasis under normal conditions,²⁶⁹ astrocytes possess a pre-programmed response that becomes activated with neuroinflammatory insults,²⁴⁰ including brain injuries such as stroke, termed ‘reactive astrogliosis.’²³⁹ When exposed to noxious stimuli, astrocytes upregulate a set of ‘pan-reactive’ genes, including increased expression of

intermediate filaments such as GFAP and vimentin,²³⁹ which allow the astrocytes to orient towards the site of inflammation, hypertrophy and form a glial scar to contain the source of the stimulus.²⁷⁰ These responses may become dysregulated with aging, necessitating the use of aged animal models to develop therapies that reflect the average human stroke patient.

Exciting new research suggests that astrocytes can tune their responses to the specific type of injury, generally falling into two broad polarization states, termed ‘A1’ and ‘A2’.²³⁹ The so-called ‘A1’ astrocytes are stimulated via microglial secretion of pro-inflammatory cytokines, including interleukin-1 β (IL-1 β), interleukin-6 (IL-6) and tumor necrosis factor- α (TNF- α), which induce a set of genes that impairs their ability to regulate synaptic function, inhibits AQP4 polarization to astrocytic endfeet, alters their production of ECM products, and causes the secretion of as-yet undiscovered products that cause direct neurotoxicity.²⁴⁰ In addition to these acute responses, baseline A1 activation also increases over the course of normal aging, and could further impact the responses of the aged brain to acute neuroinflammation.²⁷¹

Surprisingly, following middle cerebral artery occlusion (MCAO) in young animals, astrocytes instead take on an ‘A2’ phenotype,²³⁹ but comparatively little is known about their functionality or regulation. Unlike A1 astrocytes, A2 astrocytes could be stimulated by pure hypoxia, or require co-stimulation with other cytokines, such as TGF- β , to effectively make this transition to an A2 phenotype. Furthermore, while it is tempting to ascribe a ‘beneficial’ role for A2 astrocytes in brain injury, there is no definitive evidence to support this notion. As such, the functionality of the A2 astrocyte still needs to be elucidated by more mechanistic studies. Even if A2 astrocytes play a beneficial role in young animals, these responses may also change in the aged brain, which alters the extracellular microenvironment

in numerous ways, including a predisposition to increased TGF- β signaling and A β pathology. Overall, more research is needed to better understand how A2 astrocytes shape their responses to ischemia, and whether this changes with aging.

TGF- β has been shown to reverse the activation of A1 astrocytes,²⁴⁰ returning them to a more undifferentiated, ‘pan-reactive’ state. However, TGF- β signaling may play a different role in ischemia-activated A2 astrocytes. Previous work indicates that TGF- β levels are elevated in mouse models of CAA,²¹⁸ and that overexpression of TGF- β in wild-type mice leads to reactive astrogliosis, fibronectin expression and microvascular damage.^{219,220} Previous work in young animals has shown that knockout of astrocytic TGF- β signaling has been shown to reduce astrocyte activation and inhibit the formation of a GFAP⁺ glial scar after stroke, but this was associated with worse functional recovery.²²⁹ This suggests that A2 astrocytes may respond differently to TGF- β than their A1 counterparts, instead being stimulated by TGF- β , rather than inhibited. This responsiveness to TGF- β may also differ in aging, as they shift to a more A1 phenotype at baseline.²⁷¹ It is not known how TGF- β antagonism affects astrocyte activation or functional recovery in the aged animals with stroke, who may be more sensitive to its negative, pro-fibrotic effects.^{223,233}

Following stroke, aging could alter the specific levels of different TGF- β isoforms, or shift the balance of downstream signaling pathways, such as the canonical Smad signaling cascade.²²¹ While previous work has focused on post-stroke Smad2 activation by phosphorylation,²²³ Smad3 is actually the major Smad isoform that is involved in modulating protein expression via direct binding to DNA.²⁷² Phosphorylated Smad3 levels have been previously shown to disproportionately increase with fibrotic diseases in aged animals, including pulmonary fibrosis²⁷³ and skeletal muscle degeneration.²⁷⁴ Furthermore, Smad3

knockout has been shown to reduce renal and cardiovascular fibrosis, and improve function, in a mouse model of renovascular hypertension.²⁷⁵ Similar results were found in a mouse model of hepatic fibrosis, with Smad3 knockouts exhibiting reduced fibrosis after liver injury.²⁷⁶ In the brain, Smad3 induces APP expression by astrocytes, due to binding to the zinc finger nuclear factor, CTCF.²⁷⁷ Furthermore, inhibiting Smad2/3 activation in innate immune cells prevented the formation of amyloid pathology in Tg2576 mice, an animal model of Alzheimer's disease.²⁷⁸ While much of this data indicates that TGF- β -Smad3 signaling is a major driver of fibrosis in age-related diseases, it is not known how this pathway impacts the function of perivascular astrocytes in aging or stroke, and whether this is specifically associated with altered AQP4 expression and basement membrane fibrosis. As we described in the preceding chapter, these changes in the perivascular niche may sensitize the brain to the development of CAA by reducing perivascular CSF flow and increasing the affinity of the basement membrane for CSF A β ₁₋₄₀.

Overall, the role of TGF- β during brain injury remains controversial, and the few studies performed in aged animals suggest a detrimental effect of astrocytic TGF- β signaling. Astrocytic endfeet form the outer wall of the PVS, and regulate the composition of the outer basement membrane, which is involved early in the pathogenesis of CAA.^{181,196} Furthermore, reactive astrocytes are associated with impaired CSF flow during normal aging,²³⁵ multiple microinfarction,^{236,237} traumatic brain injury²³⁵ and Alzheimer's disease.^{209,238} However, the relationship between TGF- β , perivascular astrocytes and perivascular CSF flow is not well understood. Additionally, dysregulated TGF- β signaling, which may occur after stroke in the aged brain,²²³ could further impact A2 responses to ischemic injury and induce the abnormal production of ECM proteins, such as

fibronectin/integrin- α 5 complexes. Therefore, I hypothesize that TGF- β signaling in aging stimulates A2 astrocytes to further impair AQP4-mediated water uptake and increase basement membrane fibrosis. I further hypothesize that inhibiting TGF- β signaling will improve perivascular CSF flow and reduce CSF A β ₁₋₄₀ deposition in aged mice with DMCAO.

5.1.3: Experimental design.

Our first aim was to fully evaluate the molecular and cellular mediators underlying basement membrane remodeling and alterations in CSF flow after stroke. Therefore, we first hypothesized that aging worsens post-stroke reactive gliosis due to altered TGF- β signaling. We further hypothesized that TGF- β activates A2 astrocytes to secrete fibronectin and downregulate AQP4 expression, two major factors that impact perivascular CSF flow. To test this hypothesis, we first performed DMCAO and examined GFAP, vimentin, AQP4, Smad2/3 phosphorylation and TGF- β levels at 7 DPI. Then, we cultured primary cortical astrocytes from both P1 wild-type pups, and examined how oxygen glucose deprivation (OGD), an *in vitro* model of ischemia,²⁵⁷ differentially impacts activation and phenotype by gene microarray, western blot and immunocytochemistry (ICC). Next, we examined whether TGF- β and A β ₁₋₄₀ co-stimulation induced changes in gene/protein expression by the same methods, and additionally examined how they affected *in vitro* FITC-A β ₁₋₄₀ deposition and ³H₂O uptake. Finally, we verified our results *in vivo* and measured whether intracisternal TGF- β injection increased perivascular gliosis, fibronectin expression and reduced the bulk flow of CSF (measured by intracisternal injection of ³H₂O and ¹⁴C-Inulin).

We next hypothesized that TGF- β signaling to astrocytes is the major driver of basement membrane fibrosis and reductions in CSF flow after stroke. To test this hypothesis *in vivo*, we first performed DMCAO in young and aged wild-type mice, and measured astrocyte reactivity and TGF- β expression after stroke. To explore the potential translational relevance of global TGF- β inhibition, we performed DMCAO in aged mice and treated them with a continuous peripheral infusion of a TGF- β R1/R2 antagonist (GW788388 Hydrate), then measured the impact of chronic treatment on histology, physiology and functional outcomes.

5.2: Methods

5.2.1: Animals.

All assays were performed using tissues and cells derived from *Mus musculus* (C57/Bl6). For aging studies, young (3 month-old, Charles River) and aged (20 month-old, National Institute of Aging) wild-type male mice were obtained and housed simultaneously within UT Health for at least 2 weeks prior to beginning any experiments. In all cases, mice were fed standard dry chow *ad libitum*, and kept on a 12-hour light-dark cycle. Additionally, mice were examined regularly by the veterinary staff, as well as trained members of the lab for any signs of illness following DMCAO, or gross pathology following sacrifice. All protocols were approved by the UTHealth IACUC and carried out in an AAALAC-approved facility. Finally, animals were randomized to experimental conditions, and investigators were blinded to treatment.

5.2.2: Experimental stroke model.

Permanent DMCAO was performed as described in Chapter 4. Briefly, mice were anesthetized with isoflurane, the dorsolateral cranium was incised and a burr hole was drilled to expose the MCA. Following brief MCA cauterization to induce ischemia, the burr hole was closed with dental cement, and the incision sutured. Sham surgeries were performed without cauterization. All surgeries were performed under aseptic conditions, and mice were periodically monitored for signs of pain, infection or weight loss following the procedure.

5.2.3: Animal sacrifice.

Mice were deeply anesthetized with Avertin (250 mg/kg), then the ventral abdomen was incised and the ribcage was reflected to expose the heart muscle. An 18-gauge butterfly needle was then placed into the left ventricle, and the right atrium opened with a small incision. Mice were perfused with ice-cold PBS supplemented with 0.2% heparin using an automated pump set to a rate of 10 mL/min, until draining perfusates became clear. For studies requiring fresh tissue, brains were then extracted, cortices dissected from underlying structures and then snap-frozen on dry ice for future assays. For studies requiring fixed tissue, mice were first perfused with ice-cold 4% PFA for 5 minutes, and brains were then extracted and post-fixed in 4% PFA at room temperature for 24 hours, then dehydrated/stored in 30% sucrose at 4°C prior to sectioning.

5.2.4. Immunohistochemistry.

Fixed brain sections (24 µm thickness) were mounted onto slides, then washed for 3 x 5 minutes in wash buffer (Tris Buffered Saline + 0.1% Tween). Following this, heat-mediated antigen retrieval was performed in 100 mM Sodium Citrate buffer + 0.1% Tween at 95°C for 20 minutes in a vegetable steamer. Slides were washed 3 x 5 minutes, then incubated for 2 hours in blocking buffer (wash buffer supplemented with 0.5% Triton-X, 1% BSA and 5% normal goat serum) for 2 hours. Then, slides were incubated in blocking buffer with anti-GFAP-Cy3 (Mouse, 1:1000, Millipore Sigma, *cat. C9205*), *Lycopersicon esculentum* lectin (1:100, Vector Laboratories, *cat. DL-1177*), anti-AQP4 (Rabbit, 1:5000, Millipore Sigma, *cat. HPA014784*), anti-integrin- α 5 (Rabbit, 1:100, abcam, *cat. EPR7854*) or anti-fibronectin (Rabbit, 1:100, abcam, *cat. ab2413*) antibodies. Then, slides were washed 3

x 5 minutes, then incubated with secondary antibodies in blocking buffer (anti-Rabbit (Goat, abcam, Alexa-Fluor, 1:500, $\lambda = 488, 594$ or 647 nm). Following a final 3 x 5 minute washing step, slides were submerged in Tris-Buffered Saline, then cover-slipped with Vectashield containing DAPI (Vector Laboratories, *cat. H-1200*).

5.2.5: Protein isolation, SDS-PAGE and western blotting.

The right cortex was thawed on ice and manually homogenized in buffer containing 1% NP-40, 1 mM PMSF, cOmplete (Roche) and PhosSTOP (Roche). Following sonication and centrifugation, the supernatant was removed and diluted to 4 mg/mL in 4x Laemmli Sample Buffer (Bio-Rad, *cat. 161-0737*) supplemented with 4% β -mercaptoethanol, then heated to 95°C for 5 minutes. Following sample preparation, 10 μ L (40 μ g) of each lysate was run on a 4-15% Criterion TGX 26-well gels (Bio-Rad, *cat. 5671085*) at 120V for 60 minutes. Protein bands were subsequently transferred to a PVDF membrane, blocked in 5% BSA or non-fat dry milk and probed with anti-fibronectin (Rabbit, 1:1000, abcam, *cat. ab2413*), anti- $\alpha 5$ Integrin (Rabbit, 1:1000, abcam, *cat. EPR7854*), anti-Vimentin (Rb, 1:1000, abcam, *cat. ab9257*), anti-GFAP (Rabbit, 1:500, Cell Signaling, *cat. 12389S*), anti-pSmad2/3 (Rabbit, 1:500, Cell Signaling, *cat. 8828S*), anti-Smad2/3 (Rabbit, 1:500, Cell Signaling, *cat. 8685S*), anti- β -actin (Mouse/HRP conjugated, 1:50,000, Sigma, *cat. A3854*) or anti-vinculin antibody (Rabbit, 1:10,000, abcam, *cat. EPR8185*). Blots were then probed with HRP-conjugated goat anti-rabbit secondary antibody (1:10,000, Vector Laboratories, *cat. PI-1000*) and imaged using a Bio-Rad ChemiDoc Imager.

5.2.6: Multiplex assays.

The absolute level of TGF- β 1 was quantified using a Bio-Plex Pro TGF- β 3-Plex Assay (Bio-Rad, cat. 171W4001M). Briefly, cortical lysates were diluted to 8 mg/mL in NP40 buffer, then underwent acid-mediated antigen retrieval and were further diluted in dH₂O to a final concentration of 1 mg/mL, and supplemented with 0.5% BSA. Plates were loaded and incubations/washes were performed according to the manufacturer's instructions. Following this, plates were read with the Luminex-based Bio-Plex 200 (Bio-Rad) using the manufacturer's protocol, and unknown values interpolated with the Bio-Plex Manager Software (Bio-Rad).

5.2.7: Cell culture techniques

- **Harvesting of primary cortical astrocytes.** Mouse pups (P1) were anesthetized on ice, cleaned with 70% ethanol, and decapitated. Then, under a laminar flow hood, brains were extracted from the cranium with blunt forceps and placed in sterile Hank's Balanced Salt Solution (HBSS, Ca²⁺/Mg²⁺-free) in a sterile 3 cm petri dish under a dissecting microscope. The meninges were then removed and the cortex was separated from the underlying brain structures with sharp forceps. Isolated cortices were then placed in fresh, sterile, ice-cold HBSS (Ca²⁺/Mg²⁺-free) prior to digestion. Once all cortices were harvested, the tissue was placed in enzymatic digestion buffer (MACS Neural Dissociation Kit [\sim 400 μ L/brain]), manually disrupted by passing through a P200 pipet tip 15-20 times, and then digested for 30 minutes at 37°C. Digests were visually inspected for any remaining clumps, and passed through a P200 pipet tip an additional 15-20 times until a grossly homogenous solution was obtained.

The enzymes were then quenched via the addition of 600 μL of HBSS (with $\text{Ca}^{2+}/\text{Mg}^{2+}$) per brain, and the total mixture was then centrifuged at 600 x g for 10 minutes at room temperature. Cells were washed with 1 mL HBSS, centrifuged and then resuspended in 1 mL cell culture media (Dulbecco's modified eagle medium [DMEM], 10% Fetal Bovine Serum [FBS], 1% Penicillin-Streptomycin) per brain. Cells were then stained with Trypan Blue and counted using the Countess II Automated Cell Counter (Thermo Fisher). Finally, cells were then diluted and plated on Poly-D-Lysine-coated 12-well plates or glass cover slips at a density of $\sim 2 \times 10^5$ live cells/well.

- ***Maintenance and purification of primary astrocytes.*** At 1 day *in vitro* (1 DIV), the media was changed to remove dead cells and other debris, then replaced once weekly until the completion of experiments. Cells were examined periodically to monitor growth and check for signs of bacterial or fungal contamination. Following confluence of the astrocyte monolayer, the remaining microglia were then depleted at 14 DIV by exposure to a 50 mM solution of leucine methyl ester (pH = 7.4) for 2 hours, as previously described.²⁷⁹ To further increase the efficacy of the depletion, plates were then shaken at 200 revolutions per minute (RPM) for 4 hours at 37°C, and the media exchanged. The following day, the media was changed again to remove any floating (dead) microglia, and the astrocyte monolayer was visually inspected under polarized light to confirm successful microglial depletion (fewer than 5% of visible cells by area).

- ***Oxygen-glucose deprivation and peptide stimulation.*** Oxygen-glucose deprivation (OGD) and peptide stimulation experiments were carried out at 19 – 21 DIV in a balanced salt solution (BSS) containing 125 mM NaCl, 5 mM KCl, 1.2 mM NaH₂PO₄, 26 mM NaHCO₃, 1.8 mM CaCl₂, 0.9 mM MgCl₂, 10 mM 4-(2-hydroxyethyl)-1-piperazineethanesulfonic acid (HEPES), supplemented with 10 mM glucose for normoxic (NO) controls. Cultures were washed with NO or OGD media 3 times prior to the experiment to remove any serum or antibiotics present in the normal culture media. Recombinant human TGF-β1 (Peprotech) and Aβ₁₋₄₀ (Anaspec) was reconstituted in BSS, then diluted to a working concentration of 3 ng/mL and 10 μM, respectively. Immediately prior to OGD, media was equilibrated with 5% CO₂ balanced with nitrogen. Following the addition of equilibrated media, cells were placed in a warmed hypoxic chamber and OGD performed for 6 hours. Then, cells were re-oxygenated and either placed on ice and immediately harvested (acute studies), or culture media was supplemented with 10 mM glucose and cells were allowed to survive for 18 hours at 37°C (chronic studies).
- ***Isolation of protein from primary cells.*** Cells were lysed in 200 μL radioimmunoprecipitation assay buffer (RIPA) buffer (Sigma) supplemented with 1 mM PMSF (Sigma), cOmplete (Roche) and Phos-Stop (Roche). Cells were manually disrupted with a P200 pipet tip, then sonicated on ice for 10 seconds. Lysates were then centrifuged at 18,000 x g for 20 minutes at 4°C. Finally, supernatants were removed, aliquoted and stored at -80°C prior to further assays.

- ***Astrocytic $^3\text{H}_2\text{O}$ uptake studies.*** Primary astrocytes were washed 3 x 5 minutes in BSS with glucose, then exposed to 1×10^6 CPM of $^3\text{H}_2\text{O}$ at 37°C for 30 minutes at room temperature. Exposing empty wells to $^3\text{H}_2\text{O}$ controlled for background radioactivity and nonspecific binding of $^3\text{H}_2\text{O}$ to the culture vessel. Then, cells were rapidly washed with fresh BSS and immediately lysed in Solvable (see *Liquid scintillation counting* methods).
- ***Astrocytic $\text{A}\beta_{1-40}$ uptake studies.*** Coverslips containing live cells were incubated in NO/OGD culture media supplemented with $2 \mu\text{M}$ FITC- $\text{A}\beta_{1-40}$ or PBS control at 37°C for 30 minutes. Following this, coverslips were washed 3 times with PBS, then fixed with 4% PFA for 10 minutes. Fixed coverslips were stored at 4°C in PBS prior to ICC and imaging studies.
- ***Immunocytochemistry.*** Coverslips were first washed with wash buffer (50 mM Tris-HCl buffer [pH = 7.8]) 3 x 5 minutes. Then, heat-mediated antigen retrieval was performed in 100 mM Sodium Citrate buffer + 0.1% Tween at 95°C for 5 minutes in a microwave oven (10% power). After cooling to room temperature, coverslips were again washed 3 x 5 minutes in wash buffer, then blocked with triton-carrageenan-TBS (TCT) solution (1% Carrageenan, 0.5% Triton-X) for 30 minutes at room temperature. Next, coverslips were incubated overnight at 4°C with primary antibodies (GFAP, 1/1000; AQP4, 1/500; Fibronectin, 1/500; and/or Integrin- $\alpha 5$, 1/500). The following day, coverslips were washed 3 x 5 minutes with detergent wash buffer (50 mM Tris-HCl buffer + 0.1% Triton-X [pH = 7.8]), then incubated with anti-Rabbit secondary antibodies (1/1000) in TCT for 1 hour at room temperature. After washing for 3 x 5 minutes with detergent wash buffer, coverslips

were then submerged in regular wash buffer, then dipped in dH₂O and mounted with Vectashield + DAPI (Vector Laboratories), then sealed with nail polish. Slides were allowed to cure for 3 days at 4°C prior to imaging. To control for potential background fluorescence, secondary controls were exposed to identical conditions, except for incubation with the secondary antibody.

- ***Isolation of RNA from primary cells.*** RNA was harvested and purified using the RNEasy Mini Kit (Qiagen) according to the manufacturer's instructions. Briefly, cells were directly lysed by immersion in lysis buffer supplemented with 1% β-mercaptoethanol. Then, lysates were transferred to eppendorf tubes and thoroughly vortexed at high speed to ensure complete lysis of cells. Next, ethanol was added to a concentration of 35% and the mixture transferred to the RNEasy spin column. Following DNase treatment and repeated washes, RNA was then eluted into RNase free water, then stored at -80°C prior to use.

5.2.8: Synthesis of complementary DNA.

Complementary DNA (cDNA) was generated using the iScript cDNA Synthesis Kit (Bio-Rad) according to the manufacturer's instructions. Briefly, in each sample, messenger RNA (mRNA) quality and content was estimated by measuring absorbance (260/280 nm) with the Nanodrop 2000 (Thermo Fisher), and then concentrations were normalized by dilution with RNase-free dH₂O. Then, 25 µg of RNA was loaded into the cDNA synthesis reaction containing 4 µL of RT supermix. These mixtures were then incubated in a thermal cycler (Bio-Rad, CFX96 Touch) for 5 minutes at 25°C (priming step), then 20 minutes at 42°C (reverse transcription step), then 5 minutes at 85°C (RT inactivation step), and finally

cooling to 4°C. Following this, the newly synthesized cDNA was then transferred to a fresh eppendorf tube and stored at -80°C prior to performing qPCR assays.

5.2.9: qPCR measurement of gene expression.

Gene expression was measured using custom PrimePCR Microarrays (Bio-Rad). To carry out each assay, cDNA samples were diluted 1:1 with dH₂O, then 19 µL of diluted cDNA was mixed with 331 µL of dH₂O and 350 µL of SYBR green (Bio-Rad) to a final volume of 700 µL. Then, 10 µL of this mixture was loaded into wells pre-loaded with primers (**Table 6-1**), a genomic DNA control, two RNA quality controls, a no reverse transcriptase control or a PCR positive control. Then, reactions were incubated in a thermal cycler (Bio-Rad CFX384 Touch), and gene expression measured over 39 cyclic amplification steps, according to the manufacturer's instructions.

| Gene Information | | Assay Information | | |
|------------------|--|-------------------|--------|-----------------|
| Symbol | Gene Name | Assay ID | Length | Design |
| Agri | agrin | qMmuCID0006603 | 70 | Intronic |
| Amigo2 | adhesion molecule with Ig like domain 2 | qMmuCED0049592 | 99 | Exonic |
| App | amyloid beta (A4) precursor protein | qMmuCID0017777 | 88 | Intron-spanning |
| Aspg | asparaginase homolog (S. cerevisiae) | qMmuCID0027304 | 161 | Intron-spanning |
| B3gnt5 | beta-1,3-N-acetylglucosaminyltransferase 5 | qMmuCED0039654 | 120 | Exonic |
| Ccl11 | chemokine (C-C motif) ligand 11 | qMmuCED0044849 | 83 | Exonic |
| Cd109 | CD109 antigen | qMmuCED0049647 | 74 | Exonic |
| Cd14 | CD14 antigen | qMmuCED0049648 | 99 | Exonic |
| Cd44 | CD44 antigen | qMmuCED0061009 | 86 | Exonic |
| Clcf1 | cardiotrophin-like cytokine factor 1 | qMmuCED0040924 | 94 | Exonic |
| Col16a1 | collagen, type XVI, alpha 1 | qMmuCID0024725 | 167 | Intron-spanning |
| Cp | ceruloplasmin | qMmuCED0045372 | 89 | Exonic |
| Cxcl10 | chemokine (C-X-C motif) ligand 10 | qMmuCED0049500 | 84 | Exonic |
| Cxcl13 | chemokine (C-X-C motif) ligand 13 | qMmuCID0006355 | 118 | Intron-spanning |
| Cxcl16 | chemokine (C-X-C motif) ligand 16 | qMmuCED0044879 | 96 | Exonic |
| Emp1 | epithelial membrane protein 1 | qMmuCED0038081 | 115 | Exonic |
| Fbln5 | fibulin 5 | qMmuCED0044306 | 77 | Exonic |
| Fkbp5 | FK506 binding protein 5 | qMmuCED0046340 | 84 | Exonic |
| Fn1 | fibronectin 1 | qMmuCED0045687 | 61 | Exonic |
| Gapdh | glyceraldehyde-3-phosphate dehydrogenase | qMmuCED0027497 | 75 | Exonic |
| Gbp2 | guanylate binding protein 2 | qMmuCED0048024 | 74 | Exonic |
| Gfap | glial fibrillary acidic protein | qMmuCID0020163 | 107 | Intron-spanning |
| Ggta1 | glycoprotein galactosyltransferase alpha 1, 3 | qMmuCID0017837 | 108 | Intron-spanning |
| H2-D1 | histocompatibility 2, D region locus 1 | qMmuCED0041320 | 60 | Exonic |
| H2-T23 | histocompatibility 2, T region locus 23 | qMmuCED0040619 | 100 | Exonic |
| Hsbp1 | heat shock protein 1 | qMmuCED0038398 | 88 | Exonic |
| Hspg2 | perlecan (heparan sulfate proteoglycan 2) | qMmuCID0021282 | 119 | Intron-spanning |
| Iigp1 | interferon inducible GTPase 1 | qMmuCED0038266 | 77 | Exonic |
| Il6 | interleukin 6 | qMmuCED0045760 | 70 | Exonic |
| Il10 | interleukin 10 | qMmuCED0044967 | 84 | Exonic |
| Itga5 | integrin alpha 5 (fibronectin receptor alpha) | qMmuCID0015586 | 103 | Intron-spanning |
| Itgb1 | integrin beta 1 (fibronectin receptor beta) | qMmuCED0046395 | 89 | Exonic |
| Lcn2 | lipocalin 2 | qMmuCED0045799 | 64 | Exonic |
| Osmr | oncostatin M receptor | qMmuCID0005690 | 82 | Intron-spanning |
| Psmb8 | proteasome subunit, beta type 8 | qMmuCED0045963 | 114 | Exonic |
| Ptgs2 | prostaglandin-endoperoxide synthase 2 | qMmuCED0047314 | 107 | Exonic |
| Ptx3 | pentraxin related gene | qMmuCED0026777 | 105 | Exonic |
| S1pr3 | sphingosine-1-phosphate receptor 3 | qMmuCID0020240 | 190 | Intron-spanning |
| S100a10 | S100 calcium binding protein A10 (calpactin) | qMmuCED0049492 | 119 | Exonic |
| Sdc2 | syndecan 2 | qMmuCED0046013 | 97 | Exonic |
| Serpina3n | serine peptidase inhibitor, clade A, member 3N | qMmuCED0044644 | 90 | Exonic |
| Serping1 | serine peptidase inhibitor, clade G, member 1 | qMmuCED0060967 | 107 | Exonic |
| Sic10a6 | solute carrier family 10, member 6 | qMmuCID0027010 | 141 | Intron-spanning |
| Sphk1 | sphingosine kinase 1 | qMmuCED0040475 | 61 | Exonic |
| Spp1 | secreted phosphoprotein 1 | qMmuCED0061675 | 93 | Exonic |
| Srgn | serglycin | qMmuCID0009102 | 143 | Intron-spanning |
| Steap4 | STEAP family member 4 | qMmuCID0017408 | 119 | Intron-spanning |
| Tbp1 | TATA box binding protein | qMmuCID0040542 | 102 | Intron-spanning |
| Tgfb1 | transforming growth factor, beta 1 | qMmuCED0044726 | 116 | Exonic |
| Tgfb2 | transforming growth factor, beta 2 | qMmuCID0024408 | 108 | Intron-spanning |
| Tgfb3 | transforming growth factor, beta 3 | qMmuCED0045203 | 61 | Exonic |
| Tgfr1 | transforming growth factor, beta receptor I | qMmuCID0026554 | 80 | Intron-spanning |
| Tgm1 | transglutaminase 1, K polypeptide | qMmuCID0022777 | 169 | Intron-spanning |
| Thbs1 | thrombospondin 1 | qMmuCED0048851 | 105 | Exonic |
| Timp1 | tissue inhibitor of metalloproteinase 1 | qMmuCED0044729 | 92 | Exonic |
| Tm4sf1 | transmembrane 4 superfamily member 1 | qMmuCED0047458 | 113 | Exonic |
| Tnf | tumor necrosis factor | qMmuCED0004141 | 119 | Exonic |
| Uggt1 | UDP-glucose glycoprotein glucosyltransferase 1 | qMmuCID0005905 | 110 | Intron-spanning |
| Vim | vimentin | qMmuCED0046651 | 60 | Exonic |

Table 5-1. PCR assay design. Bio-Rad PrimePCR assays were selected and custom 384-well plates created to independently measure the expression of 54 genes.

5.2.10: Intracisternal injection protocols

- **TGF- β injections.** As described in Chapter 3, aCSF containing Na⁺ (150 mM), HCO₃⁻ (24.1 mM), K⁺ (3 mM), Ca²⁺ (1.4 mM), P (1.0 mM) and Mg (0.8 mM) was prepared in sterile Ultrapure Water. Then, recombinant human TGF- β 1 was reconstituted in aCSF at a concentration of 50 ng/ μ L and stored at -20°C prior to experiments. To perform the injection, mice were anesthetized with an intraperitoneal injection of Ketamine (120 mg/kg) and Xylazine (10 mg/kg), then placed in a stereotaxic frame. Following exposure of the dorsal neck musculature, the needle was inserted into the cisterna magna.¹²⁵ Then, TGF- β 1 or vehicle control was infused into the cisterna magna at a rate of 2 μ L/min over 5 minutes, after which mice were transferred to a warmed cage and allowed to survive for 24 hours prior to sacrifice.
- **Radiotracer injections.** For studies involving radioactive tracers, stock solutions of ¹⁴C-Inulin (Perkin Elmer, $\sim 2 \times 10^5$ CPM/ μ L) and ³H₂O (Perkin Elmer, $\sim 2 \times 10^6$ CPM/ μ L) were dissolved in aCSF and radioactivity normalized via liquid scintillation counting. Then, stock solutions were combined to a final concentration of 1×10^5 CPM/ μ L ¹⁴C-Inulin and 1×10^6 CPM/ μ L ³H₂O in aCSF. Tracer mixtures were kept on ice for up to 4 hours, then vortexed for 5 seconds immediately prior to infusion. Tracer was infused into the cisterna magna at a rate of 2 μ L/min over 5 minutes, after which mice were transferred to a warmed cage. Finally, 30 minutes after beginning the injection, mice were sacrificed by Avertin overdose (250 mg/kg). For radiouptake measurement, fresh brains were extracted and cortex isolated, then snap frozen and stored at -80°C for later processing.

- ***Fluorescent tracer injections.*** For studies involving fluorescent tracers, lyophilized FITC-A β_{1-40} (100 μ M stock, Anaspec) and lysine-fixable 3 kD TR dextran (TR-d3, 3,000 MW, 4% stock, Thermo Fisher) were subsequently dissolved in aCSF, then combined to a final solution of 10 μ M FITC-A β_{1-40} and 2% TR-d3. In all cases, tracer mixtures were kept on ice for up to 4 hours, then vortexed for 5 seconds immediately prior to infusion. Tracer was infused into the cisterna magna at a rate of 2 μ L/min over 5 minutes, after which mice were transferred to a warmed cage. Finally, 30 minutes after beginning the injection, mice were sacrificed by Avertin overdose (250 mg/kg). Then, transcardial perfusion with 0.2% heparin-PBS, and 4% PFA was performed, and brain tissue was then removed and stored in 4% PFA for subsequent processing.

5.2.11: Alzet pump implantation.

To administer the equivalent of \sim 10 mg/kg/day dosage of TGF- β R1/R2 antagonist (GW788388 Hydrate), 10 mg of lyophilized GW788388 Hydrate was reconstituted in a solution of 50% DMSO, 12.5% ethanol and 37.5% water, then loaded into implantable Alzet mini osmotic pumps according to the manufacturer's instructions. Additional sets of pumps were loaded with vehicle solution to serve as controls. Then, mice were anesthetized with isoflurane and the pump implanted subcutaneously over the dorsal back musculature. Following surgery, mice were examined daily for any signs of infection or excessive weight loss.

5.2.11: Liquid scintillation counting.

Samples were thawed on ice, then placed in 5 mL glass vials and dissolved in 1 mL Solvable (Perkin-Elmer) overnight at 37°C. Then, homogenates were vortexed and mixed with 4 mL Hionic-Fluor scintillation cocktail (Perkin-Elmer). Following this, β -emissions were measured using a Tri-Carb LSC (Perkin-Elmer), with $^3\text{H}_2\text{O}$ emissions counted at less than 20 keV, and ^{14}C -Inulin measured counted between 20 and 150 KeV. Control vials containing aCSF alone, aCSF + ^{14}C -Inulin and aCSF + $^3\text{H}_2\text{O}$ were used to account for background radiation, as well as to normalize emission signals from samples for subsequent analyses.

5.2.12: Fluorescent microscopy and tracer imaging.

Following perfusion, brains were extracted and post-fixed for 24 hours in 4% PFA. Then, brains were dehydrated in 30% sucrose, frozen to -20°C and sectioned to 24 μm (IHC/cresyl violet staining) or 100 μm (tracer quantification) sections. Sections were then mounted onto slides and coverslipped. For experiments involving colocalization with lectin, sections were first stained with *Lycopersicon esculentum* (Tomato) lectin (see *Immunohistochemistry*). Sections were imaged under fluorescence with a Leica DMI8 microscope at 10X magnification. A blinded investigator imaged the lateral cortex (0.38 mm anterior to Bregma, 2.5 mm lateral, 1.5 mm deep). Then, 100 μm Z stack images were obtained, and maximum intensity projections performed with LAS X software. Images were then quantified in ImageJ (see *Data Analysis*).

5.2.13: *DigiGait*.

The impact of aging, stroke and genetic/pharmacological manipulation on motor function was assessed using DigiGait (Mouse Specifics) at 6 and 13 DPI in a double-blinded manner. Mice were first acclimated to the system, and then the speed was gradually increased to 15 cm/second in young animals, and 10 cm/second in aged animals. Locomotion was recorded for 60 seconds, and then parameters of gait analyzed with DigiGait software.

5.2.14: *Data Analysis*.

- ***Quantification of protein expression.*** Intensity values for each band were measured using the Bio-Rad ImageAnalyzer software. Then, each intensity value was normalized by dividing it by the intensity of the loading control (either Vinculin or β -actin). Finally, these values were normalized to the mean value of the control group, plotted and statistically analyzed in Prism.
- ***Quantification of gene expression.*** Cycle threshold (CT) values for every gene of interest, loading control and quality control were first exported from Bio-Rad CFX software into Microsoft Excel. Given the large number of samples and genes involved (~3,840 assays), prior to further analysis, samples of poor quality were removed (~10%) based on the following pre-defined criteria: (1) presence of genomic DNA contamination, (2) poor RNA quality, (3) positive no RT control, or (4) loading control not detected. Then, relative gene expression was estimated by the following equation: $\Delta\Delta CT = (CT_1 - CT_{1/GAPDH}) - (CT_2 - CT_{2/GAPDH})$, where CT_1 is expression of the gene of interest in sample 1, CT_2 is the mean expression of the gene of interest

in the control samples (NO + Vehicle treated), and CT_{GAPDH} is the expression of the loading control (GAPDH). Since CT values are expressed on a logarithmic scale, to convert these values to fold-change, we then used the formula $Expression = 2^{-\Delta\Delta CT}$. After this last conversion step, fold-change values were imported into Prism, and any statistical outliers were removed on a gene-by-gene basis based on a positive Grubb's test (pre-determined threshold set at $p < 0.05$). Finally, to generate a heat map of genes related to astrocyte phenotype, expression values were Z-transformed based on the sample population mean and standard deviation (SD) for each individual gene.

- **Atrophy quantification.** High resolution images of cresyl violet-stained coronal brain sections (24 μm) were obtained. Then, ventricular volume and hemisphere size were quantified as previously described.^{255,256} Tissue atrophy percentage was calculated by the formula: $\% \text{ tissue loss} = 100 - ([\text{total ipsilateral tissue}/\text{total contralateral tissue}] \times 100)$.
- **Tracer intensity.** Tracer influx was quantified by measuring intensity as a function of tissue depth using ImageJ. Then, average intensity values were imported into Excel, and integrated into 50 μm bins. Absolute binned intensity values were then plotted as raw intensity (A.U.). To reduce experimental variability and further improve the quality of our data, tracer intensity in the injured hemisphere was then normalized to intensity in the contralateral hemisphere, and then converted to a percentage value prior to statistical analysis.
- **Immunohistochemical quantification.** IHC images were acquired and quantified in a double-blinded manner. Based on lectin staining, ROI's were drawn around 3 peri-infarct vessels/image across 3 brain sections for a total of 27 vessels/brain. Threshold

was held constant between brains, and the area and average pixel intensity of AQP4, GFAP, fibronectin and integrin- α 5 was measured relative to the ROI.

- **Statistics.** All statistical analyses were performed using Prism 7. Data are reported as mean (+/-) SEM with the number of animals/repetitions per group. When only two groups were compared, Student's t-test (two-tailed) was used to compare normally distributed data of equivalent variance, and Welch's correction was applied when data were normally distributed, but of unequal variance (denoted in figure legends). When three groups were compared, one-way ANOVA with Tukey's test for multiple comparisons was performed. When four or more groups were compared, two-way ANOVA with either Tukey's or Dunnet's test for multiple comparisons was utilized (denoted in figure legends). Asterisks indicate statistical significance levels based on the P-value: * $p < 0.05$, ** $p < 0.01$, *** $p < 0.001$.

5.3: Results

5.3.1: DMCAO produced widespread perivascular reactive astrogliosis that worsened with aging.

To first characterize how stroke alters perivascular astrocyte phenotypes *in vivo*, we performed DMCAO on young (3 month-old) animals and then examined their brains at 7 DPI by IHC (**Fig. 5-1A**). We found that DMCAO dramatically increased the expression of GFAP⁺ reactive astrocytes in the peri-infarct cortex, striatum and white matter, which was associated with major increases in lectin-stained glycosylated basement membrane components throughout vessels within the injured hemisphere (**Fig. 5-1A, i. - ii.**). We then performed high magnification 3-dimensional reconstruction of perivascular astrocytes and found that DMCAO also altered the morphology of glial endfeet, inducing widespread changes characterized by hypertrophy, increased GFAP expression and reduced AQP4 polarization (**Fig. 5A, iii. – viii.**).

Then, to assess whether aging also increased perivascular gliosis, we performed DMCAO in young (3 month) and aged (20 month) old animals, and similarly assessed astrocyte morphology (**Fig. 5-1B**). We found that aged animals with stroke exhibited further increases in GFAP expression within perivascular reactive astrocytes compared to their younger counterparts (**Fig. 5-1B, iv.**) Finally, to confirm age-induced changes in reactive gliosis quantitatively, we then obtained cortical lysates at 7 DPI and assessed the expression of both GFAP and vimentin, an additional marker of reactive gliosis, by western blot (**Fig. 5-1C, i.**). We found that aging ($F[1, 19] = 20.96, p < 0.001$) and DMCAO ($F[1, 19] = 50.75, p < 0.001$) both produced statistically significant increases in cortical GFAP expression, with a trending interaction effect between aging and DMCAO (**Fig. 5-1C, ii.**, $F[1, 19] = 3.51, p =$

0.076). Similarly, we also found that aging (**Fig. 5-1C, iii.**, $F[1, 18] = 11.17$, $p = 0.004$) and DMCAO ($F[1, 18] = 68.94$, $p < 0.001$) both increased vimentin expression within the cortex, with a significant interaction effect ($F[1, 18] = 8.85$, $p = 0.008$). Overall, these data indicate that stroke induces perivascular astrocyte reactivity, which worsens with aging. These stroke-induced changes are associated with altered basement membrane glycosylation and impaired AQP4 polarization to astroglial endfeet.

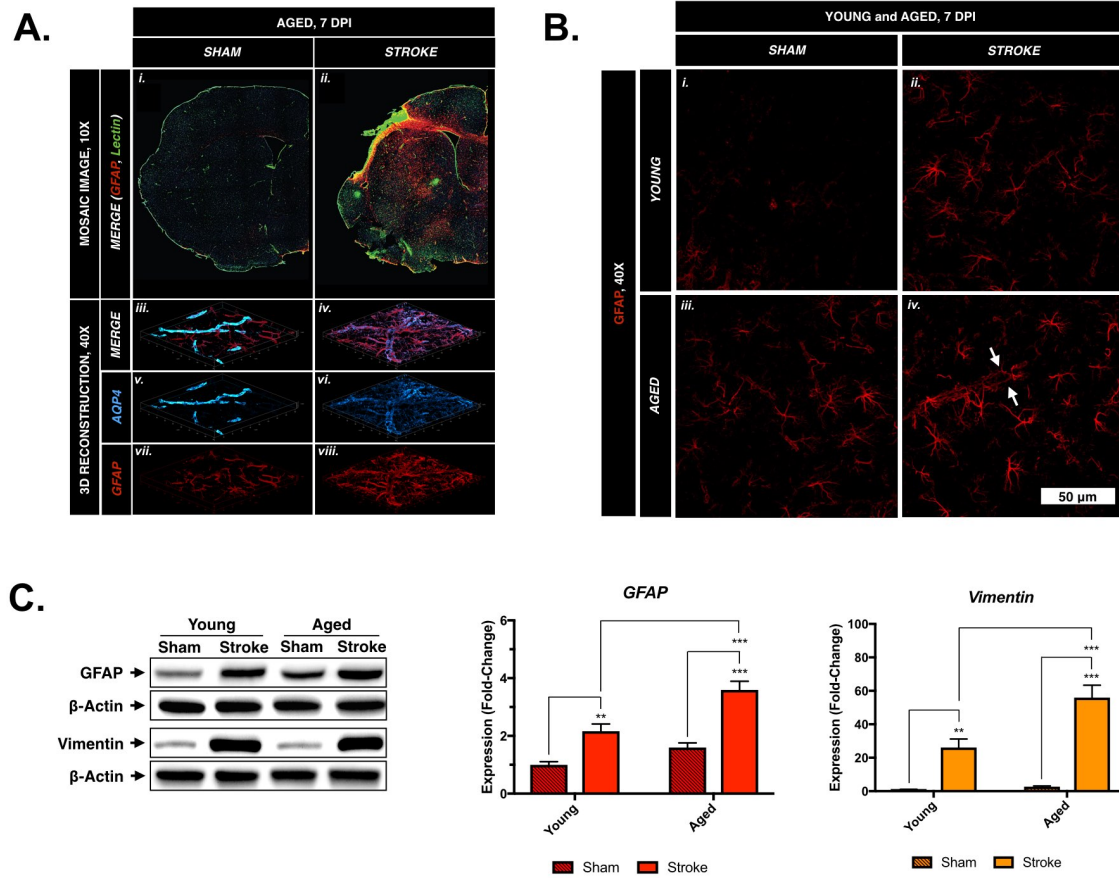


Figure 5-1. Reactive astrogliosis occurs after DMCAO and is worse in aged animals.

(A.) (i., ii.) Representative fluorescent mosaic micrographs from aged mice showing increased levels of lectin and GFAP staining throughout the injured hemisphere after DMCAO (7 DPI). (iii. – viii.) 3-dimensional reconstruction showing increased GFAP staining and reduced AQP4 polarization within the perivascular region following DMCAO in aged animals. (B.) Comparison of cortical GFAP staining outside of the ischemic penumbra between young and aged mice. White arrows denote high levels of perivascular GFAP staining in aged mice with DMCAO. (C.) Western blot analysis showed the highest levels of GFAP and Vimentin expression in aged mice with DMCAO. $n = 5 - 8$ mice per group. Data are analyzed by Tukey's post-hoc test for multiple comparisons. Significance: ** $p < 0.01$, *** $p < 0.001$. Scale Bar = 50 μ m.

5.3.2. DMCAO differentially induces TGF- β -Smad signaling pathways with aging.

Previous work has shown that stroke induces TGF- β signaling, which may increase with aging.²²³ However, there is limited data on how the absolute levels of individual TGF- β isoforms change after stroke in aged animals, or how downstream Smad phosphorylation is affected. We found that DMCAO increased TGF- β 1 levels at 7 DPI in both age groups ($F[1, 18] = 74.05, p < 0.001$), with no effect of aging (**Fig. 5-2A**). However, we observed that aging differentially affected downstream Smad2/3 phosphorylation by western blot (**Fig. 5-2B**). Total levels of phosphorylated Smad2 (phospho-Smad2) increased following DMCAO (**Fig. 5-2C, i.**, $F[1, 19] = 7.88, p = 0.013$), with a significant interaction effect between aging and DMCAO ($F[1, 19] = 11.84, p = 0.003$). In contrast, total levels of Smad2 significantly increased with aging (**Fig. 5-2C, ii.**, $F[1, 19] = 34.35, p < 0.001$), and reduced following DMCAO in aged, but not young animals (interaction, $F[1, 19] = 14.71, p = 0.001$). Relative Smad2 phosphorylation was lower in aged animals (**Fig. 5-2C, iii.**, $F[1, 19] = 9.79, p = 0.006$), with a trending increase in mice with DMCAO ($F[1, 19] = 2.81, p = 0.11$) and no significant interaction effect. In contrast, total levels of phospho-Smad3 increased with aging (**Fig. 5-2D, i.**, $F[1, 19] = 26.63, p < 0.001$), with a significant interaction between aging and DMCAO ($F[1, 19] = 16.03, p < 0.001$). There was also a weak interaction effect on total Smad3 levels (**Fig. 5-2D, ii.**, $F[1, 19] = 4.41, p = 0.049$), and a main effect of age on increasing Smad3 phosphorylation (**Fig. 5-2D, iii.**, $F[1, 19] = 7.06, p = 0.02$). Overall, these data indicate that Smad2 signaling predominates in young animals with DMCAO, while Smad3 signaling may play a more prominent role in aged animals.

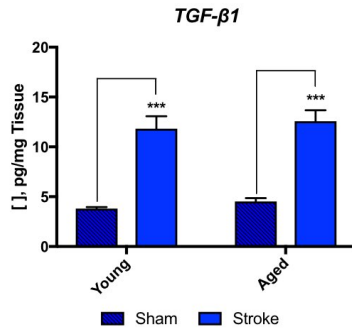
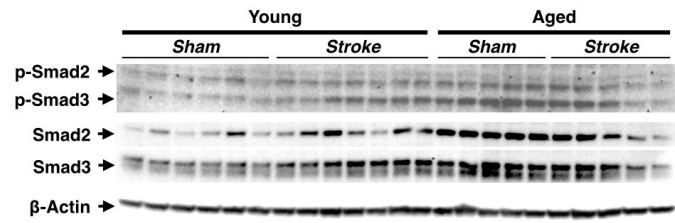
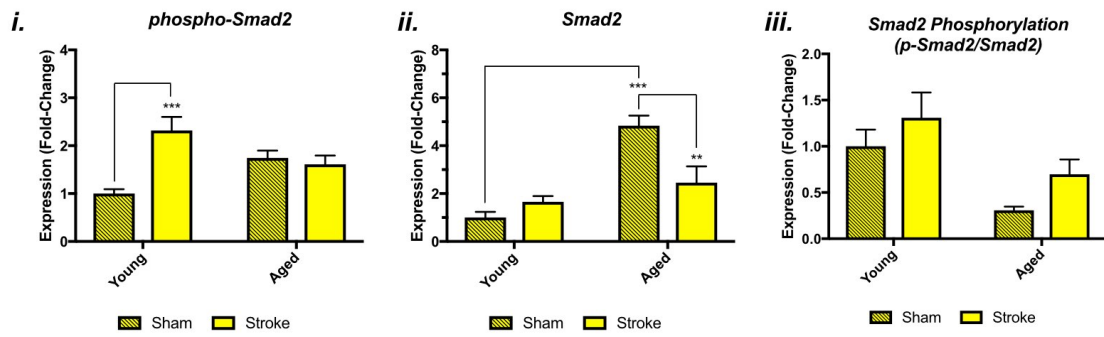
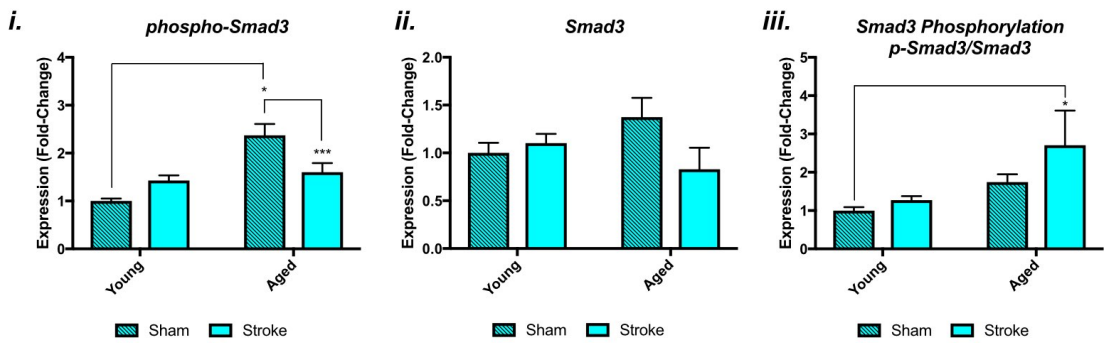
A.**B.****C.****D.**

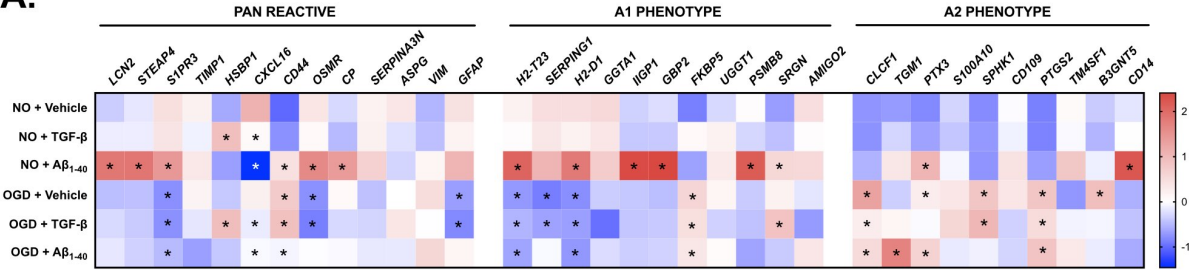
Figure 5-2. TGF- β signaling is differentially activated by aging and DMCAO. (A.)

Cortical TGF- β 1 levels similarly increase after DMCAO in young and aged mice. $n = 5 - 8$ per group. **(B.)** Representative western blot images of Smad proteins. **(C., D.)** Smad2 phosphorylation is higher in young animals, while Smad3 phosphorylation predominates in aged animals. $n = 5 - 7$ per group. Data are analyzed by Tukey's post-hoc test for multiple comparisons. Significance: $*p < 0.05$, $**p < 0.01$, $***p < 0.001$.

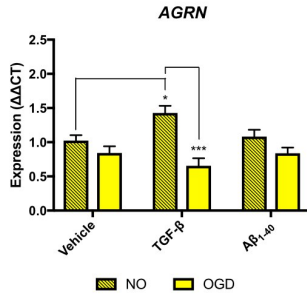
5.3.3. Exposure to OGD, TGF- β and A β_{1-40} acutely impact astrocyte polarization, ECM production and cytokine expression in vitro.

Previous studies have shown that a significant number of reactive astrocytes take on an ‘A2’ phenotype after stroke *in vivo*,²³⁹ but the relative effects of hypoxia, TGF- β and A β_{1-40} on the post-stroke induction of A2 astrocytes is not known. Therefore, we evaluated whether OGD, an *in vitro* model of ischemic stroke, would stimulate the transcription of A2 genes. We further hypothesized that this transition would be inhibited by co-stimulation with recombinant TGF- β 1 and A β_{1-40} peptides. To test this hypothesis, we generated primary astrocyte cultures from P1 mouse pups, then subjected the astrocyte monolayer to 6 hours of OGD in the presence of vehicle, TGF- β 1 or A β_{1-40} and collected RNA for qPCR microarray. As we expected, we found that OGD induced an A2 phenotype, however, this was not significantly impacted by TGF- β costimulation (**Fig. 5-3A**; see **Table 5-2** for F-values). In contrast, we found that A β_{1-40} stimulation induced a classical pro-inflammatory A1 phenotype under normoxic conditions, and suppressed the transition to A2 phenotype under OGD conditions (**Fig. 5-3A**).

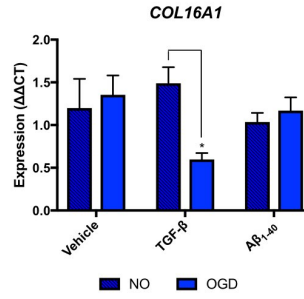
A.



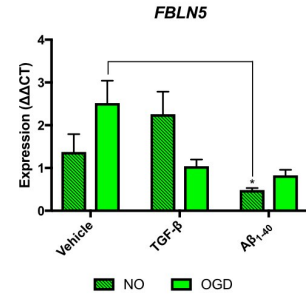
B. i.



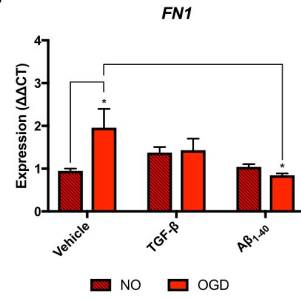
ii.



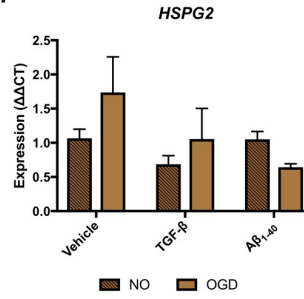
iii.



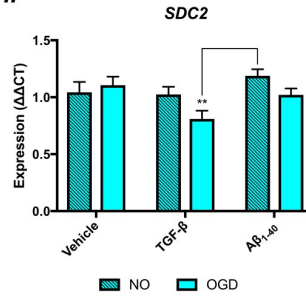
iv.



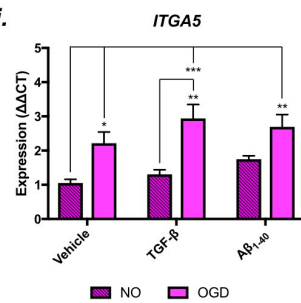
v.



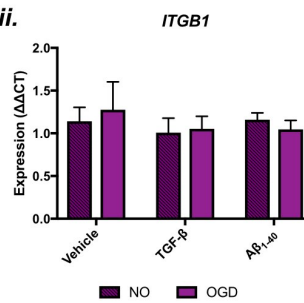
vi.



vii.



viii.



ix.

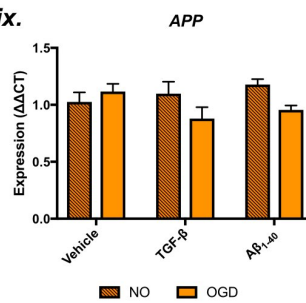


Figure 5-3. Expression of cellular phenotype and ECM-related genes in primary astrocytes following acute stimulation. (A.) Heat map showing variation in expression of genetic markers of astrocyte phenotype following with ischemia and/or co-stimulation. ddCT values are plotted as Z-scores.. **(B.)** (i. – viii.) Expression (ddCT) of ECM-related genes. (ix.) Expression of APP. $n = 5 - 8$ per group. Heat map data in panel (A) are analyzed by two-way ANOVA with Dunnet's test for multiple comparisons to compare ddCT values of experimental groups against vehicle/NO control. All other expression data in panel (B) are analyzed by two-way ANOVA with Tukey's post-hoc test for multiple comparisons. Significance: * $p < 0.05$, ** $p < 0.01$, *** $p < 0.001$.

| | Interaction | | | Perfusion | | | Co-Stimulation | | |
|-----------|------------------|----------|-----|------------------|---------|-----|------------------|---------|-----|
| | F(DFn, DFd) | P-value | S | F(DFn, DFd) | P-value | S | F(DFn, DFd) | P-value | S |
| Agrn | F (2, 47) = 5.8 | P=0.005 | ** | F (1, 47) = 25 | P<0.001 | *** | F (2, 47) = 0.7 | P=0.498 | ns |
| Amigo2 | F (2, 39) = 0.4 | P=0.661 | ns | F (1, 39) = 4.1 | P=0.05 | * | F (2, 39) = 3 | P=0.063 | ns |
| App | F (2, 47) = 3.4 | P=0.043 | * | F (1, 47) = 3.6 | P=0.066 | ns | F (2, 47) = 1.3 | P=0.281 | ns |
| Aspg | F (2, 35) = 0.7 | P=0.501 | ns | F (1, 35) = 0.1 | P=0.706 | ns | F (2, 35) = 0.6 | P=0.537 | ns |
| B3gnt5 | F (2, 47) = 2.4 | P=0.101 | ns | F (1, 47) = 5.3 | P=0.026 | * | F (2, 47) = 2.1 | P=0.137 | ns |
| Ccl11 | F (2, 31) = 3.4 | P=0.048 | * | F (1, 31) = 0.1 | P=0.764 | ns | F (2, 31) = 0.3 | P=0.744 | ns |
| Cd109 | F (2, 47) = 1.3 | P=0.281 | ns | F (1, 47) = 0.4 | P=0.506 | ns | F (2, 47) = 0.7 | P=0.483 | ns |
| Cd14 | F (2, 47) = 38 | P<0.001 | *** | F (1, 47) = 94.7 | P<0.001 | *** | F (2, 47) = 32.8 | P<0.001 | *** |
| Cd44 | F (2, 47) = 14.1 | P<0.001 | *** | F (1, 47) = 26.5 | P<0.001 | *** | F (2, 47) = 1 | P=0.375 | ns |
| Cicf1 | F (2, 47) = 3.8 | P=0.029 | * | F (1, 47) = 61.2 | P<0.001 | *** | F (2, 47) = 3.3 | P=0.046 | * |
| Col16a1 | F (2, 40) = 4 | P=0.026 | * | F (1, 40) = 1.4 | P=0.251 | ns | F (2, 40) = 0.7 | P=0.509 | ns |
| Cp | F (2, 47) = 5.4 | P=0.008 | ** | F (1, 47) = 1.5 | P=0.232 | ns | F (2, 47) = 6.4 | P=0.004 | ** |
| Cxcl10 | F (2, 46) = 90.4 | P<0.001 | *** | F (1, 46) = 60.7 | P<0.001 | *** | F (2, 46) = 101 | P<0.001 | *** |
| Cxcl16 | F (2, 45) = 9.7 | P<0.001 | *** | F (1, 45) = 0.3 | P=0.614 | ns | F (2, 45) = 14.1 | P<0.001 | *** |
| Fbln5 | F (2, 44) = 4.4 | P=0.018 | * | F (1, 44) = 0.1 | P=0.794 | ns | F (2, 44) = 5 | P=0.011 | * |
| Fkbp5 | F (2, 44) = 1.9 | P=0.159 | ns | F (1, 44) = 15 | P<0.001 | *** | F (2, 44) = 1.3 | P=0.274 | ns |
| Fn1 | F (2, 44) = 3.6 | P=0.037 | * | F (2, 44) = 2.5 | P=0.092 | ns | F (1, 44) = 2.2 | P=0.145 | ns |
| Gbp2 | F (2, 47) = 84.2 | P<0.001 | *** | F (1, 47) = 118 | P<0.001 | *** | F (2, 47) = 96.6 | P<0.001 | *** |
| Gfap | F (2, 47) = 0.1 | P=0.939 | ns | F (1, 47) = 20.2 | P<0.001 | *** | F (2, 47) = 5.5 | P=0.007 | ** |
| Ggta1 | F (2, 47) = 0.3 | P=0.714 | ns | F (1, 47) = 21.2 | P<0.001 | *** | F (2, 47) = 1.9 | P=0.16 | ns |
| H2-D1 | F (2, 47) = 11.2 | P<0.001 | *** | F (1, 47) = 114 | P<0.001 | *** | F (2, 47) = 10.7 | P<0.001 | *** |
| H2-T23 | F (2, 47) = 23.2 | P<0.001 | *** | F (1, 47) = 113 | P<0.001 | *** | F (2, 47) = 22.2 | P<0.001 | *** |
| Hsbp1 | F (2, 47) = 0.2 | P=0.858 | ns | F (1, 47) = 0.6 | P=0.44 | ns | F (2, 47) = 23 | P<0.001 | *** |
| Hspg2 | F (2, 46) = 1.2 | P=0.312 | ns | F (1, 46) = 0.5 | P=0.486 | ns | F (2, 46) = 1.6 | P=0.205 | ns |
| Iigp1 | F (2, 44) = 118 | P<0.001 | *** | F (1, 44) = 140 | P<0.001 | *** | F (2, 44) = 128 | P<0.001 | *** |
| Ii10 | F (2, 43) = 6.9 | P=0.003 | ** | F (1, 43) = 90.8 | P<0.001 | *** | F (2, 43) = 6.5 | P=0.004 | ** |
| Ii6 | F (2, 44) = 5 | P=0.011 | * | F (1, 44) = 53.5 | P<0.001 | *** | F (2, 44) = 23.5 | P<0.001 | *** |
| Itga5 | F (2, 45) = 0.5 | P=0.585 | ns | F (1, 45) = 28.5 | P<0.001 | *** | F (2, 45) = 1.9 | P=0.162 | ns |
| Itgb1 | F (2, 47) = 0.2 | P=0.861 | ns | F (1, 47) = 0.01 | P=0.918 | ns | F (2, 47) = 0.3 | P=0.767 | ns |
| Lcn2 | F (2, 46) = 9.5 | P<0.001 | *** | F (1, 46) = 14.7 | P<0.001 | *** | F (2, 46) = 14.3 | P<0.001 | *** |
| Osmr | F (2, 47) = 1.2 | P=0.312 | ns | F (1, 47) = 50.7 | P<0.001 | *** | F (2, 47) = 16.2 | P<0.001 | *** |
| Psbm8 | F (2, 47) = 33.4 | P<0.001 | *** | F (1, 47) = 64.5 | P<0.001 | *** | F (2, 47) = 22.7 | P<0.001 | *** |
| Ptgs2 | F (2, 43) = 0.3 | P=0.749 | ns | F (1, 43) = 66.4 | P<0.001 | *** | F (2, 43) = 0.6 | P=0.573 | ns |
| Ptx3 | F (2, 46) = 3.6 | P=0.034 | * | F (1, 46) = 3.9 | P=0.055 | ns | F (2, 46) = 10.6 | P<0.001 | *** |
| S100a10 | F (2, 47) = 1.3 | P=0.285 | ns | F (1, 47) = 3.7 | P=0.06 | ns | F (2, 47) = 0.2 | P=0.835 | ns |
| S1pr3 | F (2, 46) = 1.5 | P=0.224 | ns | F (1, 46) = 61.4 | P<0.001 | *** | F (2, 46) = 5 | P=0.011 | * |
| Sdc2 | F (2, 46) = 2.2 | P=0.128 | ns | F (1, 46) = 3 | P=0.09 | ns | F (2, 46) = 3.6 | P=0.036 | * |
| Serpina3n | F (2, 47) = 0.1 | P=0.91 | ns | F (1, 47) = 5.7 | P=0.021 | * | F (2, 47) = 0.6 | P=0.536 | ns |
| Serping1 | F (2, 46) = 0.27 | P=0.768 | ns | F (1, 46) = 27.4 | P<0.001 | *** | F (2, 46) = 4 | P=0.024 | * |
| Sphk1 | F (2, 42) = 3.2 | P=0.053 | ns | F (1, 42) = 48.7 | P<0.001 | *** | F (2, 42) = 3.2 | P=0.049 | * |
| Spp1 | F (2, 47) = 0.8 | P=0.467 | ns | F (1, 47) = 0.8 | P=0.366 | ns | F (2, 47) = 3.8 | P=0.03 | * |
| Srgn | F (2, 46) = 7.5 | P=0.002 | ** | F (1, 46) = 3 | P=0.089 | ns | F (2, 46) = 1.4 | P=0.251 | ns |
| Steap4 | F (2, 45) = 10.4 | P<0.001 | *** | F (1, 45) = 22.1 | P<0.001 | *** | F (2, 45) = 12.3 | P<0.001 | *** |
| Tgfb1 | F (2, 46) = 6 | P=0.005 | ** | F (1, 46) = 35.9 | P<0.001 | *** | F (2, 46) = 2.5 | P=0.096 | ns |
| Tgfb2 | F (2, 47) = 0.6 | P=0.57 | ns | F (1, 47) = 0.6 | P=0.435 | ns | F (2, 47) = 9.8 | P<0.001 | *** |
| Tgfb3 | F (2, 42) = 2.3 | P=0.115 | ns | F (1, 42) = 3.3 | P=0.077 | ns | F (2, 42) = 2.3 | P=0.108 | ns |
| Tgfb1 | F (2, 45) = 0.6 | P=0.57 | ns | F (1, 45) = 3 | P=0.09 | ns | F (2, 45) = 0.2 | P=0.856 | ns |
| Tgm1 | F (2, 35) = 1.4 | P=0.255 | ns | F (1, 35) = 7.9 | P=0.008 | ** | F (2, 35) = 12 | P<0.001 | *** |
| Thbs1 | F (2, 47) = 4.4 | P=0.017 | * | F (1, 47) = 59.6 | P<0.001 | *** | F (2, 47) = 7.9 | P=0.001 | ** |
| Timp1 | F (2, 45) = 1 | P=0.372 | ns | F (1, 45) = 1.7 | P=0.201 | ns | F (2, 45) = 0.7 | P=0.523 | ns |
| Tm4sf1 | F (2, 47) = 0.8 | P=0.443 | ns | F (1, 47) = 2.9 | P=0.094 | ns | F (2, 47) = 3.7 | P=0.031 | * |
| Tnf | F (2, 40) = 123 | P<0.001 | *** | F (1, 40) = 131 | P<0.001 | *** | F (2, 40) = 137 | P<0.001 | *** |
| Uggt1 | F (2, 47) = 1.1 | P=0.343 | ns | F (1, 47) = 0.2 | P=0.665 | ns | F (2, 47) = 0.3 | P=0.75 | ns |
| Vim | F (2, 47) = 0.6 | P=0.5730 | ns | F (1, 47) = 6 | P=0.018 | * | F (2, 47) = 1.6 | P=0.214 | ns |

Table 5-2. Effects of perfusion, co-stimulation and interaction on gene expression in primary cultured astrocytes. Tabulation of F-values, degrees of freedom and p-values for all PCR assays detailed in Fig. 5-3 through Fig. 5-5. *n = 5 – 8 per group. Data are analyzed by two-way ANOVA. Significance: ns, no significance, *p < 0.05, **p < 0.01, ***p < 0.001.*

We next broadly assessed how these stimuli impacted the production of ECM components by primary astrocytes. To accomplish this, we examined the mRNA levels of agrin (*AGRN*), collagen XVI (*COL16A1*), fibulin-5 (*FBLN5*), fibronectin (*FNI*), perlecan (*HSPG2*), syndecan-2 (*SDC2*), integrin- α 5 (*ITGA5*) and integrin- β 1 (*ITGB1*) immediately following OGD (**Fig. 5-3B; Table 5-2**). We found that exposure to OGD reduced agrin expression ($p < 0.001$) and upregulated integrin- α 5 ($p = 0.001$). Treatment with vehicle, TGF- β 1 or A β ₁₋₄₀ differentially impacted fibulin ($p = 0.011$) and syndecan-2 expression ($p = 0.036$). Finally, we also observed statistically significant interaction effects between OGD and co-stimulation on the expression of agrin ($p = 0.005$), collagen XVI ($p = 0.026$), fibrillin ($p = 0.018$) and fibronectin ($p = 0.037$). Overall, these data indicate that A2 astrocytes produce a unique compliment of ECM proteins following ischemia, which is further modulated by exposure to TGF- β 1 or A β ₁₋₄₀ in the extracellular milieu during ischemia.

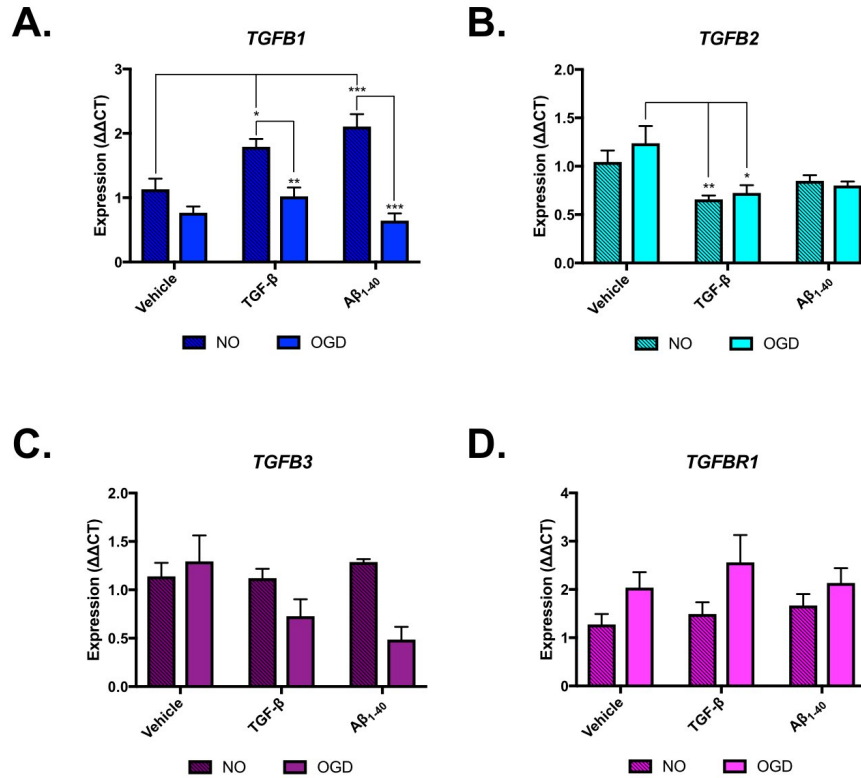


Figure 5-4. Expression of TGF-β-related genes in primary astrocytes following acute stimulation. (A. – D.) Expression (ddCT) values of TGF-β signaling genes. n = 5 – 8 per group. Data are analyzed by two-way ANOVA with Tukey's post-hoc test for multiple comparisons. Significance: * $p < 0.05$, ** $p < 0.01$, *** $p < 0.001$.

We then examined the impact of OGD and co-stimulation on the expression of TGF-β signaling components. To assess this, we measured mRNA levels of TGF-β1 (*TGFB1*), TGF-β2 (*TGFB2*), TGF-β3 (*TGFB3*) and TGF-βR1 (*TGFBR1*) immediately following OGD (Fig. 5-4; Table 5-2). We found that OGD exposure reduced the expression of TGF-β1 ($p < 0.001$) and TGF-β3 ($p = 0.038$), and concurrently increased the expression of TGF-βR1 ($p = 0.02$). Treatment with exogenous TGF-β1 or Aβ₁₋₄₀ increased astrocytic TGF-β1 expression ($p = 0.003$), but reduced the expression of TGF-β2 ($p < 0.001$). Finally, we also observed statistically significant interaction effects between OGD and treatment on the expression of

TGF- β 1 ($p = 0.002$). Overall, these data suggest that A2 astrocytes may exhibit increased sensitivity to TGF- β signaling due to increased expression of TGF- β R1, but this might be balanced by downregulation of astrocytic production of TGF- β isoforms following stimulation by OGD, TGF- β or A β ₁₋₄₀. However, further studies of downstream Smad activation are required to address this point.

Finally, we also sought to characterize the impact of OGD and co-stimulation on the expression of various cytokines related to ischemic stroke and CAA. To assess this, we measured mRNA levels of C-X-C motif chemokine 10 (*CXCL10*), C-X-C motif chemokine 16 (*CXCL16*), IL-6 (*IL6*), interleukin-10 (IL-10, *IL10*), osteopontin (*SPP1*) and TNF- α (*TNF*) immediately following OGD (**Fig. 5-5; Table 5-2**). We found that OGD increased IL-6 ($p < 0.001$) and IL-10 levels ($p < 0.001$), reduced TNF- α expression ($p < 0.001$) and had differential impacts on CXCL10 ($p < 0.001$) and CXCL16 ($p < 0.001$) expression. Treatment with TGF- β 1 or A β ₁₋₄₀ increased the expression of IL-6 ($p < 0.001$), TNF- α ($p < 0.001$), CXCL10 ($p < 0.001$), CXCL16 ($p < 0.001$), but reduced IL-10 expression ($p = 0.003$) and differentially impacted SPP1 expression ($p = 0.031$). Finally, we also observed a statistically significant interaction between OGD and treatment on the expression of IL-6 ($p < 0.001$), IL-10 ($p = 0.004$), TNF- α ($p < 0.001$), CXCL10 ($p < 0.001$) and CXCL16 ($p < 0.001$). Overall, these data indicate that stimulation with OGD, TGF- β 1 and A β ₁₋₄₀ all generally upregulated cytokine expression by reactive astrocytes, with the notable exception of the anti-inflammatory cytokine IL-10, which was suppressed by both TGF- β 1 and A β ₁₋₄₀.

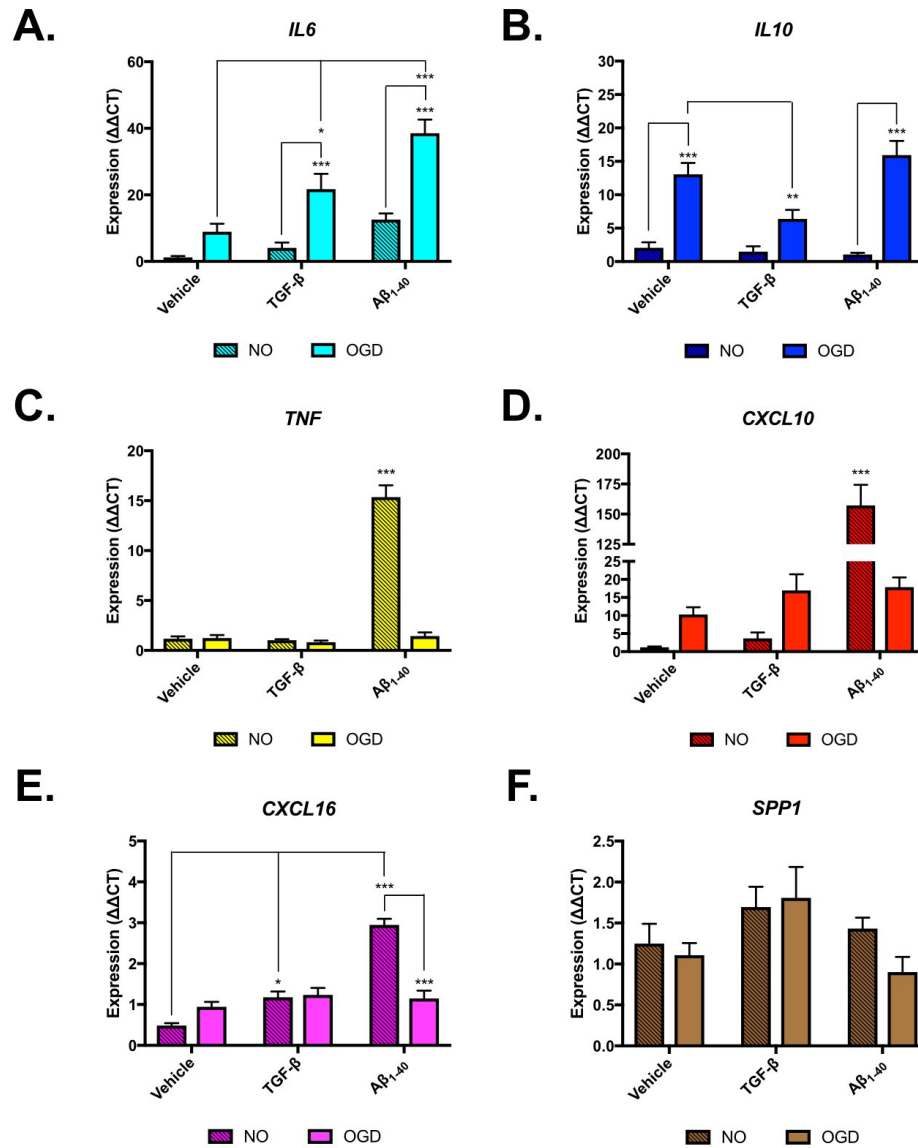


Figure 5-5. Expression of inflammatory cytokine genes in primary astrocytes following acute stimulation. (A. – D.) Expression (ddCT) of inflammatory cytokine genes. $n = 5 - 8$ per group. Data are analyzed by two-way ANOVA with Tukey's post-hoc test for multiple comparisons. Significance: * $p < 0.05$, ** $p < 0.01$, *** $p < 0.001$.

5.3.4. Chronic TGF- β exposure modulates astrocytic ECM production, and may ‘prime’ the ECM for the deposition of A β ₁₋₄₀.

Next, we sought to determine whether chronic TGF- β stimulation influences ECM composition and its affinity for A β ₁₋₄₀ deposition. Our previous studies, detailed in Chapter 4, found that fibronectin and integrin- α 5 form a complex that binds soluble A β ₁₋₄₀ within the basement membrane after stroke. However, neither the cell types nor the upstream signaling mechanisms by which stroke increases fibronectin/integrin- α 5 expression were explored in those studies. Therefore, we next hypothesized that chronic stimulation with TGF- β would induce the deposition of exogenous A β ₁₋₄₀ due to upregulation of fibronectin and integrin- α 5 by astrocytes.

To test this hypothesis, we first treated primary astrocytes with recombinant TGF- β 1 peptide for 24 hours, then measured the binding of exogenous A β ₁₋₄₀ to the ECM following incubation in a 2 μ M solution of FITC-A β ₁₋₄₀ for 30 minutes. We found that TGF- β 1 treatment increased the uptake of FITC-A β ₁₋₄₀ by the astrocyte monolayer (**Fig. 5-6A**, *i.*, $t[5] = 5.94$, $p = 0.002$). In contrast with our acute studies of gene expression, examination of total protein levels by western blot further showed that chronic TGF- β 1 treatment significantly increased the expression of fibronectin (**Fig. 5-6A**, *iii.*, $t[6] = 4.91$, $p = 0.003$), and there was also a nonsignificant trend for increased integrin- α 5 expression with treatment (**Fig. 5-6A**, *iv.*, $t[3] = 1.74$, $p = 0.172$, t-test with Welch’s correction). Chronic TGF- β 1 treatment significantly reduced GFAP expression (**Fig. 5-6A**, *v.*, $t[6] = 3.19$, $p = 0.011$), with a nonsignificant trend for decreased vimentin expression (**Fig. 5-6A**, *vi.*, $t[6] = 1.14$, $p = 0.296$), indicating reduced expression of ‘pan-reactive’ astrocyte activation markers. To determine whether increased FITC-A β ₁₋₄₀ binding was directly related to the increase in

ECM protein expression, we then performed ICC and found that FITC-A β_{1-40} binding colocalized with regions of increased fibronectin (**Fig. 5-6B**, *vehicle* [i – iii.], *TGF- β 1* [vii. – ix.]) and integrin- α 5 expression (**Fig. 5-6B**, *vehicle* [iv. – vi.], *TGF- β 1* [x. – xii.]). Overall, these results indicate that astrocytes are a source of both fibronectin and integrin- α 5 expression, and also show that fibronectin expression is stimulated by TGF- β 1 treatment *in vitro*. They further confirm that these increases in fibronectin are directly associated with increased A β_{1-40} binding, although it does not rule out increased endocytosis of FITC-A β_{1-40} as a potential contributor to this phenotype.

Next, to confirm the *in vivo* relevance of TGF- β 1-induced stimulation of fibronectin expression, we intracisternally injected naive young mice with recombinant TGF- β 1, and then collected the cerebral cortex for western blot and IHC analysis 24 hours later. Similar to our *in vitro* studies, we found that TGF- β 1 treatment upregulated fibronectin expression (**Fig. 5-6C**, *ii.*, $t[5] = 2.62$, $p = 0.047$). However, TGF- β 1 treatment had no impact on GFAP levels (**Fig. 5-6C**, *ii.*, $t[5] = 0.058$, $p = 0.956$). We further confirmed that our injections successfully activated TGF- β signaling by examining Smad phosphorylation. We found that chronic treatment with TGF- β 1 increased phospho-Smad2 expression (**Fig. 5-6C**, *iv.*, $t[5] = 4.03$, $p = 0.01$), but did not significantly alter the levels of total Smad2 (**Fig. 5-6C**, *vi.*, $t[5] = 0.64$, $p = 0.55$), producing a relative increase in Smad2 phosphorylation (**Fig. 5-6C**, *vi.*, $t[5] = 3.47$, $p = 0.018$). We verified that these changes occurred within perivascular astrocytes by IHC (**Fig. 5-6D**), and found that TGF- β 1 treatment increased the association of astrocytes with the vasculature, as well as fibronectin expression. Overall, these results confirm our *in vitro* findings that TGF- β stimulates fibronectin expression within the ECM, and further shows that these changes occur within the basement membrane *in vivo*.

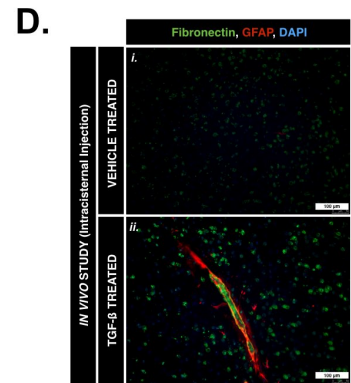
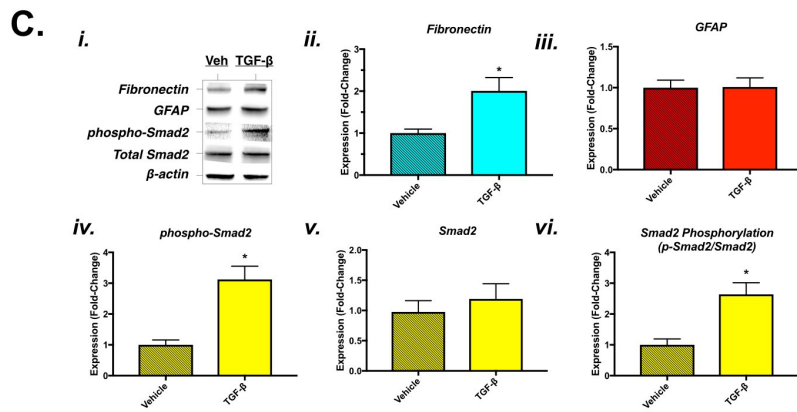
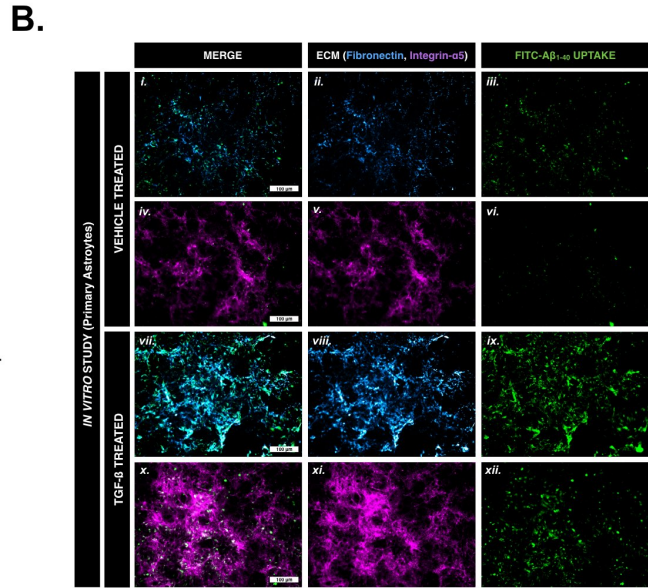
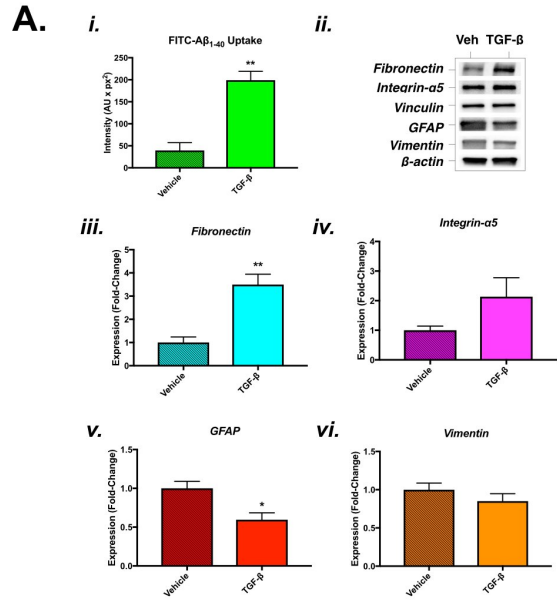


Figure 5-6. TGF- β stimulation increases A β ₁₋₄₀ binding and fibronectin expression. (A.) (i.) Quantification of A β ₁₋₄₀ binding by primary astrocyte cultures treated with TGF- β . $n = 3$ per group. (ii.) Representative western blots of primary astrocytes treated with vehicle or TGF- β . (iii. – vi.) Quantification of protein expression changes by western blot. **(B.)** ICC showing colocalization of exogenous FITC-A β ₁₋₄₀ with ECM proteins in primary astrocytes. $n = 4 – 5$ per group. **(C.)** (i.) Representative western blots of brain tissue from mice that received intracisternal injection of vehicle or TGF- β . (ii. – vi.) Quantification of protein expression changes by western blot. $n = 3 – 4$ per group. **(D.)** IHC localizing increased fibronectin expression in mice treated with TGF- β localizes with the basement membrane of brain cortical vessels. All data are analyzed by Student's *t*-test. Significance: * $p < 0.05$, ** $p < 0.01$. Scale bar = 100 μ m.

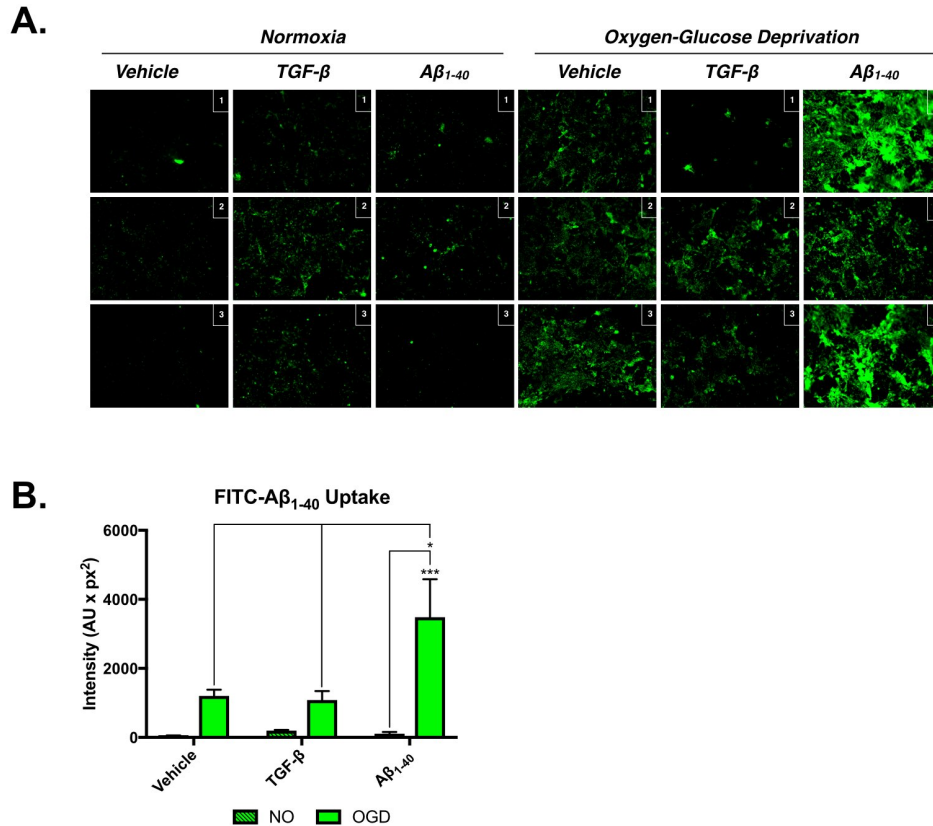


Figure 5-7. OGD increases A β_{1-40} binding in primary astrocytes. (A.) Fluorescent images showing that FITC-A β_{1-40} binding increases with OGD, and was highest in cultures that were co-stimulated with A β_{1-40} during OGD. **(B.)** Quantification of FITC-A β_{1-40} binding. $n = 3$ per group. Data are analyzed by two-way ANOVA with Tukey's post-hoc test for multiple comparisons. * $p < 0.05$, *** $p < 0.001$.

5.3.5. Ischemia, TGF- β and A β_{1-40} interact to further increase the uptake of A β_{1-40} within the astrocyte monolayer.

We next sought to further characterize how ischemia, TGF- β and A β_{1-40} interact to increase the *in vitro* binding of A β_{1-40} to the ECM produced by primary cultured astrocytes (Fig. 5-7A). We hypothesized that OGD would increase the uptake of FITC-A β_{1-40} , which

would be further accelerated by co-stimulation with recombinant TGF- β 1 and A β ₁₋₄₀. We found that FITC-A β ₁₋₄₀ uptake was increased by both OGD (**Fig. 5-7B**, $F[1, 14] = 27.78$, $p = 0.001$) and co-stimulation ($F[2, 14] = 4.95$, $p = 0.024$). We also observed a statistically significant interaction effect between OGD and co-stimulation on FITC-A β ₁₋₄₀ uptake (**Fig. 5-7B**, $F[2, 14] = 5.01$, $p = 0.023$). Overall, these data indicate that ischemia, TGF- β and A β ₁₋₄₀ interact to increase the *in vitro* uptake of FITC-A β ₁₋₄₀ within the astrocyte monolayer. However, further work is needed to address the mechanism of this phenomenon, in particular how pre-treatment with A β ₁₋₄₀ induces such dramatic increases in FITC-A β ₁₋₄₀ uptake, and why this increase in uptake appears to be conditional on exposure to OGD conditions.

5.3.6. TGF- β stimulation alters astrocytic AQP4 polarization and impairs water uptake both *in vitro* and *in vivo*.

Our initial studies showed that DMCAO upregulated TGF- β 1 expression (**Fig. 5-2A**) and altered AQP4 polarization on reactive astrocytes (**Fig. 5-1A**). Therefore, we hypothesized that TGF- β impairs AQP4 polarization, water uptake and bulk flow. To address this hypothesis, we first stimulated primary cultured astrocytes with recombinant TGF- β 1 for 24 hours, and assessed the impact on AQP4 polarization by ICC (**Fig. 5-8A**). We found that TGF- β 1 treatment altered the pattern of AQP4 staining and induced swelling of cultured astrocytes (**Fig. 5-8A, i – ii.**). To measure the functional consequences of these histological changes, we examined the *in vitro* uptake of ³H₂O, a substrate for AQP4, for 30 min into the astrocyte monolayer, and found that it was significantly reduced by TGF- β 1 treatment (**Fig. 5-8A, iii.**, $t[8] = 2.31$, $p = 0.049$). To confirm these findings *in vivo*, we injected naive young mice with TGF- β 1 and examined AQP4 polarization, as well as the

uptake of $^3\text{H}_2\text{O}$ uptake and ^{14}C -inulin (used as an extracellular space marker) from the CSF. We found that treatment with TGF- β 1 significantly reduced uptake of $^3\text{H}_2\text{O}$ (**Fig. 5-8B, ii.**, $t[10] = 3.77$, $p = 0.004$) and ^{14}C -inulin (**Fig. 5-8B, iii.**, $t[7] = 2.75$, $p = 0.029$) from the CSF. This indicates that TGF- β 1 treatment is sufficient to impair CSF flow in the healthy young brain, suggesting that it may also contribute to impairments in aging and after stroke.

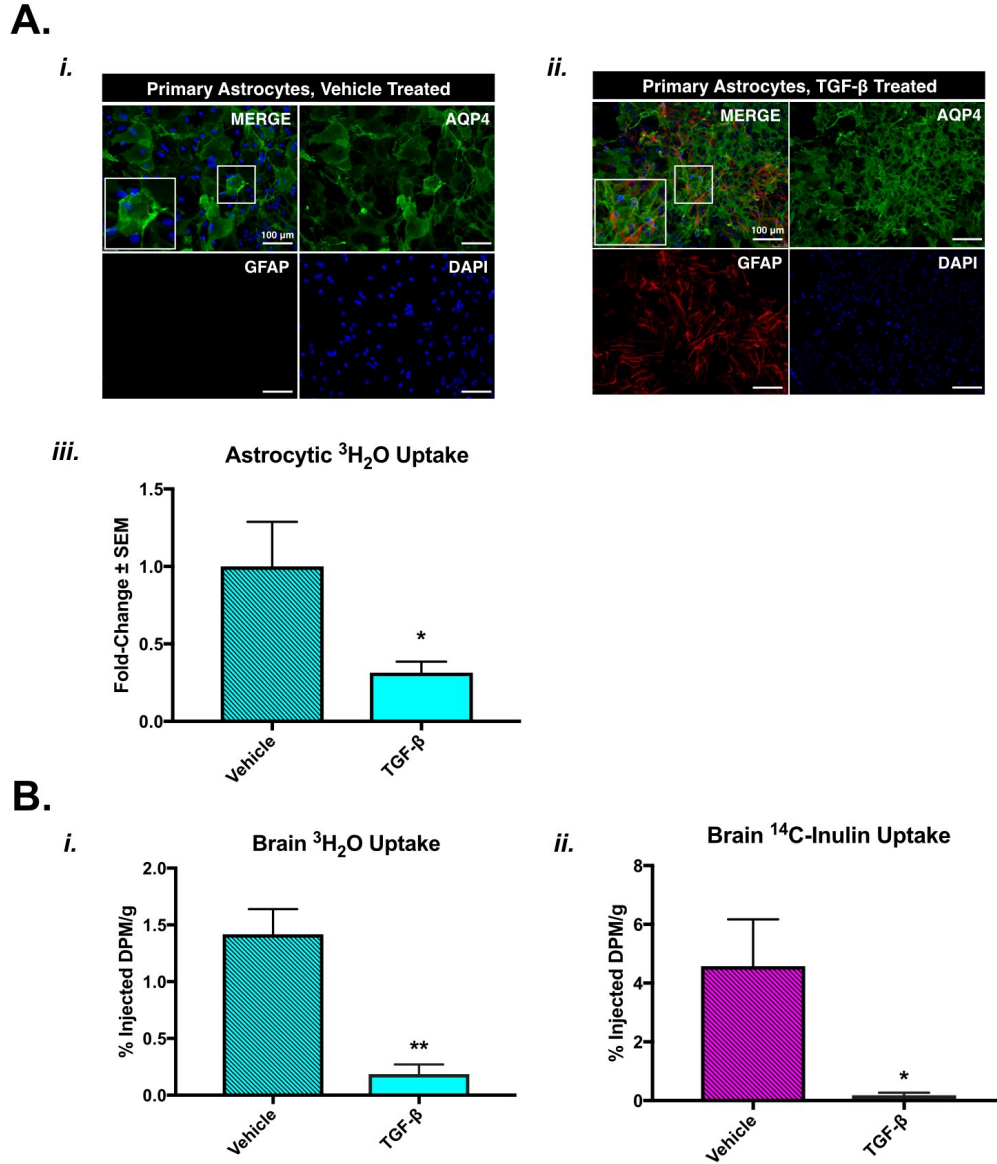
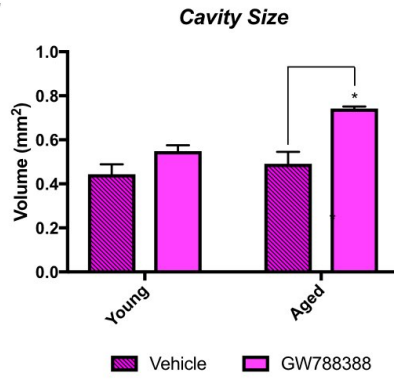


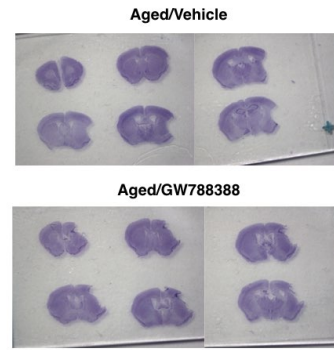
Figure 5-8. TGF- β stimulation alters AQP4 polarization and impairs water uptake. (A.) (*i.*, *ii.*) Fluorescent micrographs showing altered AQP4 polarization in TGF- β -treated primary astrocytes by ICC. (*iii.*) Quantification of $^3\text{H}_2\text{O}$ uptake by primary astrocytes treated with vehicle or TGF- β . $n = 4 - 8$ per group. **(B.)** Quantification of (*i.*) $^3\text{H}_2\text{O}$ and (*ii.*) ^{14}C -Inulin uptake by mice intracisternally injected with vehicle or TGF- β . $n = 3 - 4$ per group. Data are analyzed by Student's *t*-test. Significance: * $p < 0.05$, ** $p < 0.01$.

5.3.7: Early TGF- β R1 antagonism following DMCAO increases infarct volume and may modulate astrogliosis in an age-dependent manner. In order to further examine the translational value of TGF- β antagonism in modulating injury severity, astrogliosis and basement membrane fibrosis after stroke, we first performed a pilot study with continuous peripheral administration of GW788388 (10 mg/kg/day), a TGF- β R1/R2 antagonist, from 3 – 7 DPI in young (3 month) and aged (20 month)-old mice with DMCAO. Similar to previous studies using conditional knockout mice,²²⁹ we hypothesized that early inhibition of TGF- β signaling would slightly increase injury volume, but would have the beneficial effect of reducing gliosis. We also newly hypothesized that this would reduce fibronectin and integrin- α 5 expression in the injured cortex. Somewhat unexpectedly, we found that early TGF- β antagonism *significantly* increased injury volume (**Fig. 5-9A**, $F[1, 4] = 22$, $p = 0.009$), which worsening with aging ($F[1, 4] = 10.02$, $p = 0.034$). We next examined the impact on gliosis by western blot, and found similar trending interaction effects of aging and early TGF- β antagonism on the expression of GFAP (**Fig. 5-9B**, *i.*, $F[1, 8] = 2.92$, $p = 0.127$) and vimentin (**Fig. 5-9B**, *ii.*, $F[1, 8] = 2.54$, $p = 0.149$) at 7 DPI. Finally, we similarly examined the impact of treatment on ECM remodeling, and found similar trending interactions in the expression of fibronectin (**Fig. 5-9C**, *i.*, $F[1, 8] = 4.66$, $p = 0.063$) and integrin- α 5 (**Fig. 5-9C**, *ii.*, $F[1, 8] = 2.91$, $p = 0.127$) at 7 DPI by western blot. Overall, these preliminary data are interesting in that they show a potential age dimorphism in the role of TGF- β signaling in regulating gliosis and ECM remodeling after stroke, with a potential slight benefit to aged animals despite increases in injury volume.

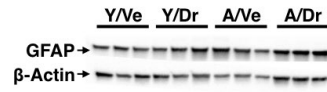
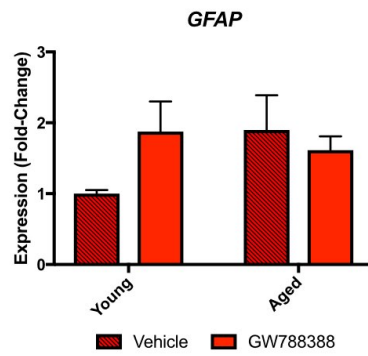
A. *i.*



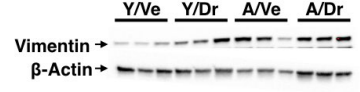
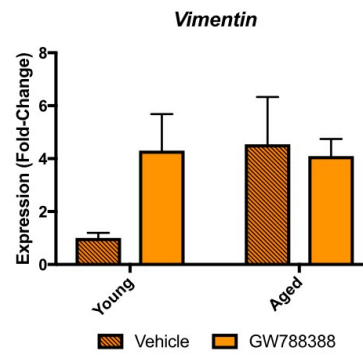
ii.



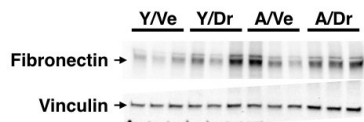
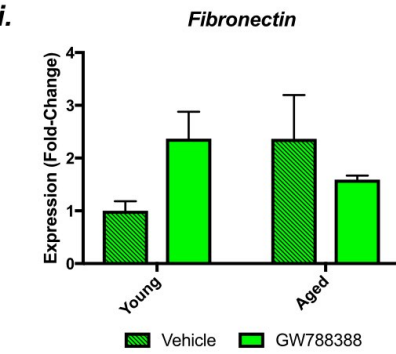
B. *i.*



ii.



C. *i.*



ii.

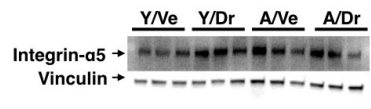
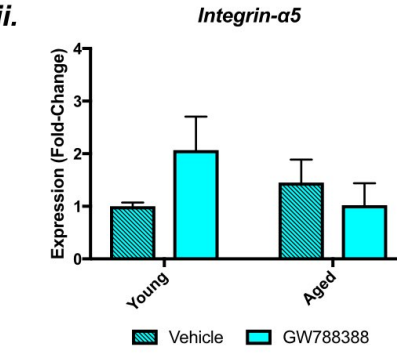


Figure 5-9. Age-specific effects of subacute TGF- β R1 antagonism following DMCAO.

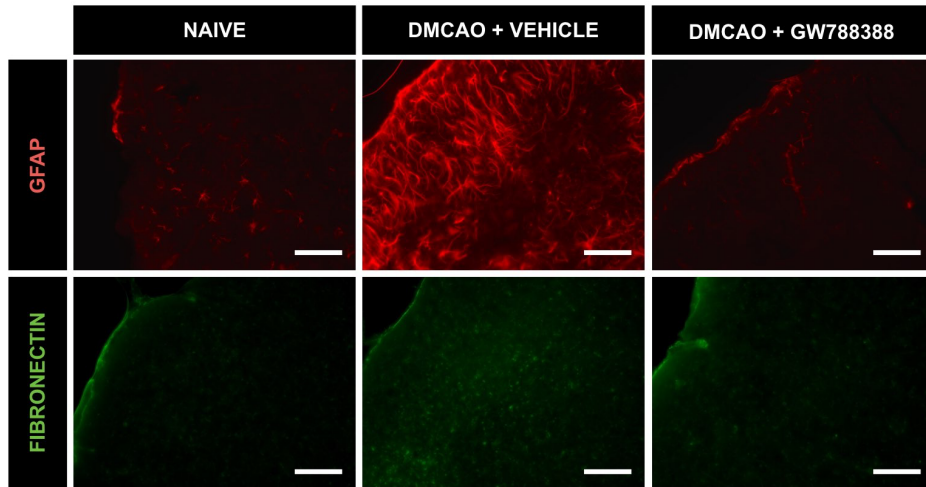
(A.) (i.) Quantification of cavity size at 7 DPI. (ii.) Representative cresyl violet stained coronal sections from vehicle and drug-treated aged mice. *n* = 2 *per group*. **(B.)** GFAP and vimentin expression at 7 DPI quantified by western blot. *n* = 3 *per group*. **(C.)** Fibronectin and integrin- α 5 expression at 7 DPI quantified by western blot. *n* = 3 *per group*. Data are analyzed by two-way ANOVA with Tukey's post-hoc test for multiple comparisons. **p* < 0.05.

5.3.8: Delayed TGF- β R1 antagonism following DMCAO reduces gliosis and ECM remodeling, while also improving perivascular CSF flow in aged animals.

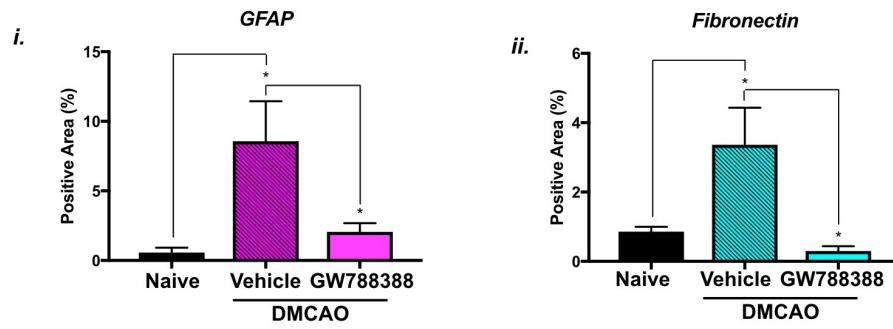
Based on the mixed results of the preceding pilot study, we next modified the dosing regimen by shifting the treatment window to 7 – 14 DPI in aged (20 month-old) mice by Alzet pump. We hypothesized that delayed TGF- β R1/R2 antagonism after DMCAO would reduce gliosis and fibronectin/integrin- α 5 expression, but have no major impact on injury volume or motor recovery in aged animals. We further hypothesized that these reductions in astrogliosis and basement membrane fibrosis would correlate with improved perivascular CSF flow and reduced FITC-A β ₁₋₄₀ deposition.

We found that DMCAO increased GFAP expression, which was rescued by treatment with the TGF- β R1/R2 antagonist ($F[2, 12] = 6.2, p = 0.014$). We also found that DMCAO increased fibronectin expression, which was significantly reduced by treatment ($F[2, 12] = 5.8, p = 0.017$). These changes in fibrosis were correlated with alterations in perivascular CSF flow. We found that DMCAO significantly inhibited glymphatic influx of CSF (measured as dextran [d3] uptake), which was rescued by treatment (**Fig. 5-10D, i.**, $F[2, 12] = 5.38, p = 0.022$). Despite these reductions in overall CSF flow, we saw no corresponding impact on relative FITC-A β ₁₋₄₀ uptake (**Fig. 5-10D, ii.**, $F[2, 12] = 0.81, p = 0.469$). However, normalization to d3 levels, which accounts for individual differences in overall CSF flow, showed a relative increase in FITC-A β ₁₋₄₀/d3 ratio with DMCAO that was rescued by treatment (**Fig. 5-10D, iii.**, $F[2, 12] = 5.93, p = 0.016$). Overall, these data show that TGF- β signaling impairs perivascular CSF flow after DMCAO, which is associated with a disequilibrium in the transport of A β ₁₋₄₀. Treatment improved CSF flow and reduced this imbalance in A β ₁₋₄₀ transport.

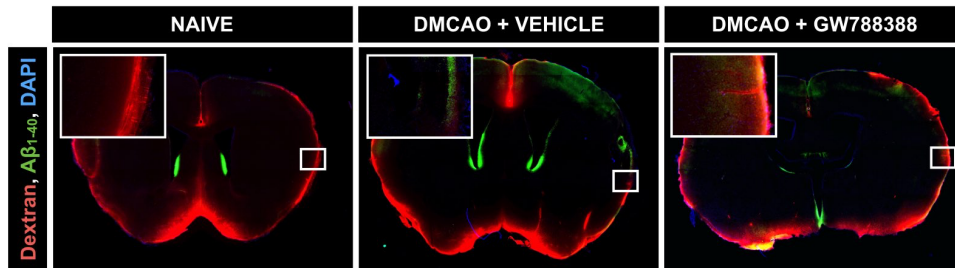
A.



B.



C.



D.

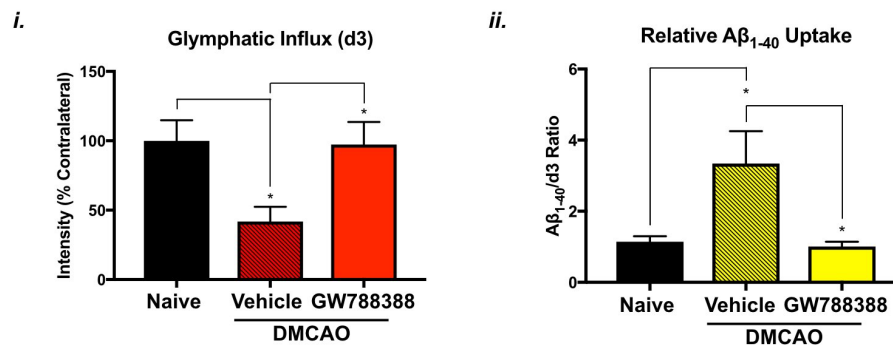


Figure 5-10. Delayed TGF- β R1 antagonism reduces fibrosis and improves perivascular flow following DMCAO in aged mice. (A.) Representative images showing increased GFAP and fibronectin expression in the peri-infarct cortex following DMCAO, which is rescued with GW788388 treatment. **(B.)** Fluorescence intensity quantification of GFAP and fibronectin expression. **(C.)** Representative images showing reduced dextran and increased A β ₁₋₄₀ distribution following DMCAO, which is rescued with GW788388 treatment. **(D.)** Fluorescence intensity quantification of tracer uptake. *n = 4 – 5 per group. Data are analyzed by two-way ANOVA with Tukey’s post-hoc test for multiple comparisons. *p < 0.05.*

5.4: Discussion.

5.4.1: Aging alters TGF- β signaling and reactive gliosis after stroke.

The current study builds on previous work examining the impact of stroke on glial scar formation in aged animals by our laboratory and others,^{223,229,233} and offers new insight into age-related alterations in canonical TGF- β signaling pathways. Similar to previous studies, we found that DMCAO produced a large, GFAP⁺ glial scar in the ischemic penumbra by 7 DPI in young animals. We further showed that this was associated with alterations in ECM glycosylation, measured by lectin staining, indicating increases in glycosylated proteins including heparan sulfate proteoglycans (HSPGs), chondroitin sulfate proteoglycans (CSPGs) and/or other glycosylated proteins such as fibronectin. While these changes have been previously shown to occur after experimental stroke, we newly observed that the glial scar extended beyond the ischemic penumbra and into the surrounding PVS, which form a continuous network through the ipsilateral cortex and striatum. We found that stroke produced a striking increase in GFAP⁺ perivascular reactive astrocytes, which was associated with abnormal lectin staining, indicating potentially major alterations in the basement membrane. We also found that the polarization of the omnipresent water channel, AQP4, was also disrupted in gliotic vessels.

Together, these changes may prime the basement membrane for the development of CAA in three ways (as described in detail in Chapter 4): (1) altering the tortuosity of the perivascular microenvironment for the diffusion of solutes (2) increasing the affinity of the basement membrane for A β ₁₋₄₀ due to alterations in protein composition (e.g. fibronectin expression), or (3) impairing water transport, and thus slowing the bulk flow of CSF, by

mislocalization of AQP4. Similar changes have been shown to occur in animal models of CAA,²⁸⁰ and with constitutive TGF- β overexpression.²¹⁹

We further found that aging induced an increase in perivascular reactive gliosis, and was associated with further increases in total GFAP and vimentin expression throughout the injured hemisphere. Since TGF- β signaling is increased in aged animals with stroke,²²³ and, in a separate paper, was also found to be a major contributor to glial scar formation by signaling to astrocytes after stroke,²²⁹ we elected to explore this further by first examining the levels of TGF- β in whole cortical lysate by multiplex ELISA, and then by probing the phosphorylation of downstream canonical Smad signaling pathways by western blot. While we found that young and aged animals exhibited similar concentrations of TGF- β 1, the predominant TGF- β isoform, we found interesting differences in the downstream Smad signaling pathways, indicating that aging induces a potentially dysregulated response to TGF- β signaling following stroke. In young animals, this TGF- β stimulation is associated with increases in Smad2/3 phosphorylation, however, this is balanced by increases in Smad2/3, potentially acting to blunt these changes. In contrast, Smad2/3 levels decline in aged animals with stroke, and the relative levels of phosphorylation increase. This decline in total Smads could help to explain the increased sensitivity of the aged brain to TGF- β signaling (and the gliotic response). In particular, relative increases in Smad3 phosphorylation could provide a potent stimulus for the transcription of 'reactive' genes following stroke, although our *in vitro* data show that TGF- β stimulation alone is not sufficient to induce increases in classical markers of astrocyte reactivity, including GFAP expression. This discrepancy suggests that TGF- β plays a role in modulating the response to

hypoxia or other stimuli, rather than directly inducing astrocyte reactivity, as was previously thought.

5.4.2: Astrocyte polarization is differentially regulated by hypoxia, TGF- β and A β ₁₋₄₀.

Recent work found that reactive astrocytes represent a more diverse population of cells than previously thought.²³⁹ While all reactive astrocytes generally express so-called ‘pan-reactive’ markers, such as GFAP and vimentin, depending on the stimulus, astrocytes can take on two distinct genotypes: A1 and A2.²³⁹ Using *in vivo* mouse models, A1 astrocytes were shown to be induced by peripheral LPS stimulation, while A2 were shown to be induced following MCAO.²³⁹ However, a very recent paper found this to be incorrect, as A1 astrocytes lack toll-like receptor-4 and, therefore, could not directly respond to LPS.²⁴⁰ Instead, the study showed that A1 astrocytes were induced by the microglial cytokines IL-1 β , IL-6 and TNF- α .²⁴⁰ To date, no such study has followed up on whether A2 astrocytes are induced by hypoxia, or if they instead similarly require co-stimulation with microglial cytokines. Furthermore, while A1 astrocytes have generally detrimental effects following activation (mislocalization of AQP4, induce aberrant synaptic function and secretion of neurotoxic products), the actual phenotype of activated A2 astrocytes is not known.

To address this gap in the literature, and to determine how A2 astrocytes are induced following stroke, we first sought to determine the specific factors that are sufficient to induce an A2 phenotype *in vitro*. We elected to model stroke *in vitro* by performing OGD on astrocyte monolayers. Although it is nearly impossible to isolate a truly ‘pure’ population of astrocytes from primary glial cultures, we chose to use microglia-depleted primary astrocyte monolayers to increase the relevance to our *in vivo* studies. When we performed OGD and

collected RNA from our cultured astrocytes, we newly found that hypoxia alone was sufficient to induce an A2 astrocyte phenotype without any exogenous co-stimulation. Additionally, while previous studies found that even delayed treatment with TGF- β inhibits A1 astrocyte activation, we found that the A2 phenotype remained intact even with TGF- β co-stimulation. Finally, to provide some insight for future studies into the role of A β ₁₋₄₀ in modulating the phenotype of astrocytes, we assessed the impact of A β ₁₋₄₀ stimulation under both normoxic and hypoxic conditions. We newly found that A β ₁₋₄₀ induces classical A1 astrocyte activation with NO, and inhibits the transition to A2 that normally occurs under hypoxic conditions. This very interesting finding suggests that stroke and AD may produce opposing astrocyte phenotypes, which may be significant in the pathogenesis of vascular dementia.

5.4.3: Reactive astrocyte subsets produce different patterns of extracellular matrix and cytokines, which can be further modified by co-stimulation.

Since understanding astrocytic basement membrane production was a major goal of our studies, we next assessed the transcription of ECM genes by astrocytes under hypoxia and co-stimulation. We found that OGD-induced A2 astrocytes upregulated fibronectin, integrin- α 5 and (potentially) perlecan expression, yet down-regulated expression of other ECM-related genes, including agrin, collagen XI and fibulin-5. They also showed no significant changes in integrin- β 1, demonstrating again that integrin- α 5 is the major subunit that changes with ischemia. These findings are in line with our previous studies, outlined in Chapter 4, which showed that stroke induced the upregulation of fibronectin and integrin- α 5 within the basement membrane *in vivo*, and newly show that astrocytes are a major source of

these proteins. Future studies should assess whether downregulation of agrin, collagen XVI or fibulin-5 also contributes to the deposition of CSF A β ₁₋₄₀ and the formation of CAA plaques after stroke.

We also examined how cytokine expression changes under hypoxia and/or co-stimulation. We first examined changes in TGF- β -related genes, and found that OGD reduced the expression of TGF- β 1, but increased the expression of TGF- β R1. This is interesting, because it suggests that activated astrocytes may be more sensitive to TGF- β 1 due to increased receptor expression. When we examined other cytokines, we found that A β -stimulated A1 astrocytes produced significantly more TNF- α , CXCL10 and CXCL16, which was inhibited by hypoxia. In contrast, A2 astrocytes produced high levels of IL-6 and IL-10. TGF- β simultaneously stimulated IL-6 (pro-inflammatory cytokine) and inhibited IL-10 (anti-inflammatory cytokine) production, suggesting that it could be shifting the phenotype of A2 astrocytes to a more pro-inflammatory state. This needs to be clarified with further studies examining a wider panel of inflammatory cytokines and surface markers.

5.4.4: TGF- β modifies multiple astrocyte functions that are involved in CSF flow.

While previous studies have shown that TGF- β induces fibrosis with injury, it was not known how it impacted astrocyte ECM production, or how these ECM changes modulate the deposition of A β ₁₋₄₀. Our results indicate that TGF- β stimulation upregulates fibronectin, which was confirmed *in vivo*. It also increased *in vitro* A β ₁₋₄₀ uptake, which colocalized with regions of increased fibronectin/integrin- α 5 expression, indicating that this deposition occurred extracellularly. In light of our results from Chapter 4, this finding supports the

hypothesis that TGF- β induces astrocytes to modify the basement membrane in a way that favors CSF A β ₁₋₄₀ deposition.

Although previous studies have shown an association between reactive astrogliosis, altered AQP4 polarization and impaired CSF flow, it was not known whether TGF- β stimulation was sufficient to induce these phenotypes. Our results indicate that TGF- β altered AQP4 expression on astrocytes and induced cell swelling, which impaired water uptake. The impact of TGF- β on these physiological parameters was also confirmed *in vivo*, which occurred in the absence of significant increases in GFAP expression. This indicates that classical markers of astrocyte reactivity do not fully predict the functionality of perivascular astrocytes, instead requiring the use of A1 and A2-specific markers.

5.4.5: Inhibition of TGF- β signaling rescued fibrosis and perivascular CSF flow in aged animals.

We first examined the impact of TGF- β R1 antagonism in the subacute phase of injury (3 – 7 DPI), and found that it increased injury volume in both young and aged animals. We also found an interesting trend, which suggests an age-specific impact of TGF- β R1 antagonism in young and aged mice. While both groups exhibited an increase in injury size, only young mice had a corresponding increase in gliosis and ECM fibrosis. This suggests that TGF- β antagonism may actually reduce gliosis in aged mice, but this effect is masked by an increase in injury volume. To test this theory, we repeated the experiment in aged mice, but delayed the inhibitor treatment until 7 – 14 DPI to further avoid potential impacts on injury volume. When we used this dosing regimen, we found that TGF- β R1 antagonism significantly reduced GFAP and fibronectin expression. Furthermore, this was associated

with increased perivascular CSF flow and a relative decrease in CSF $A\beta_{1-40}$ deposition. This suggests that this therapy could be used to favorably modulate CSF-ISF exchange in a way that boosts the bulk flow of CSF without also increasing the deposition of CSF $A\beta_{1-40}$. This could be useful in the treatment of CAA in stroke survivors.

CHAPTER 6

Serum Biomarkers of Basement Membrane Fibrosis Are Diagnostic of CAA After Intracerebral Hemorrhage

6.1: Introduction

6.1.1: Overview.

Our preclinical studies, detailed in the preceding chapters, indicate that TGF- β signaling to astrocytes may drive post-stroke CAA by inducing a set of ECM changes termed ‘basement membrane fibrosis,’ impairing CSF flow. In particular, fibronectin appears to play a major role early in the disease process by sequestering CSF A β ₁₋₄₀, potentially causing the classic “outside-in” induction of CAA pathology that is typically observed in cortical vessels. Based on these findings, we also sought to explore the contribution of MMPs, which are a set of upstream enzymes that release both of these proteins from the ECM during states of inflammation. The studies detailed in this chapter indicate that TGF- β , MMPs and fibronectin are biomarkers of CAA-related intracerebral hemorrhage (ICH) in human patients. These interesting results further validate our previous findings in animal models, and increase their potential translational value to human disease.

6.1.2: Significance.

ICH is caused by acute rupture of cerebral vessels, and affects approximately 2 million individuals each year.²⁸¹ While hypertension remains the most common cause of spontaneous ICH, accounting for half of brain hemorrhages,¹ CAA is an additional major cause of lobar ICH that will likely increase due to our aging population.⁹⁷ While probable

CAA can be diagnosed by a set of MRI-based radiologic measurements termed the Boston criteria, definitive diagnosis requires an invasive brain biopsy that is not feasible for most patients.^{20,282} In theory, identification of a CAA-specific blood biomarker profile could facilitate an earlier, cheaper and less invasive diagnosis of CAA. Additional information about the underlying pathology and the prospects for recovery could help to guide individualized patient care, significantly improving the clinical management of CAA and patient outcomes after ICH.

CAA is a chronic disease process that involves the progressive accumulation of vascular amyloid plaques, leading to reduced vessel integrity, cognitive decline and increased susceptibility to ICH.²³ Underlying CAA may alter vascular responses to acute ICH, which could produce a unique molecular signature that can be measured peripherally. This molecular signature may involve fibronectin, TGF- β and MMPs, which are all interrelated molecules that are upregulated centrally in the brains of CAA patients,^{251,283} as well as peripherally in the general response to ICH. During ICH, MMPs act to enzymatically degrade basement membrane fibronectin^{284–286} and also cleave latent TGF- β , releasing the active form into the brain extracellular space.^{287,288} Degradation of the basement membrane leads to BBB disintegration, inducing extravasation of vascular components into the brain parenchyma, leading to increased fluid uptake, and recruitment of peripheral immune cells – all contributing to secondary injury.²⁸⁹ In contrast, release of TGF- β plays a major role in the resolution of brain injury via inducing phagocytosis and the formation of fibrotic scar tissue.^{228,290} Alterations in this divergent pathway could influence recovery from ICH, and could also provide insight into the existence of underlying CAA pathology.

While the role of these mediators in ICH has been studied to a greater extent in animal models, there is less literature on whether they can be used as prognostic markers clinically. Given the central role that MMPs, TGF- β and fibronectin are thought to play in the pathophysiology of secondary injury and recovery from ICH, we hypothesize that the levels of these mediators are not only associated with initial injury severity, but also with long-term functional deficits. Furthermore, due to significant overlap between expression of these markers in CAA and ICH, opening up the potential for disease-specific interactions, we also hypothesize that these mediators can also be used to diagnose CAA in the context of ICH.

6.1.3: Experimental design.

For all experiments, we utilized ICH patient data and serum samples from clinical repositories at both UT Health and Hartford Hospital. To test the hypothesis that the serum levels of these proteins are biomarkers of injury severity, we performed spearman correlation of these putative biomarkers against clinical measures of severity, including hematoma volume, radiologic measures of edema, as well as neurological scales of acute injury. Then, to determine whether these biomarkers were independent predictors of functional recovery, we developed a multivariable model to compare initial biomarker levels (< 5 DPI) and modified Rankin Scale (mRS) score at 90 DPI, which controlled for injury severity and other confounding clinical variables. Finally, to test the hypothesis that these biomarkers can be used alone or in combination to diagnose CAA, we performed receiver operating characteristic (ROC) analysis to determine whether these cytokines can discriminate between CAA and non-CAA hemorrhage in two independent cohorts.

6.2: Methods

6.2.1: Study population.

The current study utilized ICH patient data and serum samples from Hartford Hospital and the University of Texas Health Science Center in Houston (n = 63 patients). The study was approved by the Institutional Review Boards at both institutions, and all patients participating were consented. Patient data were abstracted from prospective ICH databases detailing admission data, radiology, hospital course and functional outcomes. Patients with hemorrhages due to underlying vascular lesions or traumatic brain injury were excluded from the study. For analysis of biomarker correlation with injury etiology, patients were divided into three groups: lobar hemorrhage of suspected CAA etiology (n = 21) and deep hemorrhage (n = 42). Lobar and deep hemorrhages were defined by the location of the ictus on CT, as interpreted by an independent neuroradiologist and confirmed by an experienced neurologist. Probable CAA was defined via the Boston criteria and was supported by pathological evidence in the majority of patients.^{20,31}

6.2.2: Measurement of neurological function.

Initial ICH severity was assessed using ICH score,²⁹¹ National Institute of Health Stroke Scale (NIHSS),²⁹² Glasgow Coma Scale (GCS)²⁹³ and mRS.²⁹⁴ Additionally, long-term functional outcomes were assessed by mRS at time of discharge and at 90 DPI.

6.2.3: Radiologic measurements.

Our primary radiologic outcomes were hematoma volume and intraventricular hemorrhage (IVH) volume as quantified via computer-based analysis with MIPAV

(Medical Image Processing, Analysis, and Visualization) software. IVH was scored on a 10-point scale developed at UT Health.²⁹⁵ Hematoma and IVH volumes were determined throughout the patient's entire hospitalization via review of every head CT obtained as a part of routine clinical care until discharge.

6.2.4: Serum sample collection.

Serum samples were obtained from our study cohort at pre-specified time points from 0 to 5 days post-ictus. Serial samples were collected from each patient when possible, for a total of 136 serum samples. In order to minimize timing bias, all biosamples were timed from the onset of ICH ictus and collected by a biospecimen collection team who were blinded to the clinical status of the patient. Samples were processed within 1 hour of collection and stored at -80 degrees Celsius until use.

6.2.5: Measurement of serum analytes.

Samples were thawed on ice for 1 hour and thoroughly vortexed prior to beginning any assays. Serum fibronectin was measured using the Human Fibronectin Quantikine ELISA Kit (R&D Systems). Following activation of latent TGF- β by acidification, TGF- β 1, TGF- β 2 and TGF- β 3 were measured using the Bio-Plex Pro TGF- β 3-PLEX Assay (Bio-Rad). Similarly, MMP1, MMP2, MMP3, MMP7, MMP8, MMP9, and MMP10 were measured using the Bio-Plex Pro Human MMP Panel (Bio-Rad). All assays were performed and read according to the manufacturer's instructions.

6.2.6: Statistics.

Descriptive statistics, including frequency, percent, mean, median, SD, interquartile range (IQR), were provided for demographics and admission variables in the subgroups of CAA hemorrhage, hypertensive hemorrhage, and overall groups. Wilcoxon rank sum test was used to compare values between CAA and hypertensive hemorrhage (**Table 6-1**). Cytokine levels were averaged between repeated samples from 0 – 5 DPI. For the combined CAA and hypertensive group, spearman correlation method was used to evaluate their relation to initial injury scores. P values were adjusted by Benjamini and Hochberg procedure (1995)²⁰ to control the false discovery rate (FDR) at 0.05 (**Table 6-2**). Similar correlation analysis was done for mRS at discharge and at 90 days (**Table 6-3**). Furthermore, a multivariable model was used to study the association between mRS at 90 days and several early cytokine levels separately, adjusted for hemorrhage type, age, systolic blood pressure, hematoma volume, GCS score, IVH and coagulopathy. Descriptive statistics (median and IQR) was provided for early cytokine levels and Wilcoxon rank sum test was used to compare them between CAA and hypertension hemorrhage (**Table 6-4**). P values are adjusted to control FDR within 0.05. Univariate or multivariable logistic regression was used to provide receiver operating characteristic (ROC) curve to discriminate between CAA and hypertensive hemorrhage, which was quantified in SAS as the area under the curve (AUC) (**Fig. 6-1**). All p values were adjusted similarly to control FDR at 0.05. All data analyses were performed in SAS software 9.4 (Cary, NC).

6.3: Results

6.3.1: Fibronectin, MMPs and TGF- β are differentially associated with initial hemorrhage burden.

To assess whether peripheral markers were related to injury severity, serum samples were first obtained from a total of 62 ICH patients that were subdivided by radiologic findings; 21 were patients with acute lobar hemorrhage that met the Boston criteria for definite or probable CAA, and 41 were patients with deep hypertensive hemorrhages. Groups significantly differed by age, systolic blood pressure, stroke severity (NIHSS, GCS) as well as injury volume and IVH (**Table 6-1**).

Following correction for the FDR ($p < 0.5$), we found several cytokines correlated with injury severity in our initial univariate analysis (**Table 6-2**). All three families of cytokines were associated with initial neurological function, as measured by the Glasgow Coma Scale (GCS). Specifically, elevated serum fibronectin was associated with better neurological function on admission (GCS, $p = 0.003$). In contrast, elevated TGF- β 1 ($p = 0.003$), TGF- β 2 ($p = 0.005$) and TGF- β 3 ($p = 0.004$) correlated with worse initial neurological deficits. Similarly, patients with high levels of MMP1 ($p = 0.003$), MMP3 ($p = 0.032$), MMP8 ($p = 0.003$), MMP9 ($p < 0.001$) and MMP10 ($p = 0.002$) also exhibited worse neurological deficits on admission. When the ICH score was used to estimate injury severity, we found that MMP3 ($p = 0.041$), MMP8 ($p = 0.041$), MMP9 ($p = 0.012$) and MMP10 ($p = 0.041$) were also positively associated with increased injury severity. Finally, MMP10 also correlated with increased IVH ($p = 0.002$). In summary, these results indicate that fibronectin, TGF- β and MMP isoforms are biomarkers of initial injury severity in our cohort of ICH patients.

| Characteristics | Total Cohort (n = 63) | CAA Hemorrhage (n = 21) | Hypertensive Hemorrhage (n = 42) | P-value | Significance |
|---|-----------------------|-------------------------|----------------------------------|-----------|--------------|
| Age, years (mean [SD]) | 67.79 (14.38) | 75.76 (9.64) | 63.71 (14.78) | p = 0.003 | ** |
| Female (n [%]) | 26 (41.94) | 10 (47.62%) | 16 (39.02%) | p = 0.516 | ns |
| | | | | | |
| <u>Race</u> | | | | | |
| Black (n [%]) | 10 (16.39) | 2 (9.52%) | 8 (19.51%) | p = 0.367 | ns |
| White (n [%]) | 39 (63.93) | 16 (76.19%) | 23 (56.1%) | p = 0.367 | ns |
| Asian (n [%]) | 3 (4.92) | 0 (0%) | 3 (7.32%) | p = 0.367 | ns |
| Hispanic/other (n [%]) | 9 (14.75) | 2 (9.52%) | 7 (17.07%) | p = 0.367 | ns |
| | | | | | |
| Admission systolic blood pressure, mm Hg (mean [SD]) | 188.04 (32.34) | 171.55 (27.23) | 202 (30.44) | p = 0.03 | * |
| Admission diastolic blood pressure, mm Hg (mean [SD]) | 109.83 (35.25) | 96.45 (16.63) | 121.15 (42.99) | p = 0.145 | ns |
| GCS (median [IQR]) | 14 (4.25) | 15 (1) | 9.5 (4.5) | p = 0.039 | * |
| ICH score (median [IQR]) | 2 (2) | 1 (1.5) | 2 (2) | p = 0.667 | ns |
| NIHSS (median [IQR]) | 12 (17.5) | 7 (10) | 17 (17.25) | p < 0.001 | *** |
| Initial hematoma volume, cm ³ (mean [SD]) | 25.76 (22.74) | 37.44 (28.04) | 19.08 (15.98) | p = 0.015 | * |
| IVH score (median [IQR]) | 0 (5.5) | 0 (0) | 16 (6) | p = 0.006 | ** |

Table 6-1. Demographics and admission variables by study group. Data are analyzed by

*Wilcoxin Rank Sum Test. *p < 0.05, **p < 0.01, ***p < 0.001.*

| Admission Variable | Cytokine | Correlation | P-value, raw | Significance, raw | P-value, FDR adjusted | Significance, FDR adjusted |
|-------------------------|-------------|-------------|--------------|-------------------|-----------------------|----------------------------|
| Age | TGF-β1 | -0.293 | p = 0.021 | * | 0.144 | ns |
| | TGF-β3 | -0.271 | p = 0.033 | * | 0.144 | ns |
| | MMP9 | -0.263 | p = 0.039 | * | 0.144 | ns |
| NIHSS | TGF-β1 | 0.356 | p = 0.007 | ** | 0.058 | ns |
| | TGF-β3 | 0.34 | p = 0.01 | * | 0.058 | ns |
| | MMP1 | 0.286 | p = 0.032 | * | 0.09 | ns |
| | MMP9 | 0.296 | p = 0.027 | * | 0.09 | ns |
| GCS | Fibronectin | 0.495 | p < 0.001 | *** | 0.003 | ** |
| | TGF-β1 | -0.484 | p < 0.001 | *** | 0.003 | ** |
| | TGF-β2 | -0.431 | p = 0.004 | ** | 0.005 | ** |
| | TGF-β3 | -0.446 | p = 0.003 | ** | 0.004 | ** |
| | MMP1 | -0.472 | p = 0.001 | ** | 0.003 | ** |
| | MMP3 | -0.338 | p = 0.027 | * | 0.032 | * |
| | MMP8 | -0.471 | p = 0.001 | * | 0.003 | ** |
| | MMP9 | -0.596 | p < 0.001 | *** | p < 0.001 | *** |
| ICH Score | TGF-β1 | 0.269 | p = 0.039 | * | 0.072 | ns |
| | TGF-β3 | 0.278 | p = 0.033 | * | 0.072 | ns |
| | MMP1 | 0.327 | p = 0.012 | * | 0.041 | * |
| | MMP8 | 0.315 | p = 0.015 | * | 0.041 | * |
| | MMP9 | 0.414 | p = 0.001 | ** | 0.012 | * |
| | MMP10 | 0.345 | p = 0.008 | ** | 0.041 | * |
| Initial Hematoma Volume | TGF-β2 | 0.289 | p = 0.033 | * | 0.198 | ns |
| | MMP3 | 0.283 | p = 0.036 | * | 0.198 | ns |
| IVH Score | MMP8 | 0.49 | p = 0.018 | * | 0.065 | ns |
| | MMP9 | 0.524 | p = 0.01 | * | 0.057 | ns |
| | MMP10 | 0.609 | p = 0.002 | ** | 0.023 | * |

Table 6-2. Early cytokine levels and their relation to initial injury scores. Data are analyzed by Spearman correlation, and both raw and FDR-corrected P-values are presented. Raw and FDR-adjusted significance: * $p < 0.05$, ** $p < 0.01$, *** $p < 0.001$, ns: no significance.

| Outcome Variable | Cytokine | Correlation | P-value, raw | Significance, raw | P-value, FDR adjusted | Significance, FDR adjusted |
|------------------|-------------|-------------|--------------|-------------------|-----------------------|----------------------------|
| mRS at discharge | TGF-β1 | 0.336 | 0.037 | * | 0.143 | ns |
| | TGF-β3 | 0.352 | 0.028 | * | 0.143 | ns |
| | MMP9 | 0.326 | 0.043 | * | 0.143 | ns |
| mRS at 90 days | Fibronectin | -0.302 | 0.049 | * | 0.089 | ns |
| | TGF-β1 | 0.478 | 0.001 | ** | 0.012 | * |
| | TGF-β2 | 0.39 | 0.01 | * | 0.035 | * |
| | TGF-β3 | 0.456 | 0.002 | ** | 0.012 | * |
| | MMP1 | 0.376 | 0.013 | * | 0.035 | * |
| | MMP9 | 0.312 | 0.042 | * | 0.089 | ns |

Table 6-3. Early cytokine levels as predictors of functional outcome scores. Data are analyzed by Spearman correlation, and both raw and FDR-corrected P-values are presented. Raw and FDR-adjusted significance: * $p < 0.05$, ** $p < 0.01$, *** $p < 0.001$, ns: no significance.

6.3.2: Early elevations of TGF-β predict the degree of long-term functional deficits.

We next evaluated whether serum fibronectin, TGF-β and/or MMPs were predictive of functional outcomes in our ICH patients. Specifically, we analyzed whether cytokine levels were associated with mRS at discharge and at 90 days by univariate analysis (**Table 6-3**). While no cytokines significantly correlated with mRS at discharge, increased levels of TGF-β1 ($p = 0.012$), TGF-β2 ($p = 0.035$), TGF-β3 ($p = 0.012$) and MMP1 ($p = 0.035$) were all significantly associated with poor mRS at 90 DPI. To confirm these findings, we then performed a multivariate regression to determine whether these effects were independent of group differences in admissions data (identified in **Table 6-1**). Even when hemorrhage type, age, systolic blood pressure, hematoma volume, GCS score, IVH score and coagulopathy diagnosis were controlled for, TGF-β1 ($p = 0.013$), TGF-β2 ($p = 0.041$) and TGF-β3

| Cytokine | CAA Median (IQR) | Hypertensive Median (IQR) | P-value, raw | Significance, raw | P-value, FDR-adjusted | Significance, FDR-adjusted |
|-------------|---------------------|---------------------------|--------------|-------------------|-----------------------|----------------------------|
| Fibronectin | 238.92 (136.23) | 301.57 (120.76) | p = 0.027 | * | 0.2569 | ns |
| TGF-β1 | 33016.03 (78087.73) | 37810.92 (25226.81) | p = 0.094 | ns | 0.2569 | ns |
| TGF-β2 | 1439.43 (9633.69) | 1437.38 (197.48) | p = 0.925 | ns | 0.9248 | ns |
| TGF-β3 | 1300.95 (1795.86) | 1337.94 (307.26) | p = 0.257 | ns | 0.4035 | ns |
| MMP1 | 837.35 (1491.25) | 611.56 (2100.66) | p = 0.693 | ns | 0.7627 | ns |
| MMP2 | 21995.26 (11778.3) | 17540.91 (11822.09) | p = 0.14 | ns | 0.2569 | ns |
| MMP3 | 3384.31 (6346.49) | 4946.22 (7424.91) | p = 0.547 | ns | 0.6687 | ns |
| MMP7 | 2044.58 (1374.17) | 2702.82 (1530.49) | p = 0.129 | ns | 0.2569 | ns |
| MMP8 | 2292.1 (3026.67) | 2473.47 (4843.15) | p = 0.422 | ns | 0.5796 | ns |
| MMP9 | 22055.53 (12685.96) | 28395.04 (39910.81) | p = 0.122 | ns | 0.2569 | ns |
| MMP10 | 1670.3 (892.67) | 2237.56 (2138.41) | p = 0.071 | ns | 0.2569 | ns |

Table 6-4. Comparison of serum cytokine values in CAA and hypertensive hemorrhage patient populations. In general, individual cytokine values did not discriminate between CAA and hypertensive hemorrhage. Data were analyzed by Wilcoxon rank sum test, and both raw and FDR-corrected P-values are presented. *Raw and FDR-adjusted significance: *p < 0.05, **p < 0.01, ***p < 0.001, ns: no significance.*

(p = 0.018) remained significant predictors of mRS at 90 DPI. Overall, these data indicate that elevated serum levels of TGF-β1, TGF-β2 and TGF-β3 are biomarkers of poor long-term functional recovery, independent of initial injury, baseline characteristics or type of ICH.

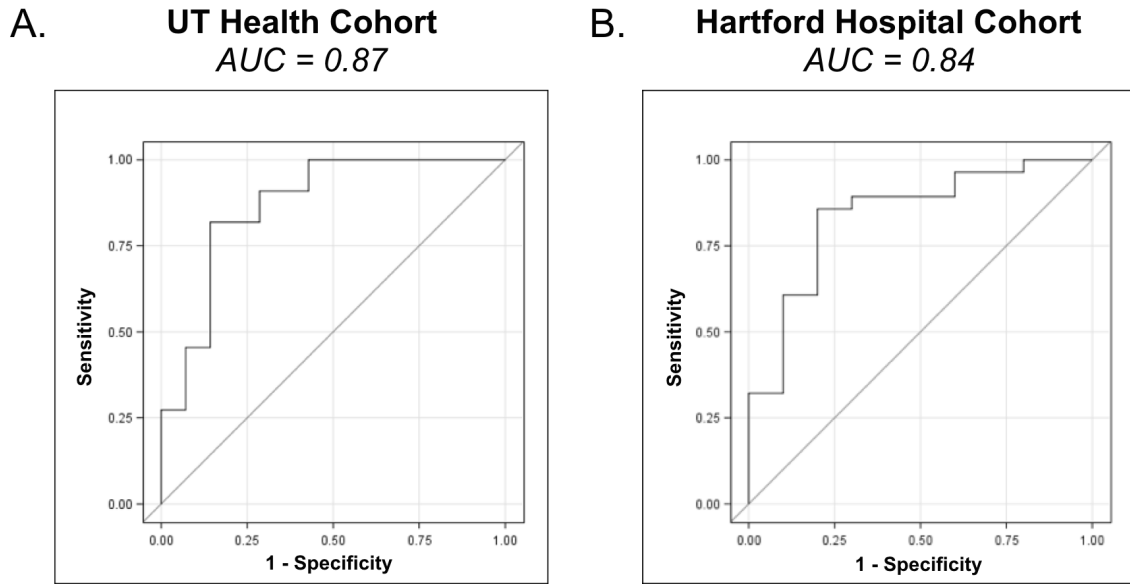


Figure 6-1. Biomarkers of small vessel fibrosis discriminate between CAA and hypertensive hemorrhage. (A) ROC curve comparing CAA and hypertensive hemorrhage within the UT Health cohort. (B) ROC curve comparing CAA and hypertensive hemorrhage within the Hartford Hospital cohort.

6.3.3: Serum biomarkers distinguish CAA from deep hypertensive hemorrhages.

In order to determine whether these biomarkers could function as a diagnostic panel for CAA, we first compared individual cytokine levels between CAA and deep hypertensive hemorrhage ICH patients (**Table 6-4**). Univariate analysis showed that CAA patients tended to have lower serum levels of fibronectin and MMPs after ICH, however, none reached statistical significance following FDR correction (**Table 6-4**). However, when fibronectin, MMPs and TGF- β were included in an exploratory multivariable ROC model, the AUC was 0.8701 (**Fig. 6-1A**), which was also found in a second exploratory cohort (AUC = 0.8393)

(Fig. 6-1B). These results indicate that this test may reliably distinguish between CAA and deep hypertensive hemorrhage, but requires further validation in larger independent cohorts.

6.4: Discussion

In the current study, we extensively characterized the expression profile of multiple MMP isoforms along with two downstream targets, TGF- β and fibronectin, in the serum of patients with CAA and hypertensive ICH. We found that these cytokines were modulated by both hemorrhage etiology and initial hemorrhage burden. Importantly, we also delineated cytokine profiles that can be associated with (1) positive diagnosis of CAA and (2) long-term functional outcomes. Overall, these preliminary findings highlight multiple candidate families of biomarkers that could one day be used to improve the diagnosis and management of ICH. Our ultimate goal is to identify candidate blood biomarkers for CAA-related ICH. CAA diagnosis is currently accomplished by cortical biopsy²⁰ or a complex set of radiologic measurements termed the Boston criteria.²⁸² However, there are disadvantages to both strategies, including cost, invasiveness and requirement for extensive technical expertise, making these tests prohibitively challenging outside of highly specialized medical centers. Therefore, identification of biomarkers could one day lead to a simple blood test that could enable CAA diagnosis in a broader clinical setting.

Previous work has shown that CAA is associated with local (e.g. brain tissue) changes in TGF- β ,^{251,296,297} fibronectin,^{251,297} and MMP activation.^{298,299} However, there is a general lack of studies examining these cytokines peripherally (e.g. in the serum) of CAA patients with ICH. We found that CAA was associated with a distinct pattern of cytokine expression. Similar to previous work, we found that TGF- β alone was not diagnostic for CAA.³⁰⁰ However, when TGF- β was included with fibronectin and MMPs, the panel as a whole could reliably distinguish CAA from deep hypertensive hemorrhage in two independent exploratory cohorts. Further studies with larger patient cohorts are warranted to

explore individual cytokines that failed to reach statistical significance, which could further improve the diagnostic potential of the cytokine panel in lobar ICH.

We also sought to determine how the expression profiles of MMPs, TGF- β , and fibronectin relate to clinical characteristics at admission. MMP9 has been previously associated with edema and neurologic deterioration after ICH.³⁰¹ While one previous study found that acute reductions in TGF- β were associated with worse long-term outcomes after ICH, that study did not differentiate patients by likely CAA and examined platelet-depleted plasma²²⁸ Finally, previous work using cellular fibronectin-specific antibodies suggested high levels of cellular fibronectin in the serum was associated with hematoma expansion and poorer outcomes,³⁰² however, cellular fibronectin likely represents a small portion of the total circulating fibronectin, measured in our study. Our data indicates that elevated expression of TGF- β and several MMP isoforms were associated with greater initial hemorrhage burden, while total serum fibronectin levels were associated with reduced injury severity. Serum fibronectin could competitively inhibit MMPs by occupying the MMP active site; further work in animal models is required to determine a potential mechanism linking fibronectin and reduced ICH severity.

Additionally, we also examined whether serum levels of MMPs, TGF- β , and fibronectin could serve as prognostic blood biomarkers of long-term functional outcome. Previous work has suggested high levels of cellular fibronectin and MMP9 are associated with hematoma expansion,³⁰² but there is minimal data regarding long-term prognostication (for instance, at 90 DPI).^{228,301} One study found that MMP3 and MMP9 levels correlated with worse functional outcomes after ICH.³⁰³ While we found a similar association between mRS and MMP9 in our univariate analysis, it did not reach the FDR threshold in our study due to

the higher number of cytokines analyzed. However, we did find that patients with higher early levels of TGF- β isoforms exhibited worsened functional outcomes after ICH. While TGF- β may be beneficial in acute injury, chronic exposure to this potent cytokine stimulates astrocytes to hypertrophy, divide, and secrete a variety of extracellular matrix proteins, leading to increased glial scarring, that has been shown to impede recovery in animal models of brain injury, in part by reducing angiogenesis and axonal reorganization.^{251,304,305,223,306} As such, TGF- β measurement during acute injury may allow healthcare providers to better identify patients who are most at-risk for long-term disability as early as 24 hours after ICH, independent of clinical severity.

Altogether, our study suggests these markers of BBB remodeling and fibrosis are differentially expressed in CAA and hypertensive hemorrhage, and may serve as serum biomarkers of initial injury severity and long-term functional outcomes. Further work is needed to confirm these findings and to refine these targets into a diagnostic panel for CAA. A better understanding of the differences in the pathophysiology of deep and lobar hemorrhage may aid in future site-specific biomarker identification and the eventual development of targeted therapeutics for different types of ICH.

CHAPTER 7

Discussion & Future Directions

7.1: Summary and overview of the literature.

CAA represents a fascinating area of research, having a wide variety of seemingly unrelated risk factors, impacting some individuals and not others, and leading to cognitive decline via multiple, potentially overlapping mechanisms. The etiology of the disease is not well understood, and there are no disease-modifying treatments available to CAA patients. Our studies represent an attempt to cast a light over the earliest stages of this disease, to determine where, when and how the initial induction of amyloid pathology can occur in individuals with ischemic stroke. While the picture is still incomplete, this work serves as a starting point for a unified mechanism of CAA induction, and new treatment strategies for this devastating disease.

The story of CAA began when the famed pathologist Rudolph Virchow first described amyloid deposits in 1854.²³ Over 50 years later, in 1906, a clinical psychiatrist and neuroanatomist named Alois Alzheimer discovered brain atrophy when he came across the case of Auguste Deter, a 55 year-old woman who suffered from rapidly progressive memory disturbances, sleep disruption, mood changes and increasing confusion before her death.³⁰⁷ At a major medical conference, he described these findings as a “peculiar severe disease process of the cerebral cortex” and theorized that her amyloid deposits were the underlying cause of her symptoms.³⁰⁷ Like most revolutionary thinkers, his presentation went largely unnoticed; fortunately, progress in the field quietly continued forward.³⁰⁷ Just three years later, a pathologist named Gustav Oppenheim found that cerebral amyloid deposits tended to

occur in two distinct extracellular locations: the parenchymal tissue between neurons, as well as the perivascular regions around cerebral vessels, a type of pathology later termed ‘amyloid angiopathy’.²³ Subsequent investigations confirmed that CAA was an independent disease process distinct from Alzheimer’s disease.²³ Finally, in 1979, a neuropathologist named Haruo Okazaki was the first to associate CAA with vessel wall stenosis, microinfarction, microhemorrhages and lobar hemorrhage in dozens of autopsy cases at the Mayo Clinic,³⁰⁸ bringing us to our current general understanding of the pathogenesis of CAA.

Since then, the most significant advances in CAA research, from a medical perspective, have to do with the detection of disease. In 1982, C.Q. Mountjoy developed the first CAA grading scheme, which assigned an ‘amyloid score’ based on the number of amyloid positive vessels in autopsy cases.³⁰⁹ However, this needed further refinement, as it did not significantly predict cognitive decline prior to death.³⁰⁹ In 1991, John Vonsattel developed a more sensitive/specific grading scheme for CAA, based on brain biopsy.^{19,20} In contrast with the earlier scheme, this method examines individual blood vessels for multiple characteristics of CAA, including the amount of amyloid present, the thickness of the tunica media, as well as the degree of vessel leakage and fibrinoid necrosis.¹⁹ Later, in 1995, John Olichney developed a separate scale, which grades the severity of CAA purely based on how many leptomeningeal and cortical vessels in a given brain section exhibit amyloid deposits, as well as how large the amyloid deposits are on each vessel (Olichney 1995).³¹⁰ While the latter two methods remain in use today, and are required to establish definitive CAA diagnosis, the use of non-invasive imaging has spurred an additional leap forward in the early detection of CAA.

In 2001, Steve Greenberg published validation of the ‘Boston criteria’, which can make a non-invasive diagnosis of CAA by counting the number of MRI-visible microhemorrhages.³¹ Since then, these criteria have been updated to include the presence of lacunar infarction, leukoairaiosis, superficial siderosis, cortical atrophy and enlarged PVS.³¹¹ Future diagnostic strategies include measurement of CSF A β ₁₋₄₀,¹⁵⁰ as well as PET imaging with fluorbetapir, a compound that binds amyloid deposits in the brain.³¹² Additionally, the development of blood biomarkers for distinguishing CAA hemorrhage from hypertensive hemorrhage could further improve the diagnosis of CAA in patients, as we have found in our research (see Chapter 6).

While earlier and more sensitive diagnosis of CAA has already improved patient care, in contrast, the search for a cure has raised as many questions as answers. The bottom line is that, while we can now detect earlier disease, the progressive vessel damage and cognitive decline cannot be stopped with current therapies. We still do not understand how this disease progresses, and why it impacts more than half of individuals over the age of 80. These outstanding questions largely have to do with a poor understanding of the underlying cause of CAA. For example, why does amyloid pathology develop around the cerebral arteries, and not the veins? Why do these arterial plaques first tend to develop in the cortex and cerebellum, rather than other areas of the brain? Is there a common thread running through the multitude of genetic and cardiovascular risk factors for CAA? Why does sporadic CAA only affect the elderly? In isolation, without predisposing risk factors, do focal events such as stroke induce amyloid pathology, or merely accelerate an existing disease process?

I began my search for answers by examining the literature, and found that a newly discovered system of perivascular flow, termed the ‘glial lymphatic’ (or glymphatic) system,

bathes the basement membrane of cortical arteries, arterioles and capillaries in a constant supply of fresh CSF.¹²⁵ My research led me to find papers indicating that CSF contains waste products such as $A\beta_{1-40}$,^{149,150,313} and to wonder whether small amounts of $A\beta_{1-40}$ could recirculate through the arterial basement membrane. Previous work suggested that stroke modifies basement membrane composition,⁹⁰ but much of this earlier work was studied in the context of angiogenesis^{155,258} or trafficking of immune cells through the BBB.^{166,169} Furthermore, the impact of aging on post-stroke basement membrane remodeling had not been defined, providing a few potential areas to add to the literature. Given that CAA is associated with basement membrane alterations,²⁸⁰ that pathology is initiated within the superficial cortical PVS,^{20,314} and that elevated levels of CSF $A\beta_{1-40}$ represents the earliest biomarker of CAA development,²⁵⁰ I proposed that we could build a coherent mechanism of CAA based around this newly discovered physiology.

7.2: Review and critical analysis of current research findings.

Upon beginning our work at UT Health, I first independently confirmed the existence of perivascular CSF flow in a series of early experiments, detailed in Chapter 3. We used intracisternal Evans blue dye injection to grossly examine CSF flow pathways through the cisterns that surround the brain, and then sectioned the brains to confirm that this dye rapidly penetrated into the deepest brain structures. Next, we verified that this dye influx occurred along perivascular routes by simultaneously labeling plasma and CSF with fluorescent dyes, and found that they co-labeled vascular structures. With this basic knowledge in hand, we then performed a series of quantitative time-course experiments to examine the influx kinetics of small tracers into the brain, as well as the clearance of $A\beta_{1-40}$ relative to larger

proteins. Over the course of these experiments, we discovered something interesting: CSF solutes were partitioned into separate layers of the basement membrane based on size. This unexpected finding provided us with early evidence that the basement membrane plays an active role in regulating the distribution of CSF solutes, which could have significant implications for our current understanding of how and why $A\beta_{1-40}$ deposits within the basement membrane in certain individuals.

Based on both my literature review and these exciting preliminary data, I developed a new hypothesis that a family of stroke-induced basement membrane changes, broadly defined as fibrosis, could impact the perivascular flow of CSF in two major ways. First, I imagined that overall hypertrophy of the basement membrane could provide focal interruptions in the flow of CSF through these perivascular pathways. This might be similar to how a blood clot occludes an artery, but outside of the vessel. Second, I predicted that increases in perivascular fibronectin, a common component of blood clots, amyloid plaques and the injured basement membrane, could bind CSF $A\beta_{1-40}$ at physiologically relevant concentrations, forming the beginnings of perivascular pathology. Together, these phenomena could lay a trap for CSF $A\beta_{1-40}$ as it circulates through the basement membrane after stroke. This could further worsen in aged animals due to their reduced CSF turnover and increased propensity to form fibrotic glial scars after injury, explaining why aged individuals are particularly vulnerable to CAA.

After some debate, we decided to model experimental stroke by using permanent DMCAO, a well-established experimental model of cortical infarction,²⁵³ which I had been introducing to our laboratory as a new technique. While the injury size in the ischemic-sensitive Balb/c mice proved to be too large for accurate physiology measurements, we found

that C57BL/6 mice exhibited a loss of just 10-15% of brain tissue within the injured hemisphere, which was not modified by aging. The latter combination provided an ideal model for several reasons, including a restricted cortical location, greater reproducibility of injury size for our physiological measurements, low mortality for our longer-term studies, and no significant impact of aging on injury volume.

Upon beginning our experiments, we quickly found that DMCAO increased the expression of fibronectin and its co-receptor integrin- $\alpha 5$, and also increased tomato lectin binding to the basement membrane (presumed to be due to increased vascular HSPG content). In particular, integrin- $\alpha 5$ and lectin⁺ matrix was highest in aged animals with stroke, which had not been shown previously. When we measured CSF influx using fluorescent 3 kD dextran particles, we discovered that aging and stroke both dramatically restricted the distribution of these solutes. The intensity of basement membrane lectin staining exhibited a weak, but statistically significant negative correlation with dextran influx in aged mice with stroke. This was our first suggestion that basement membrane proteins could impact perivascular CSF flow. At the same time, when we co-injected fluorescent A β_{1-40} , we found that they formed superficial, perivascular deposits in aged mice with stroke. This was particularly apparent in vessels around the infarct, as well as more broadly in an astrocyte and fibronectin-rich region of the brain called the glia limitans. In contrast to dextran, we found that the degree of A β_{1-40} deposition strongly correlated with lectin intensity. We also found that A β_{1-40} deposits strongly colocalized with fibronectin and integrin- $\alpha 5$ staining. Additionally, we tested the affinity of fibronectin for A β_{1-40} *in vitro*, and found that they bound each other at physiological concentrations. These fibronectin-A β_{1-40}

conjugates deposited more readily into the brains of naïve young mice, indicating that fibronectin contributes to the deposition of A β ₁₋₄₀ in aging and after stroke.

The above experiments support our hypothesis that the basement membrane specifically impacts the transport of CSF A β ₁₋₄₀, which was particularly evident in aged mice with stroke. A major strength of this study is the use of a disease-relevant injury model in aged animals, which adds significant translational value to our findings. Another strength is that, unlike many of our contemporaries,²⁰⁸ we used recombinant A β ₁₋₄₀ in addition to size-matched dextran molecules. This proved to be important, as we found that the behavior of A β ₁₋₄₀ differed significantly *in vivo*, highlighting the need to use the actual peptide to draw any relevant conclusions about its transport through the brain extracellular space.

My decision to use wild-type mice, which do not develop amyloid pathology with aging, provides some interesting benefits and drawbacks to our study. We chose to use these mice over the existing transgenic AD model mice because we were most interested in studying the very earliest stages of CAA pathology. My choice to inject recombinant A β ₁₋₄₀, rather than relying on genetic overexpression, allowed us to precisely control the timing and route of exposure, providing us with the ability to specifically study the behavior of CSF A β ₁₋₄₀ in the absence of any pre-existing amyloid pathology. However, there are downsides to our approach. The biggest weakness is that it raises the question as to whether or not we are really modeling CAA—we have no way of knowing whether these small deposits, which form over the course of just 30 minutes, are stable and could develop into mature CAA plaques. Since these wild-type mice cannot develop CAA pathology, we could not directly study the impact of CAA on post-stroke cognitive function. Additionally, due to the need to remove the brain to measure tracer distribution, we were restricted to single time-point

studies and therefore could not study the growth of these deposits over time (this has since been remedied by the establishment of an *in vivo* two-photon microscopy core). We are currently working to address these weaknesses by performing DMCAO in multiple strains of AD model mice, including Tg2576, TgSwDI, and APP/PS1, then staging plaque pathology and measuring cognitive function. This will be further elaborated in later discussions of future directions.

The other major weakness is the lack of fibronectin knockout experiments, which would be a useful final confirmation of the importance of fibronectin in the context of stroke. While we had considered this experiment, we concluded that it was not feasible for us, because fibronectin knockout is embryonically lethal, and alternative strategies, such as antibody therapies, do not cross the BBB efficiently. Future studies could be performed to engineer an inducible knockout of fibronectin using a cre/flox system, but establishing these lines is very expensive and time-consuming, forcing us to conclude that it was beyond the scope of my fellowship. However, this weakness is partially addressed in the next set of experiments, which indirectly reduces perivascular fibronectin expression by inhibiting upstream signaling pathways with a more translational approach.

After establishing the role of basement membrane fibrosis in impairing the transport of CSF A β ₁₋₄₀, I next sought to better understand how basement membrane composition is regulated in the brain, and whether manipulating these upstream pathways can reverse post-stroke increases in fibronectin in young and aged animals. Returning to the literature, I found that astrocytes, endothelial cells and pericytes all play potential roles in regulating the composition of the basement membrane,^{90,196} and that TGF- β is a major inducer of fibronectin expression and CAA pathology.^{219,251,280,304} However, it was not known which

cell types that TGF- β stimulates to produce fibronectin, or whether inhibiting TGF- β signaling would sufficiently reduce these changes after stroke. Earlier on, I had acquired some preliminary data showing that stroke increased perivascular GFAP expression, which is a nonspecific marker of astrocyte activation, and that this activation primarily occurred on astrocytic endfeet apposed to perivascular fibronectin deposits. This led me to hypothesize that TGF- β activates astrocytes to remodel the basement membrane, impair the perivascular flow of CSF, and produce fibronectin to trap CSF A β_{1-40} . Based on this idea, I further hypothesized that delayed inhibition of TGF- β could reduce perivascular gliosis, reverse basement membrane fibrosis and improve perivascular CSF flow.

We first examined how aging and stroke interact to induce astrocyte reactivity by performing DMCAO in young and aged mice, then examining GFAP and vimentin expression seven days later. We found that aging increased astrocyte reactivity at baseline and following stroke, and that this phenomenon also occurred in perivascular astrocytes. Surprisingly, while aging did not increase total TGF- β expression, it did alter the downstream signaling pathways to a potentially detrimental Smad3 phenotype. To better understand how ischemia, TGF- β and A β_{1-40} interact to regulate astrocyte phenotype (defined as A1 and A2), we then cultured primary murine astrocytes and exposed them to those stimuli in various combinations. We found that A β_{1-40} and ischemia induced opposing phenotypes (A1 and A2, respectively), and that TGF- β played more of a modulatory role in altering the expression of a variety of ECM proteins and cytokines. Beyond these acute changes in astrocyte phenotype and gene expression, we also found that chronic exposure to TGF- β induces astrocytes to express fibronectin and integrin- $\alpha 5$ at high levels, which colocalized with fluorescent A β_{1-40} *in vitro*. We further found that TGF- β altered AQP4 polarization, and

reduced water uptake by astrocytes, which has been shown to also be important for maintaining efficient CSF flow by other laboratories.¹²⁵ We confirmed our findings by injecting TGF- β into young mice *in vivo*, and found similar effects of treatment. Overall, these studies uniformly support a detrimental role of TGF- β on basement membrane fibrosis, A β ₁₋₄₀ distribution and CSF flow.

Based on all of this information, we finally sought to determine whether inhibiting TGF- β could rescue the stroke-induced changes in astrocyte reactivity, basement membrane composition and CSF A β ₁₋₄₀ transport that we had repeatedly observed in our previous sets of experiments. We initially bred GFAP^{cre/wt} x TGF β R2^{flox/flox} mice to specifically inhibit TGF- β signaling to astrocytes, but found that peripheral treatment with a TGF- β R1/R2 antagonist was a far more effective strategy. As predicted, we found that TGF- β inhibition reduced astrocyte reactivity, downregulated perivascular fibronectin expression, rescued CSF flow and reduced the binding of CSF A β ₁₋₄₀ to the basement membrane. These final experiments confirm the role of TGF- β in mediating these changes, but leave a question hanging over the sole importance of astrocytes in this process.

One strength of these experiments is the use of primary cells for our *in vitro* models, which we feel better represents the function of astrocytes in our animal models than immortalized cell lines. An additional strength is that we confirmed our most important findings with both *in vitro* and *in vivo* systems, further improving our confidence in these data. Finally, another strength is the use of a peripheral TGF- β antagonist following stroke, which provides a more translational approach for drug delivery than other potential strategies.

However, there are also some weaknesses in our approach. First, while gliosis was higher in the aged animals, the absolute levels of TGF- β did not change. We attribute this discrepancy to different patterns of Smad activation, but we were not able to confirm this with Smad mutant mice as it was beyond the scope of my aims. This could be examined by more robust follow-up studies involving knockouts of these various downstream signaling pathways. An additional potential weakness is that we elected to use *in vitro* stimulation of primary astrocyte cultures, rather than a more intensive approach involving *in vivo* stimulation of astrocytes, followed by *ex vivo* cell sorting techniques used by other laboratories.²⁴⁰ While *in vivo* stimulation may provide a more accurate representation of *in vivo* cellular responses,²³⁹ we selected our approach because it allowed us to study the behavior of these cells in isolation over longer periods of time. This gave us a chance to also measure the impact of chronic stimulation on protein expression, A β_{1-40} deposition and water uptake. However, other cells, particularly pericytes and endothelial cells, could also be playing a role *in vivo*, necessitating further studies of other cell types. Finally, the biggest weakness of these studies is that GFAP^{cre/wt} x TGF β R2^{flox/flox} genotype was significantly less effective than the inhibitor studies in our hands. While our initial experimental design dictated that we induce the knockout a full seven days after stroke to avoid detrimental effects due to increased inflammation,²²⁹ pre-stroke induction may be more effective at inhibiting TGF- β signaling. In addition to these technical issues, other cell types may respond to TGF- β in similar ways, potentially compensating for the effects of the conditional knockout compared to the more effective global inhibitor strategy.

As we completed these animal experiments, I also began to examine whether molecules associated with basement membrane fibrosis could be used as clinical biomarkers

of CAA in the serum of human ICH patients. A review of the literature revealed that there were very few studies of serum biomarkers for CAA, with the majority examining the levels of serum amyloid species and finding contradictory results.³¹⁵ I hypothesized that serum levels of levels of fibronectin, TGF- β and MMPs would correlate with CAA diagnosis, injury severity and functional outcomes. I was fortunate to collaborate with a clinical researcher who had collected serial serum samples and obtained extensive medical records from ICH patients. Based on a combination of imaging and histopathological criteria, we were able to classify patients with lobar hemorrhages due to probable CAA, and compare those with patients who had deep hypertensive hemorrhages. We found that MMPs positively correlated with injury severity in a univariate analysis, TGF- β negatively correlated with functional outcomes even with multivariate correction, and when all cytokines were included in a preliminary ROC analysis, we found that they provided a panel for CAA diagnosis that was sufficiently sensitive and specific to reliably discriminate CAA from other types of ICH.

The strengths of our study include the use of prospective ICH cohorts from two separate institutions, which allowed us to independently validate our findings with respect to the ROC analysis. Also, the use of plasma allows for minimally invasive screening of CAA, compared to other strategies that involve expensive and time-consuming MRI, or potentially dangerous collection strategies such as lumbar puncture to collect CSF, or even invasive brain biopsies requiring removal of the skull and cortical tissue. An additional strength was the overall novelty of the findings and the immediate potential for translation to human patients. The lack of a realistic and reliable screening test for patients represents a major roadblock to early intervention in the pathogenesis of CAA, which can only be remedied by the development of more reliable blood biomarkers such as these molecules.

Of course, this study has some important limitations. First, due to limited sample availability, we were faced with some underpowered comparisons and an overall lack of statistical significance of individual cytokines between CAA and hypertensive hemorrhages. This weakness will be remedied in future follow-up studies with larger patient cohorts, for which we are already seeking funding. Second, missing time-points over the five day collection period required us to average values from each patient, rather than directly comparing individual time-points. While this is not ideal, we found that cytokine values were stable over this collection period, with no statistically significant variation with time, mitigating this problem. Finally, we were unable to obtain histopathological confirmation of CAA in all of the ‘probable CAA’ patients, as it would have required an invasive brain biopsy that was sometimes not needed by the patient. This required us to rely on suboptimal MRI biomarkers to define CAA in a subset of our patients. This will be addressed in future studies with larger cohorts, which will allow us to require a definitive, biopsy-confirmed positive or negative diagnosis in all patients.

Overall, while each study has their own unique strengths and weaknesses, as a whole they provide an interesting take on CAA that deserves further study. From recombinant peptides, to cultured cells, to mouse models, and all the way up to human patients, our experiments consistently demonstrate the importance of these molecules in influencing the spread of amyloid pathology after injury. In the remainder of this discussion, I will attempt to synthesize these results with the existing literature into an updated model of CAA pathogenesis. Then, I will describe several exciting new areas of investigation, a few of which are already underway in our laboratory.

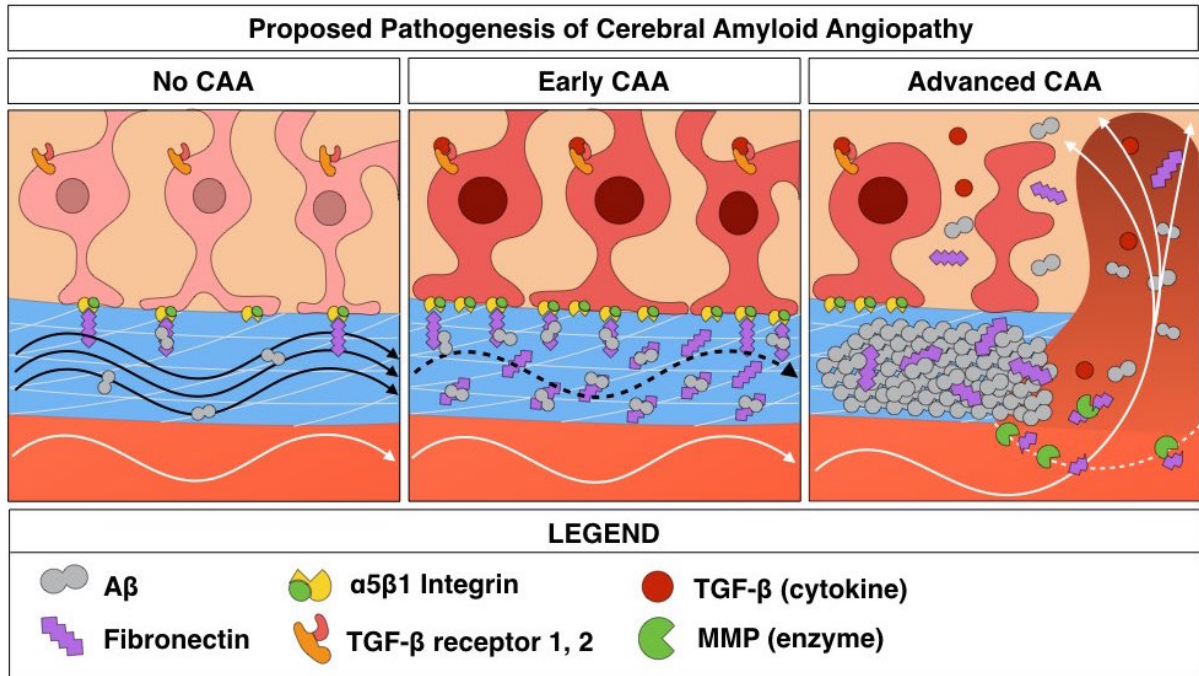


Figure 7-1: Working model of CAA pathogenesis. CAA can be divided into multiple phases, with early CAA being characterized as “pre-pathology” and advanced CAA characterized by perivascular amyloid plaques and microhemorrhages.

7.3: Developing a new model of CAA pathogenesis.

While previous disease models begin with perivascular amyloid pathology, my data indicate that there are predictable, early changes that occur within the basement membrane *before* this pathology develops. This provides a potential unified mechanism that could predict areas that are susceptible to CAA before significant damage occurs. Based on my findings and the most current literature, CAA can be broken down into three general stages: early, intermediate and late. In the early stages of CAA, insults such as ischemic stroke increase TGF-β expression, which signals to astrocytes to induce basement membrane fibrosis. These fibrotic changes include an increase in fibronectin, integrin-α5 and overall lectin⁺ matrix. In the intermediate phase, fibrosis promotes the initial sequestration of CSF

A β_{1-40} , which freely circulates through perivascular flow networks under normal conditions. As A β_{1-40} deposition increases, plaque size in affected vessels begins to increase rapidly. Finally, in the late stages of CAA, mature plaques induce chronic inflammation that leads to microhemorrhage and/or lobar ICH, as well as cognitive decline.

This proposed pathogenesis of CAA is analagous to atherosclerotic plaque formation, which occurs due to the deposition of cholesterol within areas of fibrosis that line the vessel lumen.³¹⁶ In the early stages of atherosclerosis, the walls of vessels become fibrotic due to repeated insults, including hypertension, hyperglycemia and free radicals. In the intermediate stage, cholesterol deposits within this scarred area and forms an atherosclerotic plaque. Finally, in the late stages, this deposition causes a local inflammatory response that can result in thrombi and acute ischemia. This simple model has led to the development of a plethora of disease biomarkers, pharmacological treatments and even surgical interventions to protect patients from advanced atherosclerosis, unstable plaque formation and blood clotting. Application of these ideas could lead to similar advances in the diagnosis or even treatment of CAA.

If this new model of CAA is correct, then the underlying disease process which drives cognitive decline in stroke survivors could be targeted in several places. The most straightforward method would be to prevent damage from occurring in the early stages of disease, most effectively by primary prevention of stroke and other risk factors such as hypertension, hyperglycemia and hypercholesterolemia. Following stroke, the intermediate phase could be targeted by reversing overall basement membrane fibrosis (for example, with a TGF- β antagonist) or by directly inhibiting individual receptors that bind to CSF A β_{1-40} (fibronectin, integrin- $\alpha 5$ or HSPGs). An alternative strategy would be to develop drugs that

reduce the levels of CSF $A\beta_{1-40}$, which may at least slow the development of the plaques, analogous to the use of statins in patients with hypercholesterolemia. Once the disease reaches the later stages, where secondary vessel damage has occurred and the patient has multiple microhemorrhages, it may be too late to intervene with these strategies.

Unfortunately, most patients are not diagnosed with CAA until this very late stage of disease, highlighting the need for early detection.³¹⁵ However, we found that these molecules are useful biomarkers for CAA in this population, which may help to identify at-risk patients and reduce the prescription of anticoagulant drugs, which could put them at further increased risk of repeated hemorrhage.

While this new disease model is interesting, there are several areas that require further discussion and more research to refine it into a useful predictive tool. First, translating this work to AD model mice would help to confirm that these early and intermediate changes in the basement membrane lead to CAA plaques in AD model mice. Second, a better understanding of how multiple basement membrane receptors for CSF $A\beta_{1-40}$ interact to favor the development of CAA would help to develop more selective therapeutics. Third, the number and function of different basement membrane sub-layers, and how disrupted perivascular flow in each compartment contributes to CAA pathogenesis, needs to be better understood. Further evaluation of the regulation of CSF $A\beta_{1-40}$ levels could also lead to the development of an alternative class of therapeutics for CAA. Overall, given the evidence that we have obtained from our experiments, post-stroke CAA may share mechanisms with so-called ‘sporadic’ CAA, which could significantly expand the applicability of our findings to numerous other patients, beyond stroke survivors.

7.4: Exploring the contribution of reactive astrocytes to CAA pathology.

My previous work found that TGF- β stimulates astrocytes to deposit fibronectin within the extracellular matrix *in vitro*, which is associated with reduced fluid uptake and increased A β_{1-40} deposition. We further found that inhibition of TGF- β reduced fibronectin expression, improved CSF flow and reduced CSF A β_{1-40} deposition following stroke in aged wild-type mice. While this research indicates that basement membrane fibrosis occurs prior to A β_{1-40} deposition, we do not yet know whether these changes accelerate CAA plaque formation. Furthermore, we also have not yet determined the long-term impact of CAA pathology on basement membrane composition, perivascular flow, recovery from stroke or overall cognitive function. Finally, we also do not know whether long-term TGF- β inhibition can rescue these phenotypes associated with advanced CAA.

Therefore, to better understand the significance of these findings on overall CAA pathogenesis, we propose to study the impact of DMCAO and TGF- β inhibition in Tg2576 mice, an animal model of Alzheimer's disease, using *in vivo* two-photon microscopy and cognitive testing. We hypothesize that DMCAO will accelerate CAA progression in Tg2576 mice, leading to worse cognitive function after stroke. We further hypothesize that these phenotypes will be rescued by inhibiting TGF- β signaling in Tg2576 mice with stroke.

To characterize whether stroke-induced deposition of CSF A β_{1-40} contributes to CAA, we will first place a cranial window in Tg2576 and wild-type animals, then perform DMCAO or sham surgeries one month later. Since Tg2576 mice do not generally develop CAA pathology until 13 months of age, we will examine the impact across different stages of pathology by using 3, 9, 13 and 18-month-old age-matched controls for all experiments. To evaluate CAA pathology, mice will be repeatedly injected with Methoxy-X04 (a congo red-

derivative amyloid staining fluorescent dye) and imaged by two-photon microscopy over one month. Cognitive testing (Fear conditioning, Y maze, novel object recognition test [NORT], Barnes maze) will also be performed on these animals prior to sacrifice. Finally, we will also perform IHC after sacrifice to determine how genotype, age and surgery interact to alter basement membrane composition.

In a second set of experiments, mice will receive an intracisternal injection of FITC- $A\beta_{1-40}$ at the time of two-photon imaging to determine whether CSF $A\beta_{1-40}$ contributes to the development of these mature CAA plaques. Finally, in a third set of experiments, instead of DMCAO, both genotypes will receive ICV injections of recombinant TGF- β , and the impact of treatment on the above histopathological and behavioral measures will be assessed over one month. We expect that DMCAO and TGF- β treatment will similarly increase Methoxy-X04 labeling of vessels in Tg2576 mice, which will colocalize with intracisternally injected FITC- $A\beta_{1-40}$. If successful, these experiments could definitively show that stroke is an independent risk factor for CAA, and that this acceleration occurs, in part, due to the deposition of CSF $A\beta_{1-40}$. It could also show that TGF- β alone is sufficient to induce these changes, paving the way for subsequent experiments exploring the impact of TGF- β inhibition on plaque development.

Then, to determine whether inhibiting TGF- β signaling reduces CAA development after stroke, we will perform DMCAO in Tg2576 mice and treat them with a TGF- β R1 antagonist (GW788388) or vehicle control via continuous peripheral and/or central infusion. Our previous data in aged wild-type mice found that peripheral treatment with this inhibitor reduced perivascular gliosis and fibronectin expression, as well as improved perivascular CSF flow. We expect that TGF- β R1 antagonism will have similar effects on Tg2576 mice,

with the added benefit of reducing CAA development and improving long-term cognitive function. If successful, these experiments would indicate that peripheral TGF- β R1 antagonism can blunt the impact of stroke on accelerating CAA pathology, potentially leading to a new therapy for CAA that could be explored in higher-order model systems. In the future, drugs like this could be given prophylactically to patients with stroke or other types of acute brain injuries who are at risk of developing CAA.

Overall, these experiments represent a critical next step for our research program, and we are excited to have secured NIH/NIA R01 grant funding to continue this work over the coming years. While we already have some data suggesting a potential benefit of TGF- β R1 antagonism on perivascular CSF flow, these experiments could show that these benefits extend to histopathological and behavioral improvements in animal models of CAA. There is significantly more work to be done, but following these confirmatory experiments, our findings could be rapidly translated to clinical populations, given the ongoing use of combinatorial TGF- β antagonists in other diseases, including cancer and pulmonary fibrosis.

7.5: Modulation of basement membrane receptors to improve CSF flow and reduce CAA.

While previous work has documented that basement membrane changes correlate with the severity of CAA pathology, our findings newly demonstrate that aging and stroke produce upregulation of fibronectin and its receptor, integrin- α 5. Importantly, these changes occurred *prior* to the development of pathology. We further found that these changes correlated with increased perivascular distribution of CSF A β ₁₋₄₀ and reduced CSF flow, suggesting a structure/function relationship between these basement membrane changes and perivascular transport. These new findings provide significant insight into the pathogenesis

of CAA, as it suggests that these changes could be a *cause*, not a consequence, of the development of amyloid pathology.

As one future direction, we could continue to develop this pathway as a therapeutic target by examining the impact of fibronectin and/or integrin- $\alpha 5$ knockout on the progression of CAA. For example, to test the hypothesis that astrocytic fibronectin accelerates CAA pathology, conditional fibronectin knockouts (GFAP^{cre/wt} x FN1^{flox/flox}) could be crossed with a rapidly progressing CAA model mouse, such as the TgSwDI strain, and pathology/cognitive deficits examined across the lifespan, at 3, 6, 12 and 24 months of age. Cognitive impairment could be measured using a battery of tests, including NORT, Barnes maze and contextual fear conditioning. Amyloid pathology could also be quantified histologically by staining brain sections with Thioflavin S, Congo Red or anti-amyloid antibodies such as 4G8 monoclonal antibody. I expect that fibronectin knockouts would exhibit less CAA pathology and better cognitive function by 12 months of age, and would most likely be resistant to other potential amyloidogenic stimuli such as stroke or advanced age. If these experiments are successful, an interesting next step would be to pharmacologically target fibronectin using intracisternal administration of antibody-based inhibitors, although the precise binding site of A β_{1-40} to fibronectin would need to be determined by synthesizing mutant fibronectin type I domain *in vitro*, followed by repeated binding assays with each isoform. Additionally, integrin- $\alpha 5$ small molecule inhibitors already exist (ATN-161), and could be used to reduce the binding of fibronectin to integrin- $\alpha 5$. This may also help in a more selective way by preventing the deposition of fibronectin-A β_{1-40} aggregates, without a need to identifying the exact binding site for A β_{1-40} on fibronectin.

An additional, ongoing area of study is using unbiased proteomics to discover new ECM proteins that may be involved in regulating perivascular flow. The glia limitans is an ECM-rich area that forms a barrier between the meningeal/vascular compartments and the brain interstitial fluid. As such, it may provide a first line of defense against the penetration of damaging CSF waste products, or toxic products that could enter from the peripheral circulation into the brain. We previously found that lectin staining strongly increased within the glia limitans and basement membrane following DMCAO in aged animals, indicating increased expression of glycosylated residues. This finding suggests that the composition of the glia limitans is changing, but, beyond increases in fibronectin and integrin- $\alpha 5$, we do not know how many other ECM proteins may be involved. Therefore, we hypothesized that aging and stroke would alter the glia limitans proteome, in large part due to abnormal production of ECM proteins. To test this hypothesis, we performed DMCAO in young and aged mice, then sacrificed them at 30 DPI and collected fresh brain tissue, plasma and CSF. We then sectioned the brain tissue on a cryostat, mounted it onto a PEN membrane and performed H+E staining to visualize the glia limitans. Next, we performed laser capture microdissection to isolate the outer glia limitans from the rest of the brain. We are currently awaiting LC/MS results, but our preliminary findings indicate detection of >1200 unique peptides in our test samples. Upon completion of this project, we expect that it will generate a significant amount of new information about the protein composition of the glia limitans at baseline, as well as how it changes with aging and stroke. This could provide new targets, which could then be assessed for binding potential to $A\beta_{1-40}$, using similar techniques as described in Chapter 4.

7.6: Brain perivascular flow dynamics may have a molecular size sensitivity.

Our experiments indicate that the perivascular flow rate is size-dependent, and occurs in different basement membrane layers. We found that larger particles (70 – 2000 kD) traveled through the outer region of the basement membrane, and cleared slowly from the ISF. In contrast, smaller particles (0.5 – 4.5 kD), including $A\beta_{1-40}$, were associated with the inner basement membrane and cleared more rapidly from brain tissue. These findings were surprising, as previous studies suggested that CSF solutes are transported by bulk flow, which dictates that all particles will move at the same rate, regardless of mass.^{125,199,200} The best interpretation of these data is that passive diffusion interacts with bulk flow to produce a dynamic process that cannot be described as purely one or the other.

It is important to recognize that this process of perivascular flow and solute exchange is actually dependent on two distinct compartments: the vascular basement membrane compartment (between endothelial cells and astrocyte endfeet) and the interstitial compartment (between astrocyte endfeet and other cells such as neurons and oligodendrocytes). If one were to track the movement of a single particle, initially, it may be rapidly distributed through the perivascular compartment by a process that has been historically attributed to bulk flow. However, our data suggest that this process is modified by certain biophysical properties of the basement membrane (collectively termed ‘tortuosity,’ reviewed in **Section 1.8**), which generate a size-exclusion property within the perivascular compartment.²⁰² Our data indicate that the certain regions of basement membrane are more selective for small particles, while the others permit the transport of very large particles. This property could be a function of tortuosity, which largely depends on the conformation of the ECM, which itself depends on composition. This tendency for particles to diffuse at

different rates through different regions of tissue is called anisotropy, and is best measured by sensitive techniques such as TMA iontophoresis.²⁰² However, even without this technique, we can infer from our data that the structure of the outer basement membrane must differ from the inner basement membrane to produce this divergent physiology.

Following this process of perivascular distribution, which is partly driven by bulk flow, CSF solutes must then exchange with ISF solutes. To accomplish this, particles must diffuse between the perivascular and interstitial compartments. We found that large molecules (2000 kD dextran) did not travel into the interstitium, while small molecules (3 kD dextran) easily traveled into the interstitium. If this process were solely governed by bulk flow, then one would expect that both particles would travel equally far from the PVS. Given the fact that this does not occur, and that travel distance is strongly dependent on the hydrodynamic radius (or ‘size’) of the diffusing particle, then this process must be governed by the forces of passive diffusion (as predicted by the **Stokes-Einstein** equation).²⁰² In addition to molecular size slowing down the process of diffusion, our data also suggest that the glial endfeet, which form the border between the perivascular and interstitial compartments, could also provide an anisotropic size-exclusion barrier to larger particles. This property may also contribute to the much slower clearance of intraparenchymally injected albumin, which is a measure of the reverse phenomenon: ISF-CSF exchange. An alternative interpretation is that the entire interstitial compartment excludes large particles, not just the glial endfeet. However, it is not currently possible to discern which interpretation is most accurate from the present data, and would require additional, careful studies with more sensitive techniques, such as TMA iontophoresis.

This size-exclusion barrier between basement membrane sublayers, as well as between the perivascular and interstitial compartments, may have important consequences for the pathogenesis of CAA. In CAA, there is initially a selective build-up of A β ₁₋₄₀ within the outermost layers of basement membrane of the outermost cortical vessels, which then moves inward in both directions as pathology advances.⁹⁴ This suggests that these size-exclusion properties could safeguard the vessels against this perivascular pathology, but this later becomes dysregulated and ultimately fails in CAA (potentially due to fibrosis). While monomeric A β ₁₋₄₀ is small enough to travel within the inner basement membrane layer, the assembly of these monomeric particles into oligomers and eventually much larger aggregates could form mature CAA plaques that are excluded from the inner membrane and exist within the less efficient outer membrane.

Furthermore, the segregation of the perivascular and interstitial compartments may explain the propensity of cortical pathology to begin with vessels,³¹⁷ as these larger oligomers may be able to distribute perivascularly through the outer basement membrane, but not be able to spread into the interstitial space. However, when the plaque becomes large enough to cause inflammation and damage this barrier, oligomers can spread into the interstitium and further spread pathology throughout the surrounding area. This concept is somewhat similar to metastasis of cancer, as amyloid pathology in one region of the brain (such as the hippocampus) may eventually disrupt these insulating barriers and allow for toxic oligomers to ‘infect’ the CSF and spread to distant sites via perivascular flow.

The biggest unanswered question from these experiments is: which proteins are responsible for generating this size-exclusion property? Previous studies have shown that HSPGs within the glycocalyx support the repulsive properties of the BBB,^{90,241} but it is not

know whether the HSPGs contained within the basement membrane also produce this function of size-exclusion of CSF solutes between membrane sublayers. As a next step, this question could be answered by electron microscopy, which would allow us to visualize the ultrastructure of these ECM proteins. Immunogold labeling of specific classes of basement membrane proteins (collagens, laminins, fibronectin, glycosaminoglycans) could demonstrate potential differences in the composition of these basement membrane sub-layers. Then, knocking out individual proteins that are enriched in these different layers, and examining the relative perivascular transport of small and large gold-labeled dextran particles, could begin to address the physiological significance of these differences in structure/composition within the specific sub-layer.

For example, if protein A were found to be enriched in the inner basement membrane, and knockout of protein A enabled the diffusion of high molecular weight dextran particles within the inner basement membrane, then one could conclude that protein A was responsible for generating this size-exclusion property of the inner basement membrane. Alternatively, knockout of protein B could completely abolish perivascular flow, indicating that it is required for maintaining a structure that permits the flow of CSF and solutes. Similar approaches could be used to compare the structure/function relationship of size-exclusion by the glial endfeet and/or interstitial compartment.

7.7: CSF A β ₁₋₄₀ levels may increase in aging and after stroke be by multiple mechanisms.

Our findings demonstrate that aging and stroke induce the deposition of CSF A β ₁₋₄₀ within the basement membrane. This difference in deposition occurred even though we injected the same amount of fluorescent A β ₁₋₄₀ into the CSF of each animal, suggesting that

alterations in the intrinsic $A\beta_{1-40}$ binding capacity may be altered by pathological states. However, it is important to consider that the absolute levels of CSF $A\beta_{1-40}$ may also change with aging, stroke and CAA. Previous work has shown that early increases in CSF $A\beta_{1-40}$ occur before the onset of CAA in human patients.¹⁴⁹ If aging or stroke were to also increase the levels of CSF $A\beta_{1-40}$ relative to baseline, this could further magnify the perivascular $A\beta_{1-40}$ deposition that was seen in our animal studies. As a potential future direction, we could examine how aging and stroke alter choroidal permeability and/or meningeal CSF clearance pathways, and determine whether blocking these changes could slow CAA development.

The CP undergoes several major changes with normal aging, which could lead to increases in the concentration of CSF $A\beta_{1-40}$. Beginning in old age, the barrier between the plasma and CSF becomes thinner.^{318,319} Additionally, basement membrane fibrosis occurs in both the epithelial and endothelial layers, potentially contributing to reduced absorptive capacity of the basolateral membrane.³¹⁹ Furthermore, aging causes the epithelial cells to become invested with lipofuscin granules and protein inclusions, which may also impair the secretory function of the microvilli and reduce CSF production in aging.³²⁰ Together, these changes contribute to an approximately 30% reduction in CSF secretion with aging, despite increases in total CSF volume within the ventricles and subarachnoid space, which often occur due to cerebral atrophy.^{318,319} Furthermore, Alzheimer's disease is associated with more rapid aging of the CP, with amyloid plaque formation occurring within the PVS of CP capillaries, reminiscent of CAA.³²⁰ These changes are associated with a 50% reduction in CSF turnover compared to the normal aged CP.³²¹ The net effects of these changes are reduced CSF turnover and higher CSF protein concentration with aging.³²² These reductions in CSF turnover could lead to increased transit time for $A\beta_{1-40}$ particles to be cleared from the

brain, which would increase the concentration of CSF A β ₁₋₄₀ that is recirculated along the basement membrane and lead to CAA.

Brain injury may further reduce the turnover of CSF. Following stroke, increased cellular debris can act to clog meningeal outflow, leading to increased intracranial pressure (ICP) and damage to the CP.³²³⁻³²⁵ Increased ICP further triggers a negative feedback loop involving several vasoregulatory hormones, including atrial natriuretic peptide,³²⁶ vasopressin,¹³² and fibroblast growth factor,³²⁷⁻³²⁹ which all act to reduce CSF formation. While this does prevent worsening of ICP, this feedback effectively reduces the turnover of CSF, and dysregulation of these pathways may contribute to increased CSF A β ₁₋₄₀ levels following brain injury.

In addition to slowing the clearance of CSF A β ₁₋₄₀, brain injuries can increase the permeability of the blood-CSF barrier and expose the brain to systemic waste products such as A β ₁₋₄₀. One study found that TBI increased CP permeability to plasma solutes, leading to increased osmotic uptake of water and elevated ICP.³³⁰ Following stroke, the CP upregulates lysosome expression and appears highly vacuolated, the width of the intercellular spaces increases, and the microvilli become enlarged.³³¹ These morphological changes are also associated with increased trafficking of immune cells through the CP, including increased numbers of cytotoxic T cells in aged animals.^{332,333} Similarly, the CP epithelium also provides a route for monocyte-derived macrophages to enter the brain and influence post-stroke recovery.³³⁴ While it is clear that stroke has dramatic effects on the permeability of the CP to immune cells, the effects of stroke on permeability to A β ₁₋₄₀ are not known. In older individuals, these changes could have an additive effect with baseline impairments in CSF turnover/clearance and further increase CSF A β ₁₋₄₀ levels.

As one potential new direction, we could test the hypothesis that stroke disrupts the blood-CSF barrier, newly exposing the brain to peripheral $A\beta_{1-40}$. To test this hypothesis, we could first perform DMCAO, and then intravenously inject $^{125}\text{I}-A\beta_{1-40}$ into the peripheral bloodstream. Then, we could block CSF outflow pathways by intracisternally injecting glycerol, and collect freshly filtered CSF by a microdialysis catheter placed in the lateral ventricle. Following this, in a separate group, we could intravenously inject gold-labeled $A\beta_{1-40}$, then section the brain and examine CP morphology by electron microscopy to determine whether $A\beta_{1-40}$ was being taken up transcellularly through receptors like lipoprotein receptor protein-1 (LRP1), P-glycoprotein (PGP) or receptor for advanced glycation endproducts (RAGE), or whether this uptake was occurring paracellularly. I predict that DMCAO will increase the uptake of $^{125}\text{I}-A\beta_{1-40}$ into the CSF. Depending on what route $A\beta_{1-40}$ is taken up by, different treatment strategies such as anti-inflammatory drugs to reduce damage to the CP and paracellular uptake could be explored, or utilize specific knockouts/inhibitors of the transcellular uptake processes. If successful, these experiments would determine whether stroke increases CP permeability to $A\beta_{1-40}$, and by which route this occurs. Depending on the outcome, new drugs could be utilized to reduce the uptake of $A\beta_{1-40}$ into the brain after stroke.

As an additional future area of research, we could also test the hypothesis that stroke releases necrotic debris that reduce the outflow of CSF through the dural lymphatics, impairing the removal of CSF $A\beta_{1-40}$ and worsening vascular amyloid pathology and cognitive impairment. To test this hypothesis, we could place a cranial window over the dural lymphatic vessels of Tg2576 x GFP mice, then perform DMCAO. Following this, we could then measure lymphatic outflow by intracisternally injecting fluorescent quantum dots

and measuring their flow velocity by two-photon microscopy. I would predict that DMCAO would reduce lymphatic outflow acutely after injury due to the presence of GFP-positive cellular debris within the lymphatics. We could then test whether installing a ventriculoperitoneal shunt could help to normalize CSF outflow and allow for the debris to clear more rapidly from the brain. Then, we could determine whether this treatment improves post-stroke cognitive function, and whether this impairment is greater in the transgenic Tg2576 mice. If successful, shunting could be used to improve the clearance of $A\beta_{1-40}$ in human CAA patients, particularly after an acute injury like stroke.

In conclusion, CSF $A\beta_{1-40}$ levels fluctuate over the course of CAA, with high levels observed in the early stages of disease. Degradation of the blood-CSF barrier, reduced CSF turnover and impaired outflow of through the meninges all likely contribute to early increases in $A\beta_{1-40}$ within the CSF with CAA. Aging, brain injury and Alzheimer's disease may be associated with alterations in these parameters, which could favor a build-up of CSF $A\beta_{1-40}$, worsening CAA. Further work must be done to assess how these changes in the CP impact that uptake and/or clearance of $A\beta_{1-40}$ after stroke. This could provide an additional target to reduce CSF $A\beta_{1-40}$ levels and CAA development.

7.8: Concluding remarks.

This work represents an early step in developing a new understanding of how CAA develops in survivors of ischemic stroke. CAA may be a late sign of disease within the perivascular glymphatic system, which opens up a plethora of potential treatment strategies to treat the underlying problems that are driving vascular amyloid pathology in these patients. New strategies to detect early reductions in perivascular CSF flow by imaging or serum

biomarkers could expand the treatment window for CAA. If early disease is detected, then reducing the levels of CSF A β ₁₋₄₀ by reducing distribution or enhancing clearance may help to slow the progression of amyloid pathology in distal perivascular beds. We have also shown that targeting the basement membrane with anti-TGF- β therapies can be an effective strategy for reducing perivascular amyloid burden after focal injury, which could one-day be translated to the clinic.

Overall, this work is a testament to the value of collaborative research. This project began as a far-fetched idea, but was shaped into a coherent project with much help from Dr. McCullough, Dr. Urayama and my thesis committee. With the help of other lab members, and a great deal of patience, we were able to accomplish what I once believed to be a very long shot—to reverse impairment in the perivascular drainage of waste products after stroke. Over the course of these experiments, I shared my findings with others in our research group and helped to obtain new grants, which have delivered funding that will ensure these new projects continue to grow in the coming years. While this chapter in my life is ending, it also provides a new beginning for the next wave of researchers with their own ideas. Already, others in our research group have begun to probe the contributions of diverse other systems to CAA pathogenesis, including neuroimmunology, gut microbiology and respiratory physiology. This work will provide even more of the missing pieces to the puzzle of CAA, which we can assemble into a new strategy to end dementia in the 21st century.

CHAPTER 8

References

1. Grysiewicz RA, Thomas K, Pandey DK. Epidemiology of ischemic and hemorrhagic stroke: incidence, prevalence, mortality, and risk factors. *Neurol Clin*. 2008;26:871–95, vii.
2. Impact of Stroke (Stroke statistics). Available at http://www.strokeassociation.org/STROKEORG/AboutStroke/Impact-of-Stroke-Stroke-statistics_UCM_310728_Article.jsp#.WpM5WBPwZE5. Accessed February 25, 2018.
3. Skolarus LE, Burke JF, Brown DL, Freedman VA. Understanding stroke survivorship: expanding the concept of poststroke disability. *Stroke*. 2014;45:224–30.
4. Hacke W, Schwab S, Horn M, Spranger M, Georgiadis M De, Kummer R von. “Malignant” Middle Cerebral Artery Territory Infarction. *Arch Neurol*. 1996;53:309.
5. Powers WJ, Rabinstein AA, Ackerson T, Adeoye OM, Bambakidis NC, Becker K, Biller J, Brown M, Demaerschak BM, Hoh B, Jauch EC, Kidwell CS, Leslie-Mazwi TM, Ovbiagele B, Scott PA, Sheth KN, Southerland AM, Summers D V, Tirschwell DL, American Heart Association Stroke Council on behalf of the AHAS. 2018 Guidelines for the Early Management of Patients With Acute Ischemic Stroke: A Guideline for Healthcare Professionals From the American Heart Association/American Stroke Association. *Stroke*. 2018;:STR.000000000000158.
6. Gorelick PB, Scuteri A, Black SE, Decarli C, Greenberg SM, Iadecola C, Launer LJ, Laurent S, Lopez OL, Nyenhuis D, Petersen RC, Schneider JA, Tzourio C, Arnett DK,

- Bennett DA, Chui HC, Higashida RT, Lindquist R, Nilsson PM, Roman GC, Sellke FW, Seshadri S. Vascular contributions to cognitive impairment and dementia: a statement for healthcare professionals from the american heart association/american stroke association. *Stroke*. 2011;42:2672–2713.
7. Ivan CS, Seshadri S, Beiser A, Au R, Kase CS, Kelly-Hayes M, Wolf PA. Dementia after stroke: the Framingham Study. *Stroke*. 2004;35:1264–8.
 8. Reitz C, Bos MJ, Hofman A, Koudstaal PJ, Breteler MMB. Prestroke Cognitive Performance, Incident Stroke, and Risk of Dementia: The Rotterdam Study. *Stroke*. 2008;39:36–41.
 9. Mahon S, Parmar P, Barker-Collo S, Krishnamurthi R, Jones K, Theadom A, Feigin V. Determinants, Prevalence, and Trajectory of Long-Term Post-Stroke Cognitive Impairment: Results from a 4-Year Follow-Up of the ARCOS-IV Study. *Neuroepidemiology*. 2017;49:129–134.
 10. Doyle KP, Buckwalter MS. Does B lymphocyte-mediated autoimmunity contribute to post-stroke dementia? *Brain Behav Immun*. 2017;64:1–8.
 11. Doyle KP, Quach LN, Sole M, Axtell RC, Nguyen T-V V., Soler-Llavina GJ, Jurado S, Han J, Steinman L, Longo FM, Schneider JA, Malenka RC, Buckwalter MS. B-Lymphocyte-Mediated Delayed Cognitive Impairment following Stroke. *J Neurosci*. 2015;35:2133–2145.
 12. Ritzel RM, Crapser J, Patel AR, Verma R, Grenier JM, Chauhan A, Jellison ER, McCullough LD. Age-Associated Resident Memory CD8 T Cells in the Central Nervous System Are Primed To Potentiate Inflammation after Ischemic Brain Injury. *J Immunol*. 2016. doi:10.4049/jimmunol.1502021.

13. Sorrenti V, Contarini G, Sut S, Dall'Acqua S, Confortin F, Pagetta A, Giusti P, Zusso M. Curcumin Prevents Acute Neuroinflammation and Long-Term Memory Impairment Induced by Systemic Lipopolysaccharide in Mice. *Front Pharmacol.* 2018;9:183.
14. Ye BS, Seo SW, Kim GH, Noh Y, Cho H, Yoon CW, Kim HJ, Chin J, Jeon S, Lee JM, Seong J-K, Kim JS, Lee J-H, Choe YS, Lee KH, Sohn YH, Ewers M, Weiner M, Na DL. Amyloid burden, cerebrovascular disease, brain atrophy, and cognition in cognitively impaired patients. *Alzheimer's Dement.* 2015;11:494–503.e3.
15. Li Q, Lebson L, Lee DC, Nash K, Grimm J, Rosenthal A, Selenica M-LB, Morgan D, Gordon MN. Chronological age impacts immunotherapy and monocyte uptake independent of amyloid load. *J Neuroimmune Pharmacol.* 2012;7:202–14.
16. Ameen-Ali KE, Wharton SB, Simpson JE, Heath PR, Sharp P, Berwick J. Review: Neuropathology and behavioural features of transgenic murine models of Alzheimer's disease. *Neuropathol Appl Neurobiol.* 2017;43:553–570.
17. Sanabria-Castro A, Alvarado-Echeverría I, Monge-Bonilla C. Molecular Pathogenesis of Alzheimer's Disease: An Update. *Ann Neurosci.* 2017;24:46–54.
18. Schneider JA, Arvanitakis Z, Leurgans SE, Bennett DA. The neuropathology of probable Alzheimer disease and mild cognitive impairment. *Ann Neurol.* 2009;66:200–8.
19. Vonsattel JPG, Myers RH, Tessa Hedley-Whyte E, Ropper AH, Bird ED, Richardson EP. Cerebral amyloid angiopathy without and with cerebral hemorrhages: A comparative histological study. *Ann Neurol.* 1991;30:637–649.
20. Greenberg SM, Vonsattel JP. Diagnosis of cerebral amyloid angiopathy. Sensitivity

- and specificity of cortical biopsy. *Stroke*. 1997;28:1418–22.
21. Planton M, Raposo N, Albucher J-F, Pariente J. Cerebral amyloid angiopathy-related cognitive impairment: The search for a specific neuropsychological pattern. *Rev Neurol (Paris)*. 2017;173:562–565.
 22. Kim HJ, Yang JJ, Kwon H, Kim C, Lee JM, Chun P, Kim YJ, Jung N-Y, Chin J, Kim S, Woo S, Choe YS, Lee K-H, Kim ST, Kim JS, Lee JH, Weiner MW, Na DL, Seo SW. Relative impact of amyloid- β , lacunes, and downstream imaging markers on cognitive trajectories. *Brain*. 2016;139:2516–2527.
 23. Biffi A, Greenberg SM. Cerebral Amyloid Angiopathy: A Systematic Review. *J Clin Neurol*. 2011;7:1.
 24. Schneider JA, Boyle PA, Arvanitakis Z, Bienias JL, Bennett DA. Subcortical infarcts, Alzheimer's disease pathology, and memory function in older persons. *Ann Neurol*. 2007;62:59–66.
 25. Matthews FE, Brayne C, Lowe J, McKeith I, Wharton SB, Ince P. Epidemiological pathology of dementia: attributable-risks at death in the Medical Research Council Cognitive Function and Ageing Study. *PLoS Med*. 2009;6:e1000180.
 26. Dugger BN, Davis K, Malek-Ahmadi M, Hentz JG, Sandhu S, Beach TG, Adler CH, Caselli RJ, Johnson TA, Serrano GE, Shill HA, Belden C, Driver-Dunckley E, Caviness JN, Sue LI, Jacobson S, Powell J, Sabbagh MN. Neuropathological comparisons of amnesic and nonamnesic mild cognitive impairment. *BMC Neurol*. 2015;15:146.
 27. Johnson KA, Gregas M, Becker JA, Kinnecom C, Salat DH, Moran EK, Smith EE, Rosand J, Rentz DM, Klunk WE, Mathis CA, Price JC, DeKosky ST, Fischman AJ,

- Greenberg SM. Imaging of amyloid burden and distribution in cerebral amyloid angiopathy. *Ann Neurol*. 2007;62:229–234.
28. Ly J V., Rowe CC, Villemagne VL, Zavala JA, Ma H, Sahathevan R, O’Keefe G, Gong SJ, Gunawan R, Churilov L, Saunder T, Ackerman U, Tochon-Danguy H, Donnan GA. Subacute Ischemic Stroke Is Associated With Focal 11C PiB Positron Emission Tomography Retention But Not With Global Neocortical A Deposition. *Stroke*. 2012;43:1341–1346.
29. Yang J, Wong A, Wang Z, Liu W, Au L, Xiong Y, Chu WWC, Leung EYL, Chen S, Lau C, Chan AYY, Lau AYL, Fan F, Ip V, Soo Y, Leung T, Ho CL, Wong LKS, Mok VCT. Risk factors for incident dementia after stroke and transient ischemic attack. *Alzheimer’s Dement*. 2015;11:16–23.
30. Sahathevan R, Linden T, Villemagne VL, Churilov L, Ly J V., Rowe C, Donnan G, Brodtmann A. Positron Emission Tomographic Imaging in Stroke. *Stroke*. 2016;47:113–119.
31. Knudsen KA, Rosand J, Karluk D, Greenberg SM. Clinical diagnosis of cerebral amyloid angiopathy: validation of the Boston criteria. *Neurology*. 2001;56:537–9.
32. Charidimou A, Boulouis G, Pasi M, Auriel E, van Etten ES, Haley K, Ayres A, Schwab KM, Martinez-Ramirez S, Goldstein JN, Rosand J, Viswanathan A, Greenberg SM, Gurol ME. MRI-visible perivascular spaces in cerebral amyloid angiopathy and hypertensive arteriopathy. *Neurology*. 2017;88:1157–1164.
33. Liang Y, Chen Y-K, Deng M, Mok VCT, Wang D-F, Ungvari GS, Chu CW, Kamiya A, Tang W-K. Association of Cerebral Small Vessel Disease Burden and Health-Related Quality of Life after Acute Ischemic Stroke. *Front Aging Neurosci*.

- 2017;9:372.
34. ZHANG Z, REN W, SHAO B, XU H, CHENG J, WANG Q, GU Y, ZHU B, HE J. Leukoaraiosis is Associated with Worse Short-Term Functional and Cognitive Recovery after Minor Stroke. *Neurol Med Chir (Tokyo)*. 2017;57:136–143.
 35. Liu Y, Zhang M, Chen Y, Gao P, Yun W, Zhou X. The degree of leukoaraiosis predicts clinical outcomes and prognosis in patients with middle cerebral artery occlusion after intravenous thrombolysis. *Brain Res*. 2018;1681:28–33.
 36. Zhang X, Tang Y, Xie Y, Ding C, Xiao J, Jiang X, Shan H, Lin Y, Li C, Hu D, Li T, Sheng L. Total magnetic resonance imaging burden of cerebral small-vessel disease is associated with post-stroke depression in patients with acute lacunar stroke. *Eur J Neurol*. 2017;24:374–380.
 37. Santos CY, Snyder PJ, Wu W-C, Zhang M, Echeverria A, Alber J. Pathophysiologic relationship between Alzheimer’s disease, cerebrovascular disease, and cardiovascular risk: A review and synthesis. *Alzheimer’s Dement (Amsterdam, Netherlands)*. 2017;7:69–87.
 38. Corder EH, Saunders AM, Strittmatter WJ, Schmechel DE, Gaskell PC, Small GW, Roses AD, Haines JL, Pericak-Vance MA. Gene dose of apolipoprotein E type 4 allele and the risk of Alzheimer’s disease in late onset families. *Science*. 1993;261:921–3.
 39. McIlroy SP, Dynan KB, Lawson JT, Patterson CC, Passmore AP. Moderately elevated plasma homocysteine, methylenetetrahydrofolate reductase genotype, and risk for stroke, vascular dementia, and Alzheimer disease in Northern Ireland. *Stroke*. 2002;33:2351–6.
 40. Desikan RS, Schork AJ, Wang Y, Thompson WK, Dehghan A, Ridker PM, Chasman

- DI, McEvoy LK, Holland D, Chen C-H, Karow DS, Brewer JB, Hess CP, Williams J, Sims R, O'Donovan MC, Choi SH, Bis JC, Ikram MA, Gudnason V, DeStefano AL, van der Lee SJ, Psaty BM, van Duijn CM, Launer L, Seshadri S, Pericak-Vance MA, Mayeux R, Haines JL, Farrer LA, Hardy J, Ulstein ID, Aarsland D, Fladby T, White LR, Sando SB, Rongve A, Witoelar A, Djurovic S, Hyman BT, Snaedal J, Steinberg S, Stefansson H, Stefansson K, Schellenberg GD, Andreassen OA, Dale AM, Inflammation working group, IGAP and DemGene Investigators. Polygenic Overlap Between C-Reactive Protein, Plasma Lipids, and Alzheimer Disease. *Circulation*. 2015;131:2061–2069.
41. Skoog I, Lernfelt B, Landahl S, Palmertz B, Andreasson LA, Nilsson L, Persson G, Odén A, Svanborg A. 15-year longitudinal study of blood pressure and dementia. *Lancet (London, England)*. 1996;347:1141–5.
42. Notkola IL, Sulkava R, Pekkanen J, Erkinjuntti T, Ehnholm C, Kivinen P, Tuomilehto J, Nissinen A. Serum total cholesterol, apolipoprotein E epsilon 4 allele, and Alzheimer's disease. *Neuroepidemiology*. 1998;17:14–20.
43. Ahtiluoto S, Polvikoski T, Peltonen M, Solomon A, Tuomilehto J, Winblad B, Sulkava R, Kivipelto M. Diabetes, Alzheimer disease, and vascular dementia: A population-based neuropathologic study. *Neurology*. 2010;75:1195–1202.
44. Whitmer RA, Gustafson DR, Barrett-Connor E, Haan MN, Gunderson EP, Yaffe K. Central obesity and increased risk of dementia more than three decades later. *Neurology*. 2008;71:1057–1064.
45. Groot C, Hooghiemstra AM, Raijmakers PGHM, van Berckel BNM, Scheltens P, Scherder EJA, van der Flier WM, Ossenkoppele R. The effect of physical activity on

- cognitive function in patients with dementia: A meta-analysis of randomized control trials. *Ageing Res Rev.* 2016;25:13–23.
46. Cataldo JK, Prochaska JJ, Glantz SA. Cigarette Smoking is a Risk Factor for Alzheimer's Disease: An Analysis Controlling for Tobacco Industry Affiliation. *J Alzheimer's Dis.* 2010;19:465–480.
47. van Groen T, Puurunen K, Maki H-M, Sivenius J, Jolkkonen J. Transformation of Diffuse β -Amyloid Precursor Protein and β -Amyloid Deposits to Plaques in the Thalamus After Transient Occlusion of the Middle Cerebral Artery in Rats. *Stroke.* 2005;36:1551–1556.
48. Lipsanen A, Hiltunen M, Jolkkonen J. Chronic ibuprofen treatment does not affect the secondary pathology in the thalamus or improve behavioral outcome in middle cerebral artery occlusion rats. *Pharmacol Biochem Behav.* 2011;99:468–474.
49. Sarajärvi T, Lipsanen A, Mäkinen P, Peräniemi S, Soininen H, Haapasalo A, Jolkkonen J, Hiltunen M. Bepridil decreases A β and calcium levels in the thalamus after middle cerebral artery occlusion in rats. *J Cell Mol Med.* 2012;16:2754–67.
50. Xing S, Zhang J, Dang C, Liu G, Zhang Y, Li J, Fan Y, Pei Z, Zeng J. Cerebrolysin reduces amyloid- β deposits, apoptosis and autophagy in the thalamus and improves functional recovery after cortical infarction. *J Neurol Sci.* 2014;337:104–111.
51. Mitkari B, Kerkelä E, Nystedt J, Korhonen M, Jolkkonen J. Unexpected complication in a rat stroke model: exacerbation of secondary pathology in the thalamus by subacute intraarterial administration of human bone marrow-derived mesenchymal stem cells. *J Cereb Blood Flow Metab.* 2015;35:363–6.
52. Mucke L, Masliah E, Johnson WB, Ruppe MD, Alford M, Rockenstein EM, Forss-

- Petter S, Pietropaolo M, Mallory M, Abraham CR. Synaptotrophic effects of human amyloid beta protein precursors in the cortex of transgenic mice. *Brain Res.* 1994;666:151–67.
53. Priller C, Bauer T, Mitteregger G, Krebs B, Kretzschmar HA, Herms J. Synapse Formation and Function Is Modulated by the Amyloid Precursor Protein. *J Neurosci.* 2006;26:7212–7221.
54. Zou C, Crux S, Marinesco S, Montagna E, Sgobio C, Shi Y, Shi S, Zhu K, Dorostkar MM, Müller UC, Herms J. Amyloid precursor protein maintains constitutive and adaptive plasticity of dendritic spines in adult brain by regulating D-serine homeostasis. *EMBO J.* 2016;35:2213–2222.
55. Duce JA, Tsatsanis A, Cater MA, James SA, Robb E, Wikhe K, Leong SL, Perez K, Johanssen T, Greenough MA, Cho H-H, Galatis D, Moir RD, Masters CL, McLean C, Tanzi RE, Cappai R, Barnham KJ, Ciccotosto GD, Rogers JT, Bush AI. Iron-Export Ferroxidase Activity of β -Amyloid Precursor Protein Is Inhibited by Zinc in Alzheimer's Disease. *Cell.* 2010;142:857–867.
56. Anderson JP, Chen Y, Kim KS, Robakis NK. An alternative secretase cleavage produces soluble Alzheimer amyloid precursor protein containing a potentially amyloidogenic sequence. *J Neurochem.* 1992;59:2328–31.
57. Kakuda N, Miyasaka T, Iwasaki N, Nirasawa T, Wada-Kakuda S, Takahashi-Fujigasaki J, Murayama S, Ihara Y, Ikegawa M. Distinct deposition of amyloid- β species in brains with Alzheimer's disease pathology visualized with MALDI imaging mass spectrometry. *Acta Neuropathol Commun.* 2017;5:73.
58. Zheng W, Tsai M-Y, Wolynes PG. Comparing the Aggregation Free Energy

- Landscapes of Amyloid Beta(1–42) and Amyloid Beta(1–40). *J Am Chem Soc.* 2017;139:16666–16676.
59. Head E, Phelan MJ, Doran E, Kim RC, Poon WW, Schmitt FA, Lott IT. Cerebrovascular pathology in Down syndrome and Alzheimer disease. *Acta Neuropathol Commun.* 2017;5:93.
60. Rogaev EI, Sherrington R, Rogaeva EA, Levesque G, Ikeda M, Liang Y, Chi H, Lin C, Holman K, Tsuda T, Mar L, Sorbi S, Nacmias B, Piacentini S, Amaducci L, Chumakov I, Cohen D, Lannfelt L, Fraser PE, Rommens JM, George-Hyslop PHS. Familial Alzheimer's disease in kindreds with missense mutations in a gene on chromosome 1 related to the Alzheimer's disease type 3 gene. *Nature.* 1995;376:775–778.
61. Shea Y-F, Chu L-W, Chan AO-K, Ha J, Li Y, Song Y-Q. A systematic review of familial Alzheimer's disease: Differences in presentation of clinical features among three mutated genes and potential ethnic differences. *J Formos Med Assoc.* 2016;115:67–75.
62. Lemere CA, Lopera F, Kosik KS, Lendon CL, Ossa J, Saido TC, Yamaguchi H, Ruiz A, Martinez A, Madrigal L, Hincapie L, Arango JC, Anthony DC, Koo EH, Goate AM, Selkoe DJ, Arango JC. The E280A presenilin 1 Alzheimer mutation produces increased A beta 42 deposition and severe cerebellar pathology. *Nat Med.* 1996;2:1146–50.
63. Yasuda M, Maeda K, Ikejiri Y, Kawamata T, Kuroda S, Tanaka C. A novel missense mutation in the presenilin-1 gene in a familial Alzheimer's disease pedigree with abundant amyloid angiopathy. *Neurosci Lett.* 1997;232:29–32.

64. Yamada M, Sodeyama N, Itoh Y, Suematsu N, Otomo E, Matsushita M, Mizusawa H. Association of presenilin-1 polymorphism with cerebral amyloid angiopathy in the elderly. *Stroke*. 1997;28:2219–21.
65. Dermaut B, Kumar-Singh S, De Jonghe C, Cruts M, Löfgren A, Lübke U, Cras P, Dom R, De Deyn PP, Martin JJ, Van Broeckhoven C. Cerebral amyloid angiopathy is a pathogenic lesion in Alzheimer's disease due to a novel presenilin 1 mutation. *Brain*. 2001;124:2383–92.
66. Wattendorff AR, Bots GT, Went LN, Endtz LJ. Familial cerebral amyloid angiopathy presenting as recurrent cerebral haemorrhage. *J Neurol Sci*. 1982;55:121–35.
67. Luyendijk W, Bots GT, Vegter-van der Vlis M, Went LN, Frangione B. Hereditary cerebral haemorrhage caused by cortical amyloid angiopathy. *J Neurol Sci*. 1988;85:267–80.
68. Van Broeckhoven C, Haan J, Bakker E, Hardy JA, Van Hul W, Wehnert A, Vegter-Van der Vlis M, Roos RA. Amyloid beta protein precursor gene and hereditary cerebral hemorrhage with amyloidosis (Dutch). *Science*. 1990;248:1120–2.
69. Levy E, Carman MD, Fernandez-Madrid IJ, Power MD, Lieberburg I, van Duinen SG, Bots GT, Luyendijk W, Frangione B. Mutation of the Alzheimer's disease amyloid gene in hereditary cerebral hemorrhage, Dutch type. *Science*. 1990;248:1124–6.
70. van Nostrand WE, Wagner SL, Haan J, Bakker E, Roos RAC. Alzheimer's disease and hereditary cerebral hemorrhage with amyloidosis-dutch type share a decrease in cerebrospinal fluid levels of amyloid β -protein precursor. *Ann Neurol*. 1992;32:215–218.
71. Sten H, Nilsberth C, Hammarbäck J, Engvall B, Näslund J, Lannfelt L. The Arctic

- mutation interferes with processing of the amyloid precursor protein. *Neuroreport*. 2002;13:1857–60.
72. Hsiao K, Chapman P, Nilsen S, Eckman C, Harigaya Y, Younkin S, Yang F, Cole G. Correlative memory deficits, A β elevation, and amyloid plaques in transgenic mice. *Science*. 1996;274:99–102.
73. Radde R, Bolmont T, Kaeser SA, Coomaraswamy J, Lindau D, Stoltze L, Calhoun ME, Jäggi F, Wolburg H, Gengler S, Haass C, Ghetti B, Czech C, Hölscher C, Mathews PM, Jucker M. A β 42-driven cerebral amyloidosis in transgenic mice reveals early and robust pathology. *EMBO Rep*. 2006;7:940–946.
74. Davis J, Xu F, Deane R, Romanov G, Previti M Lou, Zeigler K, Zlokovic B V, Van Nostrand WE. Early-onset and robust cerebral microvascular accumulation of amyloid beta-protein in transgenic mice expressing low levels of a vasculotropic Dutch/Iowa mutant form of amyloid beta-protein precursor. *J Biol Chem*. 2004;279:20296–20306.
75. Van Nostrand WE, Melchor JP, Cho HS, Greenberg SM, Rebeck GW. Pathogenic effects of D23N Iowa mutant amyloid beta -protein. *J Biol Chem*. 2001;276:32860–6.
76. Xu F, Grande AM, Robinson JK, Previti ML, Vasek M, Davis J, Van Nostrand WE. Early-onset subicular microvascular amyloid and neuroinflammation correlate with behavioral deficits in vasculotropic mutant amyloid β -protein precursor transgenic mice. *Neuroscience*. 2007;146:98–107.
77. Yamada M, Tsukagoshi H, Otomo E, Hayakawa M. Cerebral amyloid angiopathy in the aged. *J Neurol*. 1987;234:371–6.
78. Yamada M. Risk factors for cerebral amyloid angiopathy in the elderly. *Ann N Y Acad Sci*. 2002;977:37–44.

79. Mackic JB, Weiss MH, Miao W, Kirkman E, Ghiso J, Calero M, Bading J, Frangione B, Zlokovic B V. Cerebrovascular accumulation and increased blood-brain barrier permeability to circulating Alzheimer's amyloid beta peptide in aged squirrel monkey with cerebral amyloid angiopathy. *J Neurochem.* 1998;70:210–5.
80. Shibata M, Yamada S, Kumar SR, Calero M, Bading J, Frangione B, Holtzman DM, Miller CA, Strickland DK, Ghiso J, Zlokovic B V. Clearance of Alzheimer's amyloid- β 1-40 peptide from brain by LDL receptor-related protein-1 at the blood-brain barrier. *J Clin Invest.* 2000;106:1489–1499.
81. Hawkes CA, Härtig W, Kacza J, Schliebs R, Weller RO, Nicoll JA, Carare RO. Perivascular drainage of solutes is impaired in the ageing mouse brain and in the presence of cerebral amyloid angiopathy. *Acta Neuropathol.* 2011;121:431–443.
82. Kress BT, Iliff JJ, Xia M, Wang M, Wei HS, Zeppenfeld D, Xie L, Kang H, Xu Q, Liew JA, Plog BA, Ding F, Deane R, Nedergaard M. Impairment of paravascular clearance pathways in the aging brain. *Ann Neurol.* 2014;76:845–861.
83. Carnevale D, Mascio G, D'Andrea I, Fardella V, Bell RD, Branchi I, Pallante F, Zlokovic B, Yan SS, Lembo G. Hypertension Induces Brain β -Amyloid Accumulation, Cognitive Impairment, and Memory Deterioration Through Activation of Receptor for Advanced Glycation End Products in Brain Vasculature. *Hypertension.* 2012;60:188–197.
84. Hawkes CA, Gentleman SM, Nicoll JA, Carare RO. Prenatal high-fat diet alters the cerebrovasculature and clearance of β -amyloid in adult offspring. *J Pathol.* 2015;235:619–631.
85. Vandal M, White PJ, Tremblay C, St-Amour I, Chevrier G, Emond V, Lefrancois D,

- Virgili J, Planel E, Giguere Y, Marette A, Calon F. Insulin Reverses the High-Fat Diet-Induced Increase in Brain A β and Improves Memory in an Animal Model of Alzheimer Disease. *Diabetes*. 2014;63:4291–4301.
86. Martel CL, Mackic JB, Matsubara E, Governale S, Miguel C, Miao W, McComb JG, Frangione B, Ghiso J, Zlokovic B V. Isoform-specific effects of apolipoproteins E2, E3, and E4 on cerebral capillary sequestration and blood-brain barrier transport of circulating Alzheimer's amyloid beta. *J Neurochem*. 1997;69:1995–2004.
87. He X, Liu D, Zhang Q, Liang F, Dai G, Zeng J, Pei Z, Xu G, Lan Y. Voluntary Exercise Promotes Glymphatic Clearance of Amyloid Beta and Reduces the Activation of Astrocytes and Microglia in Aged Mice. *Front Mol Neurosci*. 2017;10:144.
88. Jacob M, Chappell D, Becker BF. Regulation of blood flow and volume exchange across the microcirculation. *Crit Care*. 2016;20:319.
89. Hakim A, Gralla J, Rozeik C, Mordasini P, Leidolt L, Piechowiak E, Ozdoba C, El-Koussy M. Anomalies and Normal Variants of the Cerebral Arterial Supply: A Comprehensive Pictorial Review with a Proposed Workflow for Classification and Significance. *J Neuroimaging*. 2018;28:14–35.
90. Thomsen MS, Routhe LJ, Moos T. The vascular basement membrane in the healthy and pathological brain. *J Cereb Blood Flow Metab*. 2017;37:3300–3317.
91. Iadecola C. The Neurovascular Unit Coming of Age: A Journey through Neurovascular Coupling in Health and Disease. *Neuron*. 2017;96:17–42.
92. Yamada M. Cerebral amyloid angiopathy: emerging concepts. *J stroke*. 2015;17:17–30.

93. Thal DR, Ghebremedhin E, Rüb U, Yamaguchi H, Del Tredici K, Braak H. Two types of sporadic cerebral amyloid angiopathy. *J Neuropathol Exp Neurol*. 2002;61:282–93.
94. Yamaguchi H, Yamazaki T, Lemere CA, Frosch MP, Selkoe DJ. Beta amyloid is focally deposited within the outer basement membrane in the amyloid angiopathy of Alzheimer's disease. An immunoelectron microscopic study. *Am J Pathol*. 1992;141:249–59.
95. Maeda A, Yamada M, Itoh Y, Otomo E, Hayakawa M, Miyatake T. Computer-assisted three-dimensional image analysis of cerebral amyloid angiopathy. *Stroke*. 1993;24:1857–64.
96. Mandybur TI. Cerebral amyloid angiopathy: the vascular pathology and complications. *J Neuropathol Exp Neurol*. 1986;45:79–90.
97. Charidimou A, Imaizumi T, Moulin S, Biffi A, Samarasekera N, Yakushiji Y, Peeters A, Vandermeeren Y, Laloux P, Baron J-C, Hernandez-Guillamon M, Montaner J, Casolla B, Gregoire SM, Kang D-W, Kim JS, Naka H, Smith EE, Viswanathan A, Jäger HR, Al-Shahi Salman R, Greenberg SM, Cordonnier C, Werring DJ. Brain hemorrhage recurrence, small vessel disease type, and cerebral microbleeds. *Neurology*. 2017;89:820–829.
98. Gregoire SM, Charidimou A, Gadapa N, Dolan E, Antoun N, Peeters A, Vandermeeren Y, Laloux P, Baron J-C, Jäger HR, Werring DJ. Acute ischaemic brain lesions in intracerebral haemorrhage: multicentre cross-sectional magnetic resonance imaging study. *Brain*. 2011;134:2376–2386.
99. Kimberly WT, Gilson A, Rost NS, Rosand J, Viswanathan A, Smith EE, Greenberg SM. Silent ischemic infarcts are associated with hemorrhage burden in cerebral

- amyloid angiopathy. *Neurology*. 2009;72:1230–1235.
100. Tabaton M, Caponnetto C, Mancardi G, Loeb C. Amyloid beta protein deposition in brains from elderly subjects with leukoaraiosis. *J Neurol Sci*. 1991;106:123–7.
 101. Pluta R, Januszewski S, Ułamek M. Ischemic blood-brain barrier and amyloid in white matter as etiological factors in leukoaraiosis. *Acta Neurochir Suppl*. 2008;102:353–6.
 102. Reijmer YD, Fotiadis P, Riley GA, Xiong L, Charidimou A, Boulouis G, Ayres AM, Schwab K, Rosand J, Gurol ME, Viswanathan A, Greenberg SM. Progression of Brain Network Alterations in Cerebral Amyloid Angiopathy. *Stroke*. 2016;47:2470–2475.
 103. Reijmer YD, Fotiadis P, Martinez-Ramirez S, Salat DH, Schultz A, Shoamanesh A, Ayres AM, Vashkevich A, Rosas D, Schwab K, Leemans A, Biessels G-J, Rosand J, Johnson KA, Viswanathan A, Gurol ME, Greenberg SM. Structural network alterations and neurological dysfunction in cerebral amyloid angiopathy. *Brain*. 2015;138:179–188.
 104. Reijmer YD, Fotiadis P, Charidimou A, van Veluw SJ, Xiong L, Riley GA, Martinez-Ramirez S, Schwab K, Viswanathan A, Gurol ME, Greenberg SM. Relationship between white matter connectivity loss and cortical thinning in cerebral amyloid angiopathy. *Hum Brain Mapp*. 2017. doi:10.1002/hbm.23629.
 105. Fotiadis P, van Rooden S, van der Grond J, Schultz A, Martinez-Ramirez S, Auriel E, Reijmer Y, van Opstal AM, Ayres A, Schwab KM, Alzheimer’s Disease Neuroimaging Initiative (ADNI), Hedden T, Rosand J, Viswanathan A, Wermer M, Terwindt GM, Sperling RA, Polimeni JR, Johnson KA, van Buchem MA, Greenberg SM, Gurol ME. Cortical atrophy in patients with cerebral amyloid angiopathy: a case-control study. *Lancet Neurol*. 2016;15:811–819.

106. Martucci M, Sarria S, Toledo M, Coscojuela P, Vert C, Siurana S, Auger C, Rovira A. Cerebral amyloid angiopathy-related inflammation: imaging findings and clinical outcome. *Neuroradiology*. 2014;56:283–289.
107. Salvarani C, Hunder GG, Morris JM, Brown RD, Christianson T, Giannini C. A - related angiitis: Comparison with CAA without inflammation and primary CNS vasculitis. *Neurology*. 2013;81:1596–1603.
108. Iadecola C. Cerebrovascular effects of amyloid-beta peptides: mechanisms and implications for Alzheimer’s dementia. *Cell Mol Neurobiol*. 2003;23:681–9.
109. Park L, Zhou P, Pitstick R, Capone C, Anrather J, Norris EH, Younkin L, Younkin S, Carlson G, McEwen BS, Iadecola C. Nox2-derived radicals contribute to neurovascular and behavioral dysfunction in mice overexpressing the amyloid precursor protein. *Proc Natl Acad Sci U S A*. 2008;105:1347–52.
110. Goodwin JL, Uemura E, Cunnick JE. Microglial release of nitric oxide by the synergistic action of beta-amyloid and IFN-gamma. *Brain Res*. 1995;692:207–14.
111. Ueda K, Fukui Y, Kageyama H. Amyloid beta protein-induced neuronal cell death: neurotoxic properties of aggregated amyloid beta protein. *Brain Res*. 1994;639:240–4.
112. Yagami T, Ueda K, Asakura K, Sakaeda T, Kuroda T, Hata S, Kambayashi Y, Fujimoto M. Effects of S-2474, a novel nonsteroidal anti-inflammatory drug, on amyloid β protein-induced neuronal cell death. *Br J Pharmacol*. 2001;134:673–681.
113. Blaise R, Mateo V, Rouxel C, Zaccarini F, Glorian M, Béréziat G, Golubkov VS, Limon I. Wild-type amyloid beta 1-40 peptide induces vascular smooth muscle cell death independently from matrix metalloprotease activity. *Aging Cell*. 2012;11:384–393.

114. Verbeek MM, de Waal RM, Schipper JJ, Van Nostrand WE. Rapid degeneration of cultured human brain pericytes by amyloid beta protein. *J Neurochem.* 1997;68:1135–41.
115. Thomas T, Thomas G, McLendon C, Sutton T, Mullan M. β -Amyloid-mediated vasoactivity and vascular endothelial damage. *Nature.* 1996;380:168–171.
116. Liu H, Yang Y, Xia Y, Zhu W, Leak RK, Wei Z, Wang J, Hu X. Aging of cerebral white matter. *Ageing Res Rev.* 2017;34:64–76.
117. Miners JS, Palmer JC, Love S. Pathophysiology of Hypoperfusion of the Precuneus in Early Alzheimer’s Disease. *Brain Pathol.* 2016;26:533–541.
118. Maier FC, Wehrl HF, Schmid AM, Mannheim JG, Wiehr S, Lerdkrai C, Calaminus C, Stahlschmidt A, Ye L, Burnet M, Stiller D, Sabri O, Reischl G, Staufenbiel M, Garaschuk O, Jucker M, Pichler BJ. Longitudinal PET-MRI reveals β -amyloid deposition and rCBF dynamics and connects vascular amyloidosis to quantitative loss of perfusion. *Nat Med.* 2014;20:1485–1492.
119. Carrano A, Hoozemans JJM, van der Vies SM, Rozemuller AJM, van Horssen J, de Vries HE. Amyloid Beta Induces Oxidative Stress-Mediated Blood–Brain Barrier Changes in Capillary Amyloid Angiopathy. *Antioxid Redox Signal.* 2011;15:1167–1178.
120. Carrano A, Hoozemans JJM, van der Vies SM, van Horssen J, de Vries HE, Rozemuller AJM. Neuroinflammation and Blood-Brain Barrier Changes in Capillary Amyloid Angiopathy. *Neurodegener Dis.* 2012;10:329–331.
121. Hartz AMS, Bauer B, Soldner ELB, Wolf A, Boy S, Backhaus R, Mihaljevic I, Bogdahn U, Klunemann HH, Schuierer G, Schlachetzki F. Amyloid-beta contributes

- to blood-brain barrier leakage in transgenic human amyloid precursor protein mice and in humans with cerebral amyloid angiopathy. *Stroke*. 2012;43:514–523.
122. Peca S, McCreary CR, Donaldson E, Kumarpillai G, Shobha N, Sanchez K, Charlton A, Steinback CD, Beaudin AE, Fluck D, Pillay N, Fick GH, Poulin MJ, Frayne R, Goodyear BG, Smith EE. Neurovascular decoupling is associated with severity of cerebral amyloid angiopathy. *Neurology*. 2013;81:1659–1665.
123. Maki T, Okamoto Y, Carare RO, Hase Y, Hattori Y, Hawkes CA, Saito S, Yamamoto Y, Terasaki Y, Ishibashi-Ueda H, Taguchi A, Takahashi R, Miyakawa T, Kalaria RN, Lo EH, Arai K, Ihara M. Phosphodiesterase III inhibitor promotes drainage of cerebrovascular β -amyloid. *Ann Clin Transl Neurol*. 2014;1:519–533.
124. Williams RJ, Goodyear BG, Peca S, McCreary CR, Frayne R, Smith EE, Pike GB. Identification of neurovascular changes associated with cerebral amyloid angiopathy from subject-specific hemodynamic response functions. *J Cereb Blood Flow Metab*. 2017;:0271678X1769105.
125. Iliff JJ, Wang M, Liao Y, Plogg BA, Peng W, Gundersen GA, Benveniste H, Vates GE, Deane R, Goldman SA, Nagelhus EA, Nedergaard M. A paravascular pathway facilitates CSF flow through the brain parenchyma and the clearance of interstitial solutes, including amyloid β . *Sci Transl Med*. 2012;4:147ra111.
126. Ghersi-Egea J-F, Strazielle N, Catala M, Silva-Vargas V, Doetsch F, Engelhardt B. Molecular anatomy and functions of the choroidal blood-cerebrospinal fluid barrier in health and disease. *Acta Neuropathol*. 2018;135:337–361.
127. MAXWELL DS, PEASE DC. The electron microscopy of the choroid plexus. *J Biophys Biochem Cytol*. 1956;2:467–74.

128. Cserr HF. Physiology of the choroid plexus. *Physiol Rev.* 1971;51:273–311.
129. Wright EM. Transport processes in the formation of the cerebrospinal fluid. *Rev Physiol Biochem Pharmacol.* 1978;83:3–34.
130. Keep RF, Jones HC. A morphometric study on the development of the lateral ventricle choroid plexus, choroid plexus capillaries and ventricular ependyma in the rat. *Brain Res Dev Brain Res.* 1990;56:47–53.
131. Pollay M, Hisey B, Reynolds E, Tomkins P, Stevens FA, Smith R. Choroid plexus Na⁺/K⁺-activated adenosine triphosphatase and cerebrospinal fluid formation. *Neurosurgery.* 1985;17:768–72.
132. Davson H, Segal MB. The effects of some inhibitors and accelerators of sodium transport on the turnover of ²²Na in the cerebrospinal fluid and the brain. *J Physiol.* 1970;209:131–53.
133. Preston GM, Agre P. Isolation of the cDNA for erythrocyte integral membrane protein of 28 kilodaltons: member of an ancient channel family. *Proc Natl Acad Sci U S A.* 1991;88:11110–4.
134. Preston GM, Carroll TP, Guggino WB, Agre P. Appearance of water channels in *Xenopus* oocytes expressing red cell CHIP28 protein. *Science.* 1992;256:385–7.
135. Nielsen S, Smith BL, Christensen EI, Agre P. Distribution of the aquaporin CHIP in secretory and resorptive epithelia and capillary endothelia. *Proc Natl Acad Sci U S A.* 1993;90:7275–9.
136. Speake T, Freeman LJ, Brown PD. Expression of aquaporin 1 and aquaporin 4 water channels in rat choroid plexus. *Biochim Biophys Acta.* 2003;1609:80–6.
137. Oshio K, Watanabe H, Song Y, Verkman AS, Manley GT. Reduced cerebrospinal

- fluid production and intracranial pressure in mice lacking choroid plexus water channel Aquaporin-1. *FASEB J.* 2005;19:76–8.
138. Wolburg H, Wolburg-Buchholz K, Liebner S, Engelhardt B. Claudin-1, claudin-2 and claudin-11 are present in tight junctions of choroid plexus epithelium of the mouse. *Neurosci Lett.* 2001;307:77–80.
139. Rosenthal R, Milatz S, Krug SM, Oelrich B, Schulzke J-D, Amasheh S, Gunzel D, Fromm M. Claudin-2, a component of the tight junction, forms a paracellular water channel. *J Cell Sci.* 2010;123:1913–1921.
140. Stratchko L, Filatova I, Agarwal A, Kanekar S. The Ventricular System of the Brain: Anatomy and Normal Variations. *Semin Ultrasound, CT MRI.* 2016;37:72–83.
141. Glimcher SA, Holman DW, Lubow M, Grzybowski DM. Ex vivo model of cerebrospinal fluid outflow across human arachnoid granulations. *Invest Ophthalmol Vis Sci.* 2008;49:4721–8.
142. Upton ML, Weller RO. The morphology of cerebrospinal fluid drainage pathways in human arachnoid granulations. *J Neurosurg.* 1985;63:867–875.
143. Louveau A, Smirnov I, Keyes TJ, Eccles JD, Rouhani SJ, Peske JD, Derecki NC, Castle D, Mandell JW, Lee KS, Harris TH, Kipnis J. Structural and functional features of central nervous system lymphatic vessels. *Nature.* 2015;523:337–341.
144. Aspelund A, Antila S, Proulx ST, Karlsen TV, Karaman S, Detmar M, Wiig H, Alitalo K. A dural lymphatic vascular system that drains brain interstitial fluid and macromolecules. *J Exp Med.* 2015;212:991–999.
145. de Leon MJ, Li Y, Okamura N, Tsui WH, Saint-Louis LA, Glodzik L, Osorio RS, Fortea J, Butler T, Pirraglia E, Fossati S, Kim H-J, Carare RO, Nedergaard M,

- Benveniste H, Rusinek H. Cerebrospinal Fluid Clearance in Alzheimer Disease Measured with Dynamic PET. *J Nucl Med*. 2017;58:1471–1476.
146. Chen L, Elias G, Yostos MP, Stimec B, Fasel J, Murphy K. Pathways of cerebrospinal fluid outflow: a deeper understanding of resorption. *Neuroradiology*. 2015;57:139–147.
147. MATSUMAE M, SATO O, HIRAYAMA A, HAYASHI N, TAKIZAWA K, ATSUMI H, SORIMACHI T. Research into the Physiology of Cerebrospinal Fluid Reaches a New Horizon: Intimate Exchange between Cerebrospinal Fluid and Interstitial Fluid May Contribute to Maintenance of Homeostasis in the Central Nervous System. *Neurol Med Chir (Tokyo)*. 2016;56:416–441.
148. Tarasoff-Conway JM, Carare RO, Osorio RS, Glodzik L, Butler T, Fieremans E, Axel L, Rusinek H, Nicholson C, Zlokovic B V., Frangione B, Blennow K, Ménard J, Zetterberg H, Wisniewski T, de Leon MJ. Clearance systems in the brain—implications for Alzheimer disease. *Nat Rev Neurol*. 2015;11:457–470.
149. Charidimou A, Friedrich JO, Greenberg SM, Viswanathan A. Core cerebrospinal fluid biomarker profile in cerebral amyloid angiopathy. *Neurology*. 2018;90:e754–e762.
150. van Etten ES, Verbeek MM, van der Grond J, Zielman R, van Rooden S, van Zwet EW, van Opstal AM, Haan J, Greenberg SM, van Buchem MA, Wermer MJH, Terwindt GM. β -Amyloid in CSF. *Neurology*. 2017;88:169–176.
151. Thomsen MS, Birkelund S, Burkhart A, Stensballe A, Moos T. Synthesis and deposition of basement membrane proteins by primary brain capillary endothelial cells in a murine model of the blood-brain barrier. *J Neurochem*. 2017;140:741–754.
152. Keski-Oja J, Mosher DF, Vaheri A. Dimeric character of fibronectin, a major cell

- surface-associated glycoprotein. *Biochem Biophys Res Commun*. 1977;74:699–706.
153. Tilling T, Korte D, Hoheisel D, Galla HJ. Basement membrane proteins influence brain capillary endothelial barrier function in vitro. *J Neurochem*. 1998;71:1151–7.
154. Kose N, Asashima T, Muta M, Iizasa H, Sai Y, Terasaki T, Nakashima E. Altered expression of basement membrane-related molecules in rat brain pericyte, endothelial, and astrocyte cell lines after transforming growth factor-beta1 treatment. *Drug Metab Pharmacokinet*. 2007;22:255–66.
155. Krum JM, More NS, Rosenstein JM. Brain angiogenesis: variations in vascular basement membrane glycoprotein immunoreactivity. *Exp Neurol*. 1991;111:152–65.
156. Schwarzbauer JE, DeSimone DW. Fibronectins, Their Fibrillogenesis, and In Vivo Functions. *Cold Spring Harb Perspect Biol*. 2011;3:a005041–a005041.
157. Li J-P, Kusche-Gullberg M. Heparan Sulfate: Biosynthesis, Structure, and Function. In: *International review of cell and molecular biology*. ; 2016: 215–273.
158. Parham CL, Shaw C, Auckland LD, Dickeson SK, Griswold-Prenner I, Bix G. Perlecan Domain V Inhibits Amyloid- β Induced Activation of the $\alpha 2\beta 1$ Integrin-Mediated Neurotoxic Signaling Cascade. *J Alzheimer's Dis*. 2016;54:1629–1647.
159. Verbeek MM, Otte-Höller I, van den Born J, van den Heuvel LPWJ, David G, Wesseling P, de Waal RMW. Agrin Is a Major Heparan Sulfate Proteoglycan Accumulating in Alzheimer's Disease Brain. *Am J Pathol*. 1999;155:2115–2125.
160. Barber AJ, Lieth E. Agrin accumulates in the brain microvascular basal lamina during development of the blood-brain barrier. *Dev Dyn*. 1997;208:62–74.
161. Lunde LK, Camassa LMA, Hoddevik EH, Khan FH, Ottersen OP, Boldt HB, Amiry-Moghaddam M. Postnatal development of the molecular complex underlying astrocyte

- polarization. *Brain Struct Funct.* 2015;220:2087–2101.
162. Utriainen A, Sormunen R, Kettunen M, Carvalhaes LS, Sajanti E, Eklund L, Kauppinen R, Kitten GT, Pihlajaniemi T. Structurally altered basement membranes and hydrocephalus in a type XVIII collagen deficient mouse line. *Hum Mol Genet.* 2004;13:2089–2099.
163. Horiguchi K, Kouki T, Fujiwara K, Tsukada T, Ly F, Kikuchi M, Yashiro T. Expression of the proteoglycan syndecan-4 and the mechanism by which it mediates stress fiber formation in folliculostellate cells in the rat anterior pituitary gland. *J Endocrinol.* 2012;214:199–206.
164. Woods A, Longley RL, Tumova S, Couchman JR. Syndecan-4 binding to the high affinity heparin-binding domain of fibronectin drives focal adhesion formation in fibroblasts. *Arch Biochem Biophys.* 2000;374:66–72.
165. Lee B, Clarke D, Al Ahmad A, Kahle M, Parham C, Auckland L, Shaw C, Fidanboyulu M, Orr AW, Ogunshola O, Fertala A, Thomas SA, Bix GJ. Perlecan domain V is neuroprotective and proangiogenic following ischemic stroke in rodents. *J Clin Invest.* 2011;121:3005–3023.
166. Engelhardt B. β 1-integrin/matrix interactions support blood-brain barrier integrity. *J Cereb Blood Flow Metab.* 2011;31:1969–71.
167. Paulus W, Baur I, Schuppan D, Roggendorf W. Characterization of integrin receptors in normal and neoplastic human brain. *Am J Pathol.* 1993;143:154–63.
168. Milner R, Campbell IL. Developmental regulation of beta1 integrins during angiogenesis in the central nervous system. *Mol Cell Neurosci.* 2002;20:616–26.
169. Milner R, Campbell IL. Increased expression of the beta4 and alpha5 integrin subunits

- in cerebral blood vessels of transgenic mice chronically producing the pro-inflammatory cytokines IL-6 or IFN- α in the central nervous system. *Mol Cell Neurosci.* 2006;33:429–40.
170. Grazioli A, Alves CS, Konstantopoulos K, Yang JT. Defective blood vessel development and pericyte/pvSMC distribution in alpha 4 integrin-deficient mouse embryos. *Dev Biol.* 2006;293:165–77.
171. Huveneers S, Truong H, Fassler R, Sonnenberg A, Danen EHJ. Binding of soluble fibronectin to integrin $\alpha 5 \beta 1$ - link to focal adhesion redistribution and contractile shape. *J Cell Sci.* 2008;121:2452–2462.
172. Mahalingam Y, Gallagher JT, Couchman JR. Cellular Adhesion Responses to the Heparin-binding (HepII) Domain of Fibronectin Require Heparan Sulfate with Specific Properties. *J Biol Chem.* 2007;282:3221–3230.
173. Wang Z, Collighan RJ, Gross SR, Danen EHJ, Orend G, Telci D, Griffin M. RGD-independent Cell Adhesion via a Tissue Transglutaminase-Fibronectin Matrix Promotes Fibronectin Fibril Deposition and Requires Syndecan-4/2 and $\alpha 5 \beta 1$ Integrin Co-signaling. *J Biol Chem.* 2010;285:40212–40229.
174. Banères JL, Roquet F, Green M, LeCalvez H, Parello J. The cation-binding domain from the alpha subunit of integrin alpha5 beta1 is a minimal domain for fibronectin recognition. *J Biol Chem.* 1998;273:24744–53.
175. Mould AP, Askari JA, Aota S i, Yamada KM, Irie A, Takada Y, Mardon HJ, Humphries MJ. Defining the topology of integrin alpha5beta1-fibronectin interactions using inhibitory anti-alpha5 and anti-beta1 monoclonal antibodies. Evidence that the synergy sequence of fibronectin is recognized by the amino-terminal repeats of the

- alpha5 subunit. *J Biol Chem.* 1997;272:17283–92.
176. Nagae M, Re S, Mihara E, Nogi T, Sugita Y, Takagi J. Crystal structure of $\alpha 5 \beta 1$ integrin ectodomain: Atomic details of the fibronectin receptor. *J Cell Biol.* 2012;197:131–140.
177. Su Y, Xia W, Li J, Walz T, Humphries MJ, Vestweber D, Cabañas C, Lu C, Springer TA. Relating conformation to function in integrin $\alpha 5 \beta 1$. *Proc Natl Acad Sci.* 2016;113:E3872–E3881.
178. Winder SJ. The complexities of dystroglycan. *Trends Biochem Sci.* 2001;26:118–24.
179. Zaccaria ML, Di Tommaso F, Brancaccio A, Paggi P, Petrucci TC. Dystroglycan distribution in adult mouse brain: a light and electron microscopy study. *Neuroscience.* 2001;104:311–24.
180. Zarow C, Barron E, Chui HC, Perlmutter LS. Vascular basement membrane pathology and Alzheimer's disease. *Ann N Y Acad Sci.* 1997;826:147–60.
181. Hawkes CA, Gatherer M, Sharp MM, Dorr A, Yuen HM, Kalaria R, Weller RO, Carare RO. Regional differences in the morphological and functional effects of aging on cerebral basement membranes and perivascular drainage of amyloid- β from the mouse brain. *Aging Cell.* 2013;12:224–36.
182. Lepelletier F-X, Mann DMA, Robinson AC, Pinteaux E, Boutin H. Early changes in extracellular matrix in Alzheimer's disease. *Neuropathol Appl Neurobiol.* 2017;43:167–182.
183. Merlini M, Meyer EP, Ulmann-Schuler A, Nitsch RM. Vascular β -amyloid and early astrocyte alterations impair cerebrovascular function and cerebral metabolism in transgenic arcA β mice. *Acta Neuropathol.* 2011;122:293–311.

184. Kiuchi Y, Isobe Y, Fukushima K. Entactin-induced inhibition of human amyloid beta-protein fibril formation in vitro. *Neurosci Lett*. 2001;305:119–22.
185. Kiuchi Y, Isobe Y, Fukushima K, Kimura M. Disassembly of amyloid beta-protein fibril by basement membrane components. *Life Sci*. 2002;70:2421–31.
186. Hawkes CA, Sullivan PM, Hands S, Weller RO, Nicoll JAR, Carare RO. Disruption of Arterial Perivascular Drainage of Amyloid- β from the Brains of Mice Expressing the Human APOE ϵ 4 Allele. *PLoS One*. 2012;7:e41636.
187. Castillo GM, Ngo C, Cummings J, Wight TN, Snow AD. Perlecan binds to the beta-amyloid proteins (A beta) of Alzheimer's disease, accelerates A beta fibril formation, and maintains A beta fibril stability. *J Neurochem*. 1997;69:2452–65.
188. Fukuda S, Fini CA, Mabuchi T, Koziol JA, Eggleston LL, del Zoppo GJ. Focal cerebral ischemia induces active proteases that degrade microvascular matrix. *Stroke*. 2004;35:998–1004.
189. Katsu M, Niizuma K, Yoshioka H, Okami N, Sakata H, Chan PH. Hemoglobin-Induced Oxidative Stress Contributes to Matrix Metalloproteinase Activation and Blood–Brain Barrier Dysfunction *in vivo*. *J Cereb Blood Flow Metab*. 2010;30:1939–1950.
190. Hamann GF, Okada Y, Fitridge R, del Zoppo GJ. Microvascular basal lamina antigens disappear during cerebral ischemia and reperfusion. *Stroke*. 1995;26:2120–6.
191. Hamann GF, Liebetrau M, Martens H, Burggraf D, Kloss CUA, Bültemeier G, Wunderlich N, Jäger G, Pfefferkorn T. Microvascular basal lamina injury after experimental focal cerebral ischemia and reperfusion in the rat. *J Cereb Blood Flow Metab*. 2002;22:526–33.

192. Wasserman JK, Schlichter LC. Minocycline protects the blood-brain barrier and reduces edema following intracerebral hemorrhage in the rat. *Exp Neurol*. 2007;207:227–37.
193. Rosell A, Cuadrado E, Ortega-Aznar A, Hernández-Guillamon M, Lo EH, Montaner J. MMP-9-positive neutrophil infiltration is associated to blood-brain barrier breakdown and basal lamina type IV collagen degradation during hemorrhagic transformation after human ischemic stroke. *Stroke*. 2008;39:1121–6.
194. Huang Q, Chen B, Wang F, Huang H, Milner R, Li L. The temporal expression patterns of fibronectin and its receptors- $\alpha 5\beta 1$ and $\alpha v\beta 3$ integrins on blood vessels after cerebral ischemia. *Restor Neurol Neurosci*. 2015;33:493–507.
195. Nakada T, Kwee IL, Igarashi H, Suzuki Y. Aquaporin-4 Functionality and Virchow-Robin Space Water Dynamics: Physiological Model for Neurovascular Coupling and Glymphatic Flow. *Int J Mol Sci*. 2017;18. doi:10.3390/ijms18081798.
196. Morris AWJ, Sharp MM, Albargothy NJ, Fernandes R, Hawkes CA, Verma A, Weller RO, Carare RO. Vascular basement membranes as pathways for the passage of fluid into and out of the brain. *Acta Neuropathol*. 2016;131:725–36.
197. Brøchner CB, Holst CB, Møllgård K. Outer brain barriers in rat and human development. *Front Neurosci*. 2015;9:75.
198. Cserr HF, Cooper DN, Milhorat TH. Flow of cerebral interstitial fluid as indicated by the removal of extracellular markers from rat caudate nucleus. *Exp Eye Res*. 1977;25 Suppl:461–73.
199. Bradbury MW, Cserr HF, Westrop RJ. Drainage of cerebral interstitial fluid into deep cervical lymph of the rabbit. *Am J Physiol Physiol*. 1981;240:F329–F336.

200. Cserr HF, Cooper DN, Suri PK, Patlak CS. Efflux of radiolabeled polyethylene glycols and albumin from rat brain. *Am J Physiol Physiol*. 1981;240:F319–F328.
201. Szentistványi I, Patlak CS, Ellis RA, Cserr HF. Drainage of interstitial fluid from different regions of rat brain. *Am J Physiol*. 1984;246:F835–44.
202. Syková E, Nicholson C. Diffusion in brain extracellular space. *Physiol Rev*. 2008;88:1277–340.
203. Rosenberg GA, Kyner WT, Estrada E. Bulk flow of brain interstitial fluid under normal and hyperosmolar conditions. *Am J Physiol*. 1980;238:F42–9.
204. Rennels ML, Gregory TF, Blaumanis OR, Fujimoto K, Grady PA. Evidence for a “paravascular” fluid circulation in the mammalian central nervous system, provided by the rapid distribution of tracer protein throughout the brain from the subarachnoid space. *Brain Res*. 1985;326:47–63.
205. Iliff JJ, Chen MJ, Plog BA, Zeppenfeld DM, Soltero M, Yang L, Singh I, Deane R, Nedergaard M. Impairment of Glymphatic Pathway Function Promotes Tau Pathology after Traumatic Brain Injury. *J Neurosci*. 2014;34:16180–16193.
206. Xie L, Kang H, Xu Q, Chen MJ, Liao Y, Thiyagarajan M, O’Donnell J, Christensen DJ, Nicholson C, Iliff JJ, Takano T, Deane R, Nedergaard M. Sleep drives metabolite clearance from the adult brain. *Science*. 2013;342:373–7.
207. Iliff JJ, Lee H, Yu M, Feng T, Logan J, Nedergaard M, Benveniste H. Brain-wide pathway for waste clearance captured by contrast-enhanced MRI. *J Clin Invest*. 2013;123:1299–1309.
208. Wang M, Ding F, Deng S, Guo X, Wang W, Iliff JJ, Nedergaard M. Focal Solute Trapping and Global Glymphatic Pathway Impairment in a Murine Model of Multiple

- Microinfarcts. *J Neurosci*. 2017;37:2870–2877.
209. Peng W, Achariyar TM, Li B, Liao Y, Mestre H, Hitomi E, Regan S, Kasper T, Peng S, Ding F, Benveniste H, Nedergaard M, Deane R. Suppression of glymphatic fluid transport in a mouse model of Alzheimer's disease. *Neurobiol Dis*. 2016;93:215–225.
210. Syková E, Vorísek I, Mazel T, Antonova T, Schachner M. Reduced extracellular space in the brain of tenascin-R- and HNK-1-sulphotransferase deficient mice. *Eur J Neurosci*. 2005;22:1873–80.
211. Syková E, Vorísek I, Antonova T, Mazel T, Meyer-Luehmann M, Jucker M, Hájek M, Ort M, Or M, Bures J. Changes in extracellular space size and geometry in APP23 transgenic mice: a model of Alzheimer's disease. *Proc Natl Acad Sci U S A*. 2005;102:479–84.
212. Vargová L, Homola A, Zámecník J, Tichý M, Benes V, Syková E. Diffusion parameters of the extracellular space in human gliomas. *Glia*. 2003;42:77–88.
213. Rees S, Cragg BG, Everitt A V. Comparison of extracellular space in the mature and aging rat brain using a new technique. *J Neurol Sci*. 1982;53:347–57.
214. Bondareff W, Narotzky R. Age changes in the neuronal microenvironment. *Science*. 1972;176:1135–6.
215. Homola A, Zoremba N, Slais K, Kuhlen R, Syková E. Changes in diffusion parameters, energy-related metabolites and glutamate in the rat cortex after transient hypoxia/ischemia. *Neurosci Lett*. 2006;404:137–42.
216. Zoremba N, Homola A, Rossaint R, Syková E. Brain metabolism and extracellular space diffusion parameters during and after transient global hypoxia in the rat cortex. *Exp Neurol*. 2007;203:34–41.

217. Maas C, Schiks B, Strangi RD, Hackeng TM, Bouma BN, Gebbink MFBG, Bouma B. Identification of fibronectin type I domains as amyloid-binding modules on tissue-type plasminogen activator and three homologs. *Amyloid*. 2008;15:166–180.
218. Grand Moursel L, Munting LP, van der Graaf LM, van Duinen SG, Goumans M-JTH, Ueberham U, Natté R, van Buchem MA, van Roon-Mom WMC, van der Weerd L. TGF β pathway deregulation and abnormal phospho-SMAD2/3 staining in hereditary cerebral hemorrhage with amyloidosis-Dutch type. *Brain Pathol*. 2017. doi:10.1111/bpa.12533.
219. Wyss-Coray T, Feng L, Masliah E, Ruppe MD, Lee HS, Toggas SM, Rockenstein EM, Mucke L. Increased central nervous system production of extracellular matrix components and development of hydrocephalus in transgenic mice overexpressing transforming growth factor-beta 1. *Am J Pathol*. 1995;147:53–67.
220. Wyss-Coray T, Lin C, Sanan DA, Mucke L, Masliah E. Chronic overproduction of transforming growth factor-beta1 by astrocytes promotes Alzheimer's disease-like microvascular degeneration in transgenic mice. *Am J Pathol*. 2000;156:139–50.
221. Zhang X, Huang W-J, Chen W-W. TGF- β 1 factor in the cerebrovascular diseases of Alzheimer's disease. *Eur Rev Med Pharmacol Sci*. 2016;20:5178–5185.
222. Mecha M, Rabadán MA, Peña-Melián A, Valencia M, Mondéjar T, Blanco MJ. Expression of TGF- β s in the embryonic nervous system: Analysis of interbalance between isoforms. *Dev Dyn*. 2008;237:1709–1717.
223. Doyle KP, Cekanaviciute E, Mamer LE, Buckwalter MS. TGF β signaling in the brain increases with aging and signals to astrocytes and innate immune cells in the weeks after stroke. *J Neuroinflammation*. 2010;7:62.

224. Letourneur O, Goetschy J-F, Horisberger M, Grütter MG. Ligand-Induced Dimerization of the Extracellular Domain of the TGF- β Receptor Type II. *Biochem Biophys Res Commun.* 1996;224:709–716.
225. Nickel J, ten Dijke P, Mueller TD. TGF- β family co-receptor function and signaling. *Acta Biochim Biophys Sin (Shanghai).* 2018;50:12–36.
226. Bai J, Xi Q. Crosstalk between TGF- β signaling and epigenome. *Acta Biochim Biophys Sin (Shanghai).* 2018;50:60–67.
227. Zhu H, Gui Q, Hui X, Wang X, Jiang J, Ding L, Sun X, Wang Y, Chen H. TGF- β 1/Smad3 Signaling Pathway Suppresses Cell Apoptosis in Cerebral Ischemic Stroke Rats. *Med Sci Monit.* 2017;23:366–376.
228. Taylor RA, Chang C-F, Goods BA, Hammond MD, Mac Grory B, Ai Y, Steinschneider AF, Renfroe SC, Askenase MH, McCullough LD, Kasner SE, Mullen MT, Hafler DA, Love JC, Sansing LH. TGF- β 1 modulates microglial phenotype and promotes recovery after intracerebral hemorrhage. *J Clin Invest.* 2017;127:280–292.
229. Cekanaviciute E, Fathali N, Doyle KP, Williams AM, Han J, Buckwalter MS. Astrocytic transforming growth factor-beta signaling reduces subacute neuroinflammation after stroke in mice. *Glia.* 2014;62:1227–40.
230. Graham JB, Muir D. Chondroitinase C Selectively Degrades Chondroitin Sulfate Glycosaminoglycans that Inhibit Axonal Growth within the Endoneurium of Peripheral Nerve. *PLoS One.* 2016;11:e0167682.
231. Starkey ML, Bartus K, Barritt AW, Bradbury EJ. Chondroitinase ABC promotes compensatory sprouting of the intact corticospinal tract and recovery of forelimb function following unilateral pyramidotomy in adult mice. *Eur J Neurosci.*

- 2012;36:3665–3678.
232. Kobayashi T, Kakizaki I, Nozaka H, Nakamura T. Chondroitin sulfate proteoglycans from salmon nasal cartilage inhibit angiogenesis. *Biochem Biophys Reports*. 2017;9:72–78.
233. Manwani B, Liu F, Xu Y, Persky R, Li J, McCullough LD. Functional recovery in aging mice after experimental stroke. *Brain Behav Immun*. 2011;25:1689–700.
234. Jha MK, Kim J-H, Song GJ, Lee W-H, Lee I-K, Lee H-W, An SSA, Kim S, Suk K. Functional dissection of astrocyte-secreted proteins: Implications in brain health and diseases. *Prog Neurobiol*. 2017. doi:10.1016/j.pneurobio.2017.12.003.
235. Kress BT, Iliff JJ, Xia M, Wang M, Wei HS, Zeppenfeld D, Xie L, Kang H, Xu Q, Liew JA, Plog BA, Ding F, Deane R, Nedergaard M. Impairment of paravascular clearance pathways in the aging brain. *Ann Neurol*. 2014;76:845–61.
236. Venkat P, Chopp M, Zacharek A, Cui C, Zhang L, Li Q, Lu M, Zhang T, Liu A, Chen J. White matter damage and glymphatic dysfunction in a model of vascular dementia in rats with no prior vascular pathologies. *Neurobiol Aging*. 2017;50:96–106.
237. Wang M, Ding F, Deng S, Guo X, Wang W, Iliff JJ, Nedergaard M. Focal Solute Trapping and Global Glymphatic Pathway Impairment in a Murine Model of Multiple Microinfarcts. *J Neurosci*. 2017;37:2870–2877.
238. Gomez-Arboledas A, Davila JC, Sanchez-Mejias E, Navarro V, Nuñez-Diaz C, Sanchez-Varo R, Sanchez-Mico MV, Trujillo-Estrada L, Fernandez-Valenzuela JJ, Vizuite M, Comella JX, Galea E, Vitorica J, Gutierrez A. Phagocytic clearance of presynaptic dystrophies by reactive astrocytes in Alzheimer’s disease. *Glia*. 2018;66:637–653.

239. Zamanian JL, Xu L, Foo LC, Nouri N, Zhou L, Giffard RG, Barres BA. Genomic analysis of reactive astrogliosis. *J Neurosci*. 2012;32:6391–410.
240. Liddelow SA, Guttenplan KA, Clarke LE, Bennett FC, Bohlen CJ, Schirmer L, Bennett ML, Münch AE, Chung W-S, Peterson TC, Wilton DK, Frouin A, Napier BA, Panicker N, Kumar M, Buckwalter MS, Rowitch DH, Dawson VL, Dawson TM, Stevens B, Barres BA. Neurotoxic reactive astrocytes are induced by activated microglia. *Nature*. 2017;541:481–487.
241. Li G, Fu BM. An Electrodifusion Model for the Blood-Brain Barrier Permeability to Charged Molecules. *J Biomech Eng*. 2011;133:021002.
242. Urayama A, Grubb JH, Sly WS, Banks WA. Mannose 6-Phosphate Receptor–mediated Transport of Sulfamidase Across the Blood–brain Barrier in the Newborn Mouse. *Mol Ther*. 2008;16:1261–1266.
243. Jin B-J, Smith AJ, Verkman AS. Spatial model of convective solute transport in brain extracellular space does not support a “glymphatic” mechanism. *J Gen Physiol*. 2016;148:489–501.
244. Asgari M, de Zélicourt D, Kurtcuoglu V. Glymphatic solute transport does not require bulk flow. *Sci Rep*. 2016;6:38635.
245. Barrow CJ, Zagorski MG. Solution structures of beta peptide and its constituent fragments: relation to amyloid deposition. *Science*. 1991;253:179–82.
246. Deane R, Du Yan S, Subramanyam RK, LaRue B, Jovanovic S, Hogg E, Welch D, Manness L, Lin C, Yu J, Zhu H, Ghiso J, Frangione B, Stern A, Schmidt AM, Armstrong DL, Arnold B, Liliensiek B, Nawroth P, Hofman F, Kindy M, Stern D, Zlokovic B. RAGE mediates amyloid-beta peptide transport across the blood-brain

- barrier and accumulation in brain. *Nat Med*. 2003;9:907–913.
247. Osgood D, Miller MC, Messier AA, Gonzalez L, Silverberg GD. Aging alters mRNA expression of amyloid transporter genes at the blood-brain barrier. *Neurobiol Aging*. 2017;57:178–185.
248. Iliff JJ, Wang M, Zeppenfeld DM, Venkataraman A, Plog BA, Liao Y, Deane R, Nedergaard M. Cerebral arterial pulsation drives paravascular CSF-interstitial fluid exchange in the murine brain. *J Neurosci*. 2013;33:18190–9.
249. Hawkes CA, Härtig W, Kacza J, Schliebs R, Weller RO, Nicoll JA, Carare RO. Perivascular drainage of solutes is impaired in the ageing mouse brain and in the presence of cerebral amyloid angiopathy. *Acta Neuropathol*. 2011;121:431–43.
250. Shoji M, Kanai M. Cerebrospinal fluid A β 40 and A β 42: Natural course and clinical usefulness. *J Alzheimers Dis*. 2001;3:313–21.
251. Wyss-Coray T, Lin C, Sanan DA, Mucke L, Masliah E. Chronic overproduction of transforming growth factor-beta1 by astrocytes promotes Alzheimer's disease-like microvascular degeneration in transgenic mice. *Am J Pathol*. 2000;156:139–50.
252. Briknarová K, Akerman ME, Hoyt DW, Ruoslahti E, Ely KR. Anastellin, an FN3 fragment with fibronectin polymerization activity, resembles amyloid fibril precursors. *J Mol Biol*. 2003;332:205–15.
253. Doyle KP, Buckwalter MS. A mouse model of permanent focal ischemia: distal middle cerebral artery occlusion. *Methods Mol Biol*. 2014;1135:103–10.
254. Attar A, Liu T, Chan W-TC, Hayes J, Nejad M, Lei K, Bitan G. A Shortened Barnes Maze Protocol Reveals Memory Deficits at 4-Months of Age in the Triple-Transgenic Mouse Model of Alzheimer's Disease. *PLoS One*. 2013;8:e80355.

255. Harris NM, Ritzel R, Mancini NS, Jiang Y, Yi X, Manickam DS, Banks WA, Kabanov A V., McCullough LD, Verma R. Nano-particle delivery of brain derived neurotrophic factor after focal cerebral ischemia reduces tissue injury and enhances behavioral recovery. *Pharmacol Biochem Behav.* 2016;150-151:48–56.
256. Verma R, Friedler BD, Harris NM, McCullough LD. Pair housing reverses post-stroke depressive behavior in mice. *Behav Brain Res.* 2014;269:155–63.
257. Milner R, Hung S, Wang X, Berg GI, Spatz M, del Zoppo GJ. Responses of endothelial cell and astrocyte matrix-integrin receptors to ischemia mimic those observed in the neurovascular unit. *Stroke.* 2008;39:191–7.
258. Huang Q, Chen B, Wang F, Huang H, Milner R, Li L. The temporal expression patterns of fibronectin and its receptors- $\alpha 5\beta 1$ and $\alpha v\beta 3$ integrins on blood vessels after cerebral ischemia. *Restor Neurol Neurosci.* 2015;33:493–507.
259. Benito-Jardón M, Klapproth S, Gimeno-LLuch I, Petzold T, Bharadwaj M, Müller DJ, Zuchtriegel G, Reichel CA, Costell M. The fibronectin synergy site re-enforces cell adhesion and mediates a crosstalk between integrin classes. *Elife.* 2017;6.
doi:10.7554/eLife.22264.
260. Jullienne A, Roberts JM, Pop V, Paul Murphy M, Head E, Bix GJ, Badaut J. Juvenile traumatic brain injury induces long-term perivascular matrix changes alongside amyloid-beta accumulation. *J Cereb Blood Flow Metab.* 2014;34:1637–45.
261. Iliff JJ, Chen MJ, Plog BA, Zeppenfeld DM, Soltero M, Yang L, Singh I, Deane R, Nedergaard M. Impairment of glymphatic pathway function promotes tau pathology after traumatic brain injury. *J Neurosci.* 2014;34:16180–93.
262. Zámecník J, Vargová L, Homola A, Kodet R, Syková E. Extracellular matrix

- glycoproteins and diffusion barriers in human astrocytic tumours. *Neuropathol Appl Neurobiol.* 2004;30:338–50.
263. Anderová M, Kubinová S, Mazel T, Chvátal A, Eliasson C, Pekny M, Syková E. Effect of elevated K(+), hypotonic stress, and cortical spreading depression on astrocyte swelling in GFAP-deficient mice. *Glia.* 2001;35:189–203.
264. Roitbak T, Syková E. Diffusion barriers evoked in the rat cortex by reactive astrogliosis. *Glia.* 1999;28:40–8.
265. Li B, Lin Z, Mitsi M, Zhang Y, Vogel V. Heparin-induced conformational changes of fibronectin within the extracellular matrix promote hMSC osteogenic differentiation. *Biomater Sci.* 2015;3:73–84.
266. Agulhon C, Petravicz J, McMullen AB, Sweger EJ, Minton SK, Taves SR, Casper KB, Fiacco TA, McCarthy KD. What is the role of astrocyte calcium in neurophysiology? *Neuron.* 2008;59:932–46.
267. Papouin T, Dunphy J, Tolman M, Foley JC, Haydon PG. Astrocytic control of synaptic function. *Philos Trans R Soc B Biol Sci.* 2017;372:20160154.
268. Magaki SD, Williams CK, Vinters H V. Glial function (and dysfunction) in the normal & ischemic brain. *Neuropharmacology.* 2017.
doi:10.1016/j.neuropharm.2017.11.009.
269. Hu X, Yuan Y, Wang D, Su Z. Heterogeneous astrocytes: Active players in CNS. *Brain Res Bull.* 2016;125:1–18.
270. Adams KL, Gallo V. The diversity and disparity of the glial scar. *Nat Neurosci.* 2018;21:9–15.
271. Clarke LE, Liddel SA, Chakraborty C, Münch AE, Heiman M, Barres BA. Normal

- aging induces A1-like astrocyte reactivity. *Proc Natl Acad Sci.* 2018;115:E1896–E1905.
272. Ueberham U, Lange P, Ueberham E, Brückner MK, Hartlage-Rübsamen M, Pannicke T, Rohn S, Cross M, Arendt T. Smad2 isoforms are differentially expressed during mouse brain development and aging. *Int J Dev Neurosci.* 2009;27:501–510.
273. Wyman AE, Noor Z, Fischelevich R, Lockatell V, Shah NG, Todd NW, Atamas SP. Sirtuin 7 is decreased in pulmonary fibrosis and regulates the fibrotic phenotype of lung fibroblasts. *Am J Physiol Cell Mol Physiol.* 2017;312:L945–L958.
274. Ito T, Yamamoto N, Nakajima S, Schaffer SW. Beta-Catenin and SMAD3 Are Associated with Skeletal Muscle Aging in the Taurine Transporter Knockout Mouse. In: *Advances in experimental medicine and biology.* ; 2017: 497–502.
275. Kashyap S, Warner G, Hu Z, Gao F, Osman M, Al Saiegh Y, Lien KR, Nath K, Grande JP. Cardiovascular phenotype in Smad3 deficient mice with renovascular hypertension. *PLoS One.* 2017;12:e0187062.
276. Latella G, Vetuschi A, Sferra R, Catitti V, D'Angelo A, Zanninelli G, Flanders KC, Gaudio E. Targeted disruption of Smad3 confers resistance to the development of dimethylnitrosamine-induced hepatic fibrosis in mice. *Liver Int.* 2009;29:997–1009.
277. Burton T, Liang B, Dibrov A, Amara F. Transforming growth factor-beta-induced transcription of the Alzheimer beta-amyloid precursor protein gene involves interaction between the CTCF-complex and Smads. *Biochem Biophys Res Commun.* 2002;295:713–23.
278. Town T, Laouar Y, Pittenger C, Mori T, Szekely CA, Tan J, Duman RS, Flavell RA. Blocking TGF- β -Smad2/3 innate immune signaling mitigates Alzheimer-like

- pathology. *Nat Med*. 2008;14:681–687.
279. Hamby ME, Uliasz TF, Hewett SJ, Hewett JA. Characterization of an improved procedure for the removal of microglia from confluent monolayers of primary astrocytes. *J Neurosci Methods*. 2006;150:128–137.
280. Wyss-Coray T, Masliah E, Mallory M, McConlogue L, Johnson-Wood K, Lin C, Mucke L. Amyloidogenic role of cytokine TGF-beta1 in transgenic mice and in Alzheimer's disease. *Nature*. 1997;389:603–606.
281. Mukherjee D, Patil CG. Epidemiology and the global burden of stroke. *World Neurosurg*. 2011;76:S85–90.
282. Knudsen KA, Rosand J, Karluk D, Greenberg SM. Clinical diagnosis of cerebral amyloid angiopathy: validation of the Boston criteria. *Neurology*. 2001;56:537–9.
283. Lee J-M, Yin K, Hsin I, Chen S, Fryer JD, Holtzman DM, Hsu CY, Xu J. Matrix metalloproteinase-9 in cerebral-amyloid-angiopathy-related hemorrhage. *J Neurol Sci*. 2005;229-230:249–54.
284. Machida T, Takata F, Matsumoto J, Takenoshita H, Kimura I, Yamauchi A, Dohgu S, Kataoka Y. Brain pericytes are the most thrombin-sensitive matrix metalloproteinase-9-releasing cell type constituting the blood–brain barrier in vitro. *Neurosci Lett*. 2015;599:109–114.
285. Kawakita K, Kawai N, Kuroda Y, Yasashita S, Nagao S. Expression of Matrix Metalloproteinase-9 in Thrombin-Induced Brain Edema Formation in Rats. *J Stroke Cerebrovasc Dis*. 2006;15:88–95.
286. Kurogi R, Kikkawa Y, Matsuo S, Nakamizo A, Mizoguchi M, Sasaki T. Upregulation of tissue inhibitor of metalloproteinase-1 contributes to restoration of the extracellular

- matrix in the rabbit basilar artery during cerebral vasospasm after subarachnoid hemorrhage. *Brain Res.* 2015;1616:26–36.
287. Imai K, Hiramatsu A, Fukushima D, Pierschbacher MD, Okada Y. Degradation of decorin by matrix metalloproteinases: identification of the cleavage sites, kinetic analyses and transforming growth factor-beta1 release. *Biochem J.* 1997;322 (Pt 3):809–14.
288. Carmichael ST, Vespa PM, Saver JL, Coppola G, Geschwind DH, Starkman S, Miller CM, Kidwell CS, Liebeskind DS, Martin NA. Genomic Profiles of Damage and Protection in Human Intracerebral Hemorrhage. *J Cereb Blood Flow Metab.* 2008;28:1860–1875.
289. Floreczak-Rzepka M, Grond-Ginsbach C, Montaner J, Steiner T. Matrix Metalloproteinases in Human Spontaneous Intracerebral Hemorrhage: An Update. *Cerebrovasc Dis.* 2012;34:249–262.
290. Amantea D, Micieli G, Tassorelli C, Cuartero MI, Ballesteros I, Certo M, Moro MA, Lizasoain I, Bagetta G. Rational modulation of the innate immune system for neuroprotection in ischemic stroke. *Front Neurosci.* 2015;9:147.
291. Hemphill JC, Bonovich DC, Besmertis L, Manley GT, Johnston SC. The ICH score: a simple, reliable grading scale for intracerebral hemorrhage. *Stroke.* 2001;32:891–7.
292. Spilker J, Kongable G, Barch C, Braimah J, Brattina P, Daley S, Donnarumma R, Rapp K, Sailor S. Using the NIH Stroke Scale to assess stroke patients. The NINDS rt-PA Stroke Study Group. *J Neurosci Nurs.* 1997;29:384–92.
293. Teasdale G, Jennett B. Assessment of coma and impaired consciousness. A practical scale. *Lancet (London, England).* 1974;2:81–4.

294. van Swieten JC, Koudstaal PJ, Visser MC, Schouten HJ, van Gijn J. Interobserver agreement for the assessment of handicap in stroke patients. *Stroke*. 1988;19:604–7.
295. Hallevi H, Dar NS, Barreto AD, Morales MM, Martin-Schild S, Abraham AT, Walker KC, Gonzales NR, Illoh K, Grotta JC, Savitz SI. The IVH score: a novel tool for estimating intraventricular hemorrhage volume: clinical and research implications. *Crit Care Med*. 2009;37:969–74, e1.
296. Weiss R, Lifshitz V, Frenkel D. TGF- β 1 affects endothelial cell interaction with macrophages and T cells leading to the development of cerebrovascular amyloidosis. *Brain Behav Immun*. 2011;25:1017–1024.
297. Wyss-Coray T, Masliah E, Mallory M, McConlogue L, Johnson-Wood K, Lin C, Mucke L. Amyloidogenic role of cytokine TGF-beta1 in transgenic mice and in Alzheimer's disease. *Nature*. 1997;389:603–6.
298. Zhao L, Arbel-Ornath M, Wang X, Betensky RA, Greenberg SM, Frosch MP, Bacskai BJ. Matrix metalloproteinase 9-mediated intracerebral hemorrhage induced by cerebral amyloid angiopathy. *Neurobiol Aging*. 2015;36:2963–2971.
299. Hernandez-Guillamon M, Martinez-Saez E, Delgado P, Domingues-Montanari S, Boada C, Penalba A, Boada M, Pagola J, Maisterra O, Rodriguez-Luna D, Molina CA, Rovira A, Alvarez-Sabin J, Ortega-Aznar A, Montaner J. MMP-2/MMP-9 Plasma Level and Brain Expression in Cerebral Amyloid Angiopathy-Associated Hemorrhagic Stroke. *Brain Pathol*. 2012;22:133–141.
300. Greenberg SM, Cho HS, O'Donnell HC, Rosand J, Segal AZ, Younkin LH, Younkin SG, Rebeck GW. Plasma beta-amyloid peptide, transforming growth factor-beta 1, and risk for cerebral amyloid angiopathy. *Ann N Y Acad Sci*. 2000;903:144–9.

301. Chang JJ, Emanuel BA, Mack WJ, Tsivgoulis G, Alexandrov A V. Matrix Metalloproteinase-9: Dual Role and Temporal Profile in Intracerebral Hemorrhage. *J Stroke Cerebrovasc Dis.* 2014;23:2498–2505.
302. Silva Y, Leira R, Tejada J, Lainez JM, Castillo J, Davalos A. Molecular Signatures of Vascular Injury Are Associated With Early Growth of Intracerebral Hemorrhage. *Stroke.* 2005;36:86–91.
303. Li N, Liu YF, Ma L, Worthmann H, Wang YL, Wang YJ, Gao YP, Raab P, Dengler R, Weissenborn K, Zhao XQ. Association of molecular markers with perihematomal edema and clinical outcome in intracerebral hemorrhage. *Stroke.* 2013;44:658–63.
304. Buckwalter M, Pepper J-P, Gaertner RF, Von Euw D, Lacombe P, Wyss-Coray T. Molecular and functional dissection of TGF-beta1-induced cerebrovascular abnormalities in transgenic mice. *Ann N Y Acad Sci.* 2002;977:87–95.
305. Smith GM, Strunz C. Growth factor and cytokine regulation of chondroitin sulfate proteoglycans by astrocytes. *Glia.* 2005;52:209–18.
306. Chio C-C, Lin M-T, Chang C-P, Lin H-J. A positive correlation exists between neurotrauma and TGF- β 1-containing microglia in rats. *Eur J Clin Invest.* 2016;46:1063–1069.
307. Hippus H, Neundörfer G. The discovery of Alzheimer’s disease. *Dialogues Clin Neurosci.* 2003;5:101–8.
308. Okazaki H, Reagan TJ, Campbell RJ. Clinicopathologic studies of primary cerebral amyloid angiopathy. *Mayo Clin Proc.* 1979;54:22–31.
309. Mountjoy CQ, Tomlinson BE, Gibson PH. Amyloid and senile plaques and cerebral blood vessels. A semi-quantitative investigation of a possible relationship. *J Neurol*

- Sci.*;57:89–103.
310. Olichney JM, Hansen LA, Hofstetter CR, Grundman M, Katzman R, Thal LJ. Cerebral infarction in Alzheimer's disease is associated with severe amyloid angiopathy and hypertension. *Arch Neurol.* 1995;52:702–8.
 311. Xiong L, Boulouis G, Charidimou A, Roongpiboonsopit D, Jessel MJ, Pasi M, Reijmer YD, Fotiadis P, Ayres A, Merrill E, Schwab K, Blacker D, Gurol ME, Greenberg SM, Viswanathan A. Dementia incidence and predictors in cerebral amyloid angiopathy patients without intracerebral hemorrhage. *J Cereb Blood Flow Metab.* 2017;:0271678X1770043.
 312. Charidimou A, Farid K, Tsai H-H, Tsai L-K, Yen R-F, Baron J-C. Amyloid-PET burden and regional distribution in cerebral amyloid angiopathy: a systematic review and meta-analysis of biomarker performance. *J Neurol Neurosurg Psychiatry.* 2017;:jnnp–2017–316851.
 313. Brkic M, Balusu S, Van Wonterghem E, Gorle N, Benilova I, Kremer A, Van Hove I, Moons L, De Strooper B, Kanazir S, Libert C, Vandenbroucke RE. Amyloid Oligomers Disrupt Blood-CSF Barrier Integrity by Activating Matrix Metalloproteinases. *J Neurosci.* 2015;35:12766–12778.
 314. Vonsattel JP, Myers RH, Hedley-Whyte ET, Ropper AH, Bird ED, Richardson EP. Cerebral amyloid angiopathy without and with cerebral hemorrhages: a comparative histological study. *Ann Neurol.* 1991;30:637–49.
 315. Senn R, Elkind MS V, Montaner J, Christ-Crain M, Katan M. Potential role of blood biomarkers in the management of nontraumatic intracerebral hemorrhage. *Cerebrovasc Dis.* 2014;38:395–409.

316. Wu M-Y, Li C-J, Hou M-F, Chu P-Y. New Insights into the Role of Inflammation in the Pathogenesis of Atherosclerosis. *Int J Mol Sci.* 2017;18:2034.
317. Yamada M, Tsukagoshi H, Otomo E, Hayakawa M. Cerebral amyloid angiopathy in the aged. *J Neurol.* 1987;234:371–6.
318. Cutler RW, Page L, Galicich J, Watters G V. Formation and absorption of cerebrospinal fluid in man. *Brain.* 1968;91:707–20.
319. Serot JM, Foliguet B, Béné MC, Faure GC. Choroid plexus and ageing in rats: a morphometric and ultrastructural study. *Eur J Neurosci.* 2001;14:794–8.
320. Wen GY, Wisniewski HM, Kascsak RJ. Biondi ring tangles in the choroid plexus of Alzheimer's disease and normal aging brains: a quantitative study. *Brain Res.* 1999;832:40–6.
321. Silverberg GD, Mayo M, Saul T, Rubenstein E, McGuire D. Alzheimer's disease, normal-pressure hydrocephalus, and senescent changes in CSF circulatory physiology: a hypothesis. *Lancet Neurol.* 2003;2:506–11.
322. Garton MJ, Keir G, Lakshmi M V, Thompson EJ. Age-related changes in cerebrospinal fluid protein concentrations. *J Neurol Sci.* 1991;104:74–80.
323. Wester P, Puu G, Reiz S, Winblad B, Wester PO. Increased monoamine metabolite concentrations and cholinesterase activities in cerebrospinal fluid of patients with acute stroke. *Acta Neurol Scand.* 1987;76:473–9.
324. Massicotte EM, Del Bigio MR. Human arachnoid villi response to subarachnoid hemorrhage: possible relationship to chronic hydrocephalus. *J Neurosurg.* 1999;91:80–84.
325. Grzybowski DM, Holman DW, Katz SE, Lubow M. In vitro model of cerebrospinal

- fluid outflow through human arachnoid granulations. *Invest Ophthalmol Vis Sci.* 2006;47:3664–72.
326. Steardo L, Nathanson JA. Brain barrier tissues: end organs for atriopeptins. *Science.* 1987;235:470–3.
327. Cuevas P, Carceller F, Reimers D, Fu X, Giménez-Gallego G. Immunohistochemical localization of basic fibroblast growth factor in choroid plexus of the rat. *Neurol Res.* 1994;16:310–2.
328. Kataoka H, Yamada E, Hazama F. Increased basic fibroblast growth factor immunoreactivity in the brain of stroke-prone spontaneously hypertensive rats. *Acta Neuropathol.* 1994;88:7–13.
329. Greenwood S, Swetloff A, Wade AM, Terasaki T, Ferretti P. Fgf2 is expressed in human and murine embryonic choroid plexus and affects choroid plexus epithelial cell behaviour. *Cerebrospinal Fluid Res.* 2008;5:20.
330. Kaur C, Singh J, Lim MK, Ng BL, Yap EP, Ling EA. Studies of the choroid plexus and its associated epiplexus cells in the lateral ventricles of rats following an exposure to a single non-penetrative blast. *Arch Histol Cytol.* 1996;59:239–48.
331. Palm D, Knuckey N, Guglielmo M, Watson P, Primiano M, Johanson C. Choroid plexus electrolytes and ultrastructure following transient forebrain ischemia. *Am J Physiol.* 1995;269:R73–9.
332. Ritzel RM, Crapser J, Patel AR, Verma R, Grenier JM, Chauhan A, Jellison ER, McCullough LD. Age-Associated Resident Memory CD8 T Cells in the Central Nervous System Are Primed To Potentiate Inflammation after Ischemic Brain Injury. *J Immunol.* 2016;196:3318–3330.

333. Llovera G, Benakis C, Enzmann G, Cai R, Arzberger T, Ghasemigharagoz A, Mao X, Malik R, Lazarevic I, Liebscher S, Ertürk A, Meissner L, Vivien D, Haffner C, Plesnila N, Montaner J, Engelhardt B, Liesz A. The choroid plexus is a key cerebral invasion route for T cells after stroke. *Acta Neuropathol.* 2017;134:851–868.
334. Ge R, Tornero D, Hirota M, Monni E, Laterza C, Lindvall O, Kokaia Z. Choroid plexus-cerebrospinal fluid route for monocyte-derived macrophages after stroke. *J Neuroinflammation.* 2017;14:153.

CHAPTER 9

Vita

Matthew David Howe was born in Providence, Rhode Island, the son of Susan Elizabeth Howe and Kevin Charles Howe. After graduating from Barrington High School, in Barrington, Rhode Island, in 2008, he entered the University of Connecticut in Storrs, Connecticut. He graduated from UConn in 2012, receiving the degree of Bachelor of Science with a double major in Physiology and Psychology, and a minor in Neuroscience. In June of 2012, he entered into the MD/PhD dual degree program at the UConn School of Medicine, then transferred with his thesis advisor in August of 2015 to the University of Texas MD Anderson Cancer Center UT Health Graduate School of Biomedical Sciences to complete his graduate research and degrees.

Permanent Address:

2718 S Belgravia Drive

Pearland, TX 77584